CRANFIELD UNIVERSITY

Academic Year 2006

H. K. Askar

DEVELOPING A MULTIPLE GLAZING SYSTEM TO MINIMIZE TRANSMISSION OF DIRECT INSOLATION FOR PARTICULAR LATITUDES

SCHOOL OF ENGINEERING

Ph. D THESIS

CRANFIELD UNIVERSITY

SCHOOL OF ENGINEERING

Ph. D THESIS

Academic Year 2006

H. K. Askar

DEVELOPING A MULTIPLE GLAZING SYSTEM TO MINIMIZE TRANSMISSION OF DIRECT INSOLATION FOR PARTICULAR LATITUDES

Supervisor: Dr. W. J. Batty
May 2006

ABSTRACT

Too often, in the last 50 years, the energy-thrift lessons of vernacular architecture have been forgotten or ignored. In the Middle East, many recently-designed commercial buildings, with large areas of glazing, incur excessively high electricity-demands to provide energy for the required air-conditioning plant. One way of reducing the magnitude of this demand is through better window design.

A new glazing system is proposed that utilizes the insertion of a clear glazing element within the cavity of a double glazed window. The main objective of this system is to achieve acceptable levels of daylight within a building by attempting to maintain the diffuse component of insolation while reducing the penetration of direct component by using the increased reflectivity of these materials with the angle of incidence of the direct beam component of solar irradiation. By using clear glazing materials the proposed system attempts to achieve acceptable performance without the need for elaborate and expensive coatings or substrates.

Because solar geometry varies with latitude a varying performance of glazing systems is expected with current glazing systems. However, the suggested system utilizes an optimal angle for overall daylighting and thermal performance that relates to the particular solar geometry of interest,

New software is also developed to assess the performance of the suggested system; this involved examining all the modes of heat transfer through the entire glazing system. Results then were assessed to calculate the optimal angle of the element that corresponds to the solar geometry of particular latitude.

Such proposal takes a new perspective, once it is acknowledged that though different forms of advanced glazing systems currently are being used to inhibit the penetration of direct solar radiation, still the main disadvantages of such advanced glazing systems are that they are relatively expensive and would reduce the penetration of a considerable part of the daylight entering the space.

ACKNOWLEDGEMENT

I wish sincerely to take this opportunity to express my gratitude to my supervisor Dr. William (Bill) Batty, for the time and effort that he gave throughout the years, putting in mind his other obligations in Japan. His efforts were also fruitful in co-publishing couple of papers on the topic.

During my stay at Cranfield, I was able to receive a great deal of knowledge and feedback, thanks to the staff at Cranfield, in the Department of Automotive, Mechanical and Structural Engineering, the computer centre, for the help and assistance.

I wish also to acknowledge with gratitude; Prof. D. Probert, for his contribution to my work, Dr. Ossama Badr who is a mentor and a friend, Dr. Ross McCluney, Head of fenestration Unit at North Berkley Laboratories-United States for his aid in supplying me with up to date copies of WINDOWS, also a big thank you to, Dr. Chris Gueymard, whose guidance on SMARTS2 was immeasurable and finally many thanks to Mr. Daryl Myers of NREL- United States for his help in supplying me with copies of their CIE daylight models.

I must also mention all the friends and colleagues who helped me in one way or another during this time; in particular my friend Mr. Yehia Al-Hadban for his help throughout the years up to the last minute.

I am immensely grateful to all the members of my family, my friend and wife Sarah and my parents whose unfailing support, encouragement and love has given me the strength when I needed it most, to them and to both of my children Lina and Jadd, I dedicate my work.

One last word is to thank God and our Lord for the unbound blessing, so I could be who I am.

CONTENTS

GLOSSARY

Aerosol Angstrom	"Coefficien*ts 1,2*", an exponent that expresses the spectral dependence of aerosol optical thickness (τ) with the wavelength of incident light (λ). Angstrom Exponent-1, based on 0.55 and 0.865 μm aerosol optical thickness (over ocean). Angstrom Exponent-2, based on 0.865 and 2.13 μm aerosol optical thickness (over ocean) Angstrom Exponent based on 0.47 and 0.67 μm aerosol optical thickness (over land)
Aliasing	Defects or distortion in images; typically seen as visibly jagged steps on diagonal lines due to sharp tonal contrasts between generated pixels; which is caused by insufficient sampling and poor filtering of the capture surface (PRQC 2005).
Arabesque decoration	Ornamental surface relief and motifs, which consist of the frequent repetition of botanical and/or geometrical shapes: these have been made of wood, glass and/or ceramics, and are usually highly colored.
Best performance	A term used in this research to refer to the preferential selection of generated results used in the optimization process, which was based on the level of contribution of the direct insolation component in heating up inner building spaces.
Birefringence	splitting a ray into two parallel rays polarized perpendicularly double refraction.
Capture surfaces/edges	planes or lines (in 2D environments), which are created to within a raytracing model to model the intersection of the rays with a specific object or plane, process is governed by differential equation.
Cermets	Class of particle-strengthened composite materials consisting of two components, one of which is an oxide, carbide, boride or similar inorganic compound and the other is a metallic binder.
Colonial-style architecture	Refers to the period from the late 18th to the early 20th century. Such types of architecture were introduced primarily by the English, Portuguese, French and Spanish, when they colonized parts of Asia, South America and the Middle East.

Although local building materials were employed, the designs of the buildings reflected, to a significant extent, the previous life styles of the immigrants, rather than the local vernacular architecture.

Commision internationale l'eclarage

I.e. *CIE,* is a group that has been working since the 1930's *de* to establish standard ways of measuring the effects on the visible band of the insolation wavelength (i.e. colour band) based on human visual physiology.

Confidence limits

an interval estimate for the mean value of data, generates a lower and upper limit for the mean, it is an indication of the uncertainty in the estimate of the true mean, it is usually expressed in terms of confidence coefficient. In practice 90%, 95%, and 99% intervals are often used, with 95% being the most commonly used.

Correlation

A measure of the association between two variables, measuring change and relations in the variables; so as if they tend to move up or down together, they are positively correlated, or negatively correlated, if moving in opposite directions. Correlations are computed in the Multiple Regression form. The most common statistic for measuring association is the *Pearson* correlation coefficient; *see definition.*

Glasses

Their structures consist of complex, continuous networks of silica-oxygen bonds, in which the individual electropositive elements are bound to oxygen. These non-crystalline solids tend to be transparent and brittle: they melt over a range of temperature.

Insolation

A term used to refer to incident solar radiation, arriving at earth un-attenuated.

Iso-lines

A term of Fluent™ terminology, which describes lines used to bisect isothermally and are applied horizontally or vertically in a CFD generated mesh to analyse heat transfer results.

International style

Predominant Class of urban architecture in the period from the late 1920s to the mid-1960s, involving the use of new applications of steel, glass and reinforced concrete showing more clearly each building's structural elements and services. Buildings depended primarily on the use of mechanical services (e.g. refrigeration plant) to achieve thermal comfort within their internal artificial environments, as the unit prices of fossil fuels were then so low.

Kriging	A form of statistical modelling that interpolates data from a known set of sample points to a continuous surface. Such technique is used in spatial analysis and geostatistics. Hutchinson et al 1984, Hulme et al 1995, Zelenka et al 1992.
Max reflection angle	The critical angle of incidence at which a light ray passing from one medium to another less refractive medium can be totally reflected from the boundary between the two.
Organic layout	This phrase is used in architecture and planning to indicate that a natural growth of an urban settlement had occurred; the expansion being dictated by immediate need, with little or no pre-planning.
Pearson coefficient	A statistic computed to calculate the correlation between two numeric variables, ranging from -1 for perfect negative correlation to +1 for perfect positive correlation. It is calculated by dividing the covariance of the variables by the square root of the product of their variances.
Regression	A mathematical technique used to explain and/or predict. The general form is $Y = a + bX + u$, where Y is the variable to be predicted; X is the variable used to predict Y, a is the intercept; b is the slope, and u is the regression residual. The a and b are chosen in a way to minimize the squared sum of the residuals.
R-squared value	an indicator from 0-1 that shows how close estimated values for the trend line correspond to actual data, being more accurate when value at or near 1, also known as the coefficient of determination.
Schlieren method	A method to measure the light deflection angle in both spatial directions, and hence the projected density gradient of a two-dimensional compressible flow. It is commonly employed as a qualitative method only.
Shading coefficient	The ratio of the solar-heat gain going through unit area of the considered type of glass to that for unit area of clear float glass, 3 mm thick, under identical applied conditions.
Ziggurat	A Babylonian (~3000–1250BC) name for a stepped pyramidal structure, with diminishing stages (i.e. podiums) with height, served by a ceremonial ramp. A small temple or shrine, with a dome of up to 20 m height, was erected on top of the uppermost terrace: it was intended to be used for observing the stars or as the location for worshiping gods.

NOMENCLATURE

A	Constant, area of heat transfer/ glazing; m^2
B, C, D, F, G, H, I	Coefficients, *see table 2.01*; dimensionless.
a, b	Coefficients; dimensionless.
C	Speed of light in a medium (in a vacuum C_0=2.988×10^8 m/s).
C_m	Monthly average fraction of the daytime sky obscured by clouds.
C_p	Specific heat capacity at constant pressure; J/kg.K
C_v	Specific heat capacity at constant volume.
D	Daily diffuse radiation received at the Earth's surface; $kWhm^{-2}$.
B, C, E, F, H, I and ***P***	Geometrical parameters (all in *m*) for the window assembly; *see Fig. 1.05.*
E_b	Total emissive power of a black body, $_b$ denotes to the black body.
f	Fraction, function, frequency of light waves; Hertz
G_{max}, G_{mean} and G_{min}	For a specific month, the daily maximum, mean and minimum amounts respectively of the incident global solar radiation at the Earth's surface, (kWh/m^2), where $G_{max}=G_0(a+b)$, $G_{mean}=G_0(a+b/2)$ and $G_{min}=G_{0a}$
G_{sc}	Solar constant: the extraterrestrial solar irradiance at normal incidence has been measured at 1373 W/m^2
G_0	For a specific month, the daily mean extraterrestrial solar irradiation incident upon a horizontal plane, i.e. the amount of insolation before experiencing attenuation and scattering by the Earth's atmosphere; kWh m^{-2}.
Gr	Formula used in convection study to express the ratio of buoyancy forces to viscosity forces; $g\alpha\Delta TL^3/\nu^2$ dimensionless.
g	gravitational force acceleration; $9.8m/s^2$
g_t	Solar transmittance plus the absorbed part of the radiation, which is re-emitted inside the building; dimensionless
h_c	Convective heat-transfer coefficient for a gas-filled vertical cavity within a double-glazed system, Wm^{-2} K^{-1}.
Kt_{max} Kt_{min}:	Maximum and minimum daily clearness-indices, i.e. the ratios of the maximum and of the minimum mean monthly daily global insolation respectively to the monthly mean

	daily extraterrestrial insolation (i.e. $G_{max}/G_o=(a+b)$ and $G_{min}/G_o=a$ respectively).
I	Spectral solar intensity; W/m^2
I_D	Direct solar intensity per unit length along the height of the glazing; W/m
K	Kelvin, Extinction coefficient; dimensionless.
k	Thermal conductivity; W/m.K
L_{lod}	The longitude of the site; degrees.
L_{lad}	The latitude of the site; degrees.
l_o	Ozone concentration in the vertical column; milli-atom-cm.
l_w	Amount of perceptible water, i.e. vapour, in the zenith direction; cm.
m	air mass; dimensionless.
p	Number of glazing panes.
Pr	Prandtl number, $C_p\mu$ /k; dimensionless.
Q	Heat flux, heat transfer rate; W/m^2
q	Type of glazing; dimensionless (1-10); *see chapter three.*
Ra	Rayleigh number, $GrPr$; $Ra_L = Gr_LPr$; dimensionless, *see chapter six.*
n_d	number of the day.
S	Number of hours of bright sunshine in one day (i.e. 24 h) averaged over a month, surface area.
Sc	Shading coefficient; dimensionless.
S_{sp}	Correction factor for the sun earth distance; $_{sp}$ denotes to Spencer model.
S_d	Number of hours per day when clouds obstruct a view of the Sun, averaged over a month.
S_{max}	Estimated astronomical mean number of hours of maximum sunshine in one day for a particular month.
t	Time; Seconds
$T_{dewpoint}$	Dew-point temperature; Kelvin.
U	Overall heat transfer coefficient; $W/m^2.K$
UV	Ultra violet
V	Velocity/volume.
VR	Metrological range of visibility; km.
vis	Visibility; m
W	Width of the cavity in the proposed double-glazing system, *see Fig. 1.23*; meters

Greek Letters

α	Absorptivity; dimensionless.
$\alpha 1, \alpha 2$	Angstrom coefficients; dimensionless.
β	Turbidity coefficient; dimensionless.
β_s	Tilt angle of the recipient surface of incidence; degrees.
ΔT	Temperature difference; either Kelvin or Celsius.
δ_s	Solar declination angle, *see chapter two*; degrees.
δ_1, δ_2	Mean solar azimuth angles for summer and winter respectively; degrees.
ε	Emissivity, of a surface; dimensionless. Wall azimuth angle (degrees) NB: equals zero at south orientation.
Φ	The solar altitude, *see chapter two*; degrees.
ϕ_B	Brewster angle; degrees.
Γ	The latitude angle, *see chapter two*; degrees.
γ_s	Solar azimuth angle, *see chapter two*; degrees.
λ	Wavelength; μm
θ_f	Inclination to the horizontal of the external glazing or inner membrane in the proposed glazing system, *see Figs. 1.23*; also the rotation angle, *see chapter four*; degrees.
θ_z	The zenith angle, *see chapter two*; degrees.
ρ	Reflectivity; dimensionless.
σ	Stefan-Boltzmann constant.
τ	Transmissivity.
τ_a	Absorptive transmissivity; dimensionless.
$\bar{\tau}_m$	Mean transmissivity of each glazing zone; dimensionless.
τ_r	Reflective transmissivity; dimensionless.
ω	The solar hour angle, *see chapter two*; degrees.
ψ	Maximum angle of reflection, *see 4.2.2*; degrees. Also, linear thermal transmittance; W/m.k

Subscript

a	Absorptivity
B	Brewster
Bn	Beam normal of solar radiation.
D	Direct
DB	Direct beam
eo	Relates to the temperature of the earth.
f	Inserted element
n	Nitrogen

o	ozone.
ro	Relates to reference temperature for wavelength 344-560nm.
S	Surface.
w	water.

LIST OF FIGURES AND TABLES

Chapter One

Figures:

Chapter Two

Chapter Three

Tables:

Chapter Four

Figures:

Tables:

Chapter Five

Figures:

Tables:

Chapter Six

Figures:

Tables:

Chapter Seven

Figures:

Tables:

Chapter Eight

Figures:

CHAPTER ONE

BACKGROUND

1.1 HISTORICAL REVIEW

Windows or any forms of openings in a building envelope are a reflection of the ambient conditions and the culture and architecture of a particular civilization. They are also associated with other building elements that accordingly would accentuate the architecture that is characteristic of that civilization.

Among the earliest signs of civilization were the agricultural settlements in Mesopotamia (i.e. present-day Iraq and the eastern part of Syria), which began more than 7000 years ago.

Subsequently, the inhabitants of this region evolved from living in villages with cottage-type settlements to the more complex and versatile city communities. During this development, the populations continually adapted their modes of living and building styles to accommodate to the terrain and climate of the local natural-environments.

Buildings and the urban environment were customised to attenuate: the severe adverse impacts of the ambient surrounding condition, the extreme effects of natural forces and the arid terrain (Fletcher B 1996).

Lifestyles and clothing were adapted as part of the survival and cultural responses to the local environment. During the millennia that have passed since those early beginnings benefits were achieved by adopting various building and environmental features, some of which are listed below:

- Ensuring that the building structure was of high thermal-mass, which attenuated the internal temperature fluctuations arising from diurnal-nocturnal ambient temperature variations.

- Sizes and locations of the openings through the outer walls and roof were optimised with respect to the heat and light transfers through them, and for defensive reasons.

- Shading by natural means (e.g. via trees) reduced the insolation incident upon adjacent buildings and the effects of wind. This was also achieved in urban environments with shaded alleys providing some thermal protection.

- Reducing the ratio of the external-surface area to the contained volume of the building thereby reduced both (i) the total insolation on its exposed surfaces (i.e. roof and walls) and (ii) the heat transfer rate per unit surface area per unit volume of the building.

- The pergola system (i.e. the repetition of shaded and sun-lit zones) inhibited the rate of heat gain and reduced diffuse reflection to surrounding dwellings.

- Narrow streets behave as cooling ducts by venting away hot dusty air (Fatthi I & Warren J 1996). Increasing the wind-exposed surface areas of the external walls and other building elements enhanced the rate of heat loss from these shaded surfaces via winds to the ambient environment. This effect was enhanced by introducing brick reliefs; motifs and alcoves (ceedex, website 1998) *see Fig.1.01.*

- Employing low-thermal-conductivity building materials as well as designs that incorporated walls with cavities that acted as air ducts for heat-exchange purposes, thus reducing the rates of heat transfer through the facades of buildings. Particularly from the exterior to the interior of the building, e.g. Badkeer, air ducts in medieval Mediterranean houses used to control humidity and temperature through built-in and connected terracotta water pipes that dissipated water droplets.

- Increasing the reflectiveness of a facade with respect to insolation could be by achieved by painting it white or utilising glazed brick-facings. The latter were used extensively in Mesopotamian temples and palaces and subsequently throughout the entire Middle East during the era of the Islamic Empire (700→1265AD).

Additionally, the microclimates within the habitable spaces of a building were controlled by:

i. Some walls were glazed preferentially to admit insolation, but where this had to be inhibited, fewer, smaller or no windows were incorporated.

ii. Appropriate location and orientation of openings in order to cool the building's fabric and, if advantageous, introduce air currents into the inhabited spaces.

iii. Employing ducts, wind-towers and shafts to promote this air circulation: the air entering the building may have been passed over intermittently-wetted cloths, thereby cooling it via latent heat extraction as well as increasing its humidity.

iv. Introducing an open-unit living space, i.e. a courtyard, within the building: this void helped by trapping cooler, denser air within the space at night, facilitating the persistence of its stratification during the day (Fatthi I & Warren J 1996).

v. Reducing the temperature of the air through evaporation and hence latent heat cooling by means of fountains and pools located in the courtyard: this increased the humidity of the air so providing a less arid environment.

vi. Having live plants, within the building and courtyard, which absorb CO_2 to promote their growth via photosynthesis, and helping to stabilize the temperature locally through the process of transpiration from the foliage: additionally, providing the shading surfaces of the leaves, that are at or below the ambient temperature, the foliage also filters out hot dust and other pollutants from the air.

vii. The building including a vented vault and dome (Fletcher B 1996),promoted the occurrence of an air currents through its internal environment.

Such features and techniques led to various zones within the building being occupied preferentially at different times of the day and year according to the daily movements of the Sun and seasonal variations in climatic conditions.

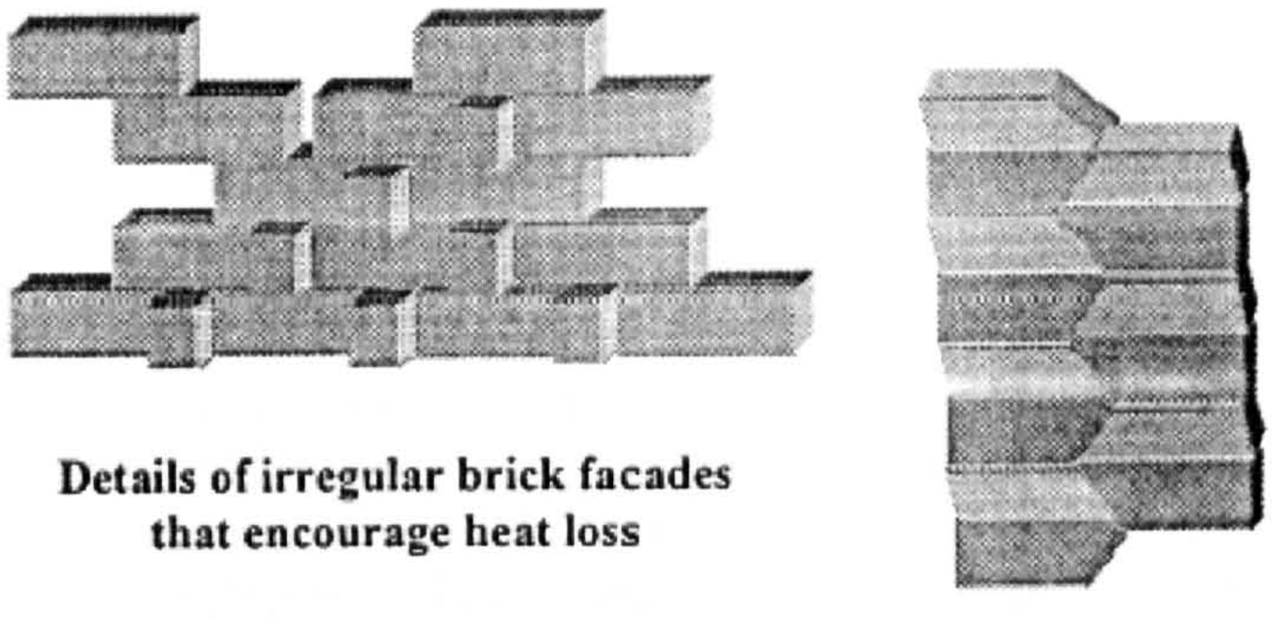

Details of irregular brick facades that encourage heat loss

Figure.1.01 Examples of brick relief, as initially employed during the first Abased era (circa 900 AD).

1.2 APPLICATIONS OF GLASS IN OPENINGS

Historically, glass technology started in the Middle East several thousand years ago. During the Stone Age (circa 50,000 BC), naturally occurring volcanic glass (i.e. obsidian) was used in cutting tools. Crude glass forms existed in the region (circa 4000 BC) as glazed cones embedded in mortar with their bases remaining exposed to the "out-doors". These glass cones served as tiling in ancient temples (e.g. the ziggurats of the Sumerians) and in the famous gate of the city of Babylon. The oldest remaining glass artefacts manufactured by humans are glass pearls, which were stolen subsequently from the graves of Egyptian pharaohs, who lived 3500 BC. The Phoenicians (circa 850 BC) were the first to produce artificial glass, on a relatively large scale (for those times), by burning earthenware, thus combining arenaceous lime-stone containing sand with natron (sodium carbonate). The clay-table library of the Assyrian king Assurbanipal (circa 700 BC) contains the oldest remaining recipe (for the formation of glass namely):''take 60 parts sand, 180 parts ash from sea plants and 5parts of chalk, heat and you get glass '' (AGSA website 1998). Glass-making techniques spread to Eastern Asia, e.g. China around 500BC (Macfarlane A. and Martin G. 2002).

The invention (circa 200 BC) of glass melting ovens and glass blowers' pipes revolutionized the manufacture of glass and made possible the production of flat glass, and window glazing. Subsequently, glass was employed extensively in the decoration of lanterns as well as for domestic artefacts, architectural decoration and personal ornament specially during the Roman Empire, which ruled most of the old world by that time.

The most common type, namely silica-based glass, had appropriate chemicals added when molten to give it the required colour. Alternatively, the use of glass in windows was rare in the Islamic Empire period (i.e.750 –850 AD), which saw still, a flourish in the technology, sophistication and the quantity of manufactured decorative glass.

The production methods, which had been introduced earlier in the neighbouring Persian and Roman Empires, were then copied frequently. Glass was used extensively in the palaces of the caliphs and in mosques. Subsequently, technological interactions ensued

with the craftsmen of the neighbouring Byzantine Empire and the crusaders, which saw the major start of flat glass manufacturing, e.g. for windows, mirrors; as can be seen in the design of windows in Byzantine palaces and churches (circa the 10th century AD). During the period from the 10th to the 12th century AD, many studies were devoted to the development of glass (Mumford L. 1970). Its coloration was achieved by adding metallic salts and oxides to the molten glass (e.g. gold produces a cranberry tint; cobalt makes blues; silver creates yellow; whereas gold and copper together can create greens or brick red, when mixed in the appropriate proportions).

Techniques for constructing stained-glass windows were written down by Theophilus, a Greek monk, in about 1100 AD. He stated ''If you want to assemble a simple window, first mark out the dimensions of its length and breadth on a wooden board, then draw the scroll work or anything else that pleases you, and select colors that are to be put in. Cut the glass and fit the pieces together with a groping iron. Enclose them with lead cams and solder on both sides. Surround with a wooden frame, strengthened with nails, and set it up in the place where you wish.'' The basis of this method has changed little during the subsequent 900 years.

During the Gothic era (circa 1200 AD), many of the great cathedrals of Europe introduced stained-glass windows. Churches became taller and lighter, with their structural weights, especially of the roofs, being supported by columns and flying buttresses. This allowed the introduction in walls of large openings, which were filled with stained-glass windows. Simultaneously, the Islamic Empire employed intricate patterns of stained glasses in motifs and designs, though not used in windows; these are referred to as Arabesque decoration (PPG Industries Inc. website 1998) During the Ottoman era (circa 1500 AD), the designs of buildings did not differ fundamentally from those of the Arabic era prior to 1260 AD. Nevertheless, during the 16th century, the designs of public buildings became increasingly decorated, through importing the flat glass from Europe. Good examples of this can be seen in the ''Al-azhar ''mosque (in Egypt), and the ''Al-qushala ''building (in Iraq).

During the late 18th to the early 20th centuries, European expatriates developed what has subsequently been called the ''colonial style'' in architecture. The associated hybrid designs introduced elements from the architectures of the expatriates 'origins, but adapted them to the more hostile climates of the Middle East. The main aim was to reduce the heat gained by the buildings from the harsh ambient environments during daytime. Local building materials with high thermal-storage capacities as well as small windows —well setback into the walls —were two of the main features of this colonial-style architecture. The maximum size of a window was limited during the 18th century to approximately 0.75m×0.75m by the then prevalent 'crown' process glass-manufacturing technique.

However, each building usually possessed individuality because its features tended to be dictated by the local weather, as well as geographical and cultural conditions of the host country. This led to the evolution of new types of inner spaces (i.e. artificial environments) that previously had not existed in indigenous vernacular buildings.

The nineteenth century saw the peak of 'post-and-lintel' construction that permitted larger window openings (i.e. up to 1.0m×1.3m) (Kob W., *et al.*1999). The improved 'cylinder'-process for making glass sheets facilitated this. When the skeletal structure for building supports was developed, first through the use of cast iron, then of wrought iron

and later of steel and reinforced concrete (Button D & Pye B. 1994), it became possible for the entire external wall facades of buildings to be constructed of glass.

The invention of refrigeration systems to cool air was rapidly followed by their use for the ''conditioning ''of air in buildings. Architects began to introduce this new technology into their buildings (e.g. Frank Lloyd Wright 's Larkin Building at Buffalo USA, in 1904,was the first air-conditioned building). Large windows were employed in offices and even residential buildings, which led to higher rates of solar-energy gains into internal spaces and therefore a greater need for mechanical cooling. This concept was exported and the American ''international style ''became especially popular after World War 2 (1939 –1945). Its rapid adoption was helped by the low unit prices of fossil fuels and hence of electricity. So high energy-dissipating systems became increasingly tolerated. This trend considered the building to be an enclosure that provides a thermally comfortable environment, which could be isolated from its hostile ambient-surroundings. Thus, mechanical systems (e.g. refrigeration plant) were installed to maintain the thermal comfort of the occupants of buildings, but at relatively high rates of energy consumption, and with insufficient concern for the ambient environment.

Changes in habitation patterns occurred as a result of the introduction of this international style. For instance, it led to the functions that occur within the various internal spaces being chosen irrespective of the orientation of the building, its location or the daily and seasonal changes of weather.

The location of human activities had previously been dictated by how well thermally comfortable conditions were achieved and maintained within the different rooms of vernacular buildings. However, thermal comfort is maintained in ''international style ''buildings primarily by air conditioning to compensate for the high rates of solar gain that they incur. During the last 50 years, the use of double-glazing gradually became a feature of contemporary architecture in some countries in order to help thermally isolate the interiors of buildings.

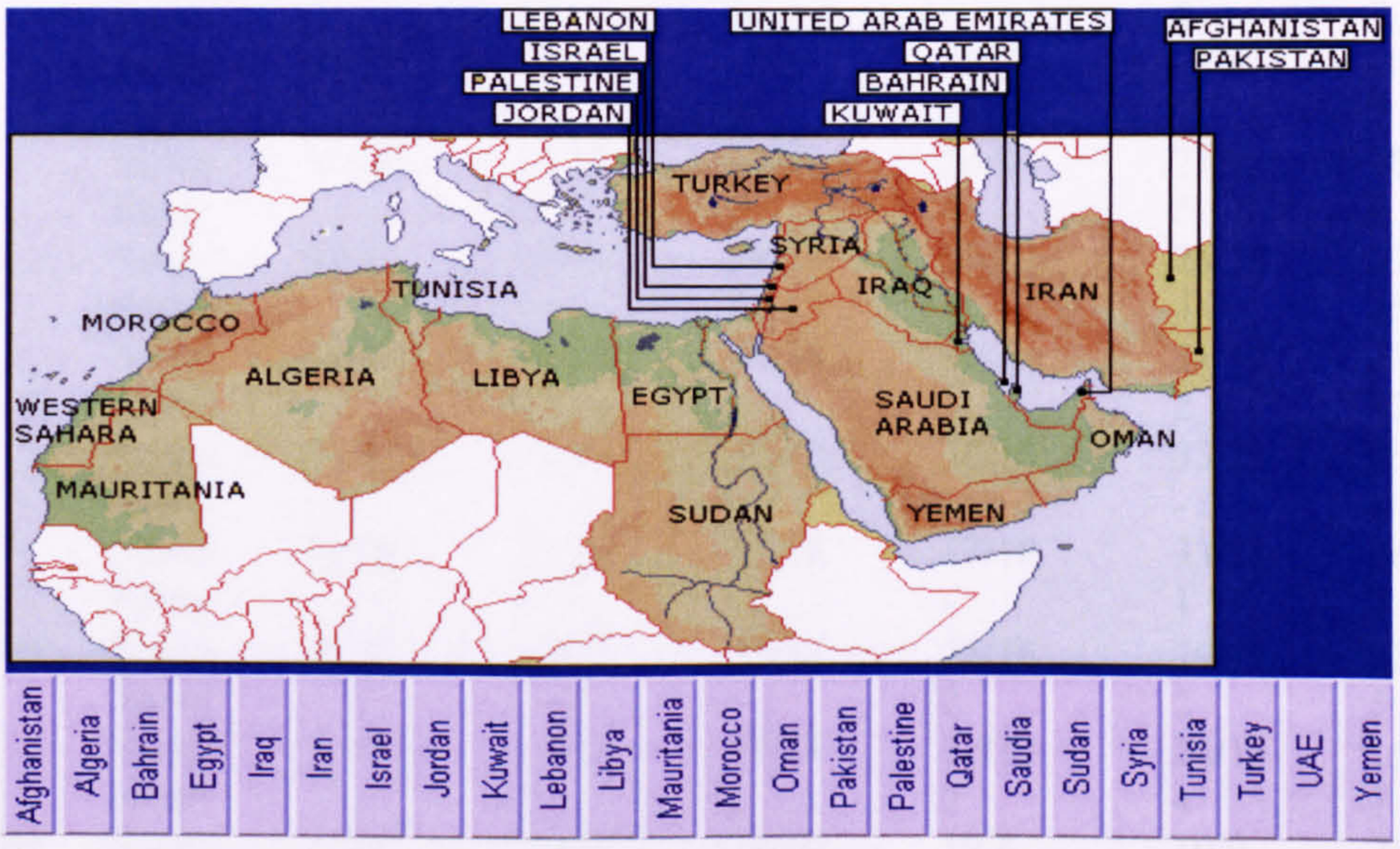

Figure 1.02 showing political and historical map of chosen zonal band (i.e. the Middle East). (Wikipedia 2006).

Another characteristic, of contemporary windows, is the utilization of tinted and/or surface coated glasses to reduce insolation transmission and glare. Excessive solar gains in summer also have been inhibited by other methods, including the use of over-hangs , reflective and light-colored external surfaces, shade screens to fully or partly obscure the windows and internal or external movable-shutters. Nevertheless, there are; as yet, no major trends to reduce the sizes of the windows in the facades of new prestige buildings in the Middle East, or to re-adopt those characteristics of the region's vernacular architecture that reduce the rates of the heat gain or loss through the fabric of a building.

Currently, in the Middle East, no statutory standards exist which are designed to limit the rates of heat transfer through the envelope elements of a building. Also, unfortunately much of the data used in predicting the thermal performances of buildings is taken from manufacturers' guides and codes of practice that emanate from foreign sources: foreign architects may pay insufficient attention to the local climate and terrain and so inappropriate, highly energy-wasteful buildings are constructed.

Table 1.01 Mean maximum and minimum temperatures for countries in the Middle East during 1996 (ceedex. UK website)
The "rainy day" description implies 9 mm of precipitation occurs whereas a "sunny day" implies ~8 h of clear-sky conditions occur, during the average day of the considered month.

Month	Day type	Monthly mean maximum and minimum temperatures in °C for the considered location (the altitudes of the locations in metres above mean sea level are given in parentheses).					
		Egypt (≈ 0)	Israel (445)	*Amman* Jordan (764)	*Damascus* Syria (709)	Izmir Turkey (27.6)	Turkey (1722)
January	Sunny	23/5	13/5	12/4	12/2	13/4	-6/-18
	Rainy		9	8	7	10	7
February	Sunny	26/7	13/6	13/4	14/4	14/4	-4/-16
	Rainy		11	8	6	8	7
March	Sunny	29/11	18/8	16/6	18/6	17/6	-1/-11
	Rainy		5	4	2	7	7
April	Sunny	35/16	23/10	23/9	24/9	21/9	10/-2
	Rainy		3	3	3	5	9
May	Sunny	40/21	27/14	28/14	29/13	26/13	17/3
	Rainy		1	1	1	4	15
June	Sunny	41/23	26/16	31/16	33/16	31/17	21/6
	Rainy		-	-	-	2	12
July	Sunny	41/24	31/17	32/18	36/18	33/21	25/9
	Rainy	-	-	-	-	-	8
August	Sunny	41/24	31/18	32/18	37/18	33/21	26/9
	Rainy		-	-	-	1	7
September	Sunny	40/22	29/17	31/17	33/16	29/17	22/4
	Rainy		-	-	2	2	5
October	Sunny	35/18	27/15	27/14	27/12	24/13	15/-7
	Rainy		1	1	2	4	7
November	Sunny	29/12	21/12	21/10	19/8	19/9	7/-5
	Rainy		4	4	5	6	6
December	Sunny	25/8	15/7	15/6	13/4	14/16	-2/-13
	Rainy		7	5	5	10	7

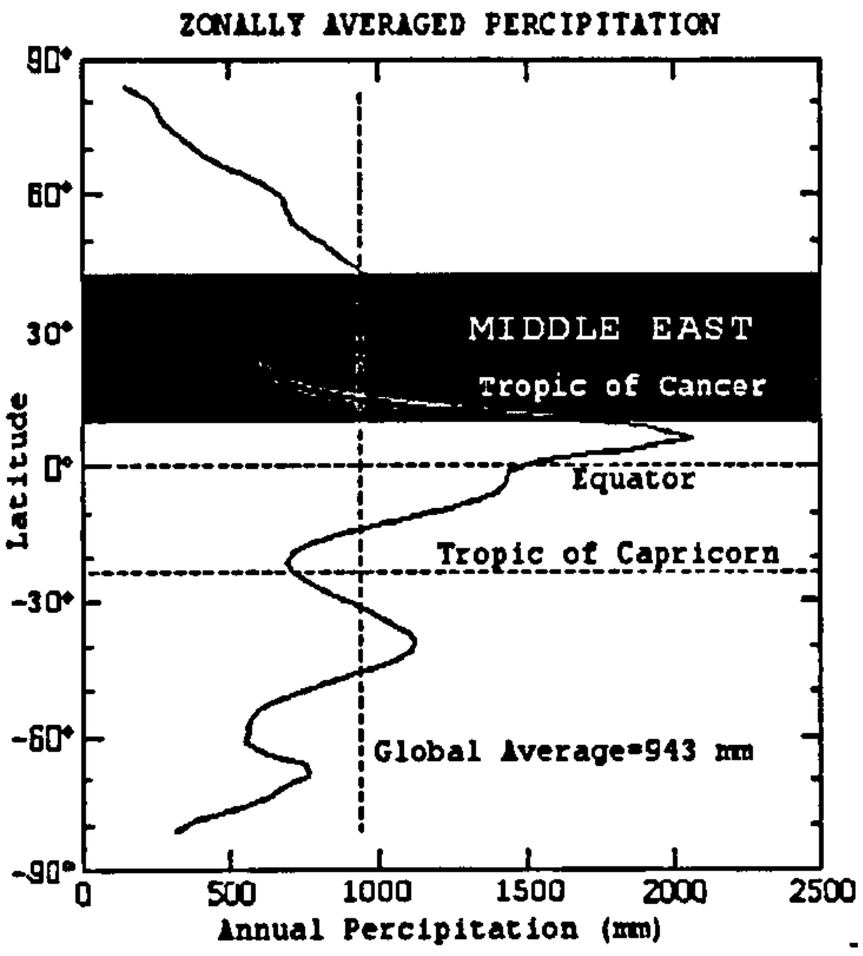

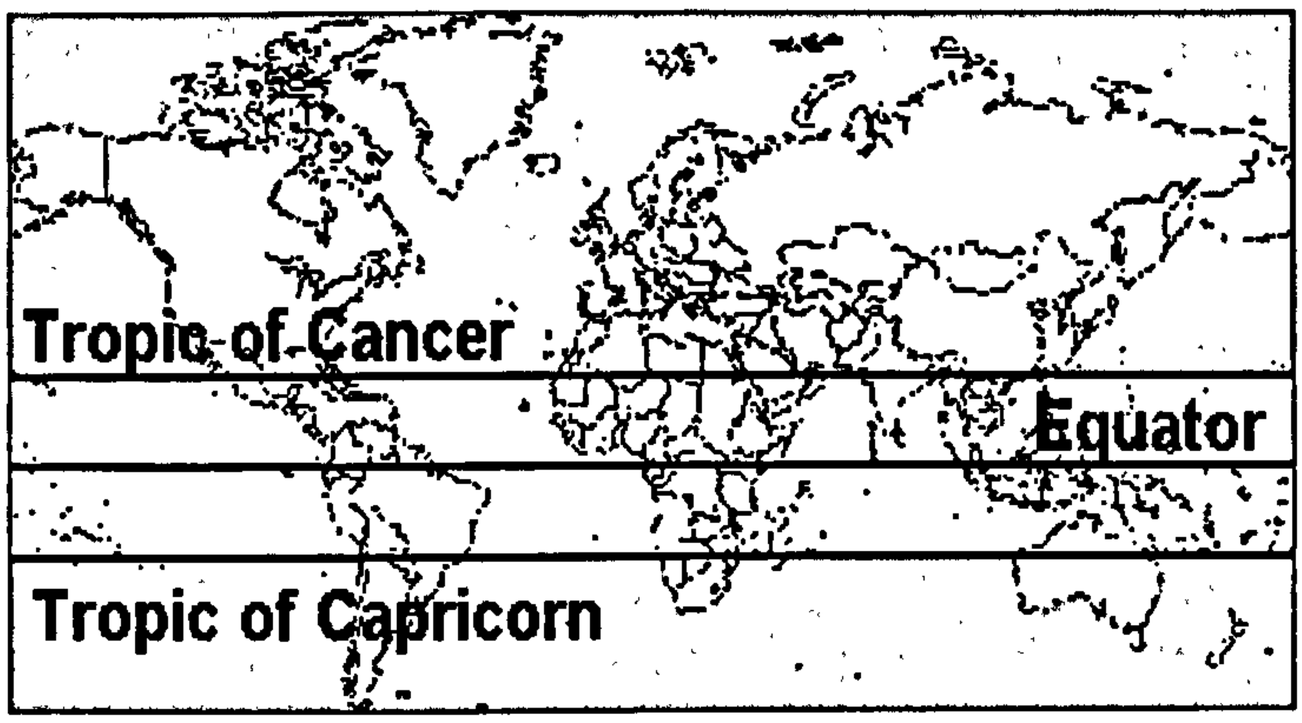

Figure.1.03 shows a comparison of the annual precipitation in the Middle East Zone in relation to the global average.

1.3 ENVIRONMENTAL CONSIDERATIONS OF THE CHOSEN BAND

The Middle East topography in general varies between mountainous and high plateaus in the northern parts to a lower and more flattened terrain in the south; *see fig 1.02*. With the exclusions of few regions, one of the main characteristics of the area is the lack of fresh water bodies, which accounts for only 1% of the freshwater volume in the world) (Charrier. B, *et al* 1998). Three major arid or desert belts encircle the zone: in the south i.e. the Arabian Peninsula, the "Sahara" desert in North Africa and the Arid plateau between Iraq, Jordan, etc. Environmental and climatic features are also dependent on other factors, those are:

1.3.1 Location

Most of the countries (e.g. part of Iran, southern Turkey, Kuwait, Iraq, Jordan, Arabian Peninsula countries, as well as the Gulf States, Egypt, Tunisia, Libya, etc.), considered in the research, lie between latitudes of 31and 37 N, and experience weather conditions characterized by high rates of insolation, *see Table1.01*. This shows the effect of rainy weather on the temperature variations experienced within each month. The presence of rain infers that cloud cover exists and so an increased reflection and absorption of insolation (i.e. especially of the infrared waveband) occurs in the higher atmosphere. This causes the indicated lower daytime temperatures experienced.

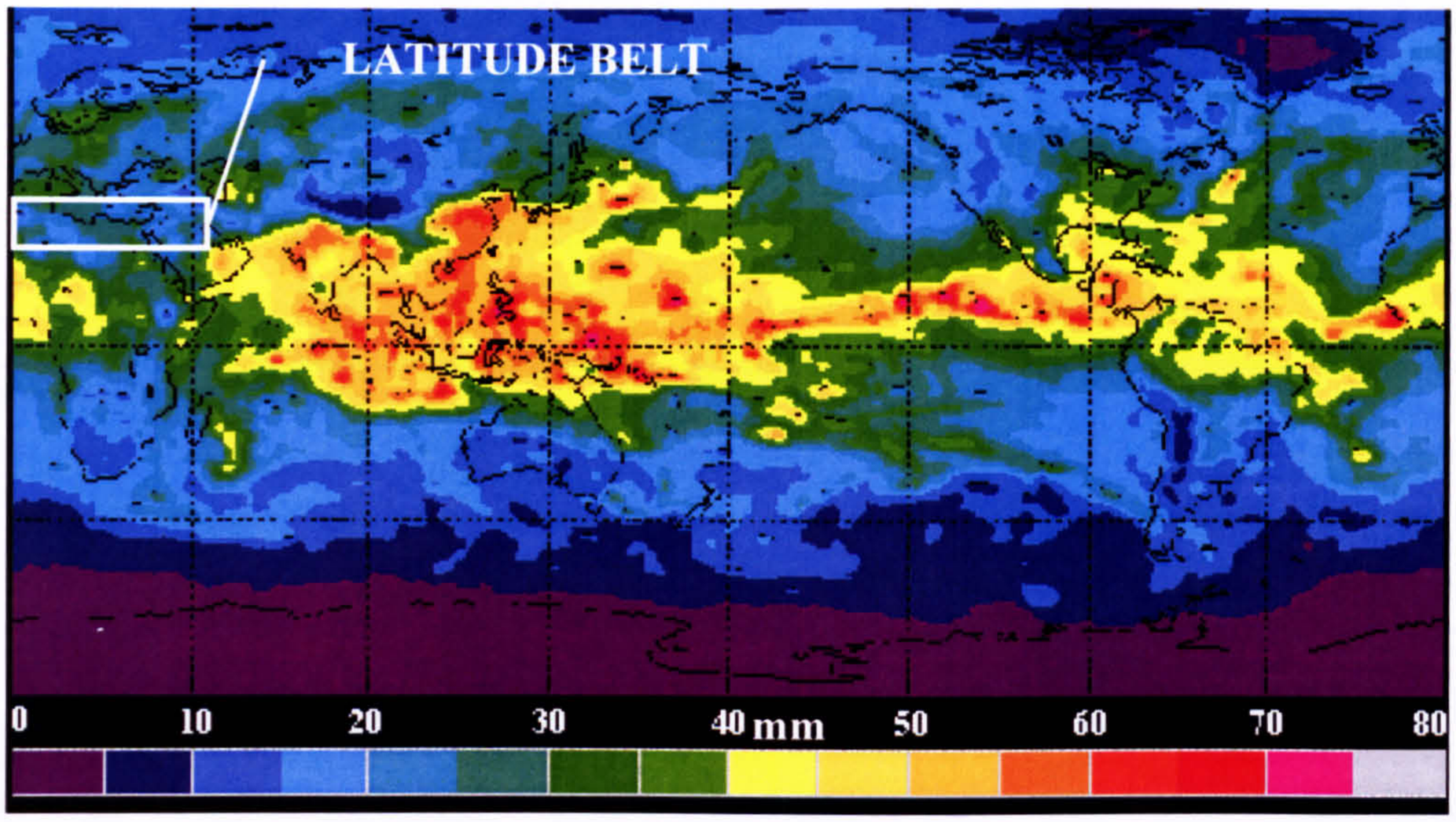

Figure.1.04 showing NASA water vapour project (i.e. NVAP) of merged total integrated perceptible water from vapours for July 10, 1989, source: NASA Lidar, Indian Ocean,

Comparing the annual average of the whole zone in general with the global average indicates the relatively low rate of precipitation, *see fig.1.03*. Furthermore, being in the tropic of Cancer would also account for the high swing in insolation rates between seasons.

Due to the lack of both in-land fresh water lakes and low rates of precipitation, large areas of this region tend to be devoid of naturally occurring green-foliage, which could provide some shelter from the exposure to insolation.

1.3.2 Global insolation incident upon a horizontal surface

This parameter is dependent upon the latitude, the diffuse solar-energy intensity and the local humidity. Direct mean daily global radiation G_{max} can attain a value of 6.8 kWh m^{-2} in Jordan and 8.5 kWh m^{-2} in Iraq and most of the Gulf States. A sample of the solar conditions for Jordan, a representative country in the region is presented in *Table 1.02*.

1.3.3 Selecting countries within the zone

As shown from the previous figures and tables, the amount of received global insolation, among other factors, is dependent upon the latitude. Additionally, there are a considerable numbers of countries that lie within the selected climate zone. Selection of the countries considered was conducted through research of weather files from countries within the zonal belt of latitudes of 31- 37N. The selection was achieved by choosing countries of same latitudes but with different longitudes (i.e. to check the parameter sensitivity) and through using an interval of 2 Degrees between latitudes (Ott. R. C., ASTRONOM software 1999-2005), *see fig 1.04 and appendices iv.1-8*. Accordingly the weather files from 8 countries were selected for simulation purposes. The chosen countries and locations, starting from the West, were:

Table 1.02 Insolation at Baqura, Jordan (32 38 0 N,35 37 0 E).The presented values of G and S were evaluated from mean monthly data (Palz W & Greif 1996).

Horizontal plane: monthly mean. (1973-1976)													
Month	Jan	Feb	Mar	Apr	May	Jun	Jul	Aug	Sep	Oct	Nov	Dec	Mean
Daily global radiation, (kWh/m^2)													
G_{mean}	2.7	3.4	4.3	5.3	6.4	6.8	6.6	6.1	5.3	4.2	3.0	2.9	4.8
G_{max}	4.5	5.6	7.1	8.1	8.6	9.0	8.8	8.1	7.1	5.9	4.7	3.9	6.8
G_{min}	1.2	1.6	2.2	2.6	3.9	7.1	7.6	7.0	5.6	3.1	1.4	1.1	3.7
G_0	5.6	6.9	8.6	10	11	11	11	10	9.2	7.5	5.9	5.1	8.6
Ratios with respect to extraterrestrial radiation													
G_{mean}/G_0	0.5	0.5	0.5	0.53	0.58	0.59	0.58	058	0.58	0.56	0.52	0.56	0.55
Kt_{max}	0.75	0.75	0.76	0.76	0.75	0.78	0.77	0.74	0.73	0.72	0.74	0.74	0.75
Kt_{min}	0.22	0.23	0.25	0.26	0.35	0.62	0.67	0.67	0.61	0.41	0.23	0.21	0.43
Mean daily diffuse radiation, (kWh/m^2)													
D *estimated*	1.2	1.3	1.8	2.1	2.0	1.8	1.9	1.7	1.5	1.2	1.1	1.1	1.6
D/G_{mean}	0.45	0.39	0.42	0.39	0.32	0.27	0.28	0.28	0.28	0.29	0.36	0.39	0.33
Daily sunshine duration, (hours)													
S	4.9	6.5	6.7	8.0	10.7	11.9	11.2	11.9	9.9	8.6	6.5	5.3	8.5
S_d	10.1	10.9	11.8	12.8	13.7	14.1	13.9	13.2	12.3	11.2	10.4	9.9	12.0
$S_{o\ max}$	10.3	11.2	12.2	13.2	13.9	14.1	14.0	13.5	12.6	11.6	10.6	9.9	-

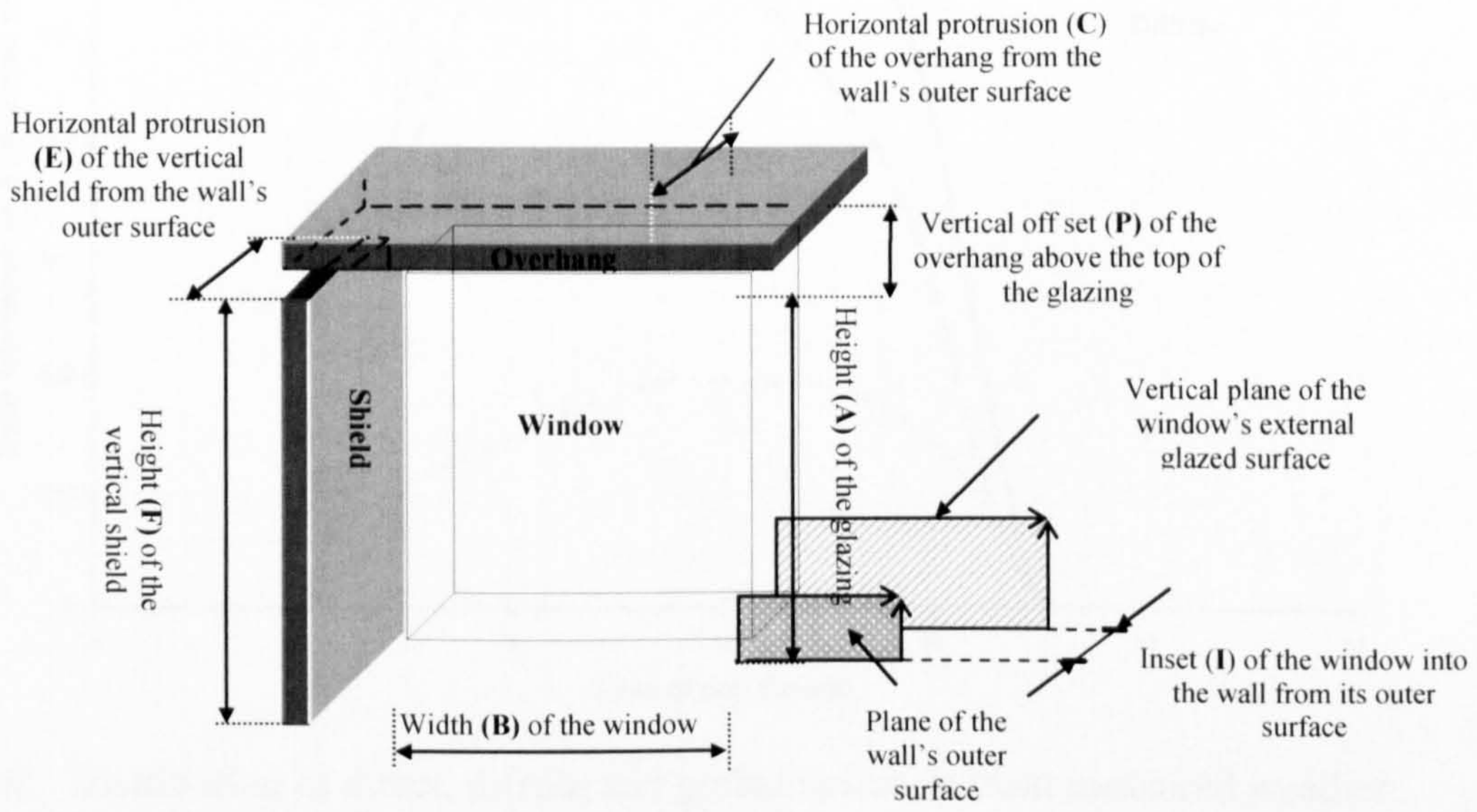

Figure.1.05 Overhang and shielding of a window.

- Algiers, city/Algiers: latitude 36.8334N (36'50'00".24), longitude: 3E (3'00'00".00)
- Egypt, city/Cairo: latitude 30.05N (30'05'00".00), longitude:31.25E (31'15'00".00)
- Israel, city/Tel-Aviv: latitude 32.0834N (32'05'00".24), longitude:34.7667E (34'46'00".12)
- Jordan, city/Amman: latitude 31.95N (31'57'00".00), longitude:35.9334E (35'56'00".24)
- Iran, city/Tehran: latitude 35.6667N (35'40'00".12), longitude:51.43334E (51'26'00".24)
- Iraq, city/Baghdad: latitude 33.33333N (33'20'00".24), longitude:4.43333E (44'26'00".24)
- Kuwait, city/Al Kuwait: latitude 29.3334N (29'20'00".24N), longitude:48E (48'00'00"E)
- Saudi Arabia, city/Al Riyadh: latitude 32.0834N (32'05'00".24), longitude:34.7667E (34'46'00".12)

Another main feature of insolation in the chosen countries is the high intensity of the direct component in relation to the total global incident rate, *see fig.1.06*; lack of green foliage cover would increase the ground reflectivity (i.e. albedo), and so augments problems in buildings associated with overheating.

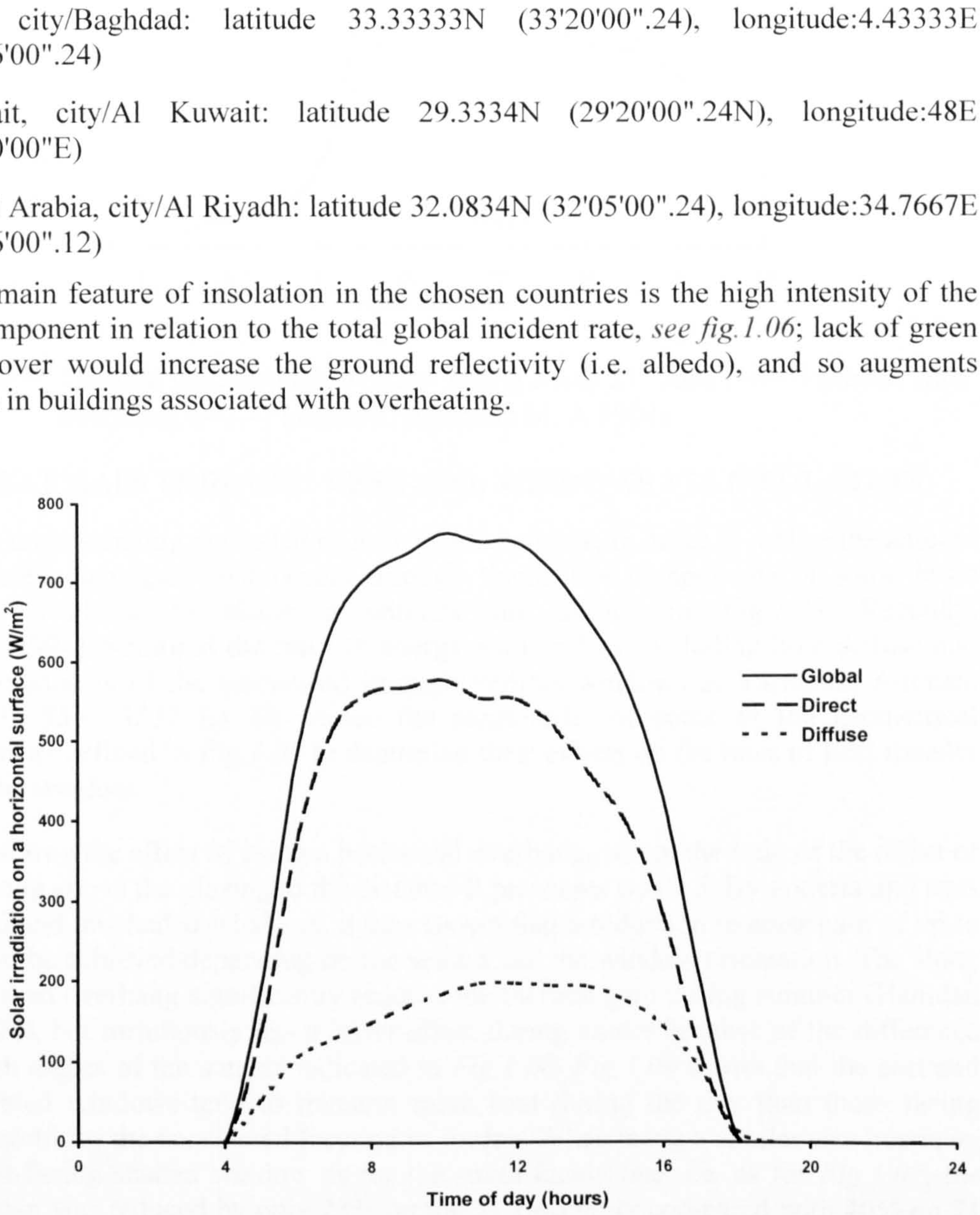

Figure.1.06 Distribution of direct, diffuse and global radiation from measured weather data for June 21st Kuwait (Latitude 24.9°N).

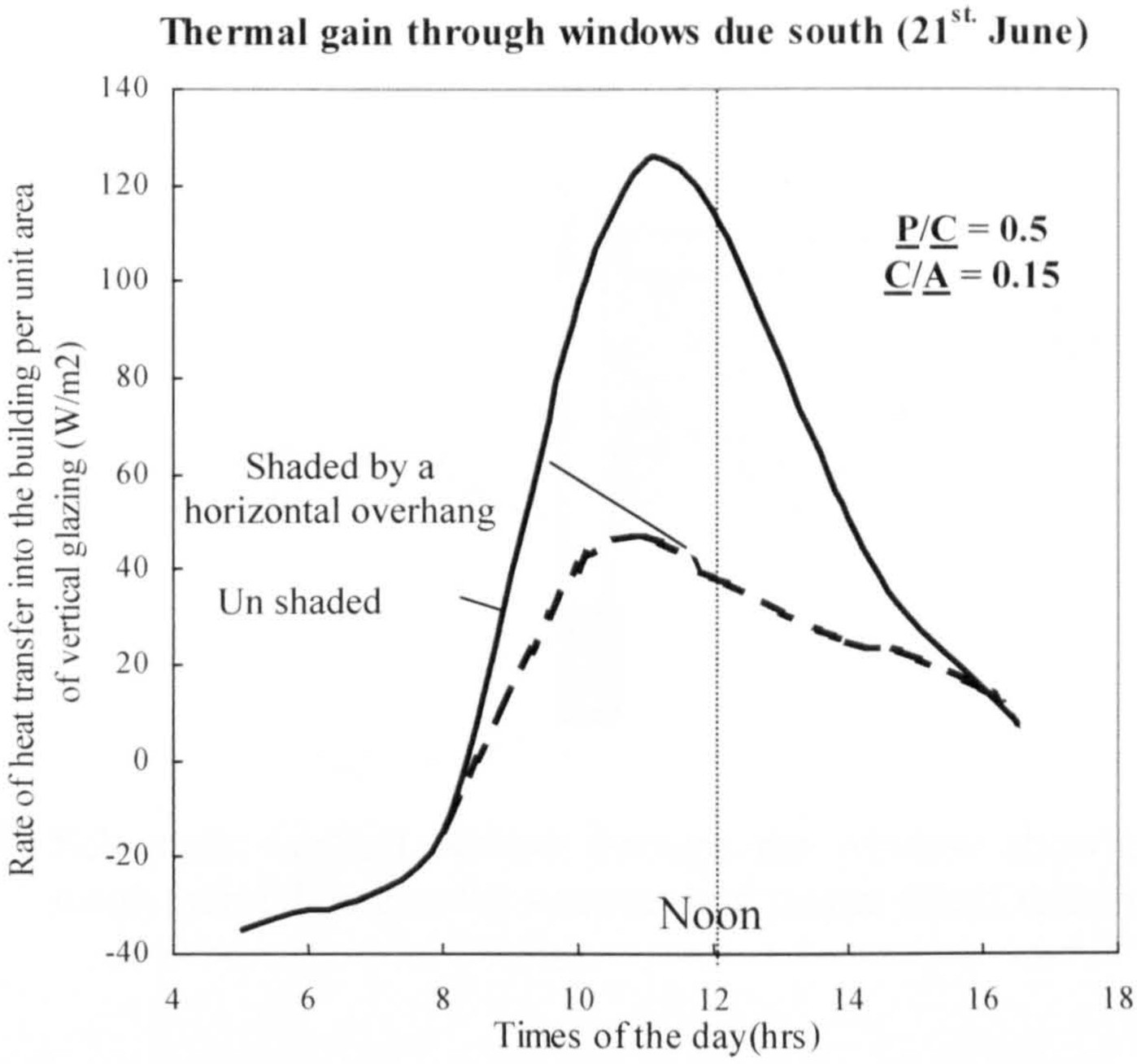

Figure 1.07 Thermal gain through window facing south 21st June (------) shaded with overhang; (——) unshaded (Hamdan M. A 1994).

1.4 HEAT GAIN THROUGH VERTICAL WINDOWS VIA INSOLATION

A greater understanding is needed of how windows work, in order to realise the amount of the excess heat gain that occurs through them. The components of some basic structures available to shade a window are shown in *Fig.1.05*. Recently, (Hamdan, 1994) measured the rates of energy gain or loss (including both diffuse and direct components of the insolation) through vertical windows at Yarmouk, Amman, Jordan (32 35N, 3537 E). He varied the magnitudes of some of the geometrical parameters as defined in *Fig.1.05* to determine their effects on the rates of heat transfer through the window.

Fig.1.07 shows the effect of using a horizontal overhang, where the ratio of the offset of the overhang above the glazing to the distance it protrudes was 0.5. By undertaking tests on shaded and un-shaded windows, it was shown that a reduction in solar gain of up to 45% could be achieved depending on the season and the window orientation. The study shows that an overhang significantly reduces the thermal gain during summer (Hamdan M. A 1994), but fortuitously has a lesser effect during winter because of the difference in azimuth angles of the sun, as indicated in *Fig.1.08*. *Fig.1.09* shows that the east and west-oriented windows tend to transmit more heat during the day than those facing south or north for the considered location in Jordan. When using a similar size overhang for a west-facing shaded window as for the south facing one, i.e. as for *Fig.1.07*, the thermal gain was reduced by only 23% on the 21 December compared with 40% on 21 June. These percentages depend upon the magnitudes of the glazing height A and the horizontal protrusion E of the vertical shield.

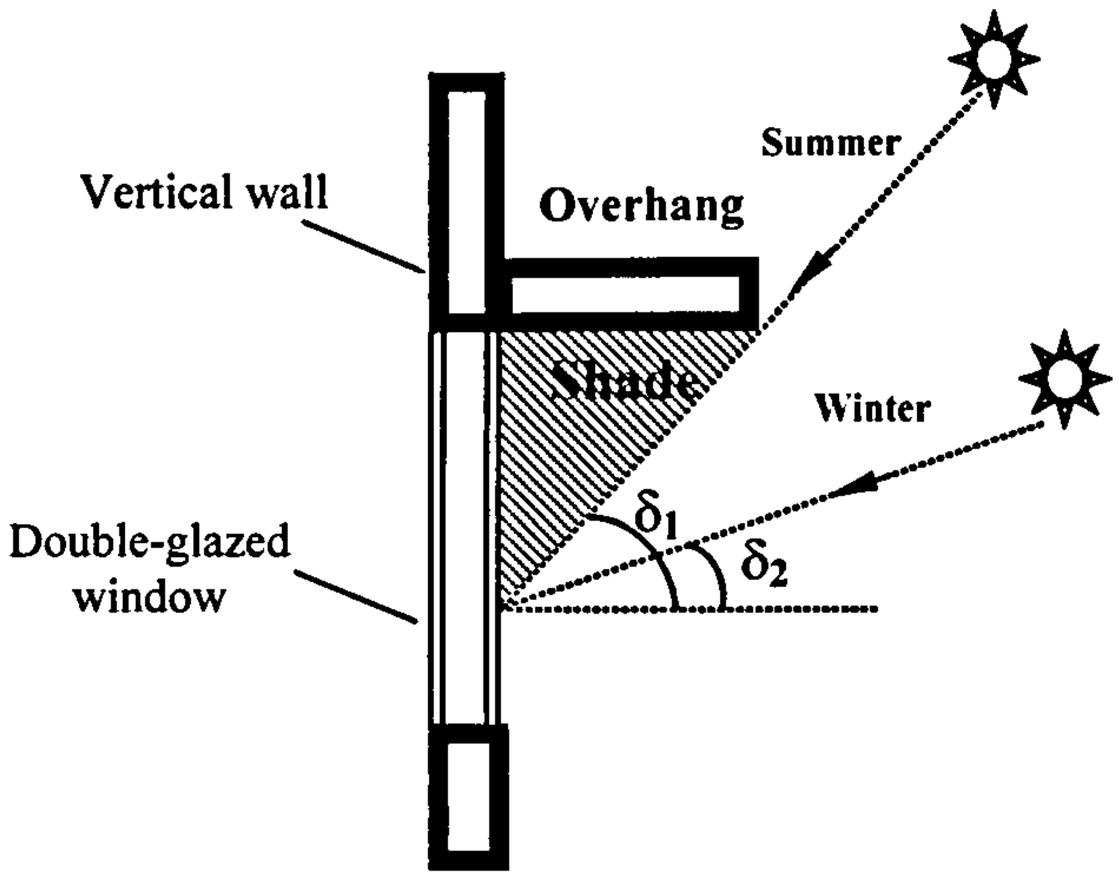

Figure 1.08 Schematic vertical section through the window showing the different mean azimuth angles for summer and winter direct sunshine.

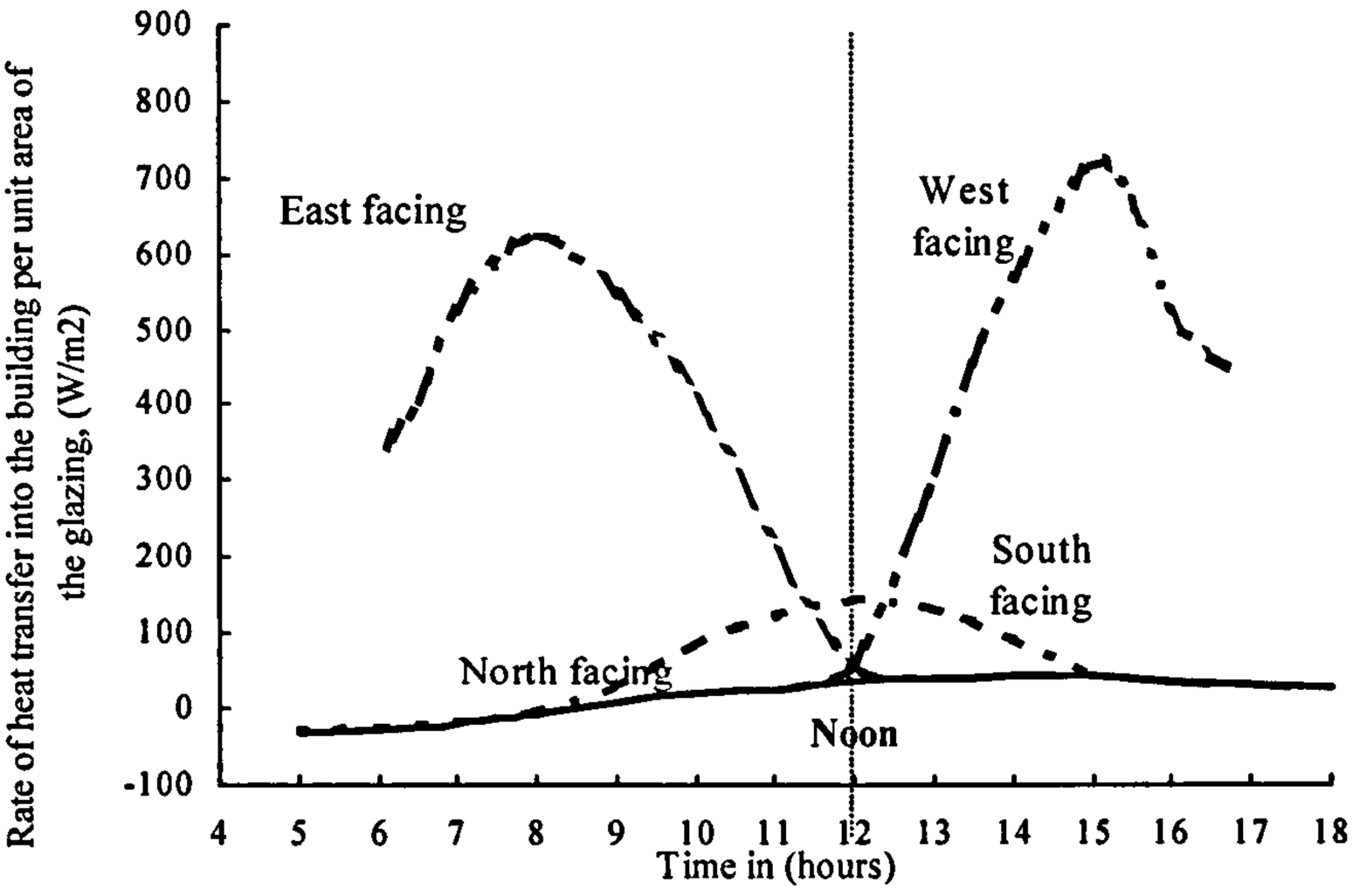

Fig.1.09 Thermal gain through unshaded identical vertical windows, 21st June (Hamdan M. A 1994)

As a result of hundreds of years of experience, with the local climate and annual changes of solar path, most windows in buildings in Amman tend to be oriented towards the southeast, and incorporate protrusions (both horizontal and vertical) of the types shown in *Fig.1.05*. The results illustrated in *Figs.1.07 –1.10* are for the cases where the horizontal overhang and vertical shield were present or absent for the various orientations.

Combination of both large overhangs and/or protrusions were not considered in this work; as they would be unlikely to be employed in current common practice.

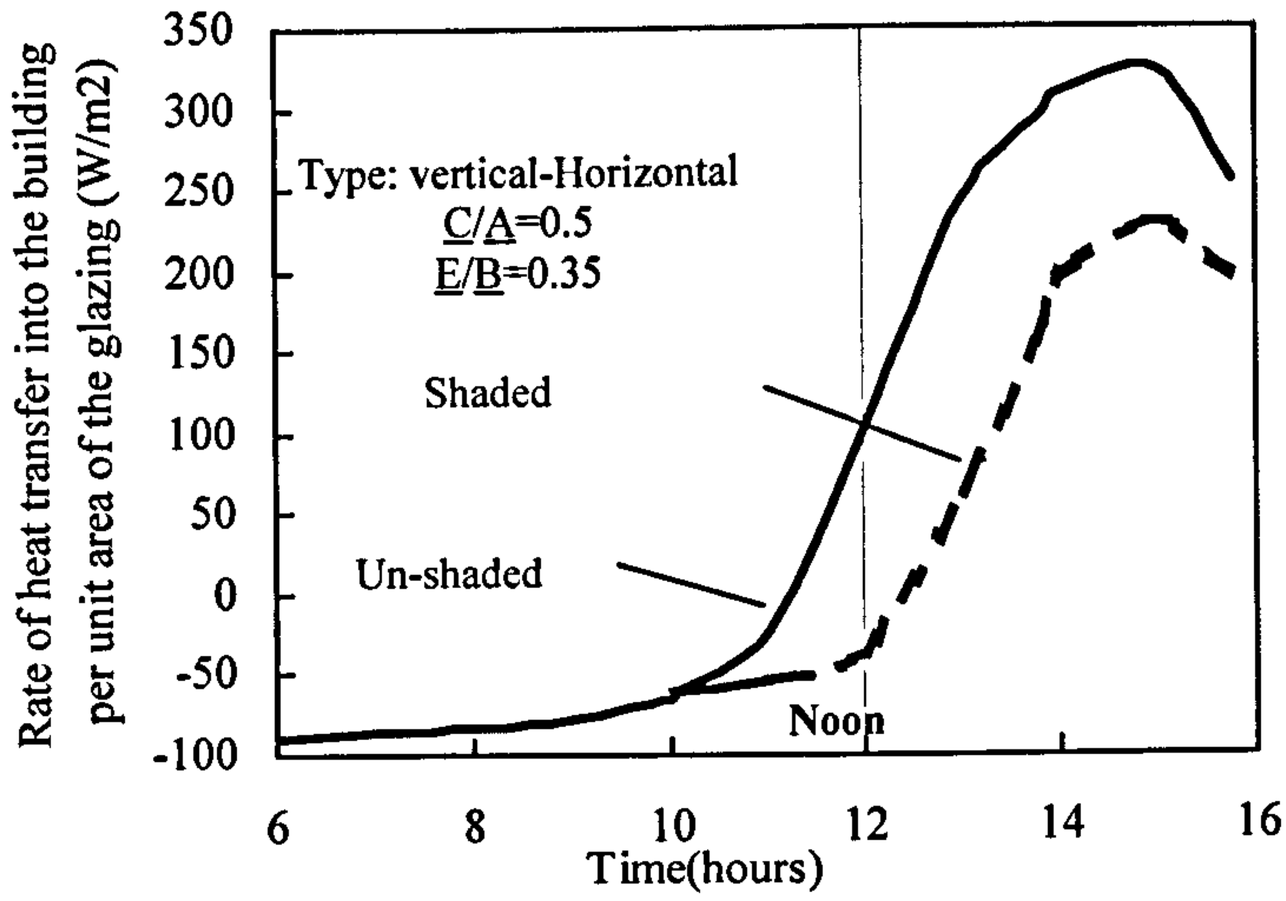

Figure 1.10 Thermal gain through vertical windows, facing due West 21 December (——) unshaded; (----) shaded with horizontal overhang and vertical shield (Hamdan M. 1994).

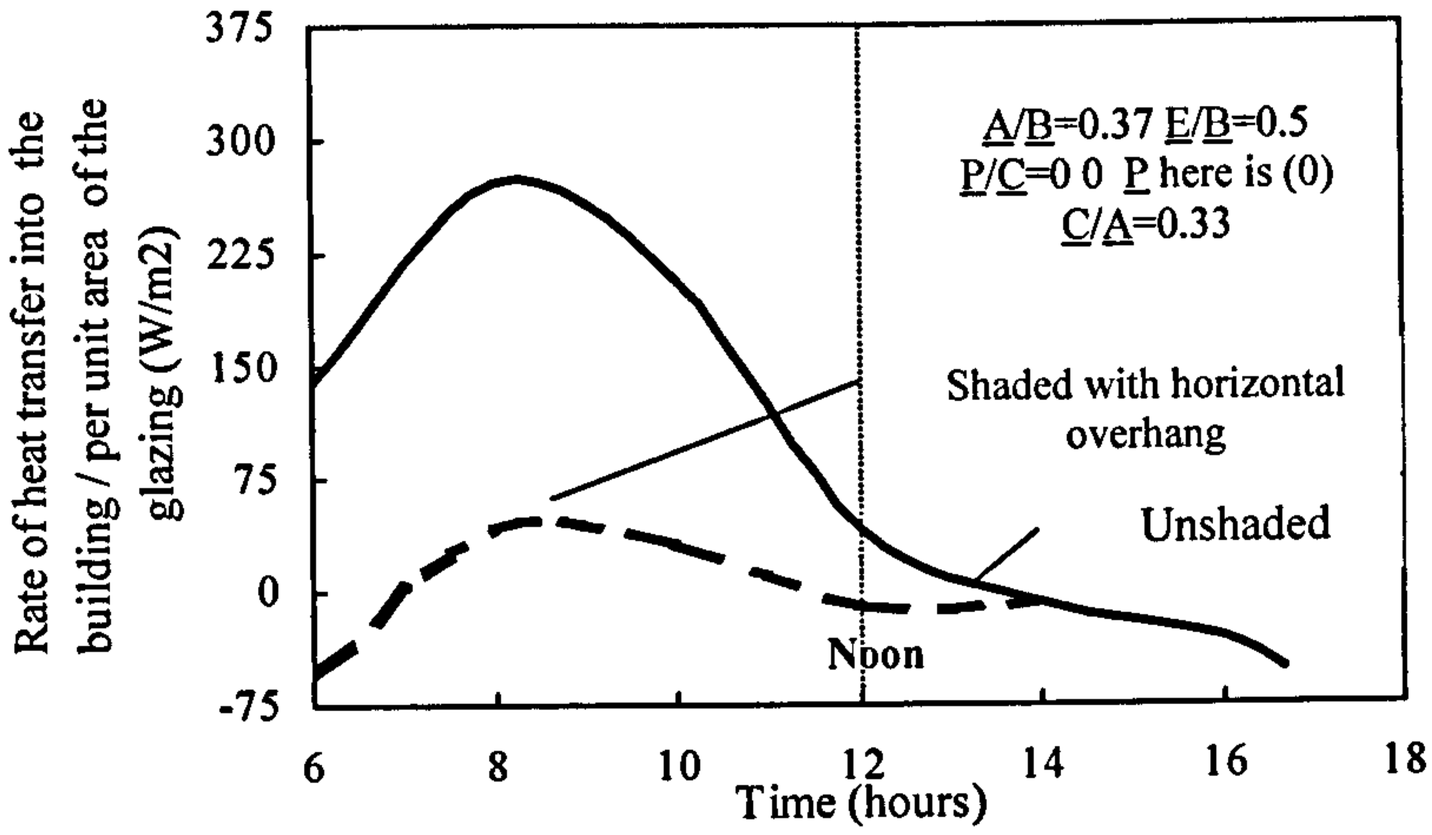

Figure 1.11 Rate of heat transfer through the vertical windows facing south-east of the building (21 June) (——) unshaded; (-----) shaded by horizontal overhang (Hamdan M. 1994).

Figures 1.09 and 1.12 also show that significant solar gains occur through an east-facing window, especially during the morning. The rate of thermal gain reaches its peak during the early hours of the day (about 8:00am): however, because of the thermal inertia of the building, the maximum temperature ensues later in the day.

Still; when comparing the effects of the overhangs over windows of similar geometry, but at different orientations; it can be seen that the shadows cast by the overhangs and vertical protrusions are more effective for the west and south orientations rather than for the easterly ones. *See figures 1.11,1.12 and 1.13* respectively. This is due to the low sun angles for the easterly orientation, which makes the two types of protrusion utilised cast relatively smaller shadows in this case.

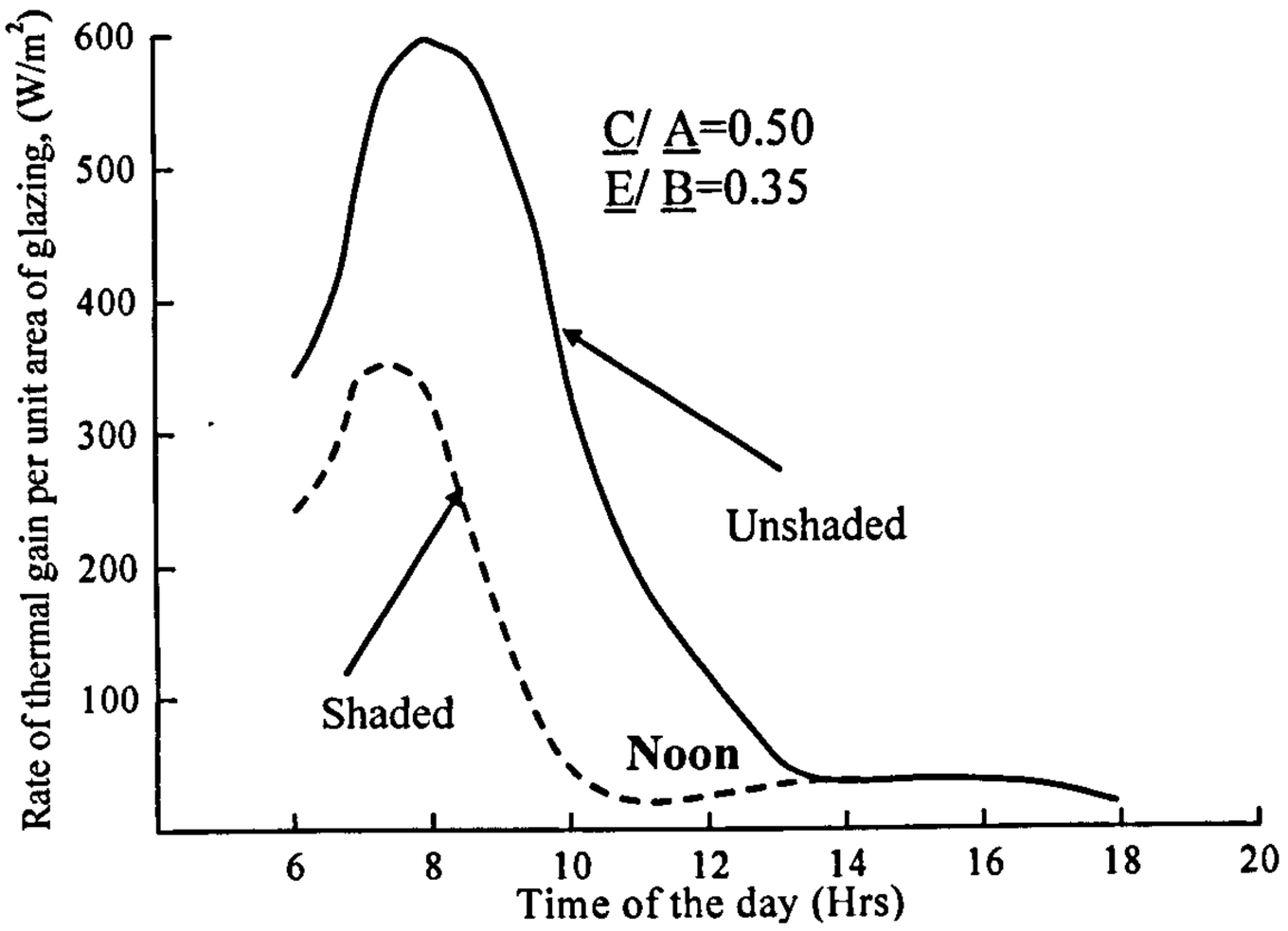

Figure1.12 thermal gain through identical vertical windows facing due east for 21June (——) unshaded, (------) shaded by vertical shield and horizontal overhang (Hamdan M.1994).

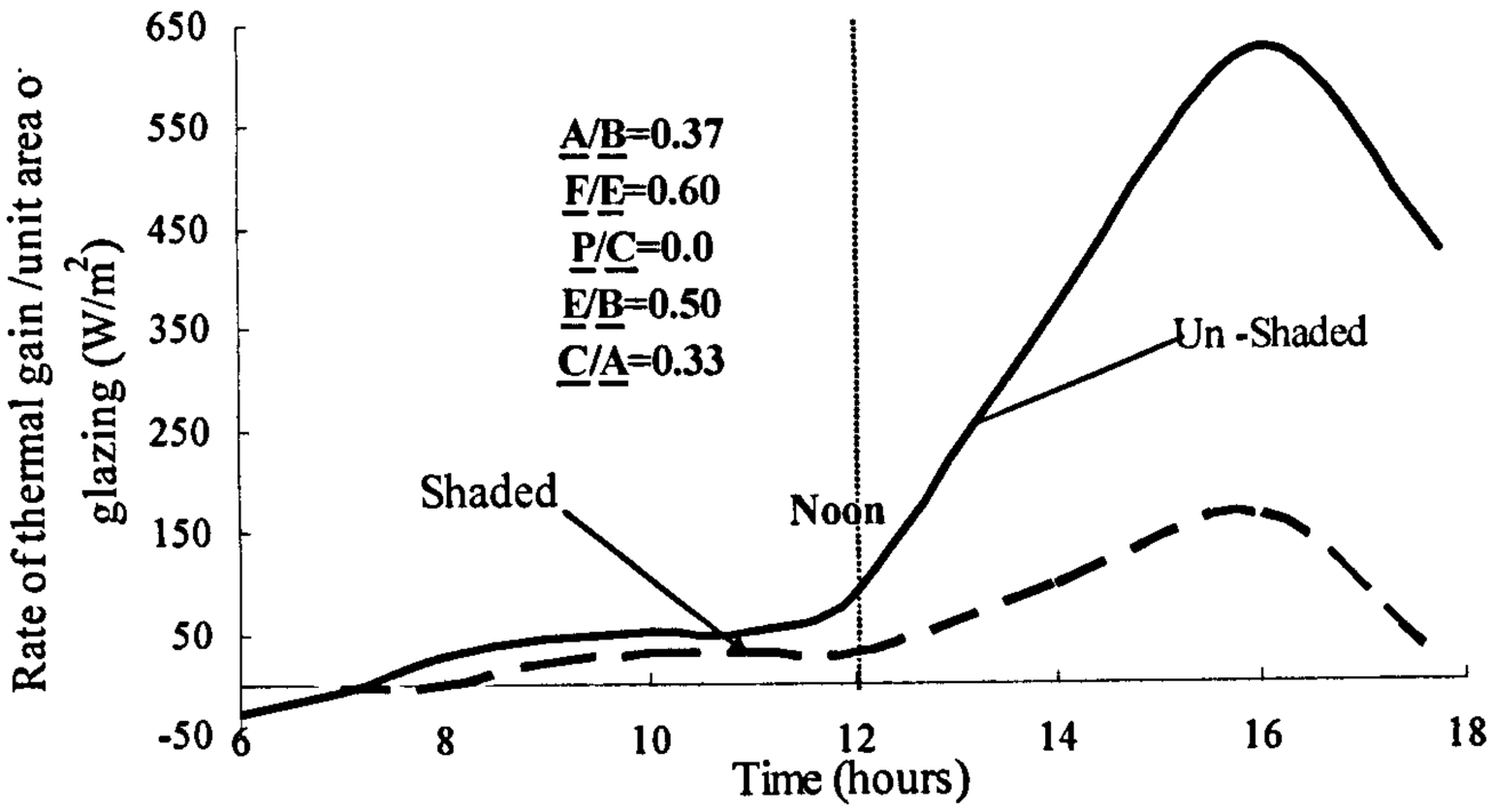

Figure 1.13 Thermal gain through identical vertical window facing Southwest, for 21 June: (------) shaded by vertical shield and horizontal overhang as in *fig 1.05*; (——) unshaded (Hamdan M. 1994).

1.5 THERMAL AND DAYLIGHTING BEHAVIOUR OF WINDOWS

There is a tendency to consider windows as apertures that allow solar radiation to enter a building, so providing both daylight and beneficial heating of its interior. This has arisen in part because of the popularity of passive-solar architecture lately and a desire for reducing the costs of heating buildings during cold seasons, while ignoring summertime discomfort in them (Loxom F. 1985-1986).

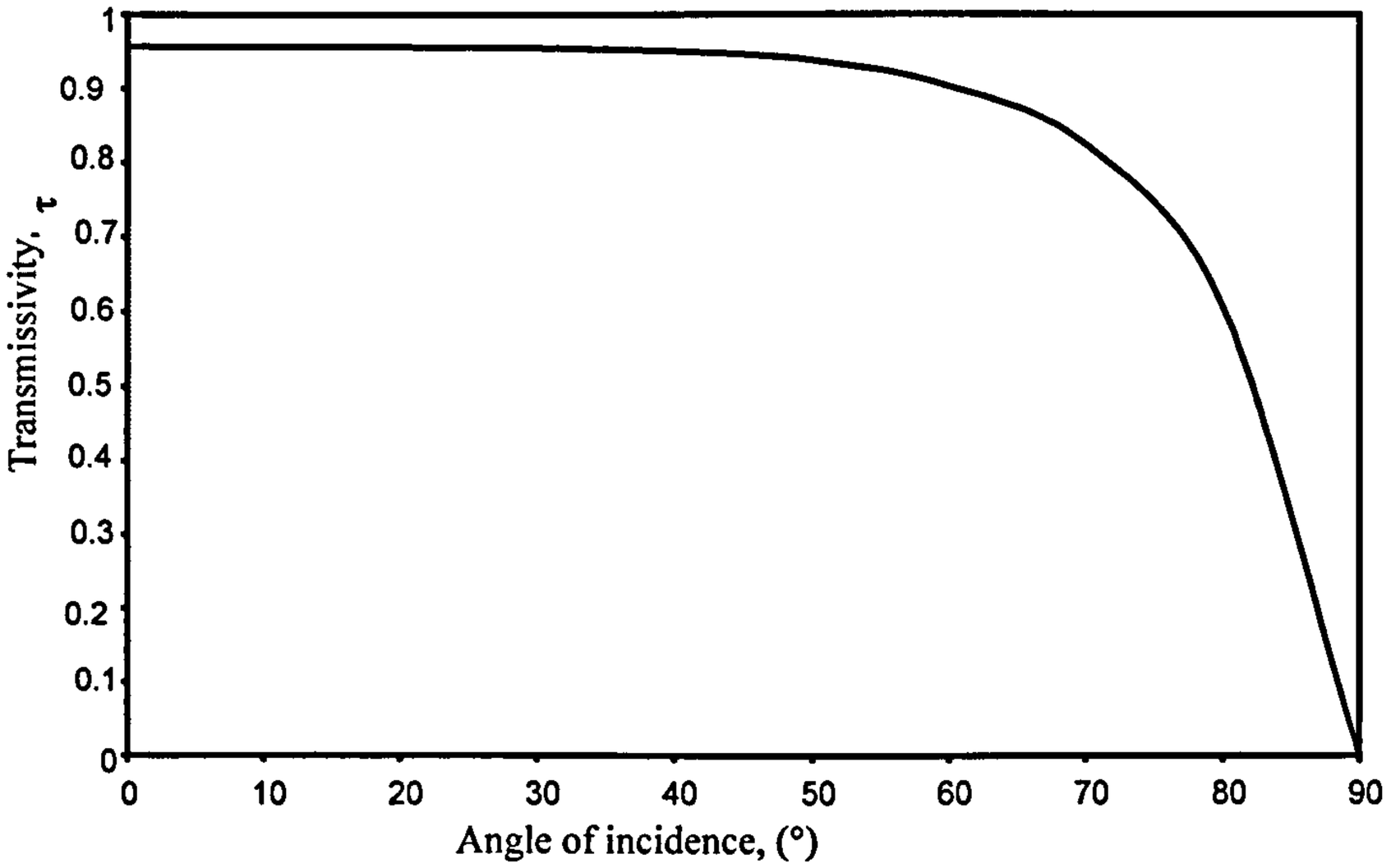

Figure 1.14 Variation of the transmissivity for clear glass of refractive index 1.53

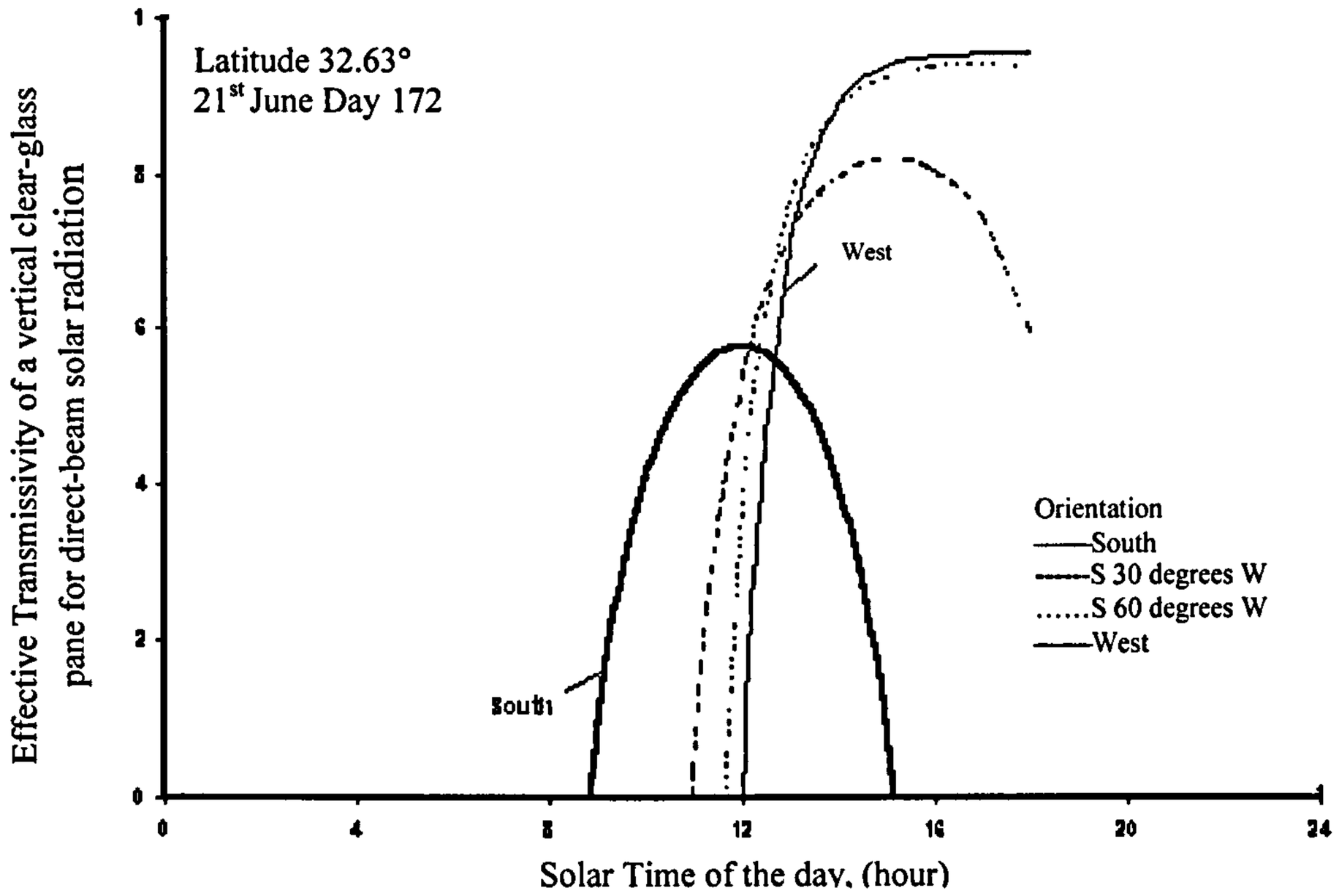

Figure 1.15 Calculated variations of the effective transmissivity of vertical glazing to direct beam solar irradiation with orientation and time of day for June 21st (Kuwait)

Consequently, much of the development of glazing systems has concentrated primarily upon reducing the rates of heat loss via them to the ambient environment from the interiors of buildings. The designs of the majority of highly glazed buildings make little attempt to take heed of façade orientation or the change of Sun angle with season. Glare and excessive solar-gains from the east through to the west during the day occur as a result in such buildings. In a relatively few cases, special coatings have been applied to the glass in some buildings in order to reflect high proportions of the incident insolation.

However, these reduce the amount of solar energy transmitted in the visible part of the spectrum as well as in the UV and the near-infrared wavebands. For general daylighting purposes, a desirable system would have daylight provided by the diffuse component of the insolation, whilst almost totally excluding the direct-beam radiation. However, as indicated, the diffuse component from the sky is much less than that from the direct the component, *see fig. 1.06.*

The tilting of glazing can be used to control the intensity of the solar radiation that is transmitted through a window. This was shown in simulations taken earlier backed by data recording, using standard glazing window against empirical insolation data of 1996 taken in Kuwait by KISR, i.e. Kuwait Institute of Scientific Research. Tilting the glazing alters the angle of incidence of direct insolation impinging on its surface.*Fig.1.14* illustrates the change of transmissivity of a typical glass surface with the angle of incidence: for angles of incidence exceeding 60, the transmissivity is reduced significantly. The variations of the transmissivity of vertical single-glazing to direct-beam radiation with the time of day for several orientations, at latitude 32.63 N, are shown in *Figs.1.15 –1.16.* The angle of incidence of the direct-beam radiation to the glazed surfaces of a building changes with the time of day. For 21 June, the effective transmissivity of south-facing glazing remains below 0.58 and the period of transmission of solar irradiation only occurs from approximately 09.00 to 15.00 hours. As the vertical glass faces an increasingly westerly direction, as indicated in *Fig. 1.16*, the transmissivity increases, from late morning and during the afternoon, to values greater than those experienced by south-facing vertical glazing.

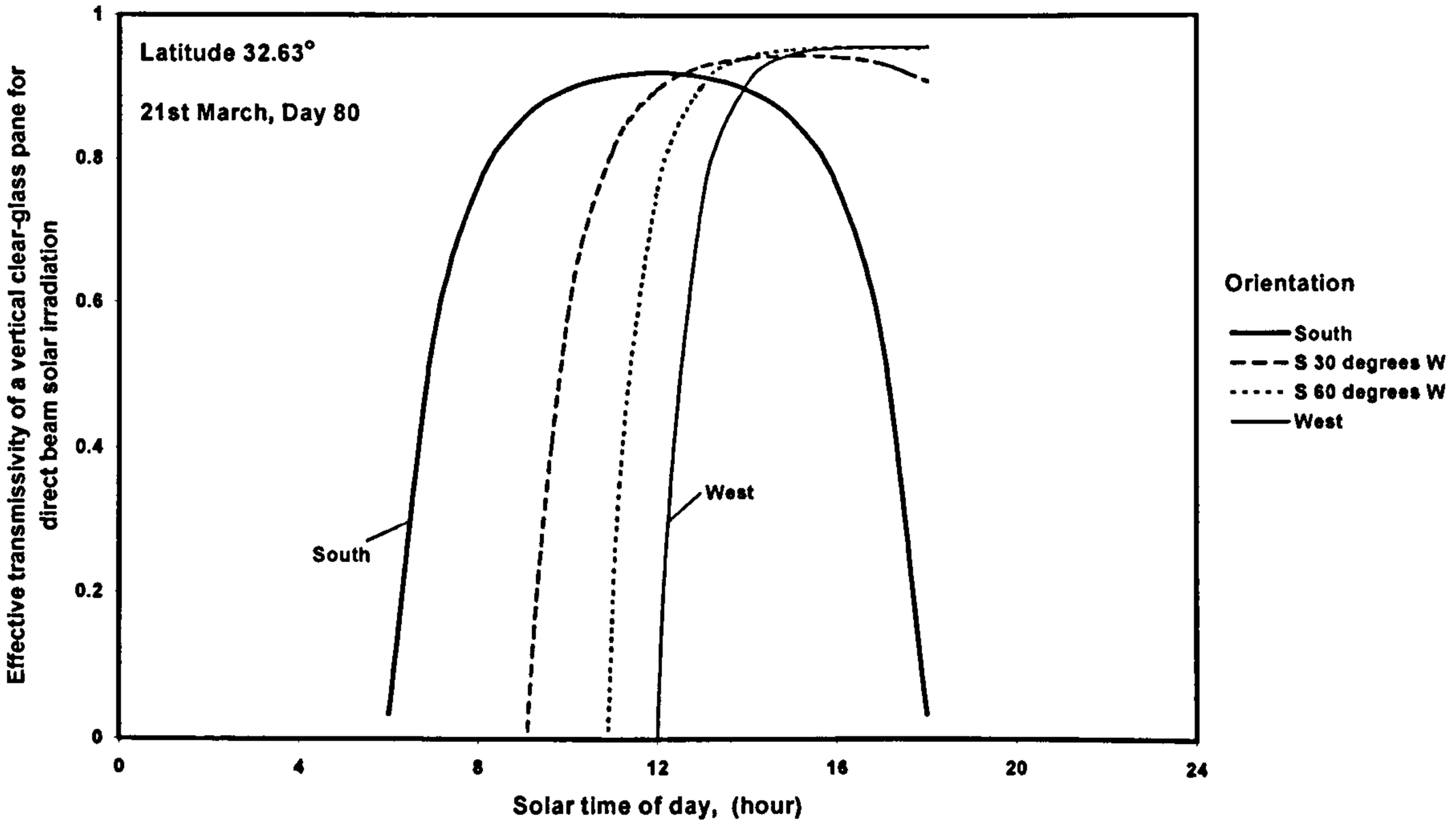

Figure 1.16 Calculated variations of the effective transmissivity of vertical glazing to direct beam solar irradiation for March 21st (Kuwait).

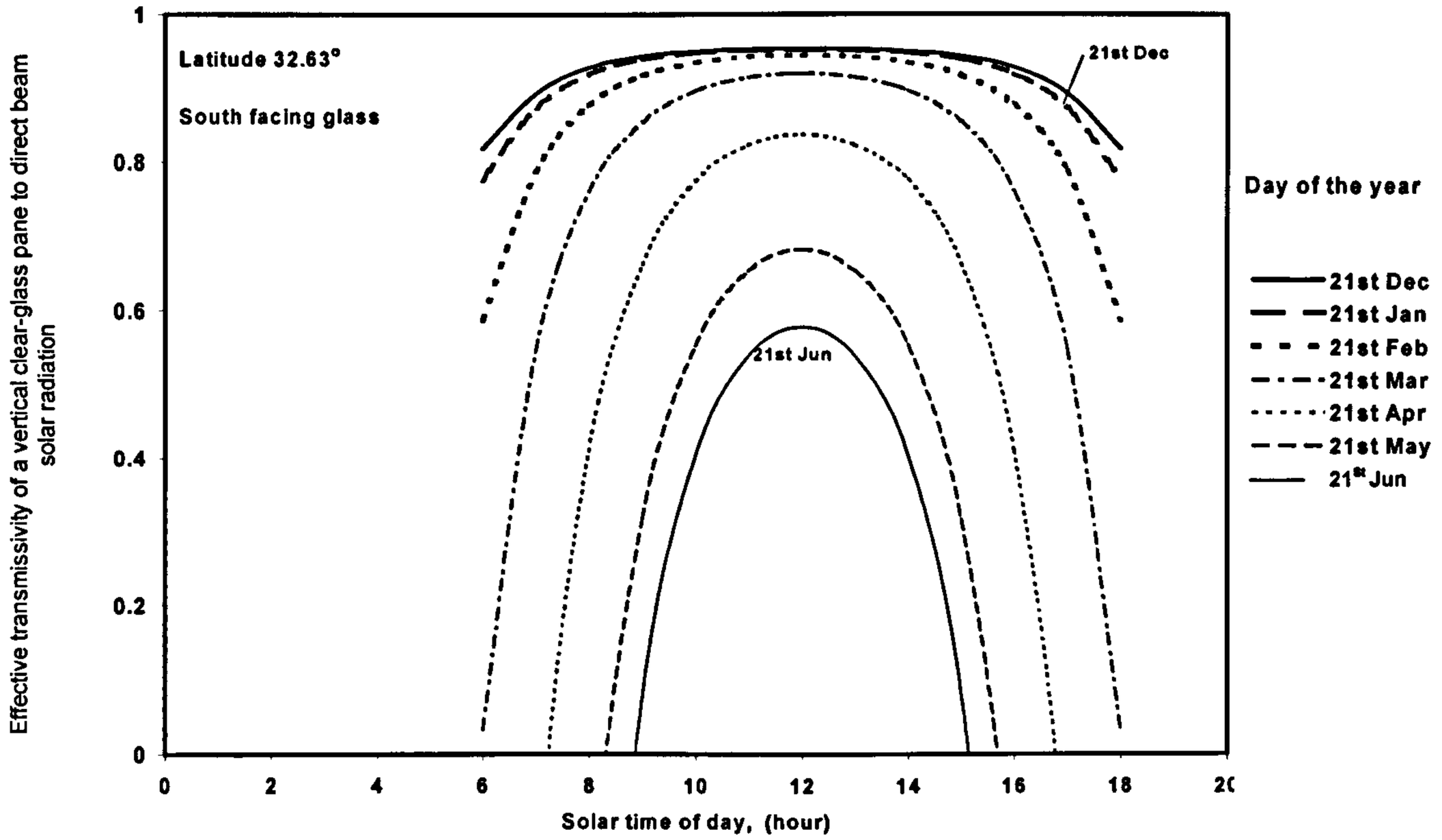

Figure 1.17 Variations of the effective transmissivity of south-facing vertical clear glazing to direct beam solar irradiation with the day of the year (Kuwait)

This occurs because the lower Sun angles (i.e. the solar altitudes) in the late afternoon result in relatively low angles of incidence of the direct-beam solar radiation on these more westerly-orientated vertical glass-surfaces.

A major change of behaviour can be observed in *figure 1.17* for the south-facing glazing where much higher transmissivities occur over a longer period of the day, with the peak values being similar to those of the more westerly-orientated vertical glazing. The behaviours of the more westerly-orientated windows are similar to those that would occur for of 21 June, but the transmission begins earlier in the morning for both the S30 W and S60 W orientations.

On 21 December, when the solar altitudes are at their lowest in the Northern Hemisphere, the transmissivities for south-facing surfaces are at their highest and the daily period during which the window transmits is most prolonged, *see fig.1.17*.

As summer approaches, the solar altitude increases: this causes both the effective transmissivity and the period of transmission to decrease.

The diffuse component of solar radiation is much less directionally dependent than the direct-beam component and so will show fewer variations with the geometry and orientation of the glazing system. The diffuse component is usually more dependent on the local atmospheric conditions, e.g. turbidity.

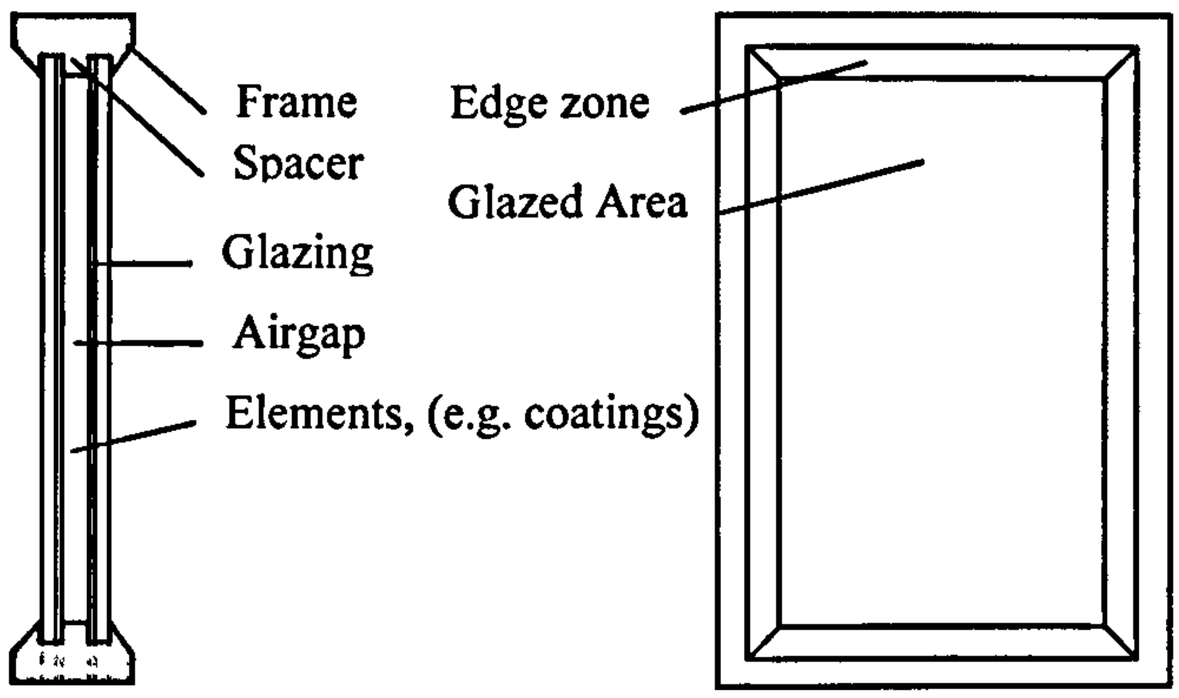

Figure 1.18 Schematic picture of typical window, consisting of frame, spacers, glazing(s), gaseous gap and coatings, if any.

1.6 HEAT TRANSFER THROUGH GLAZING

Heat can be transferred through a window via radiation, convection and conduction. In particular:

(i) Direct and diffuse components of the solar radiation enter the building during the day and heat is lost from the building by infrared radiation emitted by the exterior glass surface facing outdoor conditions.

(ii) A proportion of the insolation and the thermal radiation emitted by the building's interior surfaces and the ambient environment that are incident upon the window system are absorbed by it and then re-emitted as thermal radiation;

(iii) Convection occurs via the gas (usually air) in the cavities of a multiple-glazing system and both the exterior and the interior surfaces.

(iv) Conduction occurs through the glass panes, the trapped air in cavities and the window frames and spacers that support and separate the glass panes of the multiple-glazing system *see fig 1.18.*

The boundaries in multiple-glazing units tend to inhibit convection in the cavities: the low thermal conductivity of the trapped air contributes the major proportions of the relatively high thermal resistances of these units. This is achieved without forsaking the advantage of the window as a means for providing natural daylight. The use of partially reflective coatings on the interior surfaces of the glass panes of multi-cavity glazing has been commonly employed to minimize heat transfer by radiation.

Effective thermal transmissivities of the traditional vertical double-glazed system were studied by Robinson and Powell using a guarded-hot-box apparatus (Kusuda T. 1985). For a small horizontal temperature-difference across a narrow, vertical air-filled cavity at near-normal ambient temperatures, convective heat-transfer will occur if the cavity is wider than 12 mm, and will rise in intensity, as the width is increased, *see Fig.1.19.*

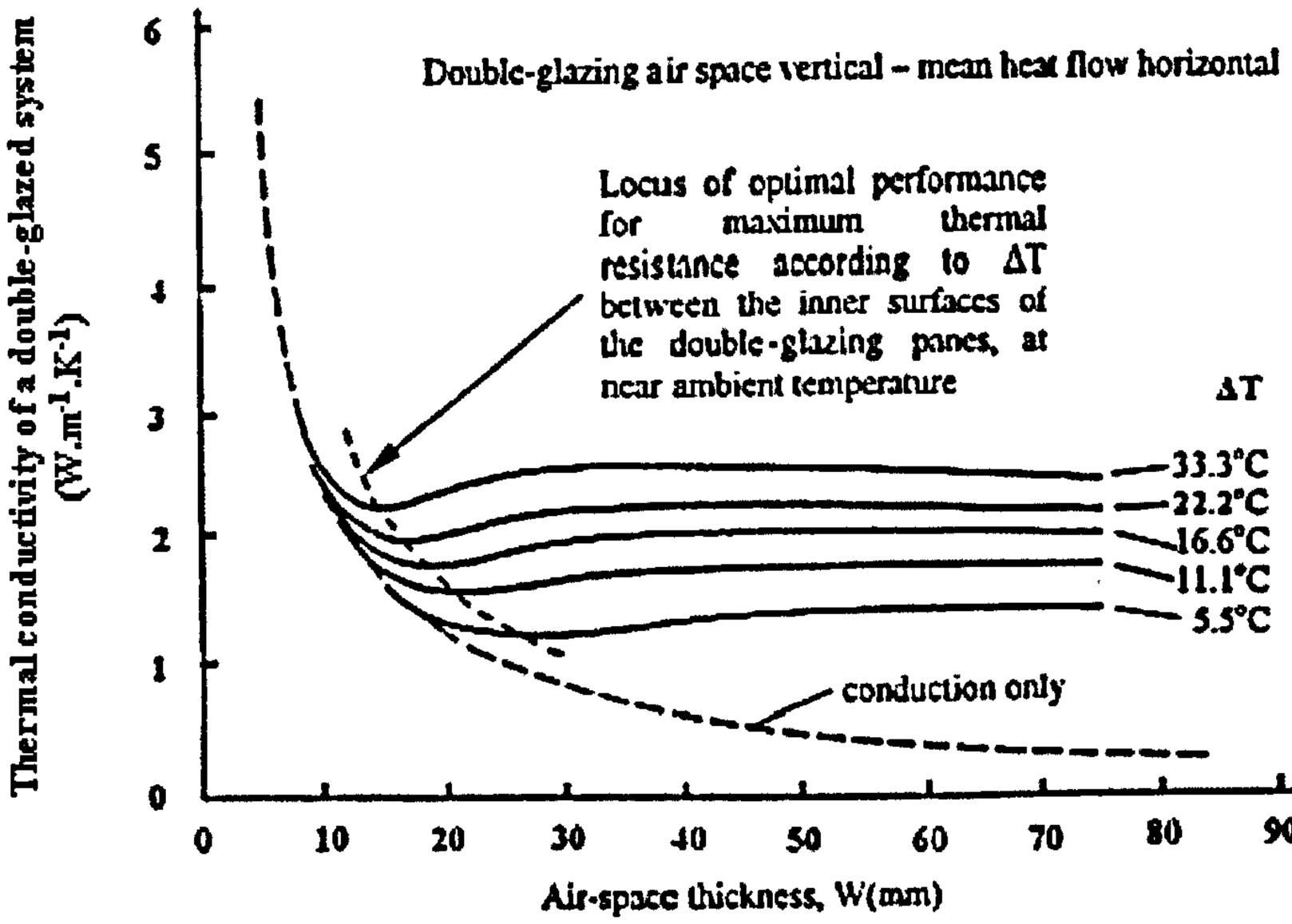

Figure 1.19 Steady state heat-transfer behaviour of a vertical double-glazed window for a fixed temperature-difference,ΔT, between the glass panes (Kusuda T. 1985).

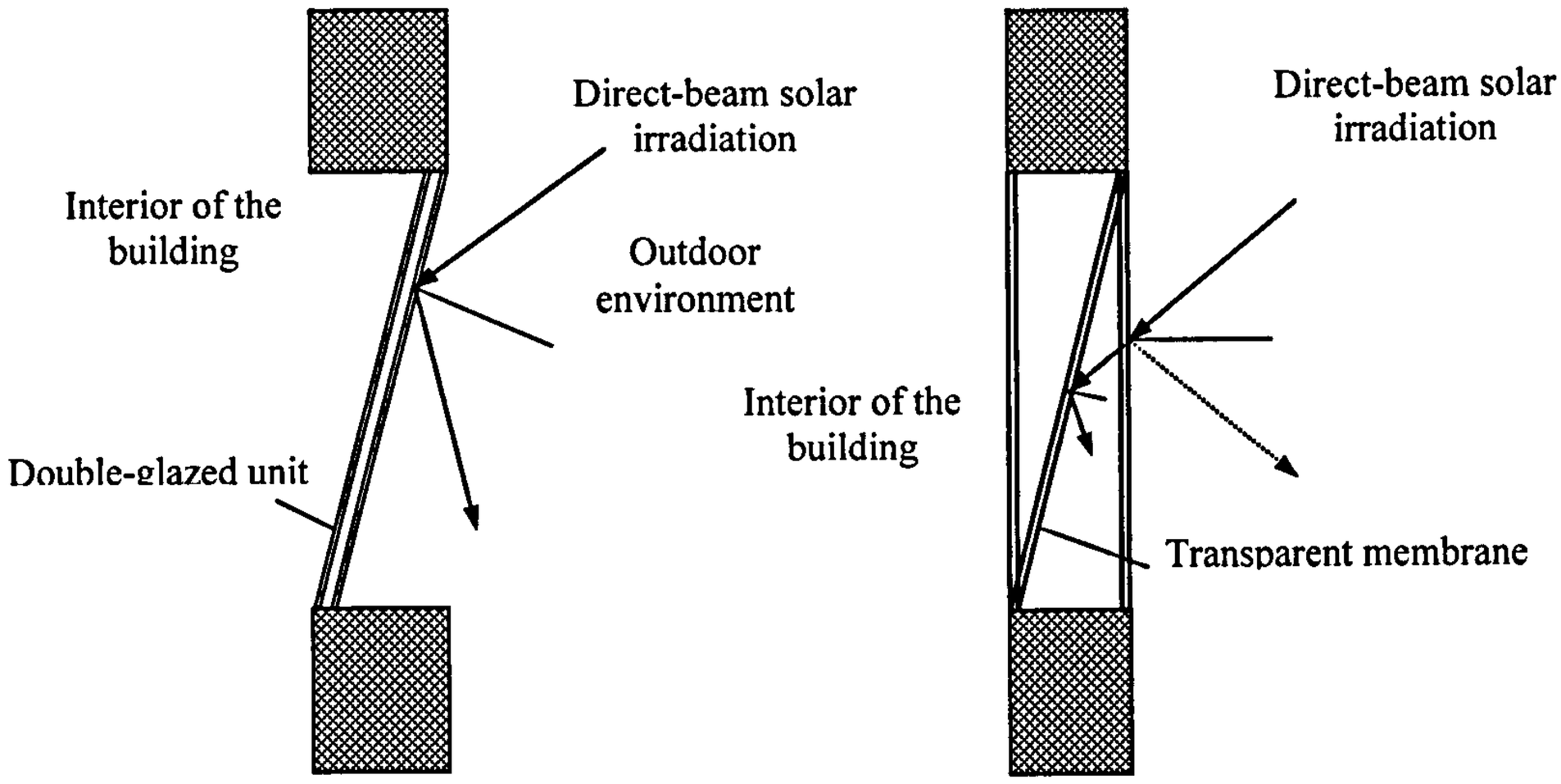

(a) Tilted double-glazed unit

(b) Angled transparent membrane within a double-glazed cavity

Figure.1.20 Vertical glazed-windows to reduce the transmission of direct-beam insolation.

However, as the width of the cavity increases, the conduction contribution to the rate of heat transfer through the cavity will decrease. Because these two conflicting processes exist, an optimal cavity width occurs at which the thermal resistance has a maximum

value. Another way to minimise the convection contribution might be through using sealed evacuated cavities in the multi glazing units, (Griffith P. W. & Norton B.1996).

For the range of air temperatures that typical building window-systems experience in the UK, the optimal cavity width is approximately 19 mm, i.e. optimal width decreases as the mean temperature of the two bounding vertical surfaces increases; *see fig 1.19.* Such an optimal width would be slightly less in the Middle East, i.e. 15-16 mm due to a higher value for the mean air temperature in the cavity.

The radiation view-factor for this system is almost unity for the range of cavity widths considered and so the radiation contribution remains approximately invariant for small temperature-differences between the vertical glass panes and does not in influence significantly the optimal width (Rubin M *et al* 1998)

1.7 THE PROPOSED GLAZING SYSTEM AND HYPOTHESIS

The proposed glazing system is set to reduce solar gain by using a tilted-glazing element, which would correspond to the range of angles of incidence of the direct-beam component experienced during the day and consequently to decrease the effective transmissivity of the glazing to solar radiation, *see fig 1.14*; while maintaining acceptable levels of the diffused daylight component, which would not be so affected as it is less angle dependant. Envisaged vertical systems, each including a tilted element, are illustrated in *Fig.1.20*; the optimal value of tilting angle θ being primarily dependent upon the latitude. Use of this optimal angle would ensure the lowest energy direct solar gain transfer from the ambient to the indoor environment, whilst attempting to maintain daylighting levels.

Systems such as that shown in *Fig.1.20 (a)* have been used previously, but are criticised usually because of their appearance. The configuration shown in *Fig.1.20 (b)* uses standard glazing-frames and a thin clear transparent plastic film/sheet to provide the reflecting element. The thermal resistive behaviours of the cavities on either side of the transparent membrane would also influence the thermal resistive behaviour of the glazed unit.

The consequences of altering the tilt of a single glass-pane from the vertical are shown in *Figs.1.21 and 1.22* respectively. The effect of the glazing's tilt angle is marked for the south facing glazing, with only a 10° glazing-angle from the vertical causing a reduction of 6.6% in the peak effective transmissivity for day 80 of the year. When the glazing tilt angle is increased to 30° from the vertical, then the peak effective transmissivity is reduced by 72%. However, the behaviour of the transmissivity with the change of glazing angle is quite different for the west-facing glazing bearing in mind the difference in time of the calculated transmissivities shown in the two figures; *see Figs.1.21 and 1.22*; in the latter figure the change in transmissivity is much smaller within the time period during which solar radiation is incident, i.e. 14-18pm.

The onset of the transmission of the direct beam solar radiation would occur later in the day as the glazing angle is increased. The sharp cut-off of the lines at approximately 18.00 hours occurs because this is the time of sunset. Consequently the validity of the proposed system has to be checked against various solar gemotry scenarios; *see also figures 1.14-1.17.*

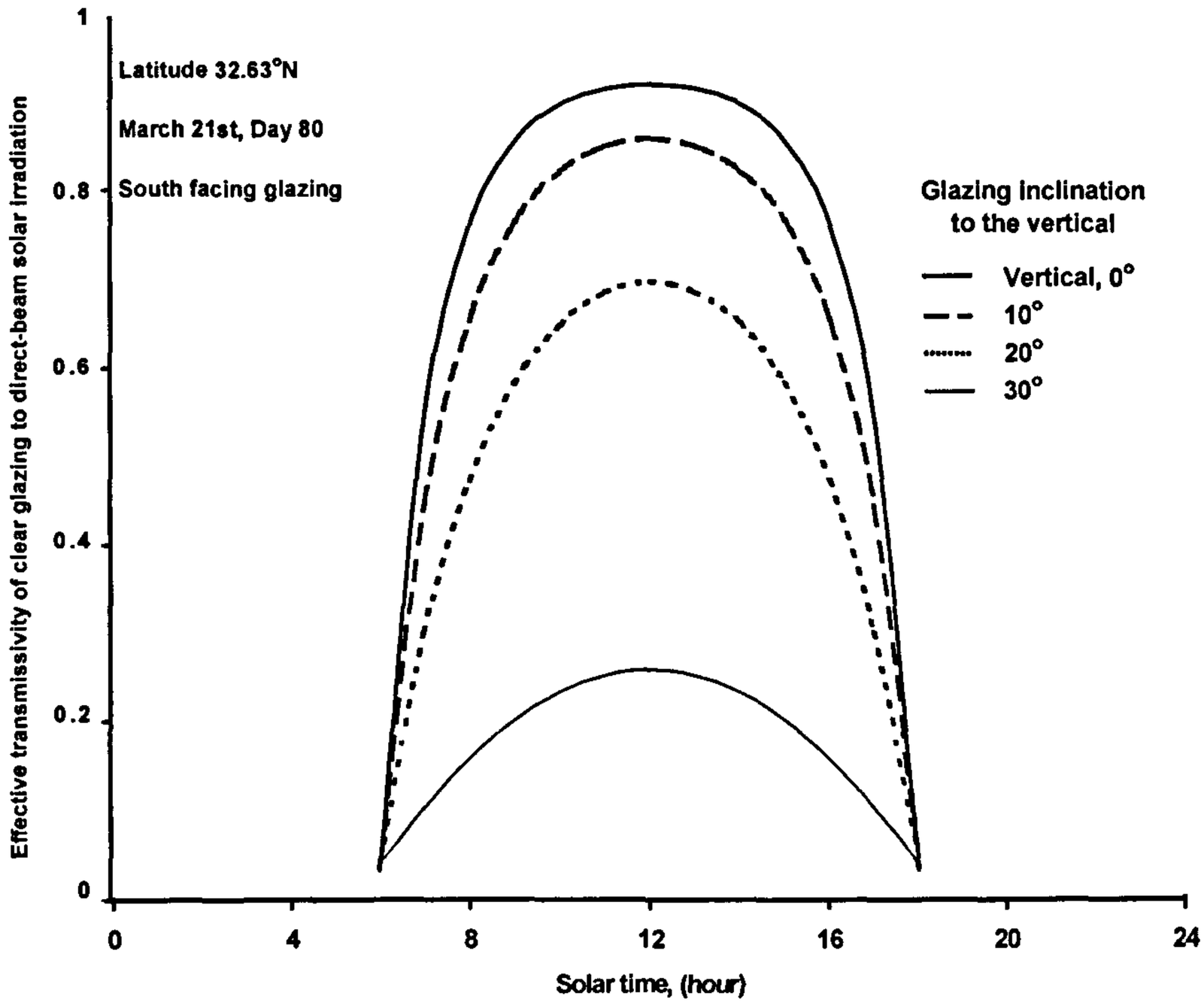

Figure 1.21 Effect of changing the inclination of the glass surface to the vertical on the effective transmissivity to direct-beam solar radiation for south-facing glazing.

Another improvement would be where the partially-reflective element bisects the air cavity between the two vertical glass panes, *see Fig.1.23*. The convective currents in the resulting triangular-sectioned cavities could affect significantly the thermal transmittance of the glazed system.

The relative magnitudes of the convective and radiative components of the heat transfer rate will be influenced by the angle θ of the transparent membrane and its effective transmissivity. As θ is decreased, for a constant height of the glazing, the cavities become wider and the convective components of the heat transfer are likely to rise with cavity width.

The optimal values of θ and H to achieve maximum thermal resistance have to be determined for each proposed application and latitude. It is proposed that such a system would allow considerable daylight to enter through the window via the diffuse component of the solar radiation, while inhibiting heat gains from the direct solar radiation component.

Additionally the units would have different thermal resistances according to whether the heat transfer is from the left to the right, or vice versa, for the configuration shown in *Fig.1.23*.

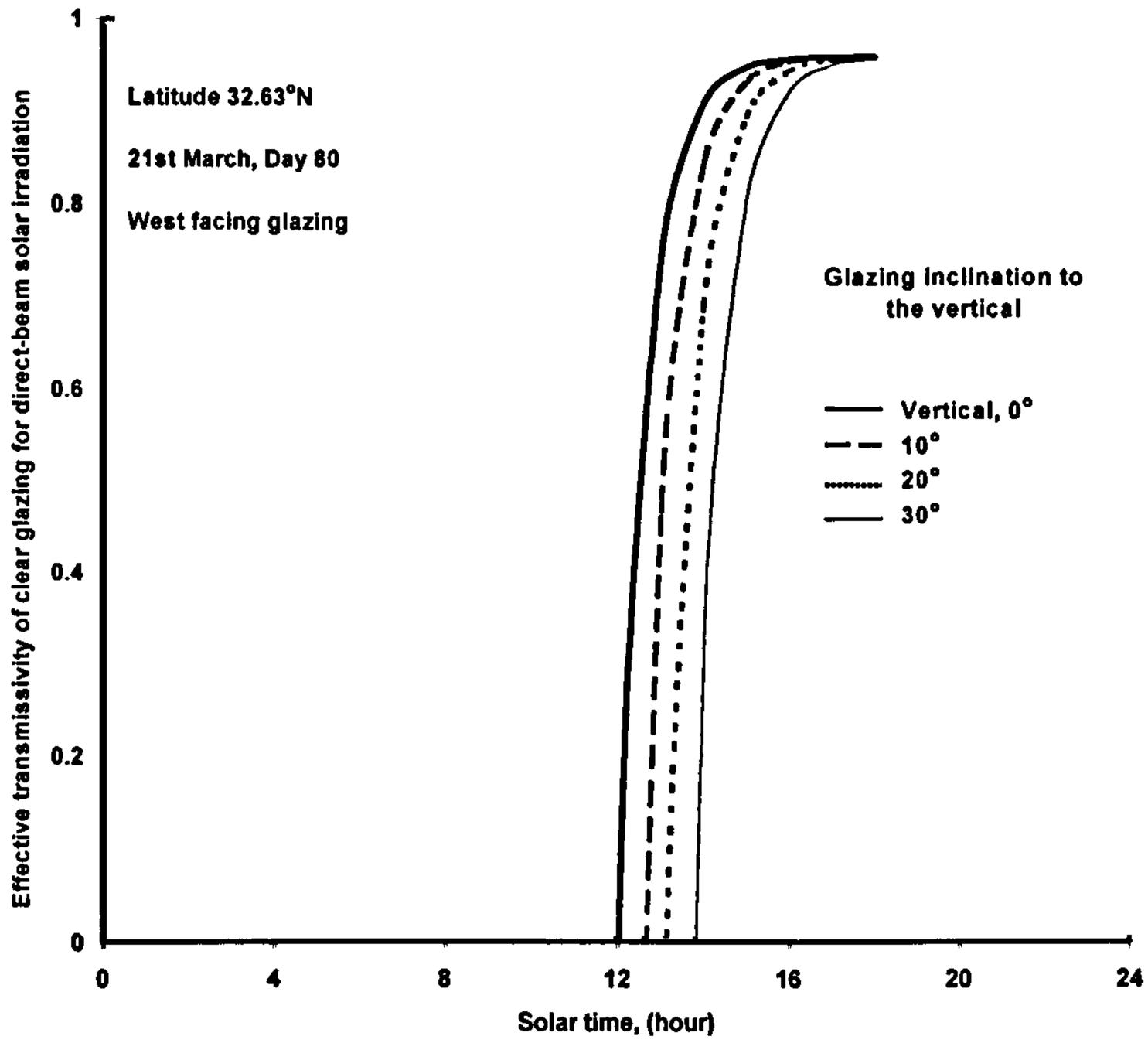

Figure 1.22 Consequence of changing the inclination of a glass surface to the vertical for the effective transmissivity to direct-beam solar radiation for west-facing glazing.

Hence in terms of thermal insulation, it would be beneficial to be able to rotate such a unit about a central vertical axis of the window within its frame, according to whether it is day or night, summer or winter, or even the imposed weather conditions.

Recently, more studies have been dedicated to understand the role of triangular stagnant core cavities in inhibiting the natural convection regimes in multiple glazing systems; (Bejan A. & Kraus D. 2003)

1.8 OBJECTIVES AND METHODOLOGY

The research then, set the Steps necessary to assess the performance of the proposed system. Those were:

(i) Modelling the insolation incident on the exterior surfaces of the glazing system in its different formats relevant to changes of parameters due to the location geographical location and time of day and year.

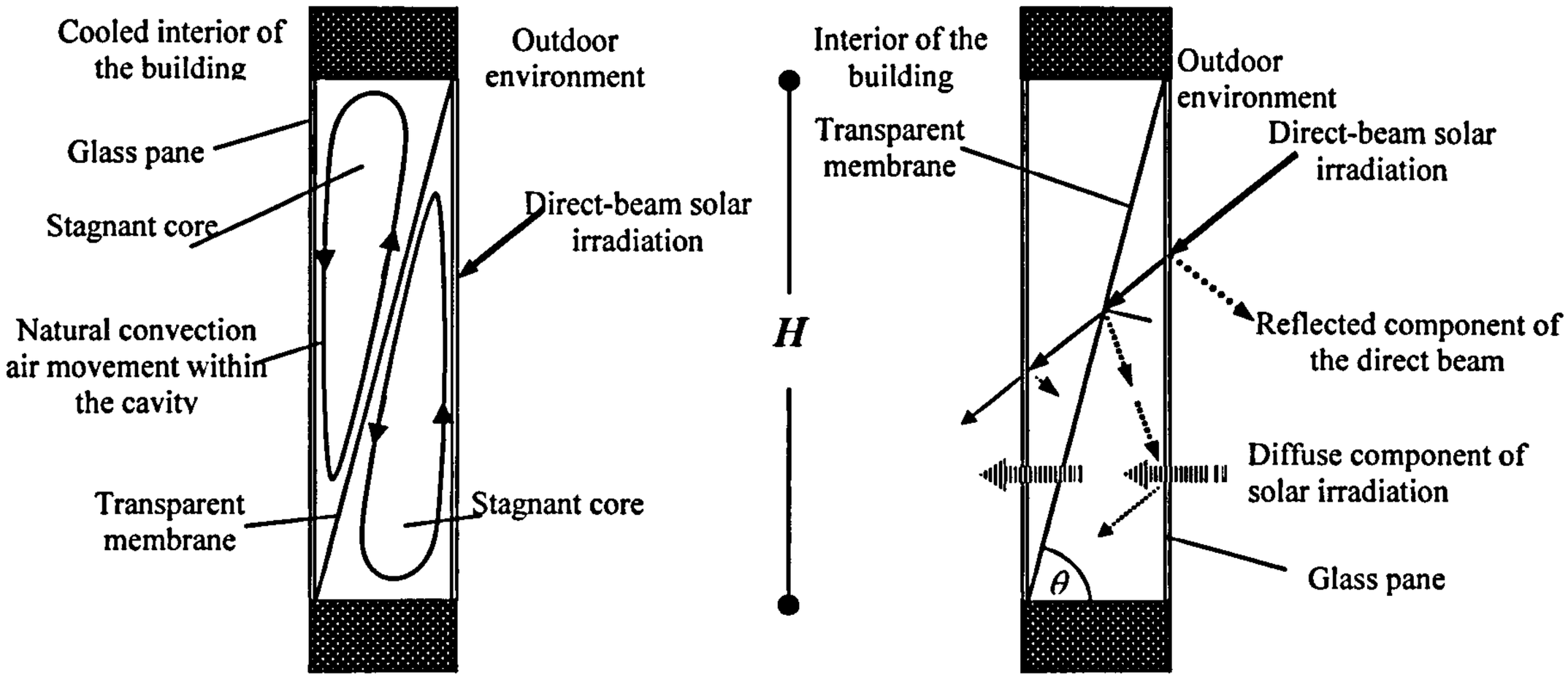

(a) Convection cells of the heated and cooled air in the glazing cavities

(b) Reflection of the incident beam component of solar irradiation at the surfaces of the vertical glass pane and the inclined transparent membrane within vertical double-glazed cavity

Figure 1.23. Schematic drawing showing the suggested system and its effect on (a) Convection and (b) radiation modes of energy transfer.

(ii) The research would develop a better understanding of the modes of heat transfer in glazing, related to the shape, size and materials of the proposed system.

(iii) The project, then, would try to develop mathematical models that can simulate such modes and their changes with the change of parameters. The performance would be tested through new software to simulate heat transfer mode using an explicit method, checking transfer behaviour at all angles of incidence and for different geometries. Consequently, the newly developed code and software would be designed to work parting conjunction with existing software where practicable.

(iv) The project would consider the feasibility of realizing the glazing system as a practical and a commercial product.

REFERENCES

1. AGSA. History of tinted glass, Art Glass Suppliers Association International; USA Janesville, OH, 1998. See also: www.agsa.org.

2. ASTRONOM 8.1, Manual, City Wageningen , USA, 2000.

3. Button D, Pye B., The building structure. In: Glass in building. Oxford, Butterworth-Heinemann, 1994.

4. Bejan A & Kraus A. D., Natural convection. In: Heat Transfer Handbook, New York: Wisley and son Inc., 2003

5. Charrier. B, Dinar S., Hiniker M, Water, conflict resolution and environmental sustainability in the Middle East, Arizona Newsletter, 1998; Autumn/Winter (44).

6. Fatthi I, Warren J., Environmental considerations, Traditional houses in Baghdad. Horsham: Coach Publishing, 1982.

7. Fletcher B. The ancient near East: Mesopotamian civilization: A History of Architecture. USA: Dan Cruickshank, 1996.

8. Griffiths P, Norton B, Eames P.C, S. Lo, detailed simulation of heat transfer across evacuated glazing, Building Research and information. 1996; 24(3): 141-147.

9. Hamdan M. A., Thermal gains through windows, Energy Conservation, 1994; 35(6): 501 –6, Elsevier Science, UK.

10. Kob W., Binder K., Baschnager J., Paul W., " Glass physics: still not transparent" Physics world, 1999; 12(12): 54.

11. Kusuda T, Rohsenow WM, Hartnett JP, Ganic EM, Heat transfer in buildings: Hand book of heat-transfer applications. New York: McGraw-Hill Book Company, 1985.

12. Lloyd-Wright F, Evolvement of the city. In: Collected writings, "The living city 1958". Minnesota, USA: Barnes & Noble, 1994. 3:250 –265.

13. Loxom F., Meteorological data for passive-solar design. Collection of reports-ETSU model-refinement study, Environment Dept., Central London Polytechnic,1985–86.

14. Macfarlane A. & Martin G. The Glass Bathyscaphe: How Glass Changed The World. USA: Chicago University Press. 2002

15. McGrath R., Glass in architecture and decoration. London: Architectural Press, 1961.

16. Mumford, L. The Myth of the Machine, The Pentagon of Power. Brace NY: Harcourt 1970.

17. Muneer T., Jorge K. & Thomas G. Heat transfer- A problem solving approach. London: Taylor & Francis, 2003.

18. Palz W, Greif J. European solar atlas radiation on horizontal and inclined surfaces. Commission of the European Community, Brussels, 1996.

19. PPG Industries Inc. for Glass Reinforcement for Thermoplastics, History of glass. Pittsburgh, PA, 15272 USA, 1998. See also: www.ppgglass.com.

20. Rubin M, Von Rottkay K, Powles R., Window optics. Solar Energy 1998; 62(3): 149 –60.

21. Volf M., Models in the chemistry and technology of glass: Mathematical approach to Glass. Sazava, Czechoslovakia, Elsevier, 1988.

22. Weather forecast for the Middle East, CNN search engine, August 1998. See also: http://www.ceedex.co.uk/outerlimits/info/weather/meast.html.

23. Wikipedia , Greater Middle East as defined by the G8, Wikipedia, the Free Encyclopaedia 2006, see also: http://en.wikipedia.org/wiki/Image:GreaterMiddleEast2.png

CHAPTER TWO

INSOLATION

Introduction

As shown in *chapter 1*, a proper insolation model is needed to measure the effect of diurnal, seasonal changes in insolation within the chosen zonal latitudes. This requires an understanding of the terminology used for the solar radiation and geometry as the source for terrestrial insolation.

2.1 SOLAR RADIATION PRINCIPLES

2.1.1 Sun geometry:

The sun, the main source of energy on Earth, is a star of intensely hot gases, with a diameter of 1.4×10^9m, at an average distance of 1.5×10^{11}m from the earth. The temperatures in the interior of the sun are on the order of 8×10^6 to 40×10^6 K; surface temperature is much lower (i.e. approximately 5800 K). The rate of energy emission from the sun is 3.8×10^{23}kW of which 1.7×10^{14}, i.e. about 4.47×10^{-8}%, is being intercepted by the earth. Of this amount 30% is reflected 47% is converted into low-temperature heat and re-radiated into space. The Earth orbit around the sun is elliptical. The period of revolution is defined as one year; the sun-earth distance varying ±1.7% over the course of the year. The plane containing the earth's elliptical orbit around the sun is called the *ecliptic plane*, while the plane containing the earth's equator is called the *equatorial plane*. An angle of 23.45° exists between these two planes. The extraterrestrial solar irradiance at normal incidence, the so-called *solar constant* G_{sc}, has been measured at 1367 W/m^2 (Gueymard "synthetic" 1995). *See fig 2.01*

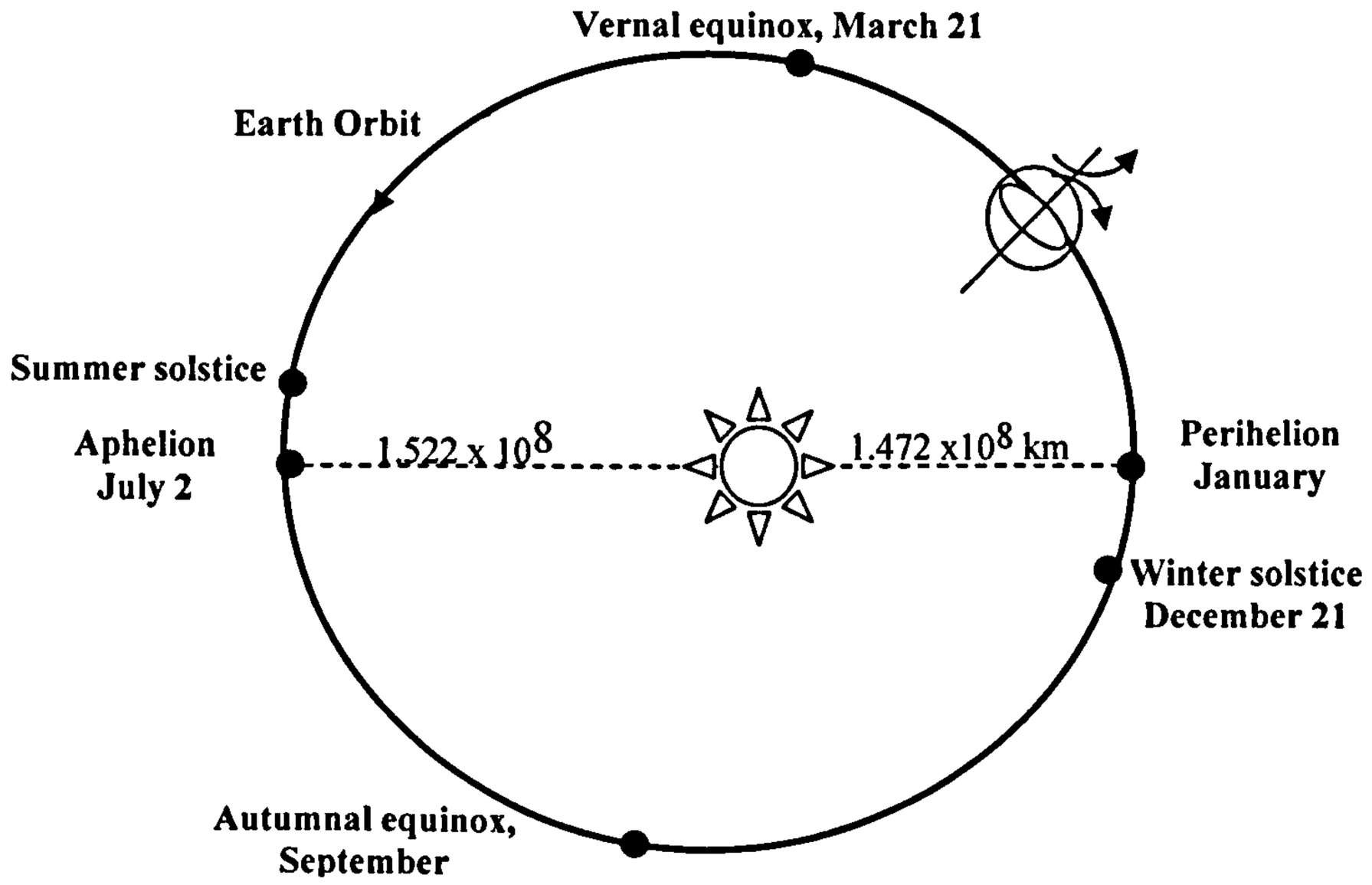

Figure.2.01 Geometry of the sun-earth system showing the Earth's various positions

The geometry evolving from "*the orbital planes*" govern the relationship between the sun and the Earth are defined by a number of geometrical parameters:

- **The solar hour angle ω:** this is defined as (15° /h) times the time period considered from the solar noon, the latter being the time of the day when the sun is highest in the sky. The observer on earth sees the position of the sun with a shift of 15 degrees per hour. Also by convention the morning values, i.e., east of the south are negative, while afternoon values are positive.

- **The solar altitude Φ**: is measured between the local horizontal plane and a line to the centre of the sun, sunrise and sunset occur when $\Phi=0°$.

- **The azimuth angle γ_s,**: is measured in the vertical plane between a line due south of a location and the projection of the line of site to the sun in the sky, it has a value that is *negative* east of south and *positive* west of south.

- **The zenith angle θ_z**: is the complement of the altitude angle, (i.e. $\theta_z=90° - \Phi$), both of these angles are related to the azimuth angle and the solar inclination and all of them are related to the solar hour angle.

- **The tilt angle of the recipient surface of incidence β_s**: is the angle, at which the surface is inclined from the local horizontal plane and it is taken positive for the south –facing surfaces.

- **The longitude angle Γ**: is the angle between the vertical line set on Greenwich meridian and the vertical line, drawn between the north and the south poles set on any other point east or west of it. The point of origin at Greenwich meridian is taken as zero and it is positive east and negative west of the meridian.

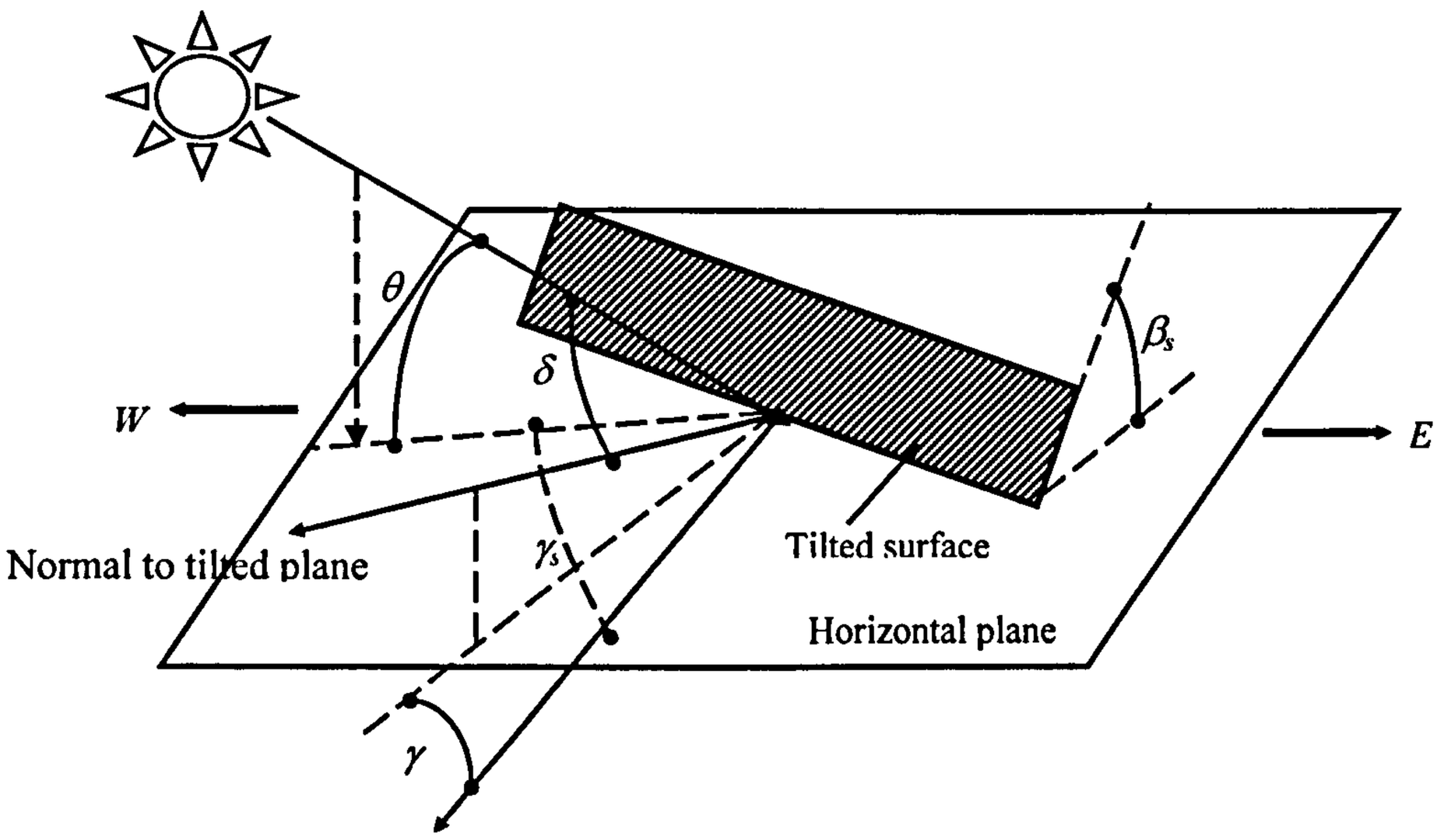

Figure 2.02 Definition of solar angles

- **The solar declination angle δ_s.:** swings between (-23.45°) on December 21to (+23.45°) on June 22. By convention it's positive when the earth-sun vector points northwards relative to the equatorial plane. The declination angle is given by the following relation (Duffet-Smith 1988):

$$\sin\delta_s = -(\sin 23.45^\circ)\cos\frac{360^\circ(n_d+10)}{365.25} \qquad (2.001)$$

Or by the relatively modified: $\delta=23.45\sin[(360°/365)+284+N]$

The solar angles are related to each other and define the amount of incident direct solar radiation that is falling on a certain surface at a certain time and in a certain place on the globe, *see fig 2.02*. The governing equation that can include all these angles is used to define the angle of incidence of the direct solar radiation ray to the receiving surface as follows (Muneer 1997):

$$\cos\theta = \sin\phi(\sin\delta\cos\beta + \cos\delta\cos\gamma\cos\omega\sin\beta) + \cos\phi(\cos\delta\cos\omega\cos\beta - \sin\delta\cos\gamma\sin\beta) + \cos\delta\sin\gamma\sin\omega\sin\beta \qquad (2.002)$$

2.1.2 The Extraterrestrial radiation:

The terrestrial solar radiation results from the emission of electromagnetic radiation from the sun. The propagation of oscillations of the electric and magnetic fields together is called *electromagnetic radiation*, since both of the electric and magnetic fields are involved in the process that radiates energy away from the source. The strength of such oscillations is measured by their amplitudes or energy *density*.

Another important characteristic of the oscillations in electromagnetic radiation is their *frequency*, which defines the number of oscillations per second occurring in the electromagnetic field. The relationship between velocity, wavelength and frequency of the electromagnetic radiation is given in the equation derived from James Clerk Maxwell's theory, i.e. $C = f\lambda$.

The electromagnetic spectrum is divided into a number of characteristic bands, *see fig 2.03(a)*. The "optical range", which includes the part of this spectrum that is visible to the human eye, is divided into three main parts, ultraviolet, visible light and infrared as shown in *fig.2.03(b)*.

Studying the physics of the behaviours of glazing systems in relation to solar and terrestrially derived electromagnetic radiation, shows that two bands within the electromagnetic spectrum are of interest: the solar spectrum that lies within wavelength interval from 350nm to 3500nm, and a second band that is from 3500nm to 50000nm*.

* One nanometer, abbreviated nm, is 10^{-9}m. 1000nm are equivalent 1micro-meter abbreviated μm or 10^{-6}m.

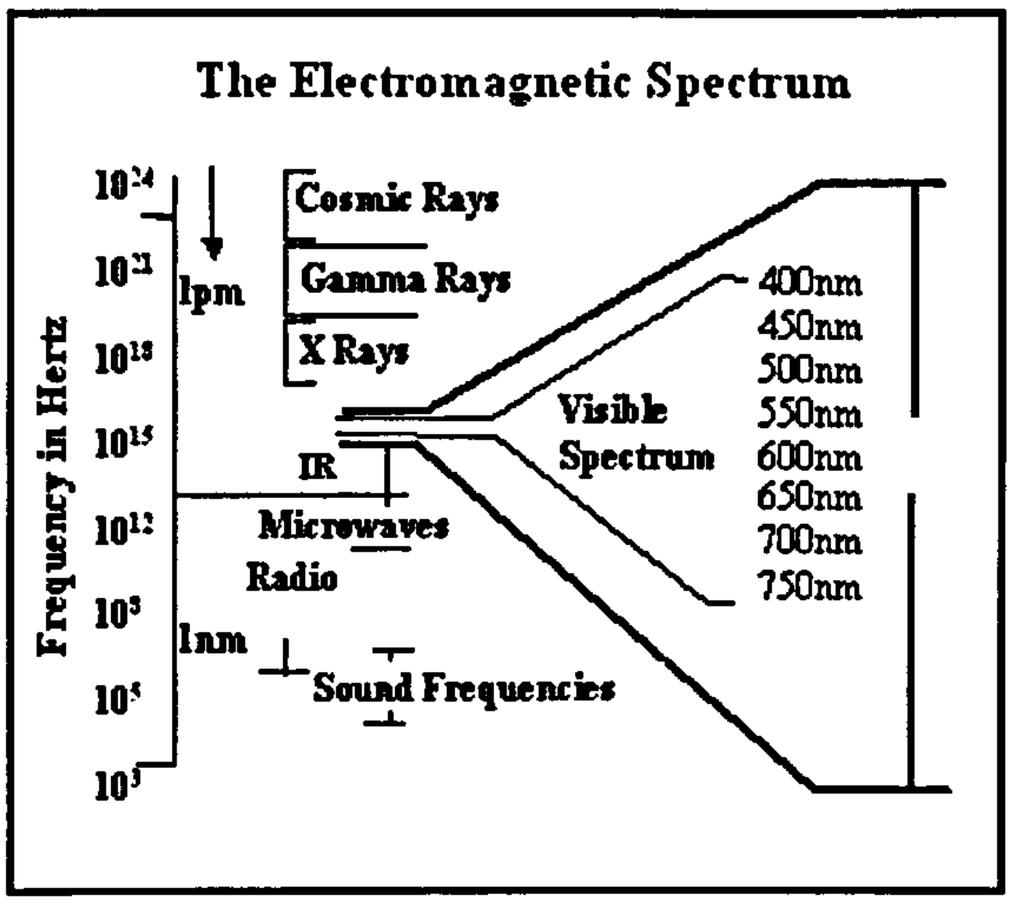

(a)

Wavelength Ranges of Optical Spectral Regions	
Name	*Wavelength range*
UV-C	100 to 280 nm
UV-B	280 to 315 nm
UV-A	315 to 400 nm
VIS	Approx. 360-400 to 760-800 nm
Purple	360 to 450 nm
Blue	450 to 500 nm
Green	500 to 570 nm
Yellow	570 to 591 nm
Orange	591 to 610 nm
Red	610 to 830 nm
IR-A, "Near IR" or NIR	780 to 1,400 nm
IR-B	1.4 to 3 μm
IR-C, "Far IR"	3 μm to 1 mm

(b)

Figure 2.03 (a) Illustration of major wavelength-frequency ranges in the electromagnetic spectrum (b) Table showing the Ranges of the Optical Spectral Region. (McCluney R 1996).

The temperature of a material defines its rate of emission of electromagnetic radiation. *See fig 2.04.*

The maximum value of the hemispherical radiative emittance of any material is 1.0 (Stefan-Boltzmann law: $E_b=\sigma T^4$), in which the surface emits the theoretically maximum amount of radiation possible (i.e. *blackbody radiation*). *Grey bodies* have been defined as having emittance that is less than unity and does not vary with wavelength. The concept of the grey body is to make radiation modelling easier to achieve. However, real surfaces (i.e. with non-blackbodies and non-grey surfaces) can have emittances that vary with wavelength. The equation for calculating the spectral distribution of blackbody radiation can be found usually in textbooks. It must be kept in mind that the sun does not function as blackbody radiator at a fixed temperature.

However, the sun is generally assumed to act as a black body sources with an effective black body temperature of 5777K [*]. The rate at which the amount energy from the sun per unit time, received on a unit area of surface perpendicular to the direction of the propagation of the radiation, at mean earth-sun distance, at the edge of the atmosphere, is called: the *sun* or *solar constant*, G_{sc}. The position of the sun in relation to a point of the earth's surface determines the amount of received energy on the surface of the Earth. The Sun's astronomical position can be determined from standard expressions for orbital geometry (i.e. Astronomical Almanac, works of Duffet-Smith, Walraven etc.1991,).

Despite the eccentricity of the Earth's orbit, it can be said that radiation emitted by the sun and its spatial relation with the earth result in a nearly fixed intensity of solar radiation at the edge of the earth's atmosphere. The emitted solar radiation is the composite result of the several layers in the sun that emit and absorb radiation of various wavelengths. Nevertheless the reason of interest in the indicated spectral range

[*]The effective black body temperature of 5777K is the temperature of a black body radiating from the sun core

is that it contains all the wavelength ranges of solar radiation, i.e. of the sun and the sky dome that are incident on the fenestration systems thus affecting the indoor temperature of the building.

It is important therefore to give several definitions associated with solar energy that can be regarded as a key to understanding the nature of changes that affect the extraterrestrial radiation upon passing through the atmosphere (Houghton J. T 1986):

- **Irradiance:** the rate at which radiant energy is incident on a surface, per unit area of the surface (W/m^2).
- **Irradiation or Radiant Exposure**: the incident energy per unit area on a surface (by integration over a specified time, i.e. an hour or a day). The term Insolation is used to refer to solar energy irradiation; usually given as *H*, units are in (J/m^2).
- **Radiosity:** the rate at which radiant energy leaves a surface per unit area, combining emission, reflection, and transmission (W/m^2).
- **Emissive Power**: the rate at which radiant energy leaves a surface per unit area by emission only.

The amount of the solar energy passing through or reflected back through the atmosphere (i.e. attenuated) or from any surface is subject to the optical properties of the atmosphere constituents (i.e. materials); as in glazing systems those properties would determine the amount of heat flux going through to the internal spaces. The solar radiation at the earth's surface consists of two components:

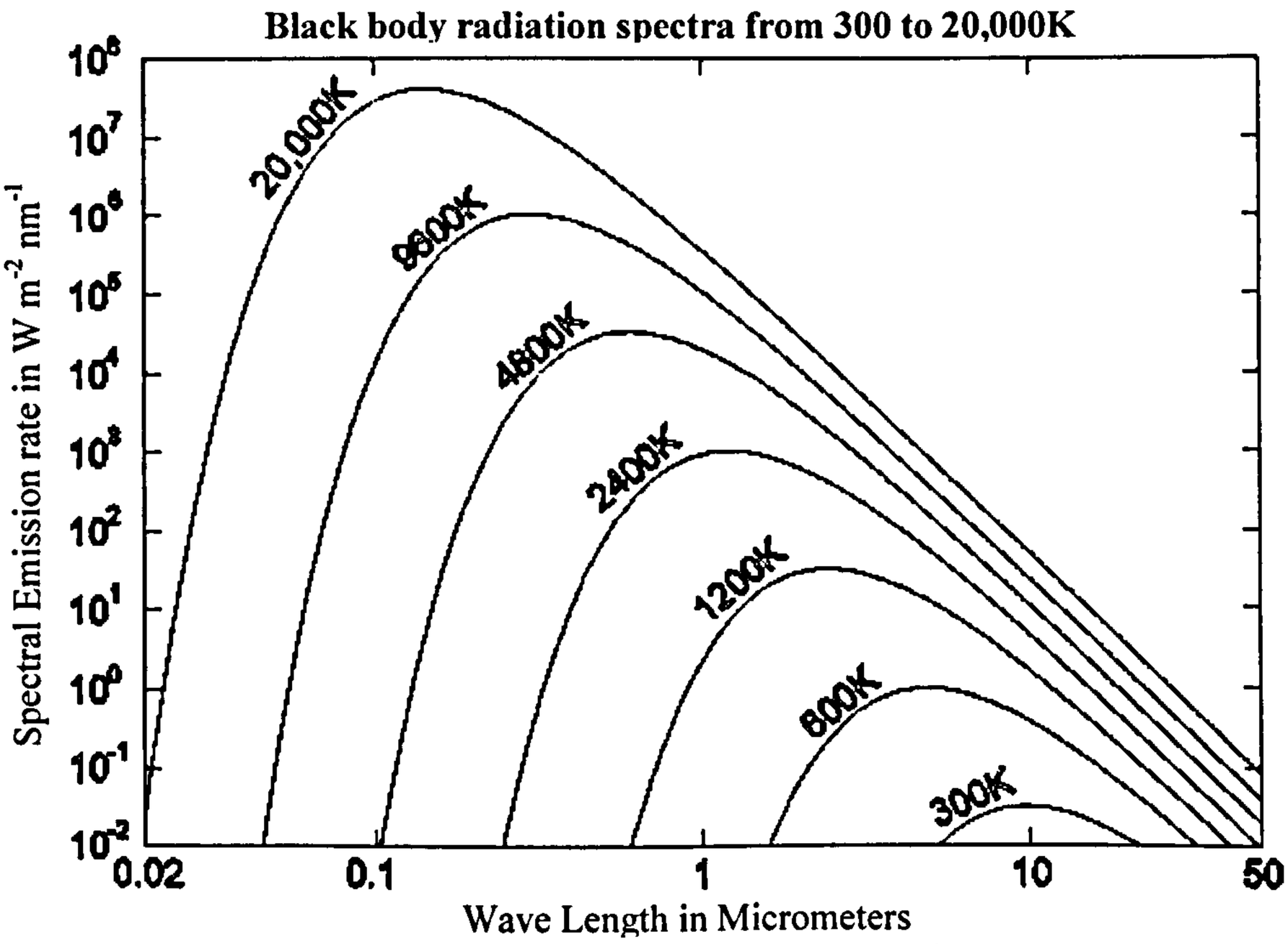

Figure 2.04 The spectral distribution of black body radiation at different source of temperature.

- **Beam Radiation** (i.e. direct solar radiation): the solar radiation received from the sun without having been scattered by the atmosphere, usually given as I_b; units are in (W/m^2).
- **Diffuse Radiation** (i.e. sky radiation or solar sky radiation): the solar radiation received from the sun after atmosphere scattering has changed its direction, usually given as I_d; units are in (W/m^2). This definition does not include the diffuse solar radiation from infrared radiation emitted by the atmosphere itself, following the absorption of solar radiation.

Total solar radiation refers to the sum of these two components. The distinction between these two components of radiation is important for understanding the behaviour of solar heat transfer through glazing. The amount of atmospheric absorption depends also on the length of the radiation path through the atmosphere. The path length can be characterised by the **air mass (m)**, which is defined as ratio of path length to unit thickness of atmosphere and this is given by the reciprocal of the cosine of the zenith angle (Garg 1992):

$$m = 1/\cos \theta_z \qquad (2.003)$$

Recently, the solar optical committee of the *NFRC* (i.e. National Fenestration Ratings Council/ USA) has selected the re-defined Air mass, based on a research by the *ASTM* (i.e. American society for standardisation and modulation/USA), and used in calculating solar optical properties of glazing. (SBIC 2003).

Air mass, in effect relates to the total molecular mass of air that the incident solar radiation travels through before arriving at the Earth's surface. The effect of this air mass on the solar radiation passing through it depends upon the path lengths and relative proportions of its optically active components, i.e. gases, vapours and particulates. For example, air is denser at sea level than it is at an altitude of 1 mile (1.6 km). For many years, solar optical properties were calculated using an air mass of 2; *NFRC* has recommended a value of 1.5 as being of more accurate. The redefined air mass gives a greater weighting to the presence of water vapour.

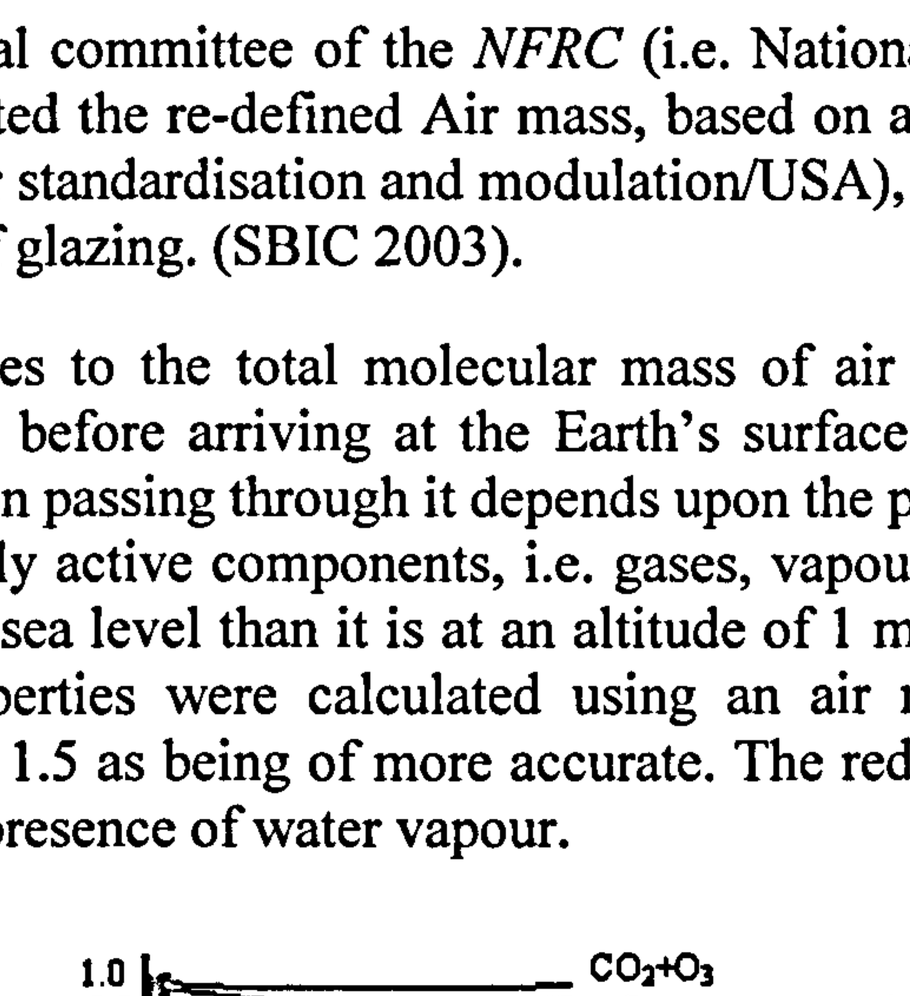

Figure 2.05 Solar transmittance for different constituents in the atmosphere versus air mass (Kerschgens-M *et al* 1976).

Justification is demonstrated in *figure 2.05* where it can be observed that the relative effect of the active component, i.e. water vapour initially reduces very rapidly, due to its diminishing concentration at higher altitudes, relevant to the changing air mass.

2.1.3 Terrestrial radiation:

The amount of the solar energy passing through or reflected back through the atmosphere or from any surface to space is subject to the optical properties of the constituents of the atmosphere. The *scattering* of the solar radiation occurs by two distinct processes:

(i) Rayleigh or molecular scattering that causes uniform scattering of radiation in all directions. Consequently only half of the scattered radiation is incident upon the earth's surface. At any point on the earth's surface, radiation scattered by this process is incident from all directions, and

(ii) Mie scattering, which is due to dust and aerosol particles within the atmosphere and occurs mainly in the direction closely aligned with the incident solar beam (an aerosol is defined as a colloidal system within a gas such as mist or fog) (Li-X, Maring- H *et al* 1996).

The amount of the cloud cover is of importance because clouds can reduce the irradiation on the earth surface up to 80% to 90%. *Absorption* of solar radiation in the atmosphere occurs in the ultraviolet range of the electromagnetic spectrum, mainly as it passes through the atmosphere, and in the infrared due to the presence of water vapour and carbon dioxide in the atmosphere. Lesser absorption effects are due to oxygen, NO_x other gases, and particulates.

The atmosphere can be considered to consist of horizontal superposed slabs of gas, each one emitting, absorbing and then transmitting solar radiation according to its concentration, temperature and spectral characteristics (Sayigh M & Mcveigh J C 1995). The gases, i.e. oxygen and nitrogen, compose about **99%** of the atmosphere and are transparent to infrared radiation (beyond **3** micrometer), while water vapour, carbon dioxide, ozone, and other asymmetrical molecules are the main constituents that affect a beam of solar radiation as it passes through the atmosphere. This section describes how the atmosphere modifies the extraterrestrial solar radiation.

- **Density, temperature and pressure:**

The properties of the atmosphere such as density, pressure and temperature change with altitude, up to a height of 100km.

From ground level to high altitudes there is an exponential decrease in pressure and density at a rate that halves their values for each additional 5km in height.

The **troposphere** has an important influence on received solar radiation and its temperature and water vapour content, which decrease rapidly with altitude. The troposphere contains 99 % of the water vapour in the atmosphere, which absorbs solar radiation and thermal radiation from the planet's surface.

Temperature decreases in the troposphere by about 6-7 C^o/km and increases in the **stratosphere** because of the ***U.V*** absorption by ozone *see fig.2.06*.

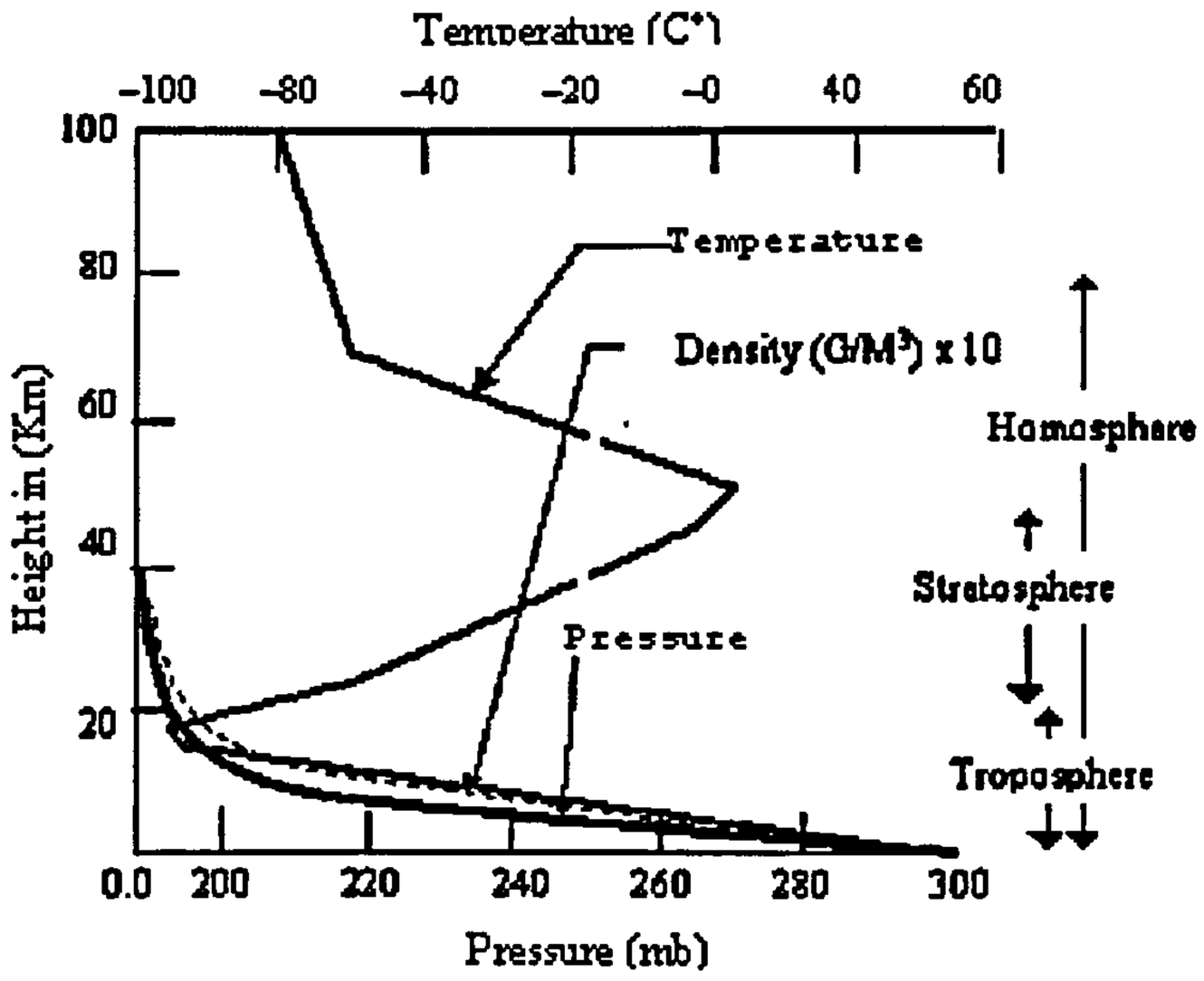

Figure 2.06 Model of vertical variation of air temperature, pressure and density, tropical conditions. (Lecture6/Sjsu 2003)

Two significant phenomena cause change in the amount of extraterrestrial radiation, these changes are:

1. Atmospheric scattering (i.e. by air molecules, water and dust).
2. Atmospheric absorption (i.e. by O_3, H_2O and CO_2).

The constituents affecting the atmosphere's transmissivity can be included in the followings:

- **Water vapour and particles:**

Air movements in the troposphere determine largely the water vapour distribution in the atmosphere and also affect its state, i.e. whether it is in the form of ice, liquid, or vapour. At a particular location, the water content in the troposphere changes continually. In return, such distribution would affect the solar radiation, as absorption or scattering.

Most of the absorption of infrared radiation occurs in the troposphere, with strong absorption occurring at wavelengths below 8μm and above 13μm. Water vapour absorbs strongly in certain bands in the infrared part of the solar spectrum, centred at 1.0, 1.4 and 1.8μm wavelengths. Beyond 2.5μm the transmission of the atmosphere is very low in the infrared due to absorption by water vapour.

Water vapour is responsible for considerable part of the sky radiation. Dust particles and water droplets in the atmosphere tend to be in larger particle sizes due to aggregation of water molecules and condensation of water on dust particles of various sizes. As a result, absorption at ground level of wavelengths beyond 20μ becomes strong.

The effects of water droplets are more difficult to treat than the effects of Rayleigh scattering by air molecules, because the nature and extent of dust and moisture particles

in the atmosphere are variable with location and time. Two approaches have been used to treat this problem; in 1940, Moon developed a transmission coefficient for perceptible water {i.e. the amount of water vapour plus liquid in the air column above the observer}, which is a function of λ^{-2} and another coefficient for dust, which is a function of $\lambda^{-0.75}$. The overall transmittance due to scattering was given as a product of different functions of λ.

The second approach uses Ångström turbidity equation to estimate of effects of scattering of dust particles and water droplets. Other models used the quantity of water vapour in an entire column of air mass as another method to calculate turbidity; this is referred to as *perceptible water* l_w., which is defined as the amount of total water vapour (cm) in the zenith direction. Cross verification can be made either by radio-sonde data or via other relevant models like those of Perez *et* al. (1990), Reian (1963) or Wright *et* al (1989):

$$lw = exp(0.07T_{dewpoint} - 0.075) \qquad (2.004)$$

Here $T_{dewpoint}$ is the dew-point temperature, which may be obtained from knowledge of dry-bulb temperature or and the relative humidity.

- **Atmospheric Gases:**

The main gases that compose the atmosphere are nitrogen, N_2, oxygen, O_2, carbon dioxide, CO_2, ozone, O_3 and Argon Ar. The relative proportions of these constituents depend upon the vertical position and the layer in the atmosphere being considered. Molecular nitrogen and Oxygen are essentially transparent to the wavelengths characteristics of solar and terrestrial radiation. However, carbon dioxide and ozone are very active and affect particular wavelength bands regarding absorption and transmittance of solar radiation.

(i) Atmospheric ozone concentration changes with latitude, it peaks at a height of 30km. **O_3** is usually associated with dry air, created at the upper atmosphere by solar radiation within the ultraviolet band. At ground levels, it is formed from the decomposition of nitrous oxide that enters the atmosphere as a pollutant.

Ozone absorbs strongly within three wavelengths bands of the layers of the ultraviolet region depending on its density within the atmosphere. Three bands have been designated as: **UV-C $100 \leq \lambda < 280$nm UV-B $280 \leq \lambda \leq 315$nm** and **UV-A $315 > \lambda \leq 400$nm)** (McCluney R 1996). There is also a weak ozone absorption band near 0.6μm wavelength.

Ozone absorbs strongly in the infrared red at 9.6μm and weaklier at 9μm and at 14μm.

The total amount of ozone contained in the atmosphere can be given in terms of a vertical column of unit area (the Red Book 1992) at normal temperature and surface pressure or Van Heuklon1979):

$$l_o = J + \{A + C\sin[D(N+F)] + G\sin[H(L_{lod}+I]\}[\sin^2(BL_{lad})] \qquad (2.005)$$

Where l_o represents the ozone concentration given as a vertical column in milli-atom-cm units, J=**235**(the equatorial annual average of l_o), N is the day number of the year,

A, B, C, D, F, G, H, I are constants, given in *table 2.01*, and L_{lod} is the longitude of the site in degrees and L_{lad} is the latitude in degrees.

(ii) Oxygen absorbs in the visible bands (i.e. between 0.4 and 0.7 μm) reaching at its highest at 0.55μm. a weak effect of O_2 also is present in the infrared band at the edge of 0.8μm..

(iii) CO_2 is the most important gas at ground level. Oceans have a stabilising action on the rate of CO_2 in the Homosphere. The main absorption and radiation of CO_2 occurs in the band of 15μm with a weaker effect at 4.3μm.

In summary most of the absorption of ultraviolet is by the ozone, for longer wavelengths than 2.5μm, a combination of scattering and strong absorption by CO_2 means that very little of insolation energy beyond the wavelength reaches the ground.

Thus form a practical point of view and for solar energy applications, only radiation of wavelengths between 0.29 ~2.5μm need to be considered. *Table 2.02* gives an information about the composition of the clean atmosphere based on the (US standard Atmosphere 1976), which is used as a reference guide to calculate the absorption and scattering for other types of atmospheres.

- **Other constituents; Aerosols**

An aerosol is defined as small solid or liquid particle that remains suspended in the air and that follows the motion of the stream, e.g. coagulated water vapour. Suspended water and ice particles in fog and clouds are also classified as aerosols, while rain, snow and hail are not aerosol particles. Aerosol particles range between 0.001~100μm, which come in many varieties, e.g. urban, maritime, dust (industrial or mineral sand), smokes, volcanic eruptions, forest fires, spores or pollens, and gas molecules. The effects of wind, which carry aerosols, contribute to the aerosol effect.

Table 2.01 Coefficients to be used in *equation 2.005*

Coefficient	Northern Hemisphere	Southern Hemisphere
A	150	100
C	40	30
D	0.9865	0.9865
F	-30	152.625
G	20	20
H	3°	2°
I. longitude>0	20°	-75°
I. longitude<0	0°	-75°
J	235	235
B	1.28	1.5
Latitude:	N= +ve. S= -ve	
Longitude:	E= +ve. W= -ve	

Table 2.02 showing the chemical composition of clean atmosphere (Muneer T. 2004).

Gas	**Content (ppm) by volume**
Nitrogen	7808400
Oxygen	20984
Argon	9340
Carbon dioxide	333
Neon	18.18
Ozone	0.012
Helium	5.42
Methane	1.5
Krypton	1.14
Hydrogen	0.5
Nitrous oxide	0.27
Carbon monoxide	0.19
Xenon	0.089
Ammonia	$4x\ 10^{-6}$
Water vapour	$4x10^{-6}$
Sulphur dioxide	10^{-6}
Nitrogen dioxide	10^{-6}
Nitric oxide	$5x\ 10^{-6}$
Hydrogen sulphide	$5x\ 10^{-8}$

Aerosols affect the absorption and scattering, the size and number of aerosol particles decreases with altitude. Models for predicting aerosols give a decrease of 60% in the particles density per kilometre for the first five kilometres above the earth's surface, for both hazy and clear skies. Particles density affects visibility; it is five times larger for a visibility of 5km than for it is of 23km.

(Kerschgens *et* al 1976) indicated that aerosols in the lower stratosphere might double the effect of absorption caused by atmospheric gases e.g. CO_2 and H_2O..

(Dietz 1963) was one of the first to discuss the effect of dust, as an aerosol on absorption; he suggested that dust could decrease the atmospheric transmittance up to 2.7% of the total insolation, especially at incident angles between (0-50°); (Duffie & Beckman.1991).

In the late sixties, serious attempts emerged to re-evaluate the effect of dust on atmospheric absorption. This work started with the pioneering studies of *eolian* sediment transport, (Bagnold 1941), followed by other empirical work/models to simulate the optical absorption (Majumdar-NC *et* al 1972).

Turbidity factors, β were introduced to simplify the method of calculating dust suspension (Ranagarajan & Mani 1984). Other models tried to simulate the dust effect as vertical column/layers in the atmosphere (Robert & Anderson 1989).

Since the eighties, more interest has been given to the effects of sand dust as an aerosol in the absorption, works like (Prodi-F; Tomasi-G, 1983) tried to take hourly and daily measurements of the solar irradiation, while others worked on deriving more reliable expression for the Ångström equations. (Alterio *et* al 1989).

Aerosols have more effect on absorption and scattering in hot arid zones like the Middle East, rather than that in temperate climates. During dust storms, visibility may fall below 2km.

Clouds cover can have a lesser effect on absorption in these altitudes due to the highly number of cloudless days (e.g. 133 days per year in Kuwait (AL Jamal K 1984). Therefore, in such conditions the effects of dust been correlated with other weather parameters, vertical effect of winds, the day-night motion, etc in predicting the absorption of infrared radiation.

Such effect becomes more evident once associated with the high reflectivity (i.e. albedo) of the ground, which is mainly covered with quartz sand, *see fig 2.07*.

Some of the recent readings in the Middle East (Kuwait, Iran/Abadan, Iraq) by the Kuwait Institute of Scientific Research have found that during summer, dust can increase the diffuse portion of the solar radiation by *0.9 times* while it only increases by *0.11 times* in other latitudes. It has been suggested that the dust effect in these latitudes should be added as a correction factor on the total sky emissivity (i.e. for the visible band and not just for the 8-13.5μm wavelength band) (Xavier Berger, Bernard Cubizolles 1992)as:

$$\Delta\varepsilon = 0.072 \ln(10900 / \text{vis}) \qquad (2.006)$$

Where **vis** is the visibility in meters. This result is restricted however to the following limits:

$$2000m < vis < 10{,}000m \qquad (2.007)$$

$$-7C^{\circ} < dewpoint < 22C^{\circ}$$

$$\Delta\varepsilon = 0.072\, ln(10900 / vis)$$

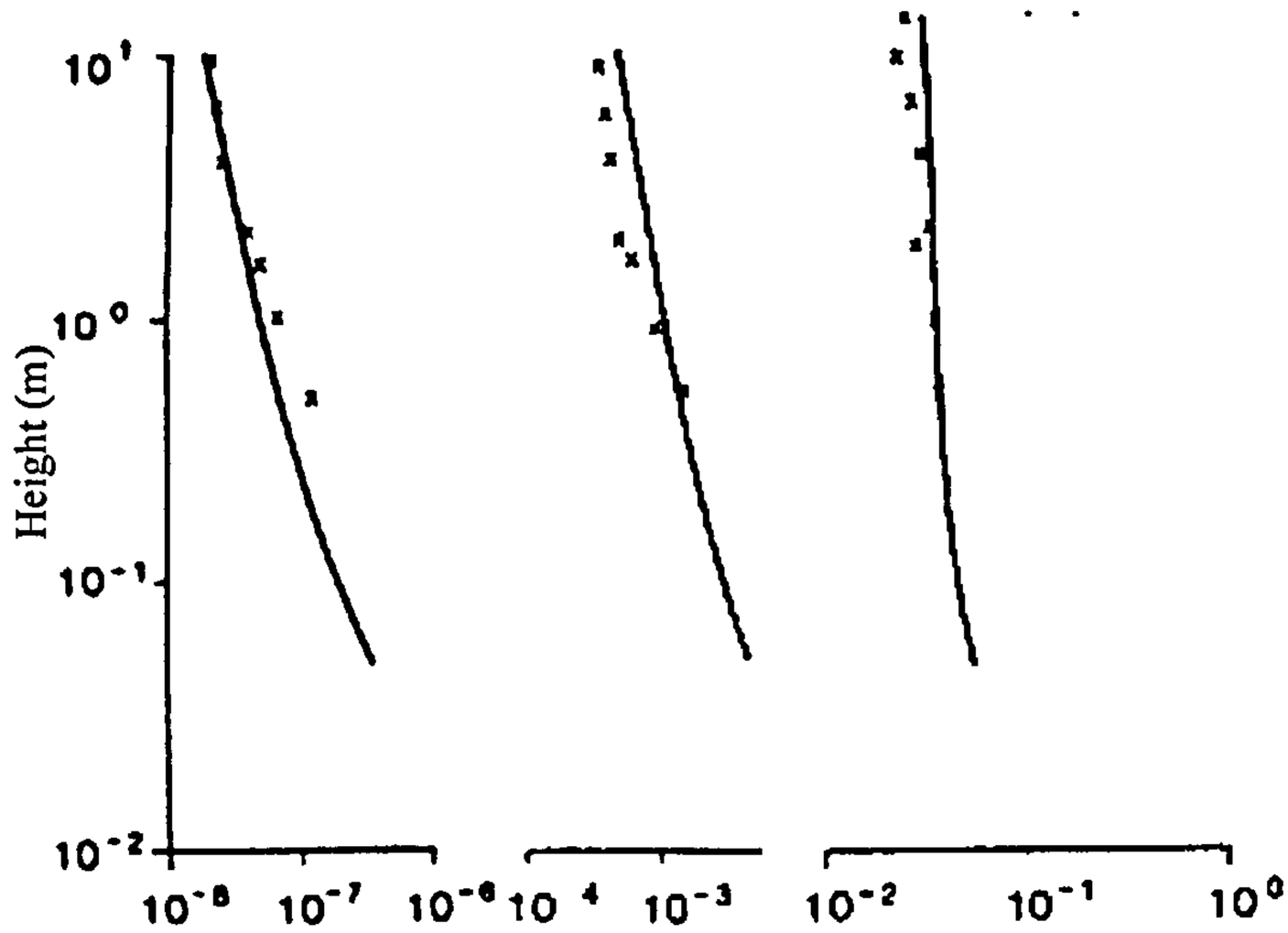

Figure 2.07 Calculated and observed concentration, mass flux and mean diameter for quartz sand as function for height (Anderson Robert S. *et al* 1986)

2.2 MODELLING OF THE INSOLATION:

Choosing an appropriate mathematical model to simulate insolation transmission through glazing systems is not simple, as it should be able to simulate both of the direct and diffused components separately.

Many models are available nowadays to describe such transmission. Those models are either theoretical or empirically based (i.e. through data gathered from observation).

The main points to be taken in any model when calculating the solar radiation are:

(i) The extraterrestrial conditions of the solar radiation: (i.e. position of the sun relative to Earth), intensity of the solar radiation outside the atmosphere for the time in question and for that place.

(ii) The received solar radiation at the Earth surface: (i.e. attenuation conditions of the atmosphere, the constituents, etc).

(iii) The type of solar radiation to be modelled: (i.e. broad wavelengths band of direct beam, diffused; or wavelength spectra models).

Historically, the development of the insolation mathematical modelling can be categorised according to assumption of the sky conditions as to: first, second and third generation models. These models were derived using the following approaches:

2.2.1 Theoretical approach:

First generation models: in the late19th century, models were derived to govern the multiple scattering of sunlight after the early works Lord Raleigh, in his theory for the illuminated sky. Early works of by Strutt in 1871-1899 &1918, and (Ångström 1929-1930) defined the factors and coefficients used precisely in equations of scattering and attenuation. This was followed by works of (Chandrasekhar 1950), then (Chandrasekhar & Elbert 1951, 1954) of direct beam radiation of plane parallel atmosphere. While, the

works of (Deirmendjian & Sekera 1954) used Chandrasekhar solution for clear sky condition to derive relative total and diffused radiation on horizontal surfaces as a function of normal incidence and inclined through the atmospheric thickness and taking the solar geometry (i.e. zenith angle) into consideration. They had to add corrections afterwards to deal with the ground reflection (albedo). Other works of (Nicolet 1951a, 1951b), (Bernhardt 1952, 1953) or (Sobolev 1963) tried to give more attention to atmospheric conditions like large aerosol particles or clouds effect.

All these models dealt with the clear sky conditions in a simplest form; nevertheless it compromised a great deal of analytical processing. The main assumption in all these models was the isotropic nature of the sky.

Second generation models: (Kondratyev & Manolova 1960) measured the radiation and intensity in 37 directions and for the tilt angles of (15°, 40 °, 65 °) in every 30 ° of the azimuth and the zenith, they showed the an-isotropic nature of the sky Irradiance. Later works of (Goody 1964), (Paltridge & Platt 1976) tried to include other sky conditions. More recent works of (Iqbal 1983) tried to take such modelling further by generating a circumsolar model assuming that the sky-diffuse component and the beam radiation emanates from the direction of the solar disk.

Third generation models: (Perez *et al.* 1990) model was based on a three component treatment of the sky-diffuse and Irradiance (i.e. the zenith angle, sky clearness, and brightness coefficients) for circumsolar and horizon brightness. Latest works of (Gueymard 1987, 1994) and (Grindley *et al.* 1995) tried to include and predict the general sky-conditions (i.e. not just clear sky). This meant dealing with the changing volumes of clouds on alternating heights, through air mass approach to predict different cast-sky conditions. Gueymard worked on monochromatic wavelength approach while Grindley took the wide band-wavelength approach. Their work had been checked through field measurements for validation.

2.2.2 Empirical approach:

All empirical models try to give expressions to estimate: (the total global horizontal Irradiance, normal beam or diffused component of the Irradiance, sunshine duration, etc). This is usually done through assessing the effect of different components of the atmosphere, the pattern of transmissivity and multiple reflections between cloud layers and through different sky conditions and for different latitudes and locations (Grindley C. 1995). After gathering of data; indices and coefficients are worked out for (sky clarity, luminous efficacy, turbidity factors, radiance factors, sunshine hours, etc).

First generation models: used the isotropic sky assumption for all slope Irradiance models. (Kimball 1919) was the first to propose a relation between the daily insolation and the extent of the cloud cover in the sky hemisphere, proposing a linear correlation, (i.e. $G_{mean}/G_o=a_2-b_2*C_m$, where C_m is the monthly average fraction of the daytime sky obscured by clouds). This was updated later on by (Black 1956) who suggested the following relation: ($G_{mean}/G_o=0.803-0.340C-0.458C_m^2$ with $C_m\leq 0.8$), after checking data from meteorological stations from around the world. (Mosby 1936) on the other hand had derived an empirical, non-spectral expression for the diffused component of the total global Irradiance for clear sky conditions.

Second-generation models: these models differentiate between the radiance distribution of clear sky and overcast skies, however they do not divorce their generic

development from the isotropic model as they refer to the latter in the overcast situation (Loxom F 1985-86). They provide better in results than the first generation models (Muneer T. 2004). E.g. (Klein 1948) added other factors to Mosby's expression to allow of separate factors of scattering by air molecules, water vapour or depletion of radiation by dust. (Hottel 1976) on the other hand proposed a simple model to calculate the amount of beam radiation, taking account of the sun zenith distance, the altitude, and other data, by assuming transmittance through a simple mix of grey gas model with a maximum error of 0.4%.

It included correction factors to allow for different climate conditions. (Lui & Jordan 1960) on the other hand analysed 149 solar Irradiance data points of studies of (Moore & Abbot 1920) and suggested a linear relation between the transmission coefficients for beam radiation and diffuse radiation. Gueymard studied the progress of clear-sky models before suggesting his own; *see table 2.03.*

Third generation models: these models took into consideration the anisotropic nature of the sky and its effect on the diffuse component of the irradiation. Some of these took luminance (or the radiance) distribution index as base, (Moon & Spencer 1942) then (Gueymard 1987) and (Muneer 1987). Others worked on air mass models with more emphasis on the role of the aerosol in scattering, especially in North America and the Middle East in the early 1990's (Kocifaj 1980 &1995 and Maring 1996,).

On the other hand, several *interpolation models* were derived across Europe in the last ten years, directly or indirectly, to measure solar radiation on a large scale. These models include spline functions, weighted average procedures or kriging, *see glossary.* Processing of satellite data provides less accurate values (compared to ground measurements) but the advantage is data coverage over vast territories at temporal resolutions of 0.5-12 hours. Significant progress has been made toward developing GIS-based solar radiation models in the last two decades, e.g. *SolarFlux, Solar Analyst, SRAD* and *r.sun.* (JRC 2003).

Table2.03 showing clear-sky models considered by (Gueymard 1993b)

Ref.	Model Type	Model Development
MAC	A	(Davies et al 1975), (Paltridge & Platt 1976), (Suckling & Hay 1976), (Davies & Hay 1978), (Davies 1980), (Davies & Mckay 1982, 1989).
IQA		(Iqbal 1983).
JOS		Joseffson quoted in Davies et al (1988).
IQB	B	(Katayama A 1966), (Sasamori et al 1972), (Hoyt 1978, 1979), (Iqbal 1983)
IQC	C	(Bird & Hulstrom 1980), (Iqbal 1983).
M&I		(Machler & Iqbal 1985)
ASHRAE	ASHRAE	(Anon 1976), (Galanis & Chatigny 1986).
POW		(Powell 1982).
EEC	EEC	(Page 1986).
CPCR2	D	(Gueymard C 1989).
PSI	1 band	(Gueymard C 1993a).

2.3 CHOOSING A MODEL:

As shown in chapter one, the pattern of insolation received on surfaces is largely governed by the specific ambient conditions in the chosen zone. The insolation model needed should therefore have the advantages of both theoretical models and the atmospheric coefficients derived from empirical local data. Consequently, two recently published models with mixed algorithms (i.e. theoretical & empirical) were selected for comparison:

- Gueymard C model of the atmospheric radiative transfer of sunshine model
- Grindley P.C, mathematical model for predicting the magnitudes of total, diffuse and direct-beam insolation.

Mathematical model for spectral radiation:

A development has been made to the spectral radiation model (*SRM* / United States Environmental Agency 1996-1997), which is the culmination of work of several authors (i.e. Spencer 1971, Leckner 1987, Gueymard 1994, Ångström 1929, McClatchey & Selby 1972, Van Heuklon 1972, Pierluissi et al. 1989). The model was developed (Gueymard 1994) and derived to simulate the solar spectral radiation working on wavelengths one by one or within specified wavelength bands i.e. 300-1700nm and for cloudless sky.

The work on this algorithm is part of new software produced by the National Fenestration Rating Council/ USA, (i.e. substituting WINDOW-4 used currently) to predict the heat transfer coefficient across different forms of fenestration systems. However a more simplified version of the algorithm was needed, as the suggested idea of the glazing system of this thesis will work on the broad band of visible spectral radiation rather than work on monochromatic spectral radiation. For simplicity reasons the clear sky conditions were taken into consideration only.

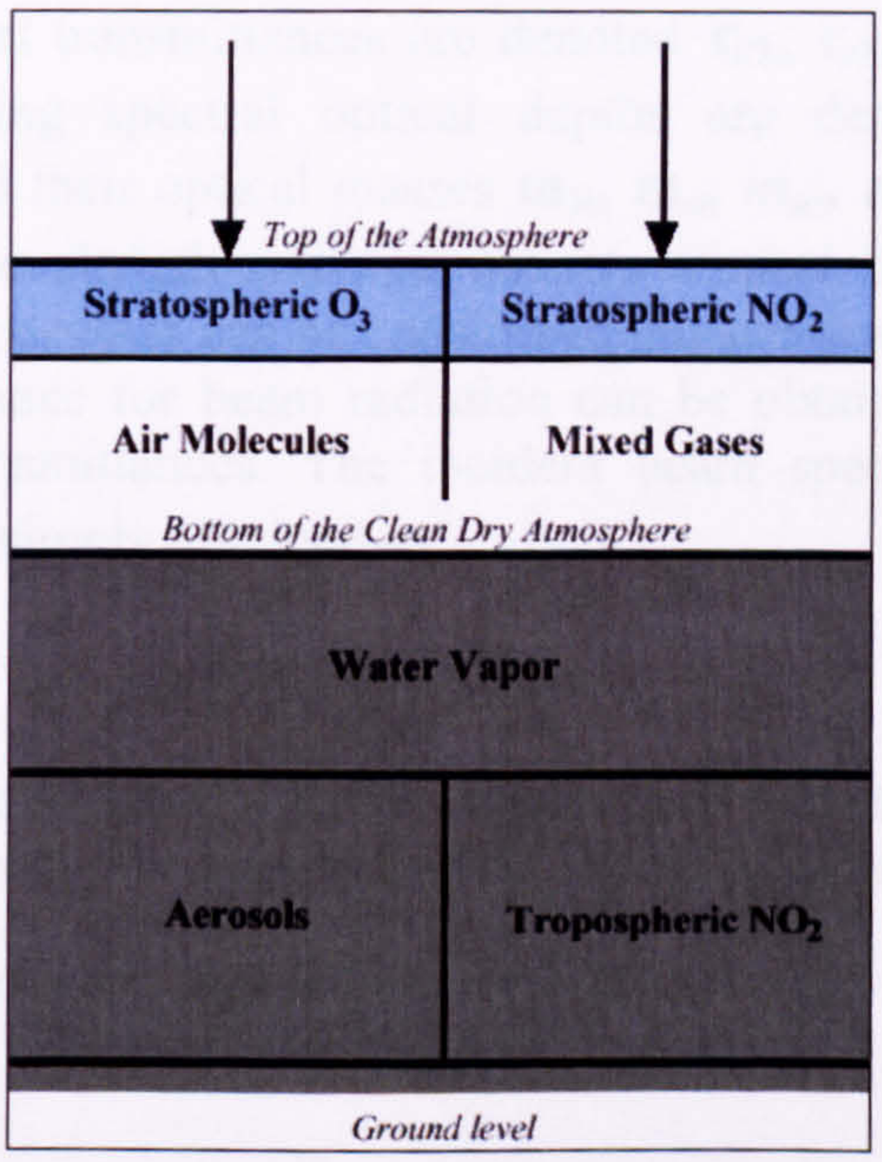

Figure. 2.08 Schematic drawing showing the different extinction layers for the insolation in the atmosphere.

(McCluney R 1996) referred to the main requirements for using the (*SRM*) are:

i. Geographical latitude and longitude.
ii. Day number for the year.
iii. Atmospheric pressure (mbar).
iv. Ambient temperature (°C).
v. Relative humidity %.
vi. Solar altitude (degrees).
vii. Reported or estimated visibility (km).

2.3.1 Model for the solar spectral radiation (i.e. Gueymard algorithm):

The model has already acquired special interest, (Kambezidis H, Muneer T 2004). This model assumes that the atmosphere is schematically considered as a succession of individual extinction layers to the insolation, to simplify calculations; *see fig 2.08*. Each layer alters the spectrum it transmits before it is incident on the next layer along the photon path, e.g. an upper stratospheric layer with O3, NO2 then a Raleigh scattering and mixed gases in the next lower layer of the clean dry strata. Thus, the correct order for all these extinction processes in large spectral bands, and especially for the visual spectrum considered, becomes significant. However, it is important to keep in mind that some effects are not obvious because both altitudinal mixing and spectral overlap occur in the real atmosphere.

Seven individual atmospheric attenuation processes are considered here: Rayleigh scattering, absorption by ozone ($\mathbf{O_3}$), stratospheric and tropospheric nitrogen dioxide ($\mathbf{NO_2}$), uniformly mixed gases (UMG), and water vapor, and extinction (mostly scattering) by aerosols. Following the nomenclature suggested by Horvath (1994),

Their respective spectral transmittances are denoted $\tau_{R\lambda}$, $\tau_{o\lambda}$, $\tau_{ns\lambda}$, $\tau_{nt\lambda}$, $\tau_{g\lambda}$, $\tau_{\omega\lambda}$, and $\tau_{a\lambda}$, their corresponding spectral optical depths are denoted $\delta_{R\lambda}$, $\delta_{o\lambda}$, $\delta_{ns\lambda}$, $\delta_{nt\lambda}$, $\delta_{g\lambda}$, $\delta_{\omega\lambda}$, and $\delta_{a\lambda}$, and their optical masses $\mathbf{m_R}$, $\mathbf{m_o}$, m_{ns}, m_{nt}, m_g, m_w, and m_a. The subscript λ refers to wavelength and thus denotes a spectral quantity. Within narrow spectral regions these processes can be considered independent of each other, so that the total spectral transmittance for beam radiation can be obtained as a direct product of individual spectral transmittances. The incident beam spectral irradiance at normal incidence $E_{bn\lambda}$, is then simply obtained as:

$$E_{bn\,\lambda} = \tau_{R\lambda} \times \tau_{o\lambda} \times \tau_{n\lambda} \times \tau_{nt\lambda} \times \tau_{g\lambda} \times \tau_{\omega\lambda} \times \tau_{a\lambda} \times E_{0n\lambda} \qquad (2.008)$$

Where $E_{0n\lambda}$ is the extraterrestrial spectral irradiance at wavelength λ, at the actual sun-earth distance. Accordingly, the intensity of the normal beam radiation would be:

Using an approach to Bouger's law or Lambert's law:

$$I_{bn\lambda} = S_{sp}\, I_{\varepsilon n\lambda} \exp(-k_{\lambda} m) \qquad (2.009)$$

Where $I_{bn\lambda}$ is the solar irradiance (W/m^2) of direct beam normal arriving at the earth for a broadband value of λ. $I_{\varepsilon no\lambda}$ is the spectral irradiance for mean value of λ entering the

Earth atmosphere. k_λ is the mean chromatic extinction or attenuation coefficient and m is the relative air mass.

S_{sp} is the correction factor for the variation of the sun-earth distance, using (Spencer model, 1971).

$$S_{sp} = 1.00011 + 0.034221\cos(\delta) + 0.00128\sin(\delta) + 0.000719\cos(2\delta) + 0.000077(2\delta) \quad (2.010)$$

Where δ is the sun angle at a particular time of the year. The value of δ is found from the following equation:

$$\delta = 2\pi(n_d - 1)/365 \quad (2.011)$$

Where the n_d refers to the day number during any given year. According to the algorithm of Gueymard (1994); constituents at various processes contribute to depletion of solar energy. These can be quantified by attenuation coefficients $k_{j\lambda}$ Subscript j includes the most important processes which are absorption of incident solar radiation by ozone, mixed gases (**CO, CO_2, O_2, N_2, CH_4** and **NO_2**), water vapour, and scattering by molecules (Rayleigh scattering) or aerosols (Mie scattering). Thus the final extinction coefficient or absorptive transmissivity τ_λ can be given by the equation:

$$\tau_\lambda = exp\left[-(k_{r\lambda}m_r + k_{a\lambda}m_a + k_{o\lambda}m_O + k_{g\lambda}m_g + k_{w\lambda}m_w + k_{n\lambda}m_n)\right] \quad (2.012)$$

Where the indices **r, α, o, g, w** and **n** respectively refer to Rayleigh and Mie scattering, absorption due to ozone, mixed gases, water vapour and NO_2.

- **Rayleigh scattering:**

Rayleigh's theory assumes that all scattering particles are spherical shape. They scatter independently of each other, for each should have a size less than **0.2λ** in diameter. Rayleigh scattering occurs usually when $\pi D/\lambda < 0.6/\eta$, D here is the diameter of the air molecules, λ is the wave length (μm) and η is the refractive index.

An approximation value for $k_{r\lambda}$ was derived by (Leckner 1978):

$$k_{r\lambda} = 0.008735\lambda^{-4.08} \quad (2.013)$$

This is applicable for the standard sky conditions such as the US Standard Atmosphere (1976). For Rayleigh scattering, Gueymard (1994) gave m_r for different incident solar angles as:

$$m_r = \left[\cos z + 1.76759\times10^{-3}\, z(94.37515 - z)^{-1.21563}\right]^{-1} \quad (2.014)$$

Where z is the solar zenith angle in degrees. More detail can be added to the formula if the local atmospheric pressure p (mbar) is to be added in relation to P_0 the reference pressure (1013.25mbar), i.e. not at sea level. The final optical transmissivity with Rayleigh scattering $\tau_{r\lambda}$ can be given in the equation as:

$$\tau_{r\lambda} = exp(-m_r k_{r\lambda} p/p_0) \quad (2.015)$$

- **Aerosol (Mie) scattering:**

The scattering process is identical in the forward and the backward directions, however Mie scattering occurs predominantly in the forward direction. Ångström (1929:1930) was the first to state that a single formula could be used for air molecules, which are within the range of $0.6/\eta < \pi D/\lambda < 5$. In the Ångström turbidity formula, the extinction coefficient of the aerosol is:

$$k_{\alpha\lambda} = \beta\lambda^{-\alpha} \tag{2.016}$$

β is called Ångström's turbidity coefficient varying in the range of 0-0.5, and α is the wavelength exponent with a typical value of 0.5-2.5. A value of **1.3** is usually taken according to empirical data for a range of atmospheric conditions examined by Ångström:

Gueymard (1994) then linked the correlation with a model for m_α, which is for air mass other than of unity in which:

$$m_\alpha = \left[\cos z + 4.29452 \times 10^{-4} z(92.24849 - z)^{-1.2529} \right]^{-1} \tag{2.017}$$

By using a correlation for β that has been given by (McClatchy and Selby 1972):

$$3.912/vis - \beta = 0.55^{\alpha}(0.01162)[0.024729(vis - 5) + 1.132] \tag{2.018}$$

vis here is the visibility in the horizontal direction in km, and a Standard value of α is **1.3** is used. The table below shows values for ***vis*** for given atmospheric conditions (Iqbal 1983):

Then $\tau_{\alpha\lambda}$ is estimated from the equation:

$$\tau_{\alpha\lambda} = exp[-m_\alpha \beta\lambda^{-\alpha}] \tag{2.019}$$

- **Absorption by ozone:**

The spectral transmission for ozone $\tau_{o\lambda}$ is expressed in the formula:

$$\tau_{o\lambda} = exp[-(k_{o\lambda} m_o \{l_o/1000\})] \tag{2.020}$$

Here the total ozone column in the atmosphere ***lo*** (milli-atom-cm) is taken form *equation (2.020)* and m_o are respectively obtained from the following model:

$$mo = \left[\cos z + 1.07489 \times 10^{-2} z(96.62667 - z)^{-1.3882}\right]^{-1} \tag{2.021}$$

Table 2.04 coefficients for different aspects of the atmosphere

Atmospheric Conditions	α	β	***Vis* (km)**
Clean	1.3	0	340
Clear	1.3	0.1	28
Turbid	1.3	0.2	11
Very turbid	1.3	0.4	≤5

Though the Gueymard model is originally supposed to work with the visible wavelength; it seemed appropriate however to include all the effects of the ozone absorption in the model. Considering the fact that ozone absorbs strongly in the ultraviolet waveband, moderately in the visible band and only weakly in the near infrared band. This depends on the temperature, i.e. ***T(K)***, $k_{o\lambda}$ is obtained the following formulation of Smith et al. (1992):

$$k_{o\lambda}(T_{eo}) = max\left[0, k_{O\lambda}(T_{ro}) + C_1(T_{eO} - T_{rO}) + C_2(T_{eO} - T_{rO})^2\right] \qquad (2.022)$$

T_{eo} here can be obtained from the formula: $T_{eo}=a_0+a_1T$ where (a_0=**332.41K**, a_0= **-0.34467** for summer; a_0= **142.68K**, a_1=**0.28498** for winter). For any other given temperature rather than the reference temperature T_{ro}, $\mathbf{C_1}$ & $\mathbf{C_2}$ are the absorption coefficients of the ozone which can be calculated from the following, depending on absorption of the UV wavelength band in three perpetual layers of ozone:

$$C_1 = (0.25326 - 1.7253\lambda + 2.9285\lambda^2)/(1 - 3.589\lambda) \qquad \lambda<310nm \qquad (2.023)$$

$$C_2 = (9.6635\times10^{-3} - 6.3685\times10^{-2}\lambda + 0.10464\lambda^2)/(1 - 3.6879\lambda) \qquad \lambda<310nm$$

$$C_1 = (0.39626 - 2.3272\lambda + 3.4176\lambda^2)/(1 - 3.5\lambda) \qquad 310\leq\lambda\leq344nm$$

$$C_2 = (1.8268\times10^{-2} - 0.10928\lambda + 0.16338\lambda^2)/(1 - 3.5\lambda) \qquad 310\leq\lambda\leq344nm$$

T_{ro}=228K is the reference temperature for the wavelength range of 344-560nm k_o* is a function of T_{ro} in the following equation:

$$k_{o\lambda}(T_{eo}) = max\left\{0, k_{o\lambda}(T_{eo})[1 + 0.0037083(T_{eo} - T_{ro})e^{28.04(0.4474-\lambda)}]\right\} \qquad (2.024)$$

- **Absorption by mixed gases:**

The gases causing further absorption in the atmosphere (i.e. mainly $\mathbf{O_2}$ and $\mathbf{CO_2}$) are uniformly mixed and their relative parameters remain constant with the altitude. (Pierluissi & Tsai 1986, 1987) had derived a formula to calculate their transmittance as:

$$\tau_{g\lambda}=exp[-(k_{g\lambda}l_g m_g)^c] \quad (2.025)$$

Gueymard (1994) defined the equation for m_g for different zenith angles as:

$$mg=[\cos z+1.76759\times10^{-3}\, z(94.37515-z)^{-1.21563}]^{-1} \quad (2.026)$$

$$lg=C_0(p/p_0)c_1\theta c_2 \qquad \theta=288.15/T \quad (2.027)$$

C_0=4.9293km, C_1=1.8849, C_2=0.1815 for O_2

C_0=4.8649km, C_1=1.9908, C_2= -0.697 for CO_2

For simplicity reasons the assumption (Gueymard 1994) was made that the atmosphere l_g consists of pure O_2 for wavelengths below **1μm**. For longer wavelengths l_g is computed with the assumption that the atmosphere consists only of CO_2 (i.e. depending on the fact that CO_2 absorbs mainly in the infrared zone). **C=0.5641** for **λ<1μm** and **C=0.707** for **λ≥1μm.**

- **Absorption by water vapour:**

For water vapour (Pierluissi et al 1989) suggested the following expression for the water vapour transmittance:

$$\tau_{w\lambda}=exp-[k_{w\lambda}(m_w l_w)^{1.05} f_w^n B_w]^C \quad (2.028)$$

Where m_w can be obtained by Gueymard (1994):

$$m_W=[cos\, z+4.29452\times10^{-4}\, z(92.24849-z)^{-1.2529}]^{-1} \quad (2.029)$$

l_w (in cm) can be obtained from the equation described by (Wright et al1989):

$$lw=exp(0.07T_{dewpoint}-0.075) \quad (2.030)$$

C and n are wavelength dependent exponents and B_w is a correction factor for the absorption process. They are obtained as follows:

$$C=0.53851+0.003262\lambda+1.5244e^{-4.2892\lambda}$$
$$n=0.88631+0.025274\lambda-3.5949e^{-4.5445\lambda} \quad (2.031)$$

$$B_W=f\, exp(0.1916-0.0785m_W+4.706\times10^{-4}m_W^2)$$

$$f=0.624m_W l_W^{0.457} \quad \text{for} \quad k_{W\lambda}<0.01$$

$$f=(0.525+0.246m_W l_W)^{0.45} \quad \text{for} \quad k_{W\lambda}\geq0.01$$

$k_{w\lambda}$ here is the spectral coefficient for water vapour. Remaining coefficients for *equation (2.032)* can be taken as follows:

$$f_w=A_w[0.394-0.26946\lambda+(0.46478+0.23757\lambda)p/p_0] \quad (2.032)$$

where A_W=1 for $\lambda\leq0.67\mu m$, or

$$A_W=(0.98449+0.023882\lambda)l_w^q,\ q=-0.02454+0.037533\lambda$$

- **Absorption by NO_2:**

As in ozone the transmittance is computed as follows (Gueymard C 1994):

$$\tau_{n\lambda} = exp[-(k_{n\lambda} l_n m_n)] \tag{2.033}$$

According to (Gueymard 1994)

$$m_n = \left[\cos z + 8.47\times10^{-3} z(96.62667 - z)^{-1.3882}\right]^{-1} \tag{2.034}$$

l_n is the total column of NO_2 in the atmosphere (atom-cm) with typical value of 1.66×10^{-3} (atom-cm) according to (Schröder & Davies 1987) so:

$$k_{n\lambda}(T_{en}) = max\left\{0, k_{n\lambda}(T_{rn})\left[1+(T_{en}-T_{rn})\sum_{i=0}^{5} f_i\lambda^i\right]\right\} \tag{2.035}$$

With definition of reference temperature as shown. For values of $\lambda<625$ nm:

f_0=0.69773, f_1=-8.18290, f_2=37.821, f_3=-86.136, f_4=96.615, f_5=-42.635 otherwise:

f_0=0.03539, f_1=-0.04985, f_2=f_3=f_4=f_5=0.

- **Gathering the model**

Following up the equations given above, the basic equation to include all the constituents of the atmosphere is for a single λ or working on **1nm** resolution:

$$I_{Bn\lambda} = SI_{En\lambda}\tau_\lambda = SI_{En\lambda}\tau_{r\lambda}\tau_{\alpha\lambda}\tau_{o\lambda}\tau_{g\lambda}\tau_{w\lambda}\tau_{n\lambda} \tag{2.036}$$

While for the entire wavelength region of $300nm \le \lambda_1 \le \lambda \le \lambda_2 \le 1700nm$:

$$I_{Bn} = \sum_{\lambda=\lambda}^{\lambda_2} I_{Bn\lambda} = S\sum_{\lambda=\lambda_1}^{\lambda_2} I_{Eon\lambda}\tau_{r\lambda}\tau_{\alpha\lambda}\tau_{o\lambda}\tau_{g\lambda}\tau_{w\lambda}\tau_{n\lambda} \tag{2.037}$$

Points to be taken in favour of this model:

(i) Comprehensive detailing in simulation of the constituents of the atmosphere.

(ii) By using continuously updated information on the atmosphere, it has the versatility to be applied in different locations.

(iii) Ability to simulate the incident irradiation on a wavelength by wavelength basis or within a customised wavelength band in the visible spectrum. Such feature is useful upon checking the performance of special types of glazing (i.e. selective or special reflective types), or to calculate the scattering effects of various constituents of the atmosphere.

(iv) Accuracy of the simulation of the terrestrial radiation by taking the relative solar geometry, location and elevation into consideration (i.e. incident angle dependent).

(v) Detailed account of albedo radiation, diffused radiation, etc., making it useful in calculating separately the insolation components.

Points to be taken into consideration when using the model:

(i) The model tends to return high values at low solar altitudes when using some of the air mass and transmission models, (*although this was modified in a later version by integrating over more than one turbidity factor to give more accuracy*).

(ii) Some albedo calculation files would return a fixed value for all wavelengths exceeding a certain limit, i.e. 900nm, thus affecting accuracy in the calculation of spectra surface/ ground reflection.

(iii) The difficulty in supplying all the necessary input data (i.e. the model is not user friendly).

(iv) As the model is more of an empirical approach, it depends to a great extent on the accumulation of gathered at each stage data, before implementing the output values into to the next step. Such approach could have both its own advantages and disadvantages, on the level of accuracy obtained.

2.2.2 Model for the diffused and the direct beam Insolation of wide band wavelengths:

(Grindley C.1995) introduced this theoretical model and validated the hypothesis against gathered data. The mathematical model works on the theory of successive reflections (Lacis A. & Hansen E. 1974)and transmissions through an atmosphere consisting of layers of "mixture of grey gases and suspended particles" that are varying in thickness, density and of infinite lateral extent.

As the Earth is of a great distance from the sun, the incident non-scattered radiation is a parallel beam. So assuming properties for uniformly absorbing grey gas in terms of radiative heat transfer, and considering the intensity for a monochromatic beam of radiation incident on a layer of thickness **dx**. It can be said that radiation transmitted through the layer can be calculated by assuming a coefficient of attenuation for this purpose:

$$dI_\lambda = -k_\lambda I_\lambda dx \qquad (2.038)$$

k_λ= the monochromatic attenuation coefficient and assuming the equation can be integrated over the distance range of (**0~*x***); therefore:

$$\int_{I_{\lambda o}}^{I_{\lambda x}} \frac{dI_\lambda}{I_\lambda} = -\int_o^x k_\lambda dx \qquad (2.039)$$

Therefore:

$$\frac{I_{\lambda x}}{I_{\lambda o}} = e^{-k_{\lambda x}} \qquad (2.040)$$

So the optical transmittance of the medium can be defined as:

$$\tau_\lambda = e^{-k_\lambda x} \tag{2.041}$$

While for the absorption as in grey gas applications:

$$\alpha_\lambda = 1 - \tau_\lambda$$

Unlike other complex models (i.e. Gueymard 1994), this model deals with the absorption of incident solar radiation that is selectively dependent upon wavelength and upon the different levels of non-homogenous atmosphere; in a simpler way to avoid uncertainty in inherent results. It uses the broad band selectivity for the clear-sky atmosphere as a model, thus:

$$\tau = \mathbf{e}^{-k m_z} \tag{2.042}$$

With multiple scattering likely to happen in each unit layer of the atmosphere, which are dependent on wavelength and angle of incidence. It can be said that portion of the radiation will be reflected while other portion will be back scattered. Thus taking such probability; and assuming that half of the intensity of the incident radiation scattered will be reflected backwards to the atmosphere and half downwards, it can be said that the probable absorptivity ρ after N successive scattering will be:

$$\alpha_b = (1-2\rho)^N - e^{-k m_z} \tag{2.043}$$

So it can be said that for the transmittance of normal beam:

$$\tau_b = (1-2\rho)^N - \alpha_b \tag{2.044}$$

While the diffuse component can be given by:

$$\tau_b = (\rho)^N - \alpha_d \tag{2.045}$$

The global horizontal transmittance is given by:

$$\tau_g = \tau_b + \tau_d \tag{2.046}$$

Incident on a unit layer thickness of atmosphere, (Grindley C. 1995) stated that probability would be that **3-4%** of the incident solar radiation would be scattered. (This assumption is taken for higher altitudes, as the present exercise is looking into checking that probability), taking the multiple scattering up to four successive scattering (as the effect of further scattering will be marginal. Estimated clear-sky transmittance at normal incidence will be:

$$\begin{aligned} \tau_b &\approx 0.867 - \alpha_b \\ \tau_d &\approx 0.068 - \alpha_d \\ \tau_g &\approx 0.935 - (\alpha_b + \alpha_d) \end{aligned} \tag{2.047}$$

Resultant albedo was taken as 6.5% and 6.9% (Houghton J. T. 1986). Raleigh scattering effect was taken into consideration though it involves only **8.03%** of the total energy of the extraterrestrial solar radiation (*see 4.2.2*) and with similar small absorption in the

infrared part. (I.e. **1%** though when it compared with the total share of the infrared to the solar constant 46.4%, it is significant). Thus it can be said that the broadband absorptivity integrated for the visible will be relatively small:

$$\alpha_b \approx 0.037 \tag{2.048}$$

Reflectivity therefore can be expressed in relation to the solar zenith angle (Lacis & Hansen 1974):

$$\rho = \frac{0.28}{(1+6.43\cos\theta_z)} \tag{2.049}$$

The simple broad model can be taken therefore to:

$$\tau_{gm_r} = Ae^{-c\rho\alpha m_r} \tag{2.050}$$

So for relative air mass m_r:

$$\tau_{gm_r} = \frac{I_g}{I_0} \tag{2.051}$$

A is scaling factor, for the transmittance of radiation in a clear atmosphere with an air mass of unity at standard conditions. $c_{\rho\alpha}$ is the attenuation factor of depletion of the incident radiation by the whole atmosphere, (i.e. both reflectivity and absorptivity due to scattering). It can be defined as:

$$c_{\rho\alpha} = f(\rho + \alpha_b) \tag{2.052}$$

On the assumption that atmospheric albedo for back scattering for the short wave is equal to the one in the forward direction in clear sky conditions (Kimball 1932):

$$\tau_g + \tau_d + (\alpha_d + \alpha_b)m_r = 1 \tag{2.053}$$

As assuming Rayleigh clear-sky boundary condition, value of coefficient A can be calculated for *equation (2.050)*:

$$A = 1 - [m_r(\alpha_b + \alpha_d) + \rho] \tag{2.054}$$

The above equation is for clear-sky conditions only:

$$\tau_{gm_r} \approx [\tau - (\alpha_b + \alpha_b\rho)m_r]\mathrm{e}^{[-(\rho+\alpha_b)m_r]} \tag{2.055}$$

The diffuse fraction of the global clear sky irradiance can be given as:

$$\tau_{dm_r} \approx 1 - (Bm_r + \tau_{gm_r}) \tag{2.056}$$

Where:

$$B = \alpha_b + \alpha_d \approx \alpha_b + \alpha_b\rho \tag{2.057}$$

In case of increased scattering due to the presence of water vapour, *equation (4.2.48)* can be amended to:

$$\tau_{dm_r} \approx 1-[m_r(B+\rho)+\tau_{gm_r}] \quad (2.058)$$

The model therefore deal with the effects of excessive water vapour or more aerosol, for coefficients A and $c_{\rho\alpha}$ in equation (44.2.42) can be calculated for two relative air masses as:

$$ln\tau_{gm_r} = ln A - c_{\rho\alpha} m_r \quad (2.059)$$

So for two relative air masses, i.e. say m_{r1} and m_{r2}:

$$\begin{aligned} ln\tau_{gm_r} &= ln A - c_{\rho\alpha} m_{r1} \\ ln\tau_{gm_r} &= ln A - c_{\rho\alpha} m_{r2} \end{aligned} \quad (2.060)$$

The value of $c_{\rho\alpha}$ can be calculated by eliminating ln A, as:

$$ln[{}^{\tau gm_{r1}}/_{\tau gm_{r2}}] = -c_{\rho\alpha}(m_{r1} - m_{r2}) \quad (2.061)$$

Then by giving two values for τ_{gmr1} and τ_{gmr2} for relative air masses, the value of A can be obtained by substituting the resultant of $c_{\rho\alpha}$ in *equation (2.059)*.

Points to be taken in favour of this model:

(i) Ability to give simulation for both the direct beam component and the diffuse part separately or collectively as required.

(ii) By using the updated information on the atmosphere it has the versatility to be applied in different locations.

(iii) Simplicity and user friendly.

(iv) Accuracy of the simulation of the terrestrial radiation and taking all the solar geometry and location into consideration (i.e. incident angle dependent).

Points to be taken into consideration when using the model:

(i) The model was not tested for different latitudes to verify the hypothesis; it has a limitation that it can be used for zenith distances up to **60°** only. That might impair its usage on latitudes where zenith angles exceed that amount.

(ii) Depending on the clear-sky conditions formulas to predict the semi covered or the over cast depending only on the water vapour as part of the relative air mass assumptions.

(iii) The model assumes conditions of ideal turbidity factors, (i.e. size and nature of aerosols); as assumptions to calculate the back scattering of the atmosphere. However, latest calculations showed that this is not valid for all types of weathers, thus limiting the use of the model.

(iv) It assumes that smaller role for the ground albedo in the calculations, e.g. when accounting for the level its contribution to the whole diffused portion (Earth Moon, and-Planets. Vol.68 1995).

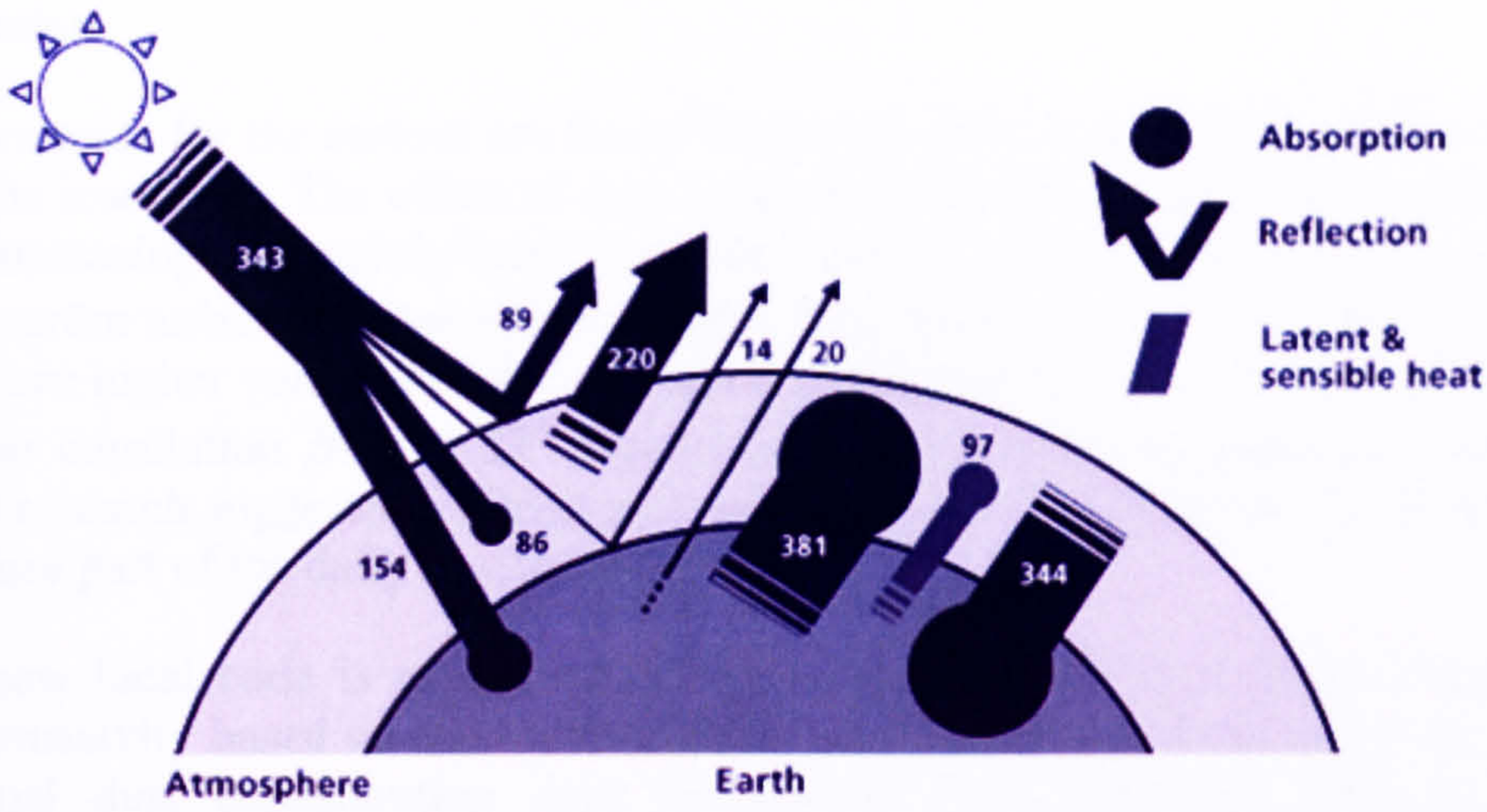

Fig. 2.09 Schematic drawing showing the energy flow generated by the solar radiation averaged over the surface of the whole planet at any given time. (FAE 2005)

Discussion

The solar spectrum compromises several distinctive bands of wavelengths: A small band of UV radiation (0.28-0.4 μm) which comprises about **2%** of the solar spectrum, visible light which range from (0.4 to 0.78 μm) and accounts for around **49%** of the spectrum and finally of infrared radiation with long wavelength (0.78-3.0 μm), which makes up most of the remaining **49%** of the solar spectrum. Figure 2.09, shows an example of the energy flow generated by the overall interaction of the extraterrestrial radiation with the Earth atmosphere, i.e. multiple scattering, reflection, absorption and remission; (FAE 2005).

Any trial to calculate the amount of incident irradiation reaching the Earth surface has to go through detailed study of the effects of the constituents of the atmosphere.

Many studies have been devoted to work the role of those factors individually, collectively and their interactive role in attenuating the incident solar. Empirical and theoretical models were derived to calculate the diffuse portion of the insolation, which is a resultant of the successive scattering and absorption that the extraterrestrial insolation undergoes upon entering the atmosphere.

Derived solar models vary in nature according to their level of accuracy, detailed output, localised conditions, type of atmosphere, and the type of application needed for. Thus, e.g. Broad band and Hourly Horizontal irradiation and illuminance models, which rely in their accuracy on the availability of corresponding horizontal global and diffuse energy data, may not be adequate as a tool to estimate the different insolation components on a sloped surface. It also indicates that solar models, which use sky clarity indices model might not be adequate for latitudes which has clear sky most of the year and clouds cover do not constitute the governing factor. For such conditions a spectral solar model for clear sky conditions would be more adequate especially if the needed empirical atmospherical data could be provided. It would also be more accurate to estimate separately the different constituents of solar radiation incident on the tilted surface of glazing.

Conclusion

- More roles for the aerosol are found by the research in the scattering and absorption of the insolation. The effect of dust as aerosol is highlighted in this section showing its increasing role mainly due to increased rate of industrial and ecological pollution. Ångström turbidity factor and β absorption coefficient to the wavelength were found to have higher values than the average (i.e.**0.3**) usually taken in other altitudes. The linear correlation $\beta=\alpha +\Delta T^{o}$ was found to have more dependence on time factor. The research suggested a bigger role to be given to dust as aerosol in calculating the diffuse part of the daily irradiation.

- A new local code is suggested by the research for Aerosol (Mie) scattering and tranmissivity based on the local turbidity conditions, calculated from the empirical annual dust concentration data for Kuwait 1996. Through using a modified Ångström's turbidity coefficient, which was shown to have higher values than the normal range. Modified α_1, α_2 and eventually modified β were also suggested, details of the code are discussed in details in *chapter 4*.

- The research analysed different solar models; though each of the investigated models had its own advantages and disadvantages, yet the research took the decision to adopt Gueymard algorithm as a base for the insolation model for the following reasons:

  (i) It is updated periodically by the author, with added refinements to the low insolation angles that creates uncertainty in results in most of the relevant models.

  (ii) Having extensive level of detailing for the atmospheric constituents, it provides the opportunity to apply local weather files conditions with more accuracy.

  (iii) The model is currently used a base for WINDOW-5 software, which is adopted by the National fenestration rating standard USA.

  (iv) A basic code was obtained (with the author permission) that would be used, thus saving time for other stages of the research.

  (v) Though that both models can predict a direct radiation component that can be calculated for both vertical and horizontal surfaces. Still, Gueymard's algorithm delivery of spectra calculation can better predict the values for both of the ground albedo and the diffused components, which are essential to account for all the real time contributors to the radiation incident on glazing surfaces.

REFERENCES

1. AL Jamal K., Quinn M., Jarrar D, Shaban N, Yagoub Y & D'Sousa J; Dust effect on infrared sky radiation in Kuwait. Solar and Wind technology 1984; I (2): 109-114.

2. Alterio S, Barbaro S, Cannistraro G, Giaconia C, Orioli A, Trapani S, A more reliable between Angstrom & Linke atmospheric turbidity parameters, Solar & Wind-Technology 1989; 6(3): 253-5.

3. Anderson Robert S., Hallet Bernard, Sediment transport by wind: towards a general model. Geological society of America Bulletin 1986; 97(5): 523-535.

4. Angstrom A, on the atmospheric transmission of sun radiation on dust in the air. Geografiska Annaler 1929; 2:156-165.

5. Berger X., Cublizolles B., report no. 26, L'aboratoire D'Ecothermique, Centre National de La Researche Scientifique, France 1992.

6. Duffie john A, Beckman W. A., solar engineering of thermal processes, USA: Wiley Inter-science, 1991.

7. Earth, Moon, and-Planets. Journal 1995; 68(1-3): 385-388.

8. Enviroene. United States Environmental Protection Agency, 1996-1997. See also: http://es.epa.gov/techinfo/facts/

9. Foundation for Alternative Energy (FAE), Slovakia 2005, "Solar Energy" Dieret website See also: http://www.fae.sk/Dieret/Solar/solar.html

10. Grindley P.C, Batty W. J, Probert S.D. mathematical model for predicting the magnitudes of total, diffuse and direct beam Insolation. Applied Energy 1995; 52:89-110.

11. Grindley P.C, mathematical model for predicting the magnitudes of total diffuse, and direct-beam insolation, A PhD. thesis 1995. Cranfield University. p.140-152.

12. Gueymard C., an anisotropic solar irradiance model for tilted surface and its comparison with selected engineering algorithms. Solar energy 1999 38: 40.

13. Gueymard C., simple model of the atmospheric radiative transfer of sunshine (SMART2): algorithms and performance assessment. Rep no. FSEC-PF-270-94, cocoa, FL, Florida solar energy centre, 1994.

1. Houghton J. T, the physics of the atmospheres. Cambridge: Cambridge University press, 1986.

2. Hutchinson M F, Booth T H, McMahon L P, and Nin, H A Estimating monthly mean values of daily total solar radiation for Australia. Solar Energy 1984; 32: 277-90.

3. Iqbal M, an introduction to solar radiation. Toronto, New York: Academic press 1983.

4. Joint Research Centre: JRC, EUROPA, Commission of European Countries, *CEC*, the GIS solar project 2003. See also: http://iamest.jrc.it/pvgis/pv/solmod/solmod0.htm

5. Kambezidis H, Solar spectral radiation, chapter 5. In: Solar radiation & Daylight Models. Editor: Muneer T, Oxford: Architectural press, 1997.pp156-162.

6. Kerschgens M; Raschke E, ReuterU. The absorption of solar radiation in model atmospheres. Contributions-to-Atmospheric-Physics1976; 49 (2): 81-97.

7. Kocifaj-M, Theory of optical identification of sub-micron particles in high atmosphere, NY: Elsevier Publishing. 1980.

8. Lacis A. & Hansen E. a parameterisation for the absorption of solar radiation in the Earth's Atmosphere. Journal of Atmospheric science 1974; 31:118-132.

9. Lecture 6, Department of Meteorology, San Jose State University, California/ USA 2003. See also:

www.met.sjsu.edu/-steffens/SPRING05/MET10/Lecture6.ppt

10. Li- X, Maring- H, Savoie-D; Voss-K, Prospero-JM, dominance of mineral dust in aerosol light-scattering in the North Atlantic. Nature 1996; 380(6573): 416-419.

11. Loxom F., Meteorological data for passive-solar design. Collection of reports-ETSU model-refinement study, Environment Dept., Central London Polytechnic, 1985– 86.

12. Majumdar NC, Kanshik SB, Mathur BL, Prediction of direct solar radiation for low atmospheric turbidity. Solar-Energy 1972; 13(4): 383-94.

13. McCluney R, fenestration solar energy gain analysis, Rep. no. FSEC-GP-65, cocoa, FL, Florida solar energy centre, 10 October 1996.

14. McCluney R, sensitivity of fenestration solar gain to source spectrum and angle of incidence. ASHRAE TRANS. 1996; 102(2): 112-122.

15. Muneer T., solar radiation & daylight models for the energy efficient design of buildings, London:Elsevier. 2004

16. Perez R., Ineichen P, Seals R. modelling daylight availability and irradiance components from direct and global irradiance. Solar energy 1990; 44: 271-276.

17. Ranagarajan-S; Mani-A, A new method for the determination of atmospheric turbidity, Chemical-and-Physical-Meteorology. 1984; 36B(1): 50-54.

18. Red book: Ozone data for the world, atmospheric environment service, Rep. 33:no.6 Downs-view, Ontario Canada, 1992.

19. Sayigh A.M, Mcveigh J.C, solar air conditioning and refrigeration, London: Pergamon press, 1995.

20. SBIC guideline and software. Washington DC: Sustainable building Industry council, 2003. See also: http://www.sbicouncil.org/soft/index.html.

21. Zelenka A, Czeplak G, D'Agostino V, Josefson W, Maxwell E and Perez R. Techniques for Supplementing Solar Radiation Network Data,. Technical Report, International Energy Agency, Report no. IEA-SHCP-9D-1, Switzerland1: Swiss Meteorological Institute, 1992.

CHAPTER THREE

GLAZING SYSTEMS

Introduction

Glazing materials are at the core of any fenestration system. Their thermal and optical properties are used to assess the performance of any window system as a whole. Specific terminology is used to describe glazing materials.

Optical materials or semi transparent materials are not always considered as grey objects (see sec.2.1.3) as unlike grey objects, the emittance varies with wavelength. Their main properties of interest are the *transmittance*, *reflectance*, and *absorptance*. These quantities are distinguished from the related quantities: *transmissivity*, *reflectivity*, and *absorptivity*. The *"-ivity"* ending refers to the inherent properties of a volume or bulk sample of the material. The *"-ance"* ending refers to the property of a specific thickness or sample of a substance or a combination of substances.

In 1927, Fresnel developed a formula for calculating the interface reflectivity of transparent media such as air, glass and plastic by using the refractive index of the media considered. Optical properties decide the amount of transmitted radiation passing through a material. An example is given in *fig 3.01*; it shows how the transmittance and reflectance of a single pane of transparent material vary with the angle of incidence.

Optical properties like transmissivity, reflectivity and absorptivity may not necessarily have the same value on both sides of a given sample. Accordingly, optical materials can be defined in two types in relation to their properties (i.e. reflectance and transmittance):

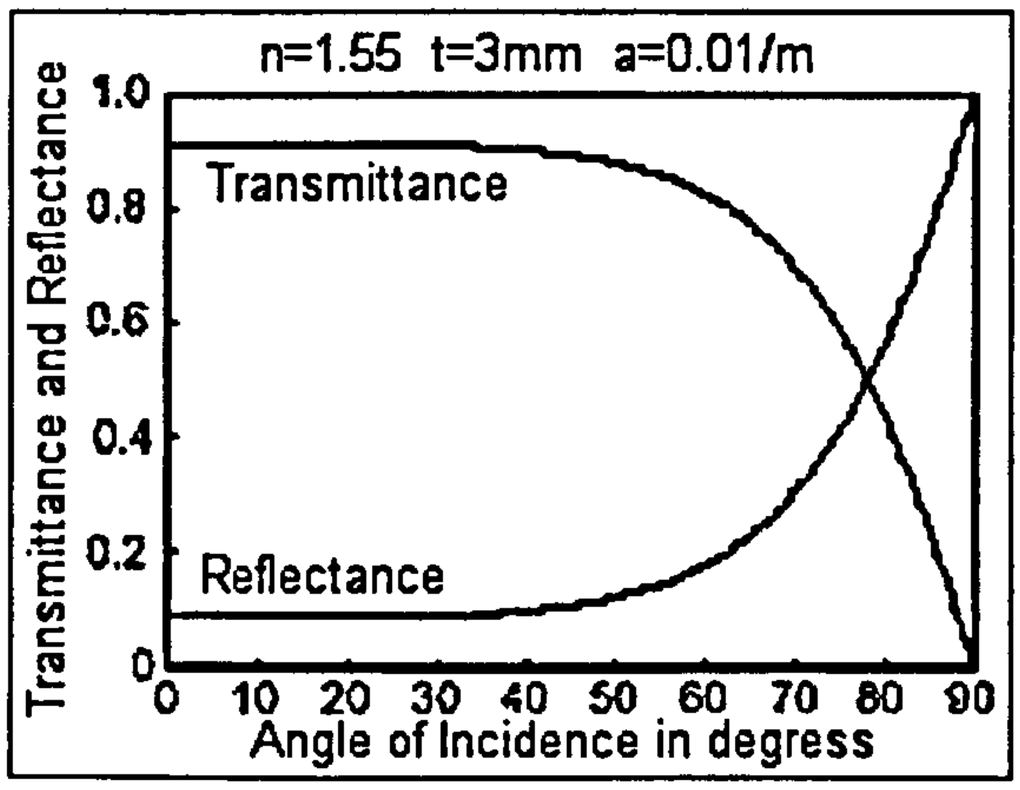

Figure 3.01 Fresnel transmittance and reflectance of a plane parallel to a plate of glass. n = refractive index, t = thickness, a = absorptivity (McCluney R.1994).

(i) Spectral optical properties, which relate to incident parallel beams of radiation, reflected and transmitted according to the laws of geometrical optics (i.e. Snell's law).

(ii) Asymmetrical optical properties displaying a strong scattering effect of their surfaces, and uneven reflecting and transmitting mechanism for the incident radiation. Such materials also exhibit strong absorption at the same time.

3.1 CURRENT TYPES OF GLAZING SYSTEMS

The widespread utilisation of solar energy in different applications has led to the continual development of durable, optically efficient solar selective surfaces. Selective coating materials and surfaces means that certain materials are applied to one or more surfaces of a system to control the amount of the transmitted irradiance through that system related to the chosen wavelength bands from the solar spectrum. The applications of solar selective materials vary, however, depending on the function needed, and other factors such as the solar geometry and geographical location. The main methods derived were for:

(i) Passive solar applications in cold climates; where the need is to allow as much solar energy as possible to enter the building through the glazing, and as little long wave transmission as possible to transfer through the window from within the building to the outside. These systems provide low emissivity surfaces that reduce long wave radiant losses from the external surfaces of the glazing to the sky, as also used in solar collectors for producing hot water.

(ii) Reflective applications; where the need is to reflect a large proportion of the incident solar radiation thus preventing excessive gains of solar energy to the internal spaces. In other applications, the reflective surfaces are applied to the internal layer of a solar collector to enhance the reflectivity and to direct the reflected insolation.

(iii) Shading elements, where the need is to minimise the direct component of the insolation coming from certain orientation while allowing diffused light to enter the building. Shading also means absorbing certain wavelength bands within the incident solar radiation, while allowing others to enter the internal space.

(iv) Smart glazing systems, where the need is to develop materials, which react according to different external influences with a reversible colour modification or clouding. Such approaches started recently, (Granqvist, 1990) and are frequently called "intelligent" or "smart windows". Further potential applications are large area displays for information and traffic engineering, as well as temperature sensoring applications in medical technology.

The deployment of selective properties for materials in solar applications started as long ago as the late 1950s (i.e. H. Tabor 1955, Holland 1958). Different methods and materials were derived to achieve the required effects. The main features of the adopted methods and materials were; i.e.] (i) the stability to operate under different temperatures (Agnihotri & Goupta 1981) (ii) the need to be resistant to atmospheric corrosion; and (iii) The economical viability, (i.e. low-cost materials used in large area techniques). The techniques employed varied between the use of transparent conducting materials

such as metals (i.e. to produce heat mirrors), plated or etched coatings, paint coating, gel-materials or films and magnetron sputtering.

The specification of coatings and materials used in these systems varies depending on the applications; some of them (e.g. the solar collectors) were derived so it can absorb all the band of the IR (infrared) with minimum losses (anti-reflecting in the infrared) while still not transmitting in the visible band. The research investigated only those systems relevant to windows and glazing systems to be applied in hot climates.

A primary purpose of windows is not just to provide daylight and a view out of the building, but also to maintain the internal thermal comfort within the space that they enclose. In regions where heating of the internal spaces is the main concern, this means glazing systems that can maintain high visibility reducing or blocking the long wave, infrared range of the electromagnetic emissions from heated internal surfaces. In such systems a large portion of the solar energy in the visible band is allowed to be transmitted through the glazing system. However, in climatic regions where overheating of internal spaces bounded by walls that are highly glazed is a significant danger for much of the year, the visibility is often reduced or sacrificed in favour of reducing the transmitted energy gain to the internal space from the visible region of the incident solar radiation. Two main approaches have emerged to provide selective surfaces:

- Glazing with wavelength selective properties (i.e. chromogenic glazing that selects particular wavelength bands within the spectrum to transmit or reflect).
- Glazing with incorporated angular selectivity (i.e. working on direct or diffused solar irradiation providing a shading element at special angles within the solar geometry). *Fig.3.02* shows the selective transmittance in the visible wavelength band for some types of commercial glazing.

3.1.1 Wavelength spectral selectivity:

The concept of spectral selectivity depends on the fact that a good reflector in one part of the solar spectrum, e.g. the infrared portion, can be a poor reflector and consequently a good transmitter in another part, e.g. the visible portion.

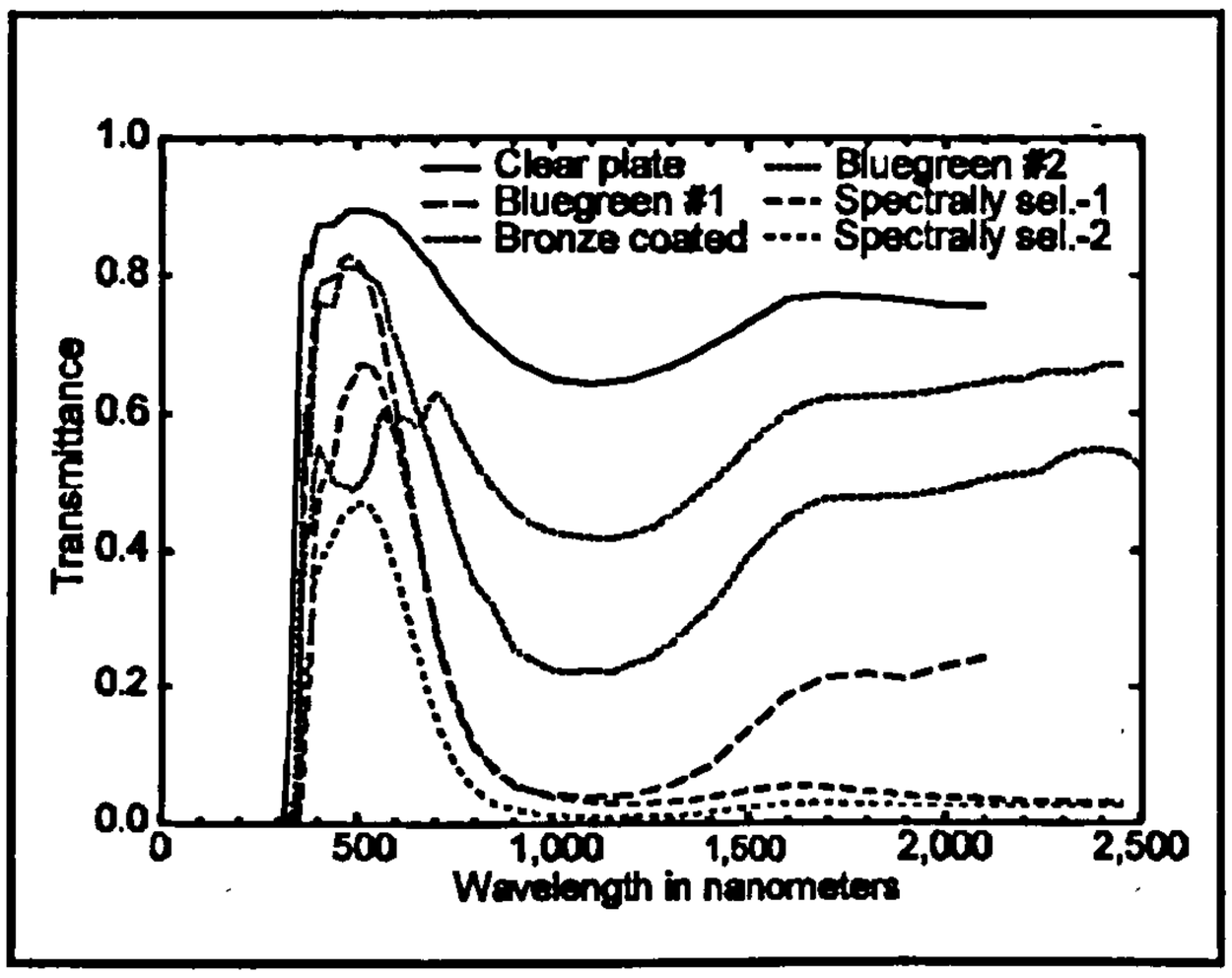

Figure 3.02 Spectral transmittance of several glazing systems (Glaubitt 1998).

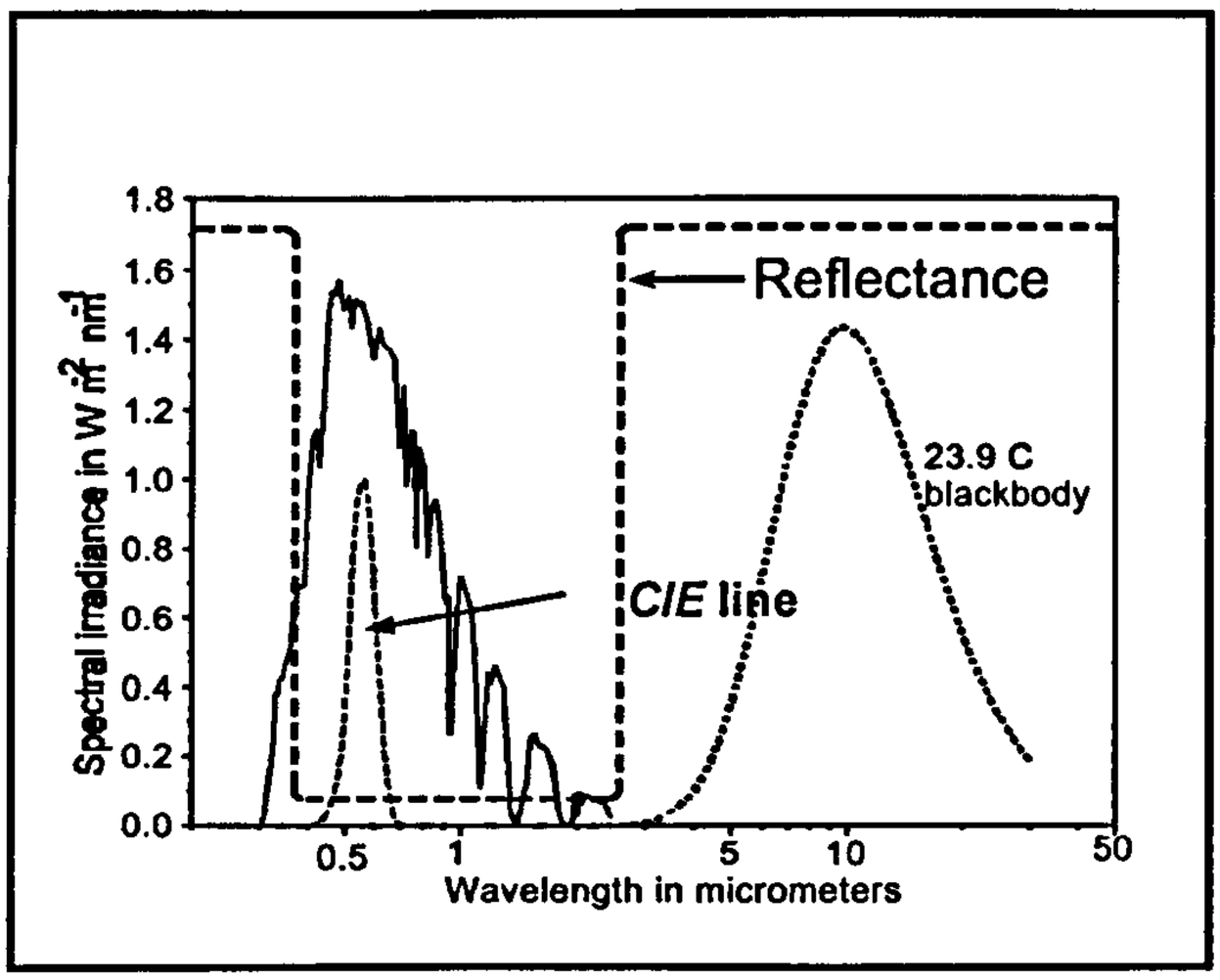

Figure 3.03 An ideal form of spectral selectivity of a coating (McCluney R. 1996)

This principle was adopted for low-*e* coatings on window glass. These had coatings that produced low emissivities and high refelectivities in the infrared.

This was achieved by inserting films with high reflectance and low-emittance in the infrared region on the inner side of the outer pane of a multiple glazing system. In cold climates such a system is useful in reducing the rate of heat losses from the internal space through the glazing. However, for hot climates such a system would be counterproductive and so spectral selectivity had to be adapted to generate glazing systems with relevant performances. (Gombert, Glaubitt *et al* 1998).

Fig 3.03 shows idealised reflectance for a low-e coating film, where the sharp edge of reflectance occurs close to the edge of the visible portion of the spectrum, thus limiting reflectance within the visible band and so maximising the transmittance of the glazing to solar radiation.

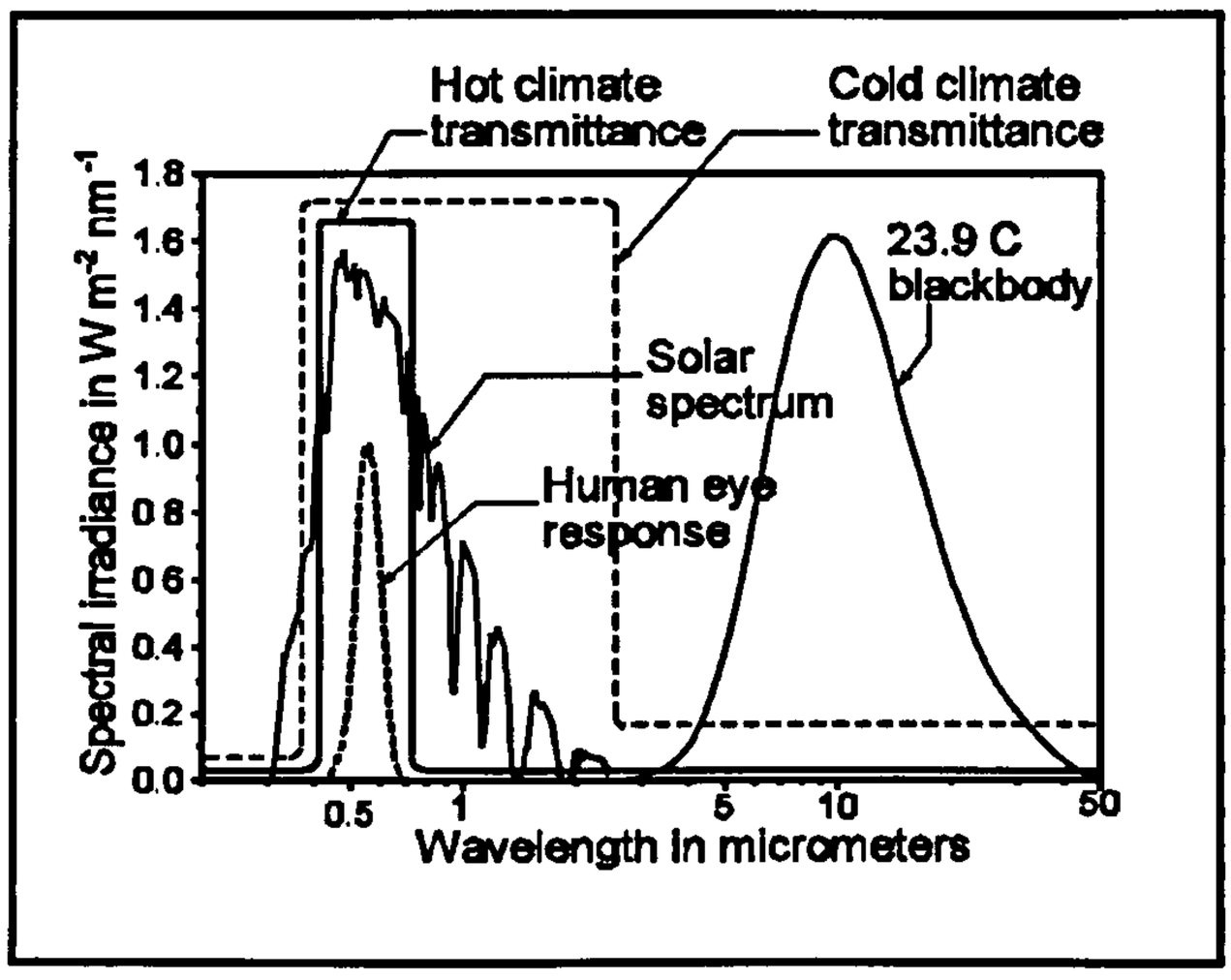

Figure 3.04 Spectral selectivity for hot and cold climates (McCluney R. 1996)

This is further demonstrated in *fig 3.04*; it shows a drop of the transmittance at the longer wavelengths of the visible band. The effect is to reflect the infrared portion and thus minimise the heat gain while maintaining an acceptable transmission for wavelengths below the 800nm. Such an effect is usually achieved by:

(i) High reflectance of the surface to the IR (i.e. infrared) and low absorptance of the visible band.

(ii) It can be also gained by high IR absorptance after insulating the multi-glazing system cavities either by using an insulating gas [usually an inert gas] or an insulated second glazed pane. Usually the coating will have a low emittance over both the near infrared (i.e. near the visible) and the far infrared (i.e. the thermal).

Different methods were introduced to validate the performance of new systems by different manufacturers; *see sec.3.4*.
The main types of the selective wavelength coatings applied to glazing include:

- Optical trapping systems (i.e. one dimensional relief or more), (Gombert, *et al*, 1998); *see fig3.05*.
- The Electro-chromic devices (i.e. ECD) (Seeboth *et al*., 2000); see *fig3.06*.
- The thermo-tropic e.g. Hydrogels and polymer blends, Lyotropic liquid crystalline Hydrogels.
- Composite materials coating (i.e. composite films of small metal particles embedded in dielectric), conductors and semi-conductors application, inorganic and organic paints etc.

Different types of selective glazing have been introduced to the market over time. Consequently a need has arisen to be able to compare and calibrate the performance of such systems

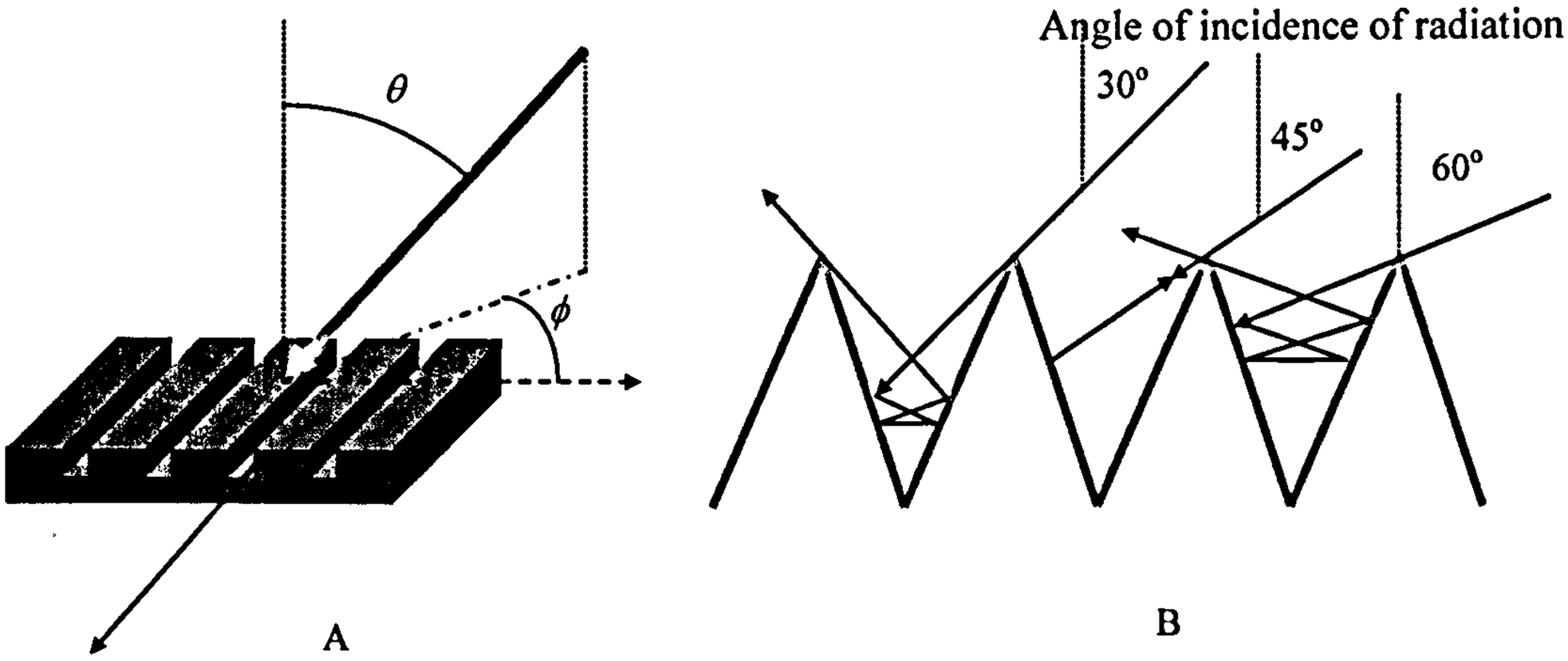

Figure 3.05 A) General incidence on a one-dimensional surface with relief grating. B) Absorption of solar radiation due to successive reflection on V-corrugated surface (Trombe et al, 1961).

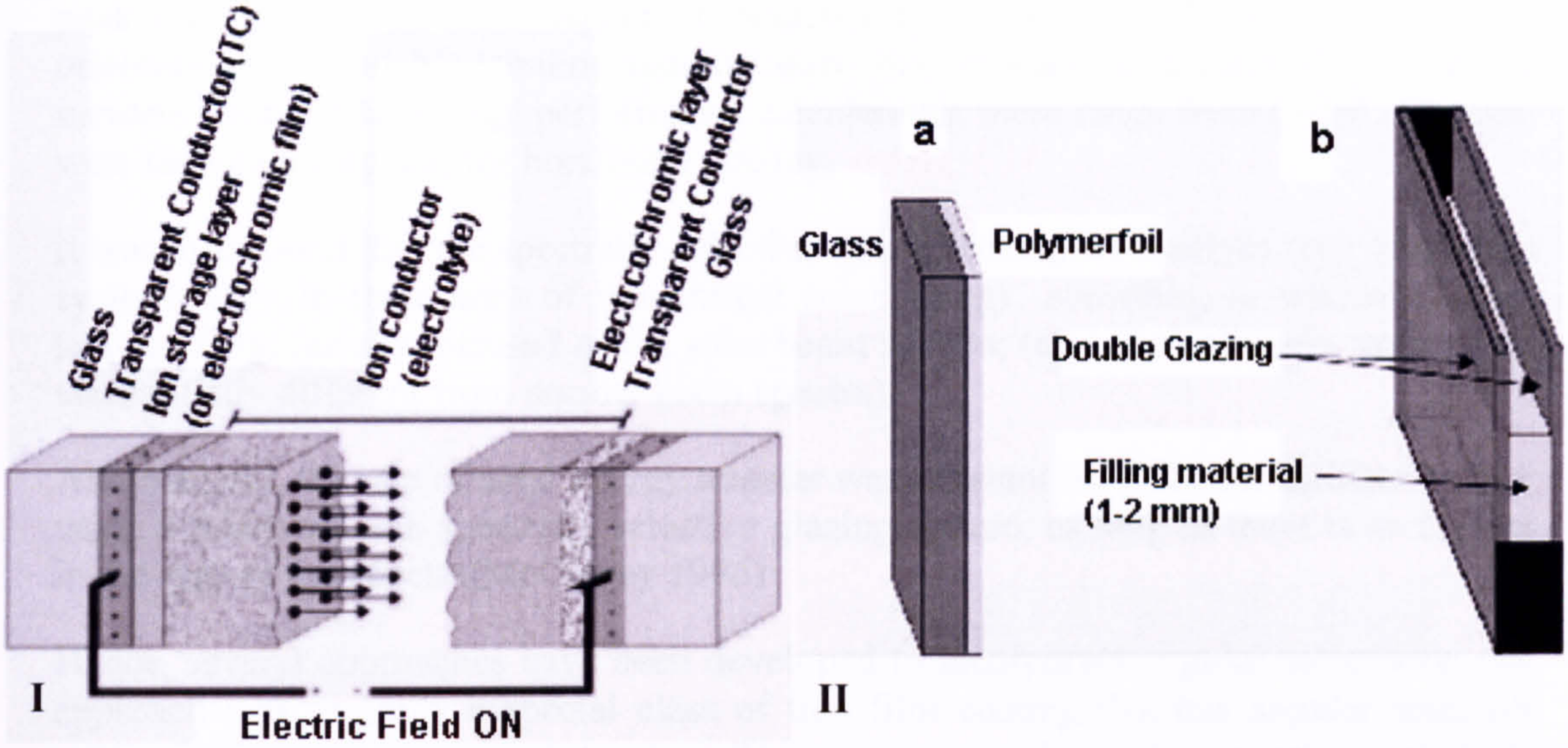

Figure 3.06 (I) Schematic diagram of an ECD with five layers in transmittance mode. With electrical field feed of cations or protons takes place into the electro-chromic layer.

(II) Possible Smart windows: [a] polymer blend [~0.2mm] coated directly onto the glazing. [b] Glazing filled with a thermo-tropic polymer gel; thickness of the layer is 1-2 mm.

The "Shading coefficient"[*Sc.*] was introduced to fulfil this role, *see sec.3.4*. It is defined as the ratio of the solar heat gain coefficient of a glazing system at a particular angle of incidence and incident solar spectrum to that of a standard reference glazing at the same angle and spectral distribution of incidence:

$$Sc = \frac{F(\lambda,\theta)_{\text{Test}}}{F(\lambda,\theta)_{\text{Ref}}} \qquad (3.001)$$

However, the simple relation between the [*Sc.*] and solar heat gain is not sufficient to define easily the shading coefficients for new advanced and complicated glazing systems with angular selective multiple panes and special coating; as those systems don't have the same spectral response as of a single pane of glass (i.e. where optical properties could be calculated from a base ratio). Heat gain calculations cannot be achieved from assessments of the relative bulk samples only.

3.1.2 Incorporated angular selectivity:

Recent technologies in glazing systems are incorporating angular selectivity methods. As reflectivity and transmissivity vary with the change of incidence angle, *see sec.1.7*, the amount of heat gain arising from transmission through a system will depend on direct and diffused solar energy component incident angles. (McCluney 1994), pointed out that transmissivity of glass stays constant for angles between (0-40^{o}), while

peak solar gains in summer happen at incidence angles between (25-55°) for east-west orientations. As such recommendations were put forward to specify the angles of incidence for annual energy performance calculations; these range from (5-80°) for east-west facing glazing and for horizontal glazing, *see fig 1.14*.

It was also found that the spectrally selective (i.e. wavelength selective) type of glazing systems vary in their rates of transmitted solar energy, according to whether it was sourced from the sky diffused or the solar beam spectra; (e.g. clear blue-sky spectra are substantially different from normal beam spectra).

Alternatively, the rate of solar energy transfer was constant for different incident angles, using a relatively non-spectrally selective glazing system, as long as there is no change in the type of the spectra(McCluney 1996).

Hence, several approaches have been developed to incorporate angular selectivity; one approach was to apply a special class of thin film coating that has angular selective properties in its multi-layered structure. The other approach was to use internal physical structure in the glazing element or cavity, using polymer-glazing elements, to divert radiation at specified directions. Other developed technology was to provide clear transmission through incidence from one direction while scattering incident light coming from other directions (Maeda *et al*., 1991).

Newer techniques were derived to manufacture well-bonded and hard-filmed surfaces that can still have the same or better optical performance, by using composite films containing metal and insulator (Smith et al 1992), these are often referred to as *cermets*. In this thin film system the angular selectivity relies on an inclined columnar structure with the *cermets* having columns consisting predominantly of an oxide. Metal columnar films can also give the same effect as they rely on the inhomogeneous structure with fine metal columns and voids forming the mixed composition. The angular selective films also have structural features that enable them to control radiation depending on the angle of incidence making them not randomly inhomogeneous.

Fig3.07 shows the manufacturing principle for such *cermets*; where those columns are typically smaller than the wavelength in cross section, and line up closely together, making it similar to Venetian blinds design; forming lines of obstacles normal to the deposition direction [also the column tilt direction]. The main difference in the control mechanism between the cermets and the metal thin films is that absorption occurs too, not only reflection. Hence, leading to bi-axial rather than uni-axial behaviour (Smith *et al* 1996).

Most of the film deposition techniques used to manufacture angular selective coatings for glazing, would utilise obliquely deposited metal films as these types work better than other techniques. This is due to the high melting points of the metals that allow better column formation because of their reduced mobility after deposition.

There is evidence that the optical properties of cermets with metal columns set less randomly, are better in performance when compared to those found in films where metal columns are set distinctively in the structure. Another problem with such types of films is their structural and mechanical strength, which are adversely affected by the method of formation of layers of metal columns and the void content used to enhance their optical properties.

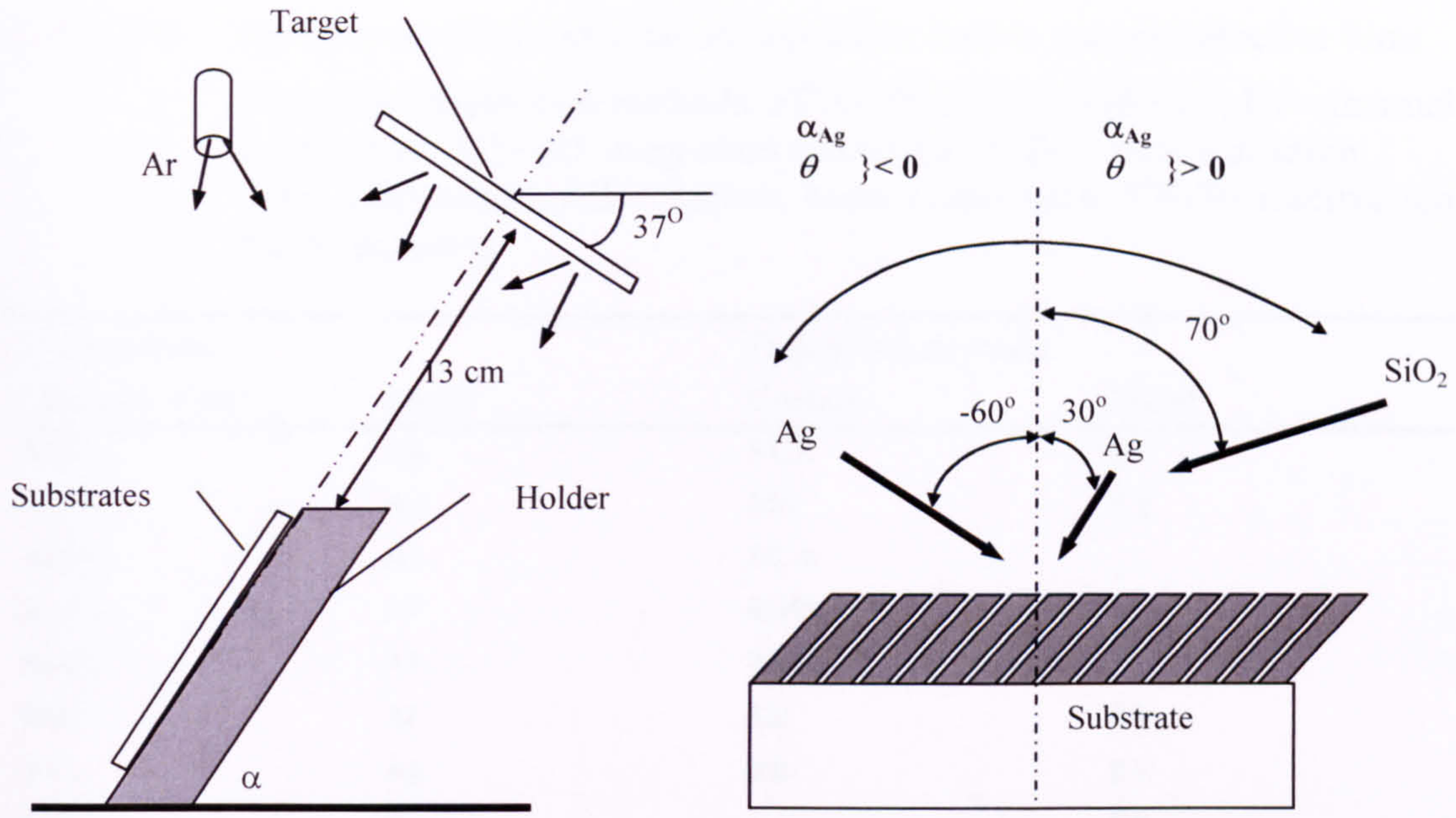

(A) **(B)**

Figure 3.07 showing: A) Deposition used for sputtering chromium (Le Bellac *et al.* 1995)

B) Deposition arrangement for bi-oblique deposition of cermets (Suzuki and Taga 1992).

Techniques to deposit thin films successfully are:

(i) *Sputtering*: that can be used for large-scale applications (i.e. large panes) by using thermally evaporated metals like silver e.g. works of (Smith *et al* 1995, Smith & Dligatch 1996).

(ii) *Thermal and electron beam evaporation*: in which an electron-beam is used to evaporate silicon oxide during deposition. Such systems work with a variety of angles (i.e. ranging between 20~30 ^{o}) to the opposite side of normal axis thus creating cermets on the samples with oblique angles corresponding to relevant insolation angles.

(iii) *Filtered cathodic Arc*: the technique was developed to deal with the inherent technical problems that arise with the presence of macro-particles in the thermal beam technique, thus, producing divergent deposition beams. However, still it has restriction on the type of the materials that can be used and conditions of application.

(iv) *Multilayers for low emittance and improved solar control*: by using ITO or SnO_2 as substrates coating.

Alternatively, a combination of these methods could be deployed with a special caution in the case of cathodic arc.
In general, the optical performance of these films depends on their microstructure and composition; other parameters that are important include the column tilt angle to the vertical, film thickness, metal content, oxide or void fraction. *Table 3.01* shows the types of these films and their methods of application.

Table 3.01 showing material combination deposition used in angular selective films

Legend for deposition methods: FCA= filtered Cathodic arc; EV= thermal evaporation; MS= RF magnetron sputtering; REB= reactive electron beam evaporation; EB= electron beam evaporation; RIBS= reactive ion beam sputtering.

Composition		Deposition methods	
Ceramic/ void	Metal	Ceramic	Metal
Al_2O_3	**Ag**	**FCA**	**EV**
Al_2O_3	**Ag**	**MS**	**EV**
Al_2O_3	**Al**	**FCA**	**_**
Al_2O_3	**Al**	**RMS**	**_**
Al_2O_3	**Al**	**REB**	**_**
SiO_2	**Al**	**EB**	**EV**
SiO_2	**Ag**	**EB**	**EV**
Air	**Cr**	**_**	**EB**
Air	**Cr**	**_**	**MS**
Air	**Al**	**_**	**EV**
Air	**Ag/Al/alloy**	**_**	**EV, EV [Ng, 1994]**
TiO_2	**Ti**	**FCA**	**_**
Ta_2O_5	**Ta**	**RIBS**	**_**
TiO_2	**Ti**	**RMS**	**_**
TiO_2	**Ag**	**FCA**	**EV**
WO_3	**W**	**RMS** [le Bellac et al., 1995]	
Cr	**Cr_2O_3**	**FCA**	**_**

3.2 CURRENT METHODLOGIES OF MODELLING GLAZING SYSTEMS:

Explicit and implicit approaches:

Simulating heat transfer (i.e. for radiative, convectional and conductional modes) through windows is a complex issue; the complex physics of energy flow in and out of the buildings makes it difficult to establish total congruence between the different approaches. Two different methods can be classified to manage the problem, *see fig3.08*.

In the more common method (**A**), values of optical constants at normal incidence are multiplied for the whole window with an approximate angular profile; this would result in equations governing the behaviour of energy flow through glazing, by normalising the performance for other angles. An angular function can then be used to generate a fixed profile or a function for a number of panes or substrates used in the system (Karlsson, 2000).

Different angular refined simulation models (i.e. mainly 10°, 20-40°, 60-80° profiles) are used to reproduce the angle dependence, and to lower the errors especially in the

case of multiple glazing or substrates coatings, building on a database of Optical Library, (e.g. / Window 4.1, 1998 and M. Rubin's optical data library 1995, etc.)

Nowadays more effort is directed towards creating a manufacturer library that has all the technical information about the angle dependent behaviour of optical properties of most of the enlisted glazing, coatings and films. (Rubin, Powles & Von Rottkay 1998).

In method (**B**), *see fig 3.08*, each glazing system is treated separately; T and R-values (i.e. transmissivity & reflectivity respectively) are calculated at normal incidence for each wavelength. The properties generated by this physical model can be used to produce physical constants that can be used to construct an equivalent bulk-glazing model that would be used to calculate its optical properties through standard Fresnel equations. E.g. if a coated bulk glazing sample is used, R&T-values are calculated for the coating first, then the glazing system properties would calculated as if it is not coated to obtain pseudo-optical values that are used to simulate the properties of the bulk sample.

In general method (**A**) is simpler, and it does not consume excessive central processing unit (CPU) time. However, being empirical and dependent on the interpolation of normal incidence properties, it requires knowledge of the whole bulk section sample to generate detailed and highly accurate data for all angles. Method (**B**), on the other hand, would lead to very low errors, upon working on a layer-by-layer basis, but is likely to require considerable CPU time, i.e. though using computational fluid dynamics techniques. Most CFD modelling, though becoming more user friendly, still requires high levels of expertise to get meaningful results, long execution time for natural convection models, and large memory space *Random Access Memory* (RAM), which is typically not available in computers of average users; (Ćurčija 2002).

As a result different methods have been developed that lie between these two extreme modelling techniques for calculating the optical properties of glazing.

In summary, relatively simple models, which apply angular dependence techniques, can be used to simulate behaviour of coated monolithic glazing materials [i.e. clear or single tinted glass, plastic substrates], with small errors in calculation, provided that they have the available properties data. These methods might not work particularly well for other un-coated glasses of different tint (Furler, 1991).

Alternatively, transmittance and reflectance measurements could be made over the full solar spectrum (250-2500 nm) at normal incidence using a spectrophotometer. Most of the radiometric measurements and spectral averages are made in accordance with the standard practice of NFRC 1994, which is based in turn on the technical procedures of ASTM 1988. (Karlsson 2000).

However, while using method (**B**) for modelling complex samples (i.e. those involving multiple coatings or substrates), it was found that optical angular properties, specially those averaged in the visible or long wave/ thermal range of the spectrum, are not strongly dependant on the detailing of the assumed model (e.g. thickness of the film samples, film in-homogeneity) but rather on the good reproduction of the near normal incidence spectra data for the whole sample. Such approach eased the way to the evolution of what are referred to as "*Equivalent Models*"(EM), (Montechi *et al.* 1999).

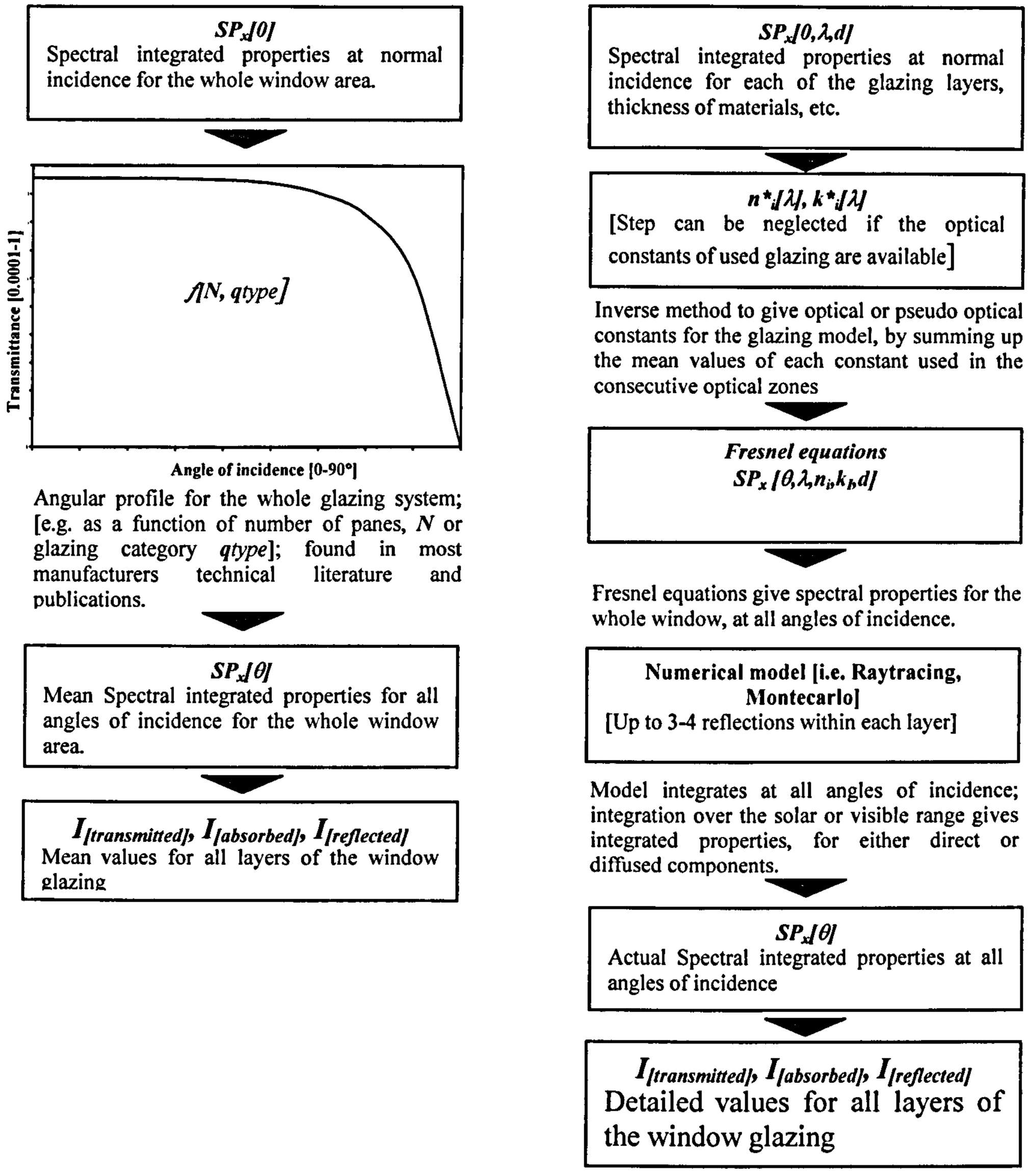

Figure 3.08 Schematic block diagram of two different methods to determine amount of energy passing through the window. The star [*] is to note that the optical constants maybe assumed physical properties.

Using the principle of the inversion of the Fresnel formula to derive optical constants for a certain coating from normal-incidence transmittance and reflectance might lead in most cases to multiple outputs. EM models generally deal with imaginary samples and could lead to better results if they are to work on the principle of neglecting the coherent effects (i.e. those yielding errors in calculation of optical properties at the interfaces of the composite materials samples, specially when including the effects of the adhesive materials bonding the different materials forming the bulk sample of glazing.

Thus a number of different "*Incoherent Equivalent Models*"(IEM) evolved of which the following are discussed in this research:

(i) *Equivalent Uncoated Model* (EUM); consisting of a slab of homogenous material with plane and parallel interfaces, characterised by the complex refractive index ***n-ik*** of the material and a thickness ***d***, *see fig 3.09.*

(ii) *Equivalent Uncoated Bi-slab Models* (EUB1 and EUB2); as more complex types of IEM. The only differences between them depend on the position of the transparent and optically dense slabs with respect to the incident radiation, and having the complex refractive index $N_t=n_t-i0$ and $N=n-ik$ respectively.

(iii) *Equivalent uncoated Triple Slab Models* (ETS1 and ETS2), similar to the above but with triple coating, *see fig 3.09.*

(iv) *Minimum of Fringe Coherent Model or the Coherent Equivalent Model* (MFCM), which takes advantage of the coherent effect of calculating the multiple refractive index, and at the same time avoiding the problem of multiple solutions. It is an imaginary slab model consisting of an optically dense substrate, coated on both sides with identical transparent films of index ***n*** and thickness equals to $n\lambda/4$ at every wavelength.

Consequently, all explicit or mixed modelling techniques are in need of reliable numerical tools to simulate the random propagation or incidence of insolation rays across the glazing systems and their surrounding environments.

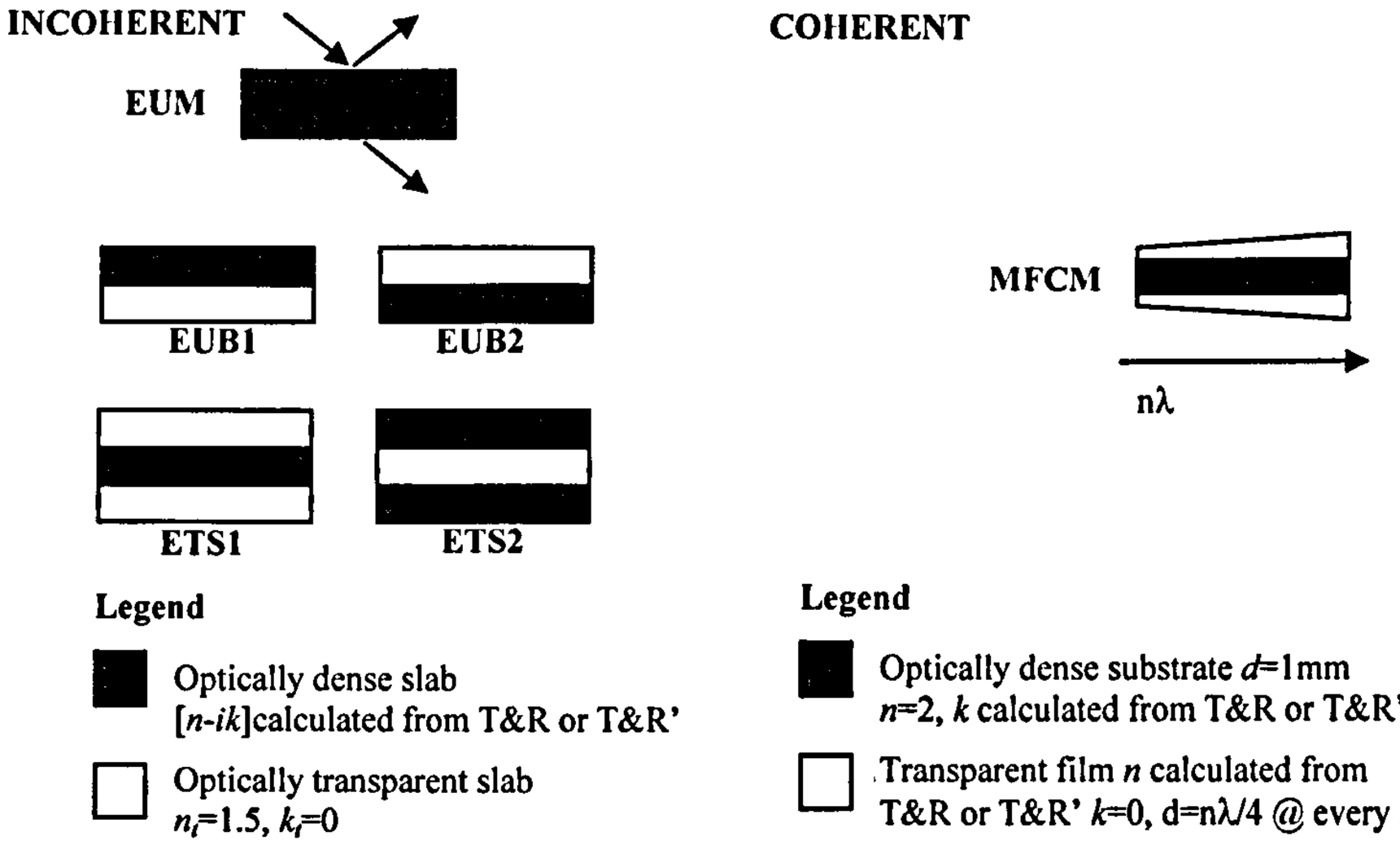

Figure 3.09 Incoherent and coherent models for the prediction of angular glazing properties, coating thickness that is set at nλ/4 is pictorially represented as a variable thickness along the n_λ axis.

3.3 MODELLING OF INSOLATION IN GLAZING USING NUMERICAL TOOLS:

The main challenge for heat transfer modelling in windows or environments where semi transparent or transparent materials are used is usually in simulating the radiative component of the energy transfer. This is due to the dual nature of the light as having quantum and wave qualities, thus leading to error in the results when grey object properties, e.g. of emissivity or diffuse reflectivity, are used to generate results.
As such algorithms with statistical nature are used to increase accuracy. Light and radiative-transport algorithms can be roughly divided into two main groups: finite element methods and Monte Carlo methods. The two groups are used to produce graphical and simulative output depending on the purpose and complexity of tools used.

3.3.1 Finite Element method:

Finite element methods for light transport were originally adapted from the radiative heat transfer literature. In 1984 Goral *et al* introduced these methods to the graphics community, where they are typically known as *radiosity algorithms*. Many improvements have been made to the basic introduced method, including sub structuring by Cohen *et al*. in 1986, progressive refinement, and hierarchical basis functions in the early nineties.

Other extensions include the handling of participating media, and finite element methods for non-diffuse surfaces. Methods have also been proposed that combine both features of Monte Carlo and finite element approaches. Typically, these would take the form of *multi-pass methods*, which combine radiosity and ray tracing passes in order to handle more general scene models as in the works of Wallace *et al.* 1987, Sillion & Puech 1989, Chen *et al*. 1991.

However, when modeling radiation heat transfer in glazing by using finite element algorithms their relevant software is faced with various limitations incurred by the nature of the theoretical background of those algorithms. Those algorithms usually treat all transparent materials as grey objects with regard to their thermal behaviour, thus assuming uniformly scattered and re-emitted irradiation. Consequently, such a modelling approach would not be able to accurately emulate the solar beam radiation behaviour both in terms of reflections at the various surfaces within the system and upon passing through the inserted semitransparent element.

(Anderson *et al* 2003); approved that using raytracing in Monte Carlo technique would be cheaper in CPU time and return more accurate results when compared to other costly techniques. Looking at the available algorithms of radiation used in most CFD software, i.e. DTRM, P-1 radiation, the Rosseland radiation, the Discrete Ordinates (DO) radiation; the research noted that they all shared the following limitations:

- The models assume that all surfaces diffuse the incident radiation. This means that the reflection at the surface is isotropic with respect to solid angle calculation and media scattering.
- The effect of scattering is not included in some of them (i.e. DTRM).
- The implementation assumes grey radiation.

- Solving a problem with a large number of rays (i.e. specially in case of an angle dependent insolation) is CPU-intensive, as it would need to divide the task into small batches handled by parallel servers.

The fact that radiation is only one of the aspects of heat transfer modes makes its calculation more integrated within the output results of deterministic algorithms, such those used in computational fluid dynamics software. An explanation is that finite element methods compute a representation of the entire solution, rather than isolated measurements, which makes it easier to locate design problems. Second, a full solution also makes it easier to include the effects of conduction and convection, and to follow the evolution of the system over time. Finally, finite element methods are considered as a standard tool in civil and mechanical engineering, so it was natural to extend these methods to heat transfer problems (Hughes 1987).

Another main inherited property in CFD modelling, which would affect the CPU time and convergence of solution is that it mostly works with the explicit representation of the scene, leading to lengthy calculation for specular calculation of radiation heat transfer.

3.3.2 Monte Carlo method:

The method is considered as a class of numerical techniques based on statistical characteristics of physical processes, or the analogue models that try to simulate such processes. A main difference between Monte Carlo algorithm, which uses random numbers, and any deterministic algorithm, e.g. as in finite element; is that the first being generic, it can virtually model any geometrical environment, while deterministic algorithms, would have several restrictions on the modelling of the geometry, participating media of the simulation environment. The technique is appropriate to deliver complex physical simulation codes by simplifying the simulation process into "packages" in order to effectively use the parallel processors in computers.

The first reported application of Monte Carlo techniques to radiative heat transfer was in 1964 by Howell and Perlmutter simulating an enclosure with non-isothermal participating medium. (Corlett R.C 1966) was the first to model photons as discrete packets (i.e. quantified) of equal energy and to include provisions for *diffuse and specular reflections.* His algorithm was developed for a non-participating medium. On the other hand, Toor and Viskanta used the Monte Carlo method to present numerical experiments for radiant heat transfer with directional material properties.

Two types of analysis techniques are used in Monte Carlo, depending on applications, method of obtaining results, etc.

- *Straightforward design analysis*: in which conditions of the sample environment are used as input parameters in random probability techniques to find output results.

- *Inverse design analysis*: here, a reverse way is used to check if the placement of the setting of the rig and the results will match the outcome of the requirements sought after. If they don't match some of the requirements, some of the conditions would be changed and the solution is run again. This is repeated till a satisfactory solution is found. The method seeks to use the required outcome as problem input, and then satisfactory results will be obtained without iteration.

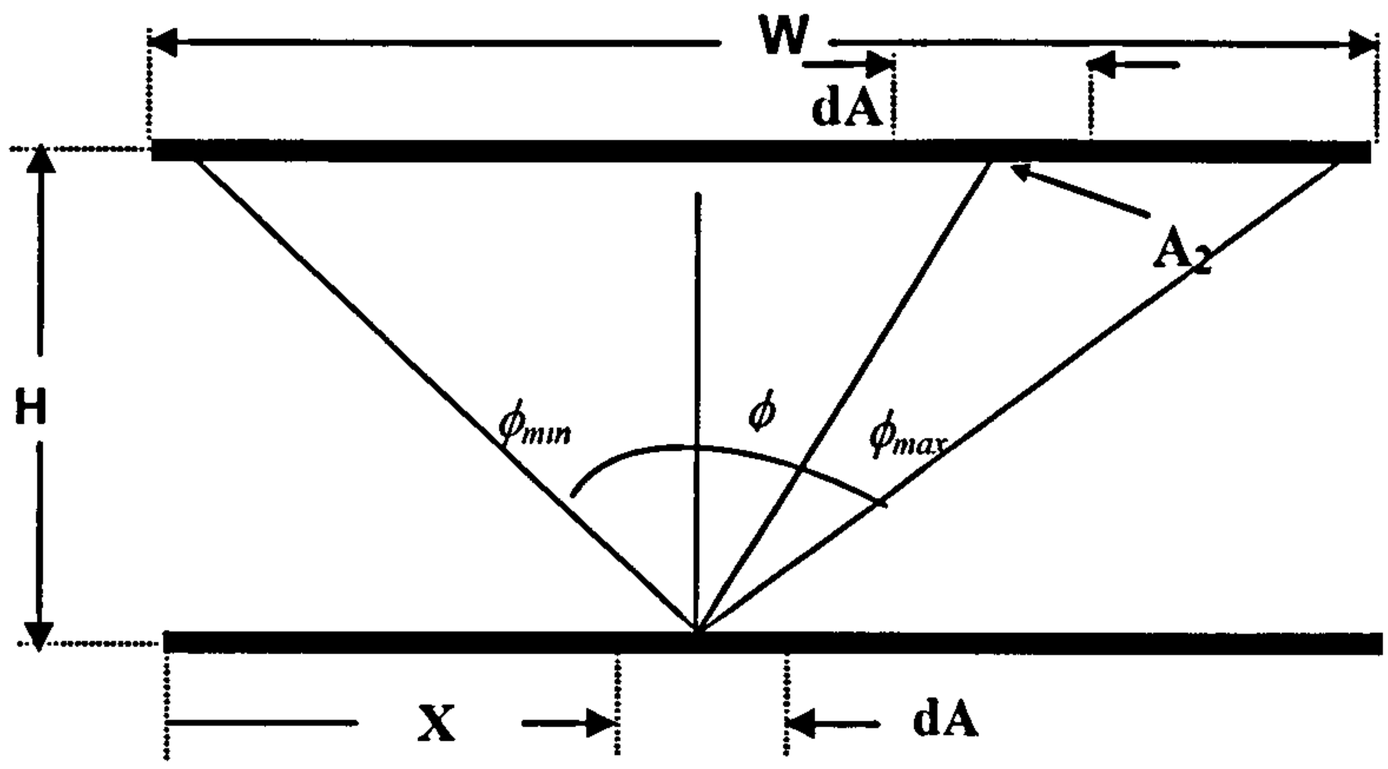

Figure 3.10 Geometry for configuration factor between strip element and plane.

Simulating radiative transfer by Monte Carlo uses the assumption that radiative energy is made of discrete packets of energy leaving a surface (e.g. dA_1), *see fig 3.10.* A fraction of the total packet of energy will strike anywhere on A_2, this will be the *configuration factor*, which is used to define the geometrical effects of the surrounding environment.

In straightforward Monte Carlo, a large number of energy packets are to be shot from dA_1 and then register the number that reaches A_2. However, the directions of which the packets leave dA_1 have to obey the laws of governing radiation (Howell 1998)

In more complex examples every event of such procedure is to be taken as an independent package to minimise time of the simulation. Directions of the outgoing packets therefore should be chosen randomly from the correct distribution of the outgoing directions. This is done by relating the outgoing direction to a number N chosen at random from a uniform set of numbers in the range of $0<N<max$.

The governing relation between a random number and a known probability is:

$$N = \int_{\xi^* = -\infty}^{\xi} dP(\xi^*) \qquad (3.002)$$

This relation is often called the *fundamental theorem of Monte Carlo*. If the probability of occurrence (ξ) of any event is know then random choices can be made by applying, *equation 3.002*. By choosing random numbers to determine the variable ξ, which is given successive values accordingly.

Running the probabilities for enough values of ξ a probability distribution $d\mathbf{P}[\xi]$ can be established:

$$N = \int_{\phi_{min}}^{\phi} = -\pi/2 \; dP(\phi^*) = \int_{\sin\phi^* = -1}^{\sin\phi} \frac{d(\sin\phi^*)}{2} \qquad (3.003)$$

Then the angle ϕ for an individual energy packet leaving dA_1, which can be found by choosing a random number R and recasting, *equation 3.003,* into:

$$\sin\phi = 2R - 1 \qquad (3.004)$$

When a large sample of packets is sent forward, they would follow the probability distribution $d\mathbf{P}[\phi]$. Alternatively, determining the value of probability requires knowing the histories of large number of these packets, checking for each one if the value of ϕ from, *see equation 3.004*, would be between ϕ_{max} and ϕ_{min}. When the sample packet will strike A_2, a relevant computer program would be able to simulate such probability and determine the mean value for each configuration factor.

Main features of the technique in heat transfer applications:

- *Approximation:* The technique solves the mathematical models of radiative transfer generally by approximating on various degrees (i.e. sub-division of related geometry, angles, etc.). The solution will approach exactness as the numbers of the sub-division elements increase (Maltby & Burns 1991)..
- *Statistical characteristics*: The nature of Monte Carlo technique is that the results inherently possess such characteristics This can be a benefit if the uncertainty in the results, in terms of variance or standard deviation, could be always determined by means of *configuration factors*.
- *Scattering*: This is relatively easy to treat in Monte Carlo problems compared with other methods that solve multiple equations of heat transfer. Works of (Walters & Buckius 1994) showed its importance in inhomogeneous media and the use of backward Monte Carlo algorithms. This is important when investigating anisotropic scattering effects by comparing anisotropic and isotropic scattering results of (i.e. the model of diffuse radiation using air mass techniques).
- *Easy application to practical systems:* Such feature makes Monte Carlo technique widely applied to practical problems with any participating media. This statement is further highlighted by the recent advances in the technique through using it in raytracing algorithms, for lighting and heat transfer simulation. Utilising super computers, it was easier to divide the bulk of the calculations into packages processed by Massively Parallel Processor (MPP) computers. *Figure 3.11* shows an example of such application in radiative heat transfer, in which the bulk of simulation is divided into deliverable packages ;(DLA 2002).

Inbuilt obstacles when using the technique:

- *Long CPU time relation*; which can be defined as the time that is required to calculate uncertainty in the projection of radiative flux to the surface to within one percent of analytical results. Though this problem has been largely addressed, as shown earlier by the new development of fast and super computer, working on network of parallel processors Still, it is noted that those machines are expensive and are not accessible to average users, where most of the calculation are performed on serial processes (e.g. in desktop computers).
- *Inaccuracy;* when dealing with problems of large grey linearly anisotropic scattering medium with spatially varying properties i.e. the atmosphere. Monte Carlo can have difficulties in simulating the movements of packets; especially those emitted from a *very large to relatively small surfaces*, i.e. paths of diffused radiation packets targeted from the hemisphere to the surface of the glazing system. These can go in any direction, thus minimising accuracy, also the distance to absorption or scattering for each packet must be individually computed along a vector with varying absorption and/or scattering coefficients.

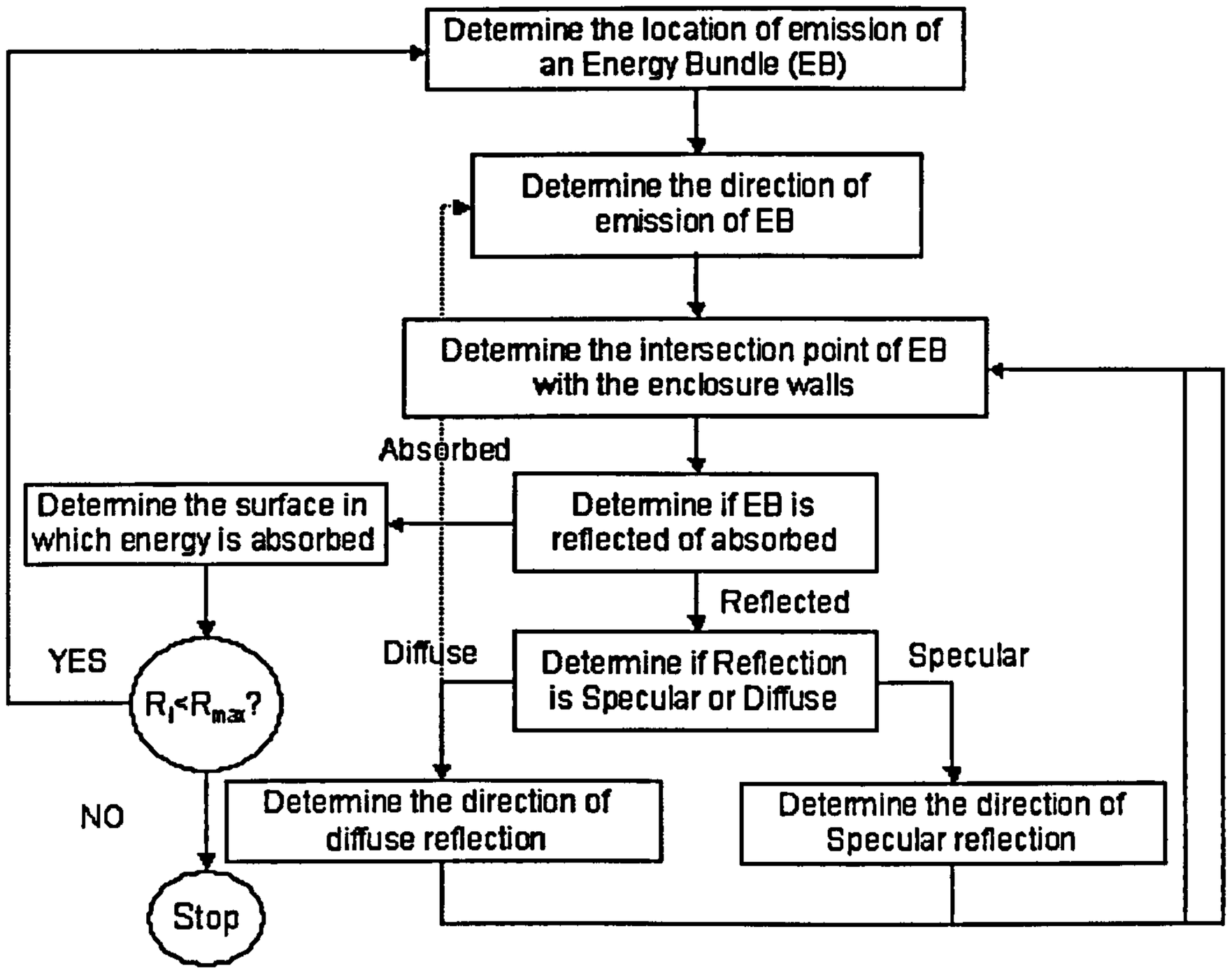

Figure 3.11 Logic flow chart for implementing the Monte Carlo ray-trace method for a given source surface in a diffuse-Specular, gray enclosure.(DLA 2002)

3.3.3 Ray tracing method:

Ray tracing is a technique of Monte Carlo for image synthesis; by creating a 2-D picture of a 3-D world. It is one of the main techniques used nowadays to simulate objects graphically in the virtual three-dimensional-space, by using the same basics of the light behaviour incident on objects (i.e. transmission, reflection, etc.). This Monte Carlo technique has been used for neutron transport problems since the 1950's and has been studied extensively since. In graphics, Monte Carlo methods arose independently, starting with Appel in 1968 who computed images using random particle tracing.

The methodology with its present algorithms can be dated back to the principles of the televised pictures; however, the real start for the present techniques is relatively new, i.e. the mid seventies (Sutherland, Sproull & Schmacker 1974), (Blinn & Newell 1976). In 1980, Whitted introduced ray tracing for the evaluation of surface appearance, and also suggested the idea of *randomly perturbing viewing*, thus was followed by contributions from Cook 1984, who added the algorithms of random sampling of light sources, lenses and time to the modeling.

Ray tracing techniques are used to address the main three light simulations:

- Neutron transport, for simulations on the micro geometric level, e.g. simulations of roughness of surfaces, thin films.
- Light transport, which is used in different graphical applications.

- Heat transfer, which is similar to the techniques of the previous, with the only difference is that the photons in heat transfer have longer wavelengths, in the infrared portion of the spectrum..

As the light emanates as an infinite number of rays from a source and is propagated to the eye or a viewpoint, it is difficult to try to trace all those rays. Accordingly, in implementation, the rays are traced backward from the viewpoint through each pixel and into that scene or angular space (Maekawa & Lord 1994). This is because interest lies eventually in a fixed number of rays, those that pass through the view plane (i.e. one per pixel). The complexity of the technique and its associated algorithms mainly depend on the purpose of the simulation, degree of accuracy sought in mimicking the view scene, geometry of the environment and the participating media, if any. As the technique inherits the quantum and abstract nature of Monte Carlo and also deals with radiation and light transfer; it can be said that the main types of algorithms used are:

- Those relevant to the geometric optics; i.e. covering wide range of optical phenomena, including emission, diffuse and specular reflection, refraction, and absorption.

- Those relevant to wave optics; i.e. would cover the previous algorithms plus those related to the wave effect of the light, e.g. diffraction.

- Finally those relevant to the quantum optics: which would cover both of the previous methods plus other effects that cannot be modeled otherwise, e.g. *fluorescence*. This occurs when photons are absorbed by a molecule, and then new photons are emitted at a different wavelength.

Two types of raytracing are used for heat transfer applications

Sequential Ray Tracing: Image-forming systems, such as heat cameras, and even the human eye, typically use such method. Systems are called sequential, when the exact order in which the rays strike the system surfaces is exactly known, thus minimising the number of rays needed.

Nonsequential Ray Tracing: In such systems, the order of ray surface intersection is not known, and these systems are typically not image forming. Non-imaging systems include fibre optics, light pipes, solar concentrators. It is much more complex than sequential ray tracing since the surface (i.e. identified as capture plane), which is to traverse the propagated ray, has to be determined additionally. Due to its nature, many rays need to be traced in order to analyse system performance. A detector is placed at the area of interest to collect, and analyse the rays.

It is computationally unattractive, as it expands virtually the limits of the particular image being generated, still it is favoured for its accuracy. As the main tasks of the method are to provide accurate solutions while minimising CPU time, there are three distinctive strategies to consider:

(i) Reducing the average cost (i.e. number of intersection of rays needed to model a certain body in an environment.

(ii) Reducing the total numbers of rays needed to emulate an object in the environment.

(iii) Replacing individual rays with a more general entity (Computer Graphics Rendering magazine 1996)..

Consequently, in heat transfer applications a *Tree form* of hierarchy is typically used in ray tracing acceleration schemes. The node in a tree has only a single parent. A tree typically has only a single root; *see fig 3.12*. In the shown example: $\mathbf{S_1}$, $\mathbf{S_2}$, etc. stands for source rays coming from light/ radiative sources. $\mathbf{R_1}$, $\mathbf{R_2}$, etc. stands for (first, second, etc.) reflections, coming from objects in the path of the rays. $\mathbf{T_1}$, $\mathbf{T_2}$, etc. stands for transmitted light through the objects. The method is also used extensively nowadays to *visualise* heat transfer, and related boundary layers (i.e. mainly for solar radiation and natural convection). New techniques of raytracing (i.e. the Schlieren, etc.) were derived that can be used in conjunction with other graphical methods to have a better understanding of such phenomena; i.e. images obtained can be enhanced using current graphical visualiser software, such as Aldus Photo-Styler, Corel Draw Graphics, (Wojciech & Konka 1996). This technique gives more detailed visualisation than conventional numerical tools; *see fig3.13*.

Drawbacks of the technique:

As in other numerical techniques, inherent drawbacks that exist in the technique affect the degree of precision in its applications, (e.g.. aliasing, time aliasing), some of these problems could be reduced in effect to a minimum. Others problems, like long periods required for running a program can be minimised with time-sharing by other algorithms of visual simulations. There are still some aspects that this method cannot tackle like the bleeding effect (Watt & Watt 1994), (i.e. the gradual diffusion of two adjacent different wavelength dependant rays) or the caustics (i.e. focused light shimmering on another reflecting object) successfully.

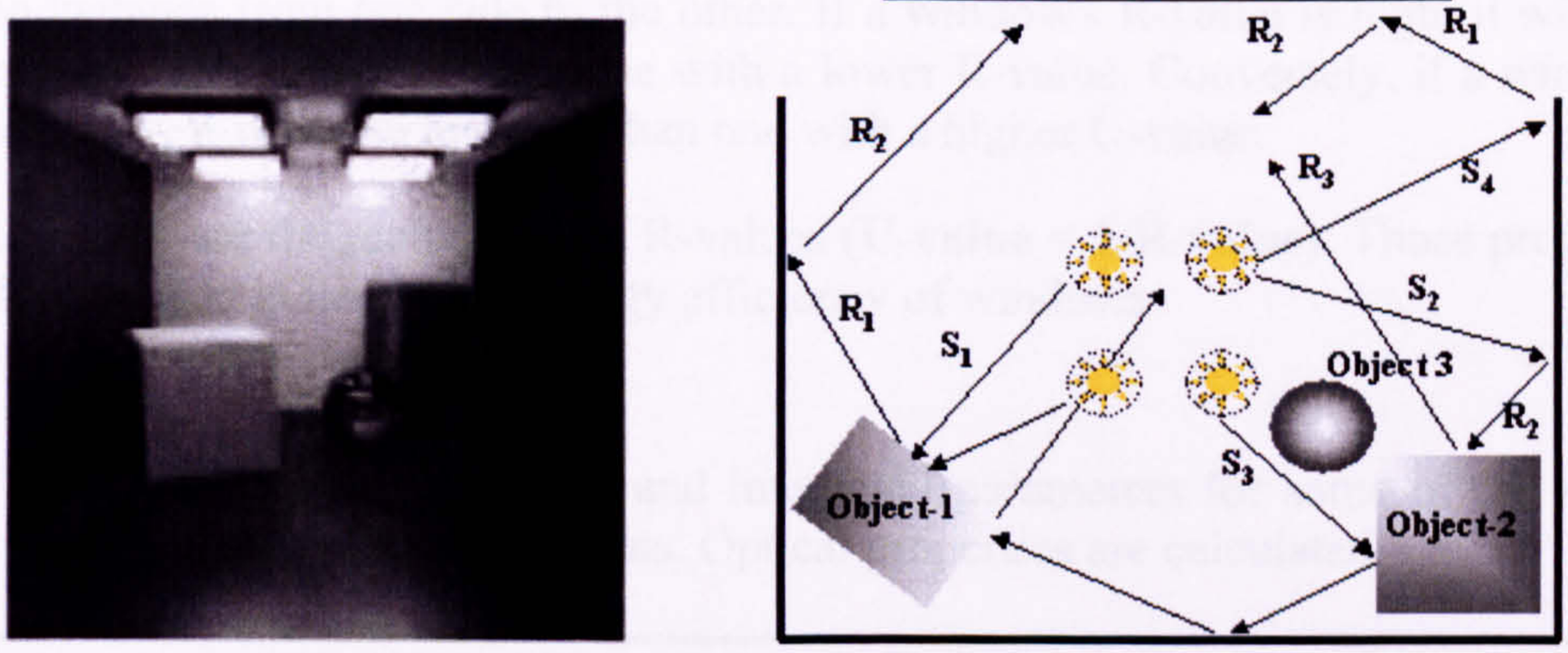

(a) (b)

Figure 3.12 showing a schematic drawing for a heat transfer raytracing tree in an enclosed space containing several objects, heated from an overhang source and looked through a glass pane: (Lafortune 1998)
(a) A generated image view of the space.
(b) Schematic plan, showing the formation of the tree, e.g. $T_1 \rightarrow R_1 \rightarrow S_4$, $T_1 \rightarrow R_2 \rightarrow R_1 \rightarrow S_1$, etc.

3.4 COMPARATIVE CALIBRATION TOOLS:

Different types of advanced selective glazing are in the market nowadays. Consequently, there is always an urgent need to have a general concept of calibrating the performance of such systems. Physical properties of glazing systems usually represent only part of a general system of measuring tools for any "*window rating*". Most of the current ratings should indicate all or some of the following:

(i) Optical properties:

Transmittance, reflectance, absorptance and emittance, as wavelength functions or as spectral averages, are used for energy and comfort assessment. Two categorisations for window solar transmittance are generally used for most referencing; T_{sol}, T_{vis}, i.e. transmittance within the whole solar spectral region and transmittance within the visible spectral region respectively. Optical properties are usually calculated for glazing systems using Fresnel formulas for normal profiles, which can then be integrated for the rest of angles. However this usually becomes more difficult through multiple glazing systems or upon adding substrates or coatings. ISO 9050 tackled this problem, by assuming either semi-transparent (Zeegers & Djik 1994) or grey object properties for the inner glazing. Computation procedure is then is introduced to give separate optical properties for each substrates/layer/ pane of the glazing system (Rubin 1985, Ross 1991). *Table 3.02* shows examples of different analysed glazing that uses this method of categorisation.

(ii) Thermo-optical properties:

Two classifications are used here, the *U-value*, i.e. related to heat conductance, which is an indication to the level of thermal leakage, therefore it should be low for good practice) or their *R-values* (resistance to heat flow. This is a rating of its ability to resist heat conductance from one side to the other. If a window's R-value is high, it will lose less heat through conduction than one with a lower R-value. Conversely, if a window's U-value is low, it will lose less heat than one with a higher U-value.

Thus, U-values are the reciprocals of R-values (**U-value = 1/R-value**). Those properties are widely used as indication of energy efficiency of windows.

Table 3.02 shows layer thickness and integrated parameters for some of the known substrates, coatings films. Optical properties are calculated.

	Float[4mm]thickness	SnO_2:F "Low-e"	Ag+" solar control
Coated layers	-	SnO_2: F/SiO_2	SnO_2/ Ag/SnO_2
Coating thickness	-	300/100nm	30/20/60nm
T_{sol} [%]	82	67	38
R_{sol} [%]	7	9	51
T_{vis}	89	90	59

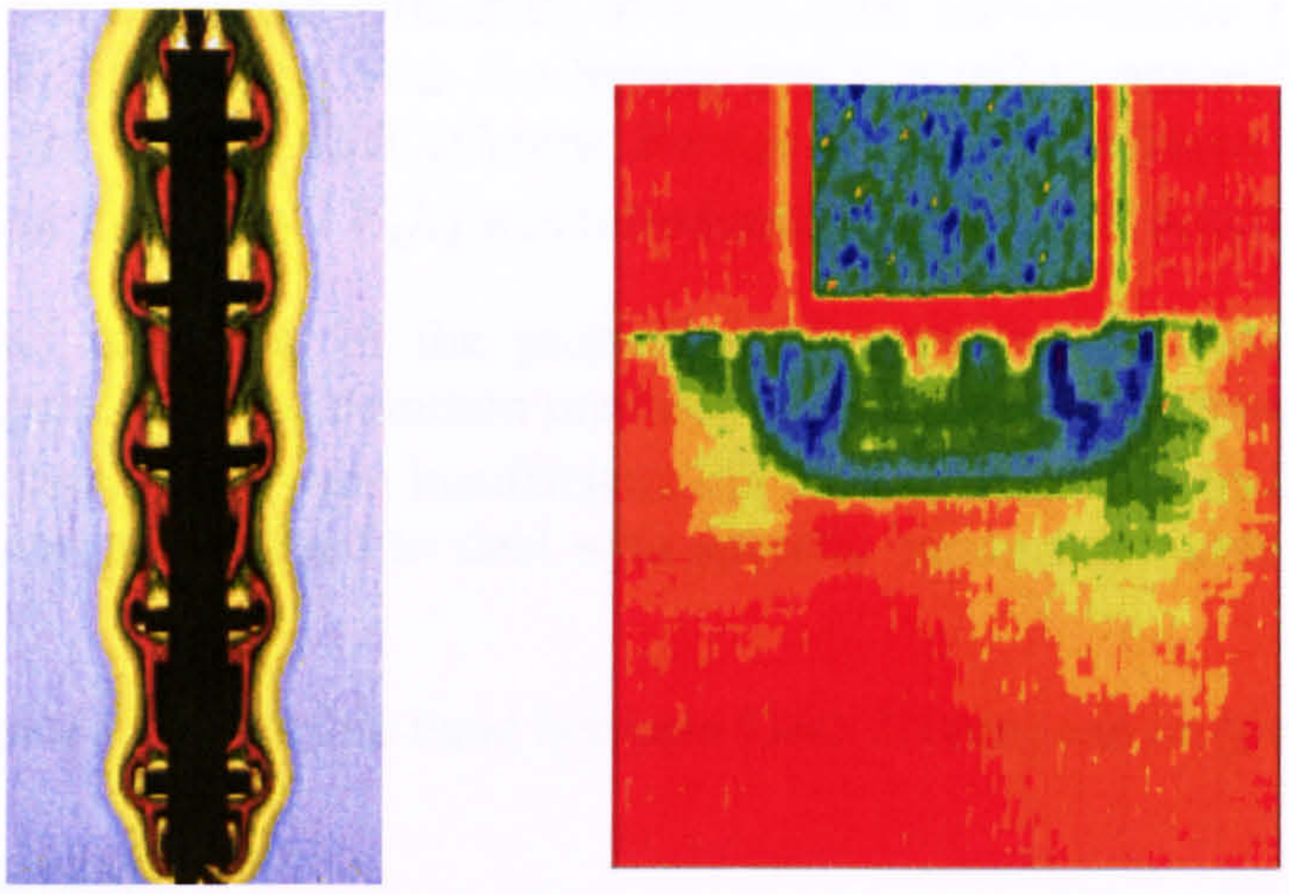

Figure 3.13 Showing a typical colour schelerian images (Tanda 1999);
a) Flow of hot air around a ribbed heated vertical plate.
b) Coloured temperature gradients of hot cylinder (side view).

(iii) Customised ratings:

These are usually based on current Standards set by recognised bodies e.g. the American Society of Heating, Refrigerating, and Air-conditioning Engineers (ASHRAE – USA) or the Chartered Institute of Building Services Engineers (CIBSE – UK). Ratings are usually calculated for a sample of an entire window, including the frame, not only for the centre of the glass, i.e. as indicated in the optical property calculation. *Colour neutrality*, *scattering properties* are also some of the important properties used to evaluate visual comfort so as the visible transmittance $\boldsymbol{T}_{vis,}$ that is used as an indicator of glare problems.

(iv) Mixed ratings:

A combination of optical and thermal properties is used sometimes to calibrate performance of glazing and/or shading, *see fig 3.14*. This standard is called, *the shading coefficient*, which is simply the fraction of solar radiation transmitted by the specified device, compared to that transmitted by an unprotected sheet of 3mm clear float glass. The higher the *shading coefficient SC* the more solar heat would pass through. That is to say:

$$Shading\ coefficient\ SC = \frac{Solar\ heat\ gain\ for\ glass\ Y}{Solar\ heat\ gain\ for\ 3mm\ clear\ float\ glass}$$

With the introduction of advanced and complicated systems of glazing with angular selective multiple panes and special coatings, the simple relation between the shading coefficient ***Sc*** and the solar heat gain was not considered to be sufficient to define the "shading" effects of such glazing systems, as multiple glazing systems do not have the same spectral response as the single pane of the glass used as a base to calculate the ratio. Consequently, a different method had to be introduced to validate performance of new systems from different manufacturers.

The first step was to set the difference between solar transmittance T_{sol} and the visible transmittance $\boldsymbol{T}_{vis}$ that deals with the human eye spectral response. This function has been standardised by the ***CIE*** (*Centre Bureau de la Commission Internationale de l'Eclairage*), and the symbol $\boldsymbol{V(\lambda)}$ was introduced to define this function.

Due to the fact that most of the properties of a glazing selectivity are angle and wavelength dependents, the common methods to calculate performance based on wide-band spectral distribution were insufficient. As a result the $\boldsymbol{V(\lambda)}$ method (*see fig 3.15*) became more commonly used to deal with specific bands and zones of interest within the spectrum.

The transmittance of the visible band between [360-720nm] can be given as:

$$T_v = \frac{\int_{360}^{720} T(\lambda) E_\lambda V(\lambda) d\lambda}{\int_{360}^{720} E_\lambda V(\lambda) d\lambda}$$

For the specific spectral band of the eye response

And that gives:

$$T_v = \frac{\sum_{i=1}^{N} T(\lambda_i) E_{\lambda i} V(\lambda_i) \Delta\lambda}{\sum_{i=1}^{N} E_{\lambda i} V(\lambda_i) \Delta\lambda} \qquad (3.005)$$

As the goal of most of the glazing systems, is to have a high visible transmittance while controlling the heat gain and to simplify calculations and regulating supplied data by the different manufacturers of glazing; three main zones of interest were identified, which relate the visible transmittance to solar heat gain coefficient. *Fig 3.16* shows these zones:

- **The neutral zone**, where it is possible to have a colourless glazing with a uniform transmittance over the visible portion.

Figure 3.14 Comparison of shading coefficients values for a range of external & internal shading devices [March 1999].

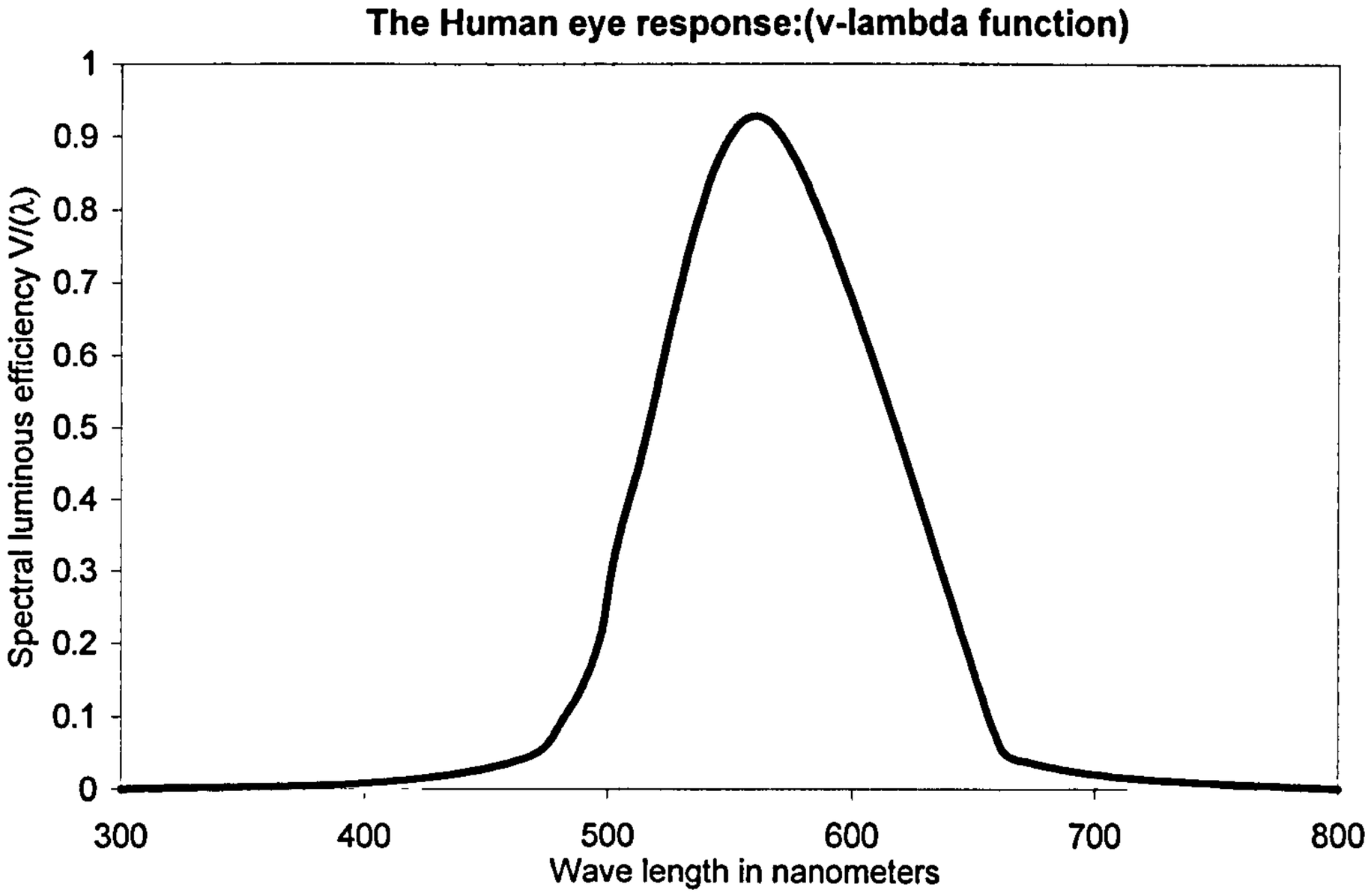

Figure 3.15 standarised *CIE* human eye spectral response

- **The colour zone:** where to achieve a certain heat gain coefficient a coloured glazing has to be applied eliminating the outer edges of the visible band (i.e. at the red and the blue edges of the $V(\lambda)$ function) or it can be done by changing the value of the $V(\lambda)$.

- **The forbidden zone:** where no combination of visible transmittance and heat gain coefficient can place a point on the graph; *see fig. 3.16.*

In *fig 3.16*, it can be noticed that there are transition boundary lines between the three zones. These lines are determined by assuming a hypothetical glazing with absolute properties for each case; i.e. an absorptance and spectral transmittance of zero outside the visible range and 1.0 within the visible wavelength region.

By decreasing transmittance within the visible band steadily to 0.0 a plot line will evolve versus the heat gain coefficient, etc. Countries have developed certified ratings or labels for windows, e.g. the *NFRC-label* in the U.S., which is attached to the windowpane and is based upon this system.

Table 3.03 The accepted optical and thermal performance of the three general categories of glazing systems. (Efficient window collaboration program 2001).

Type	Single Glazing	Double glazing (clear)	Triple glazing (moderate)
U- value	5.4-6	2.3-2.6	0.17-0.24
SHGC	0.8-0.86	0. 7-0.76	0. 45-0.5
T_{vis}	0.85-0.9	0.7-0.81	0.6-0.65

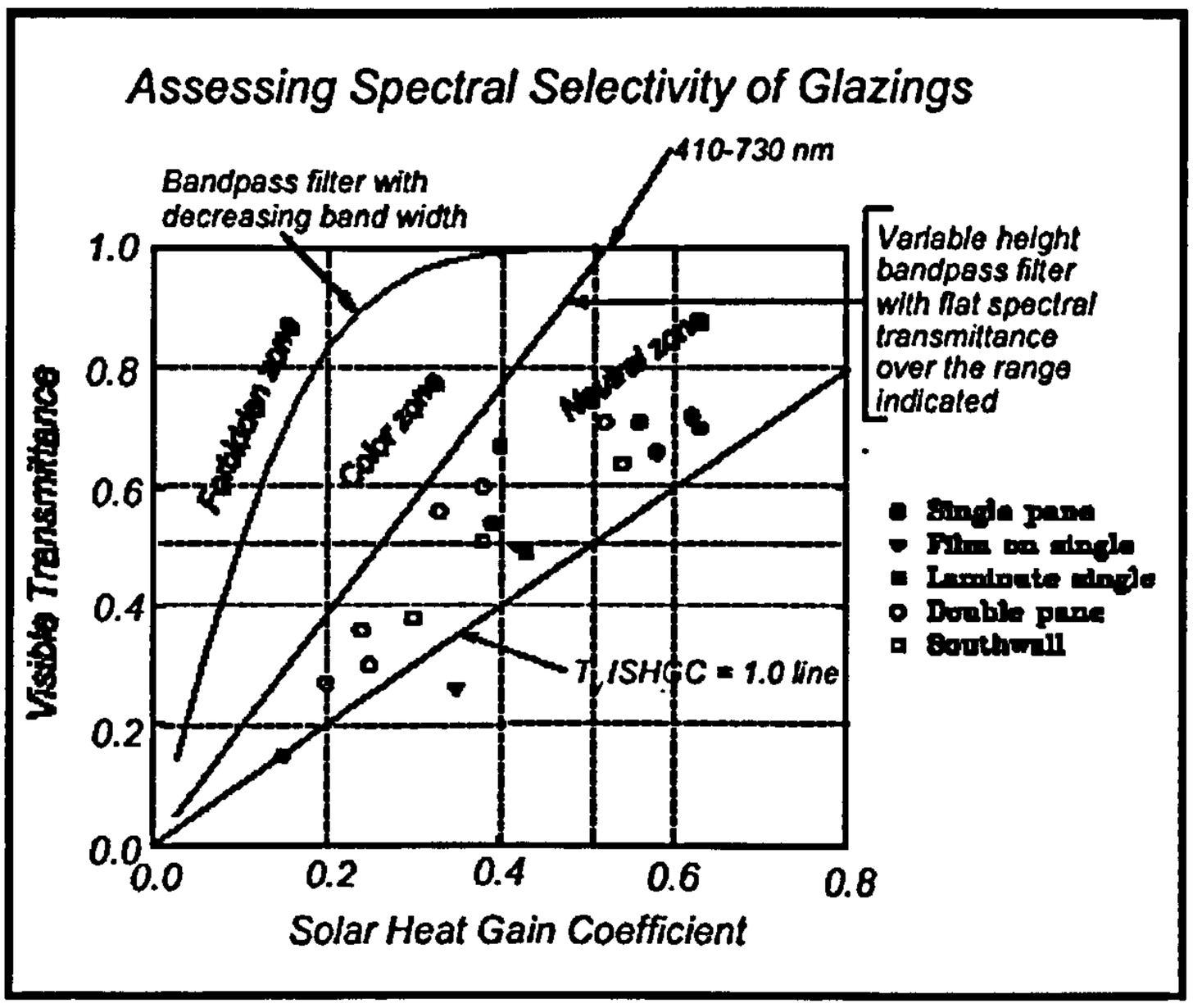

Figure 3.16 showing the zoning used commercially for some of the available glazing systems. (McCluney R 1996).

The *NFRC-label* contains the U-value, T_{vis}, and g-value (defined as defined as the solar transmittance plus the absorbed part of the radiation, which is re-emitted inside the building. the air leakage for the window including the frame.

However it is difficult to translate such output values to more understandable statements (e.g. kWh/m^{2}yr), thus more attempts are now in progress to produce an energy-rating figure to be added to the label. This could, for instance, be in the form of saved energy value compared to that of a base case window, e.g. uncoated SGU or DGU (i.e. single glazing unit, double glazing unit respectively). Energy rating of windows would then require first, dividing the world into climate zones with similar solar radiation and temperatures. Second, a general model or algorithm that would able to describe the energy impact of the window, depending on climate zone, type of shading, orientation and type of window. *Table 3.03* shows a sample of label referencing using a mixture of both the thermo-optical properties as way of labeling glazing systems, specially the ones that come with integrated frames.

3.4.1 Commercial software:

Several types of software are available nowadays in the market for evaluating glazing systems and shading devices. Algorithms used in such software vary according to the purpose, degree of complexity, and end user category, *see fig 3.17*. In general, the more complex of the methods of simulation the more extensive is the data that is required. Much of this data is not available easily to common interface users (i.e. architects, building designers) who would be concerned primarily with overall guidelines rather detailed prediction of energy behavior (Balcomb1992).

Enlisted below are some of the software packages recommended by EREC (US energy efficiency and renewable energy council).

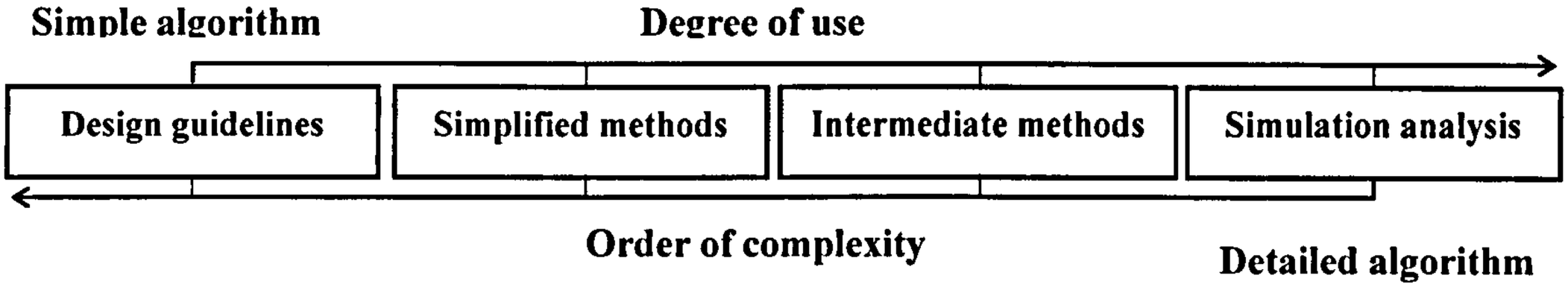

Figure 3.17 shows relation between degree of use and the complexity in regard to the level of algorithm used and detailing of energy behaviour.

- DLEB/E-10 software; was developed by SBIC, the National Renewable Energy Laboratory, Lawrence Berkeley National Laboratory, and Berkeley Solar Group with support from the U.S. DOE 9 (i.e. United States Department of Energy).

- WINDOWS' series; software developed by Lawrence Berkeley Laboratory With the U.S. Department of Energy, to help manufacturers and building professionals optimise the thermal and Daylighting performance of window systems. Another part of the software is THERM, which is a module of the WINDOW+5 program under development by LBNL. WINDOW+5 is the next generation of the WINDOW software and is being developed for the Microsoft Windows™ operating environment [Lawrence Berkeley Laboratory, 1999-2003]

- THERM, can model two-dimensional heat-transfer effects in building components such as windows, walls, foundations, roofs, and doors; appliances; and other products where thermal bridges are of concern. It has a two-dimensional conduction heat-transfer analysis. The program also uses graphic interface to create two dimensional cross section models. Results can be used with WINDOW's centre-of-glass optical and thermal models to determine total window product U-factors and Solar Heat Gain Coefficients. Output files can be used, in turn, with the RESFEN program, which calculates total annual energy requirements in typical residences throughout the United States.

- aveSARC 3.0: calculates solar angles and average-day solar radiation intensities on glazing.

- AWNSHADE (Version 2.0) calculates the unshaded fraction of diffuse sky irradiance or illuminance incident on a rectangular window for any given solar position co-ordinates relative to the window.

3.4.2 Customized algorithms:

A number of algorithms have been derived to rate the performance of glazing systems. One of these new models uses the q-value of the glazing; which is defined as the annual mean energy transmittance for any incidence angle at glazing in the cardinal direction (e.g. of East, West North and South), by trying to predict the angle dependence of the g-value [karlsson & Ross 1998].

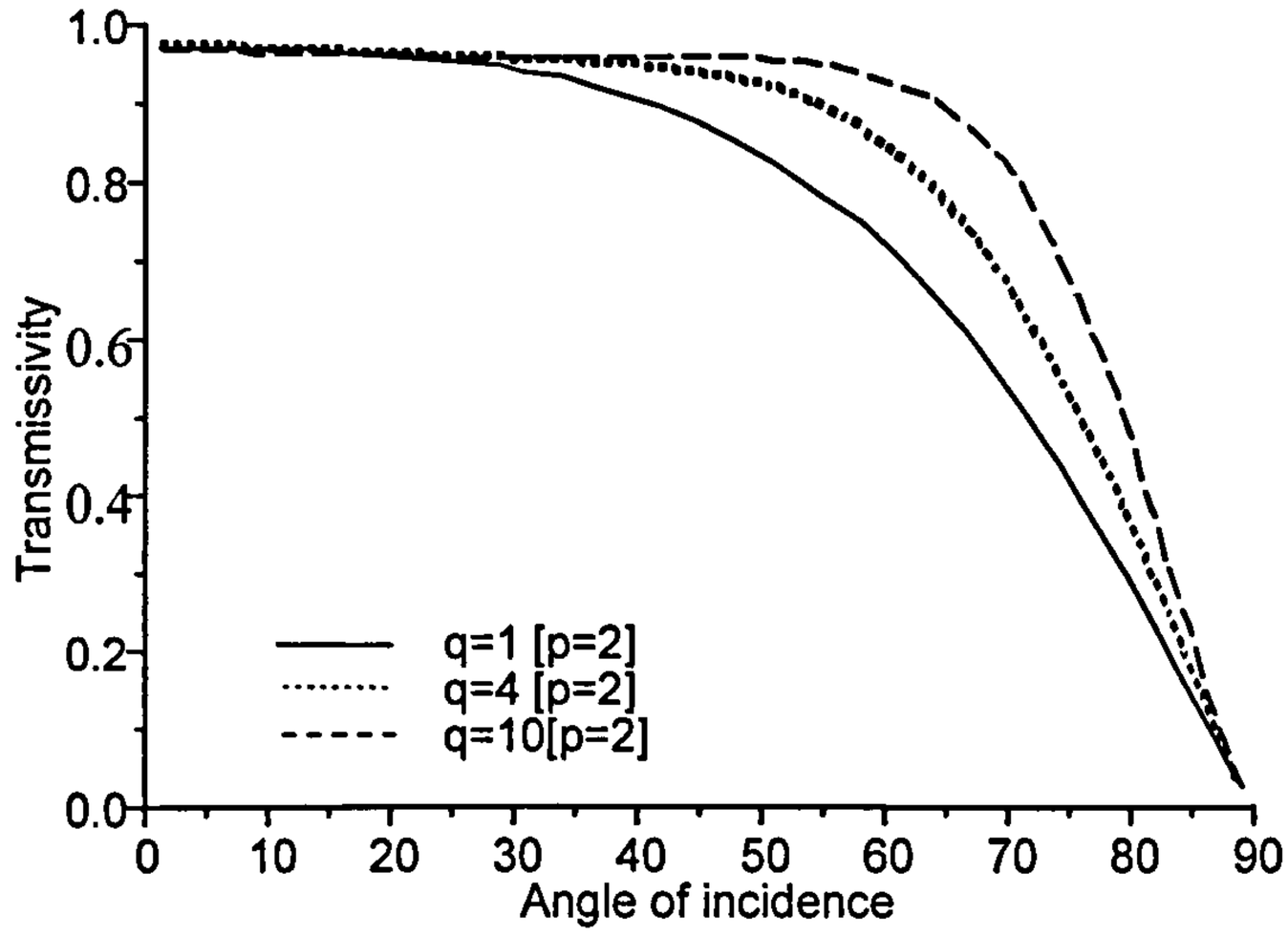

Figure 3.18 shows plot of 3 types of q value for different types of glass, based on a fixed number of panes p=2 per sample.

Its values for glazing systems should usually be low in hot and sunny climates. The model is empirical; it takes the number of panes, *p*, and the type of glazing *q*, into consideration.

The two parameters would then be determined, through using a normalising fitting curve of an angular profile, *see fig 3.18*, which is calculated using the g-value, calculated at normal incidence for the whole window:

$$f(p,q)_{\theta=0-90} = q(i)^{*}\, p(i)^{*}\, g_{t(\theta=90)} \qquad (3.006)$$

Parameter *q* is empirical and can vary from 1-10 to indicate the type of glazing (i.e. assuming the normal float glass as base of ***q=4***); so as curves representing specific glazing above this reference curve line would be considered as *reflective glazing* while the ones that are below this base curve would be considered as *absorptive types*.

By using the optical properties of this reference glazing, a profile for *q* can be generated, where the lower or higher *q*-values would correspond to glazing having lower (i.e. solid curve in *fig 3.18*) and higher (the dotted curve) profiles respectively. *Figure 3.18* shows two assumed glazing (q=1 and 10 respectively) plotted against a base reference curve of q=4 for comparison.

Consequently, glazing with a low q-value is treated as absorbing type (i.e. coated glazing with an absorbing layer and a high extinction coefficient ***k***) while a high q-value would mean a glazing that has a high reflectivity and a high refractive index n.

According to this model, the angle dependence of g-value was found to be dependent mostly on the number of panes and type of glazing or coating rather than the thickness of coating. This agrees with the predictions of the Fresnel equations.

Conclusion:

- Selective glazing technology has advanced significantly since the late fifties and early sixties. The main concern was minimising the amount of the heat gain in the hot climates and to increase it in the higher latitudes of where cold climates predominate. The literature survey indicates that two main trends of solar selective glazing could be roughly redefined:

(i) Glazing with wavelength selectivity.

(ii) Glazing with incorporated angular selectivity.

Each one of these approaches has its own advantages and disadvantages; with the wavelength selective glazing working in the region of visible transmissivity and trying to minimise the amount of heat gain by "dealing" with the extreme edges [the far blue and the far red] from the visible spectrum. On the other hand, it can have a negative effect on minimising the amount of light needed for visibility.

The glazing with incorporated wavelength selectivity has progressed rapidly in the last nine years, working on the wide wavelength band, trying to shun the direct beam radiation coming from the high solar angles and trying to maintain good visibility and view. Alternatively, trying not to be affected by the physical or optical obstacles, it worked on developing shading devices working on the microstructure of selective films and glazing. These systems have several distinct advantages over the main rivals in this technology, which are the various chromogenic systems (e.g. electro-chromic and thermo-tropic). They are simple to manufacture and relatively cheap to produce. The simplicity and cost advantage is partially compromised in the best performance of the low-*e* versions that stay well ahead in this respect.

It was shown that for best performance of the angular selective types, they should be used in multi-layers to enhance their solar control performance, which will weaken respectively their visible transmittance and view maintenance. On the other hand using a single layer film might be useful for glare control and maintenance of view but it would have a poor performance when it comes to solar blocking ability. This leads to the conclusion that a more basic approach is needed in angular selective glazing that can maintain their best features while enhancing their solar control ability at the same time. The basic approach should be to develop a compromise between good performance, cheap application, and versatility.

- When comparing the numerical methods for modelling the radiative transmission of glazing systems, it was found that each method had its advantages and disadvantages. Simulations using Monte Carlo technique have the ability to be more accurate especially in small environments as all the physical properties and materials data (i.e. conductivity, refractive index and emissivity) could be included in the calculation. Still, one of its main disadvantages is in the simulation of radiation in a large environment (i.e. atmosphere) projected to a smaller one (i.e. that of a glazing enclosure). The other disadvantage is in simulating selected wavelength spectra because of the difficulty of assigning packets of light for each wavelength band used, then following the reflection and the transmission of the system accordingly. On the other hand, the ray-tracing technique of Monte Carlo would deal with the visualisation of simulations and optical properties of a material. Thus, it needs to be

used in conjunction with other techniques to give a detailed simulation (i.e. to be part of a complete program that can counts physical properties other than the optical ones). Ray tracing is widely used in graphical simulation and has the adaptability to work in conjunction with other PC software. In addition, programmers do not need special feedback about the topic (i.e. here heat transfer) it simulates. As part of the requirements of the study is to include a software program that can simulate the hypothesis, it would be more appropriate for the task of this research to use raytracing. Similar demonstrations of the technique (Eames & Norton 1994) have shown that even multiple reflections and tracing of the diffused light could be simulated successfully.

- Consequently, raytracing technique was chosen to be used in the modelling of the radiative heat transfer aspect for the suggestion. Also, *non sequential forward ray tracing* is preferred. It follows the light rays from the source of the propagated light in the same direction in which they travel following them till they become sufficiently weak or have minimal effect on the result. This decision was made to control, thus minimise the number of rays projected, in comparison with the *sequential backward raytracing* that depends on visualising the received rays on capturing surfaces to solve the problem, thus increasing the number of probabilities, and hence CPU time.

- The complexity of glazing models is relevant to the purpose of the end user of the model. Interest in mathematical modelling of heat transfer in glazing systems is increasing proportionally with the diversity of the systems introduced to the market. Difficulty is arising in modelling new types of glazing systems that have multiple coating or layers.

- Rating of current glazing systems varies with different countries, manufacturers and the purpose of the glazing. No unified base exists upon which most systems could be calibrated. Different software exists to rate advanced glazing; in most of them, the theoretical base for calculation assumes grey object properties for the glazing. Such definition could lead to normalising of all relevant properties (i.e. transmittance, reflectance and absorptance) without relevance to incidence angles. Using Fresnel formulas as a base for software could lead to more actual inter-operational complications of insolation transfer on glazing and through glazing. Though lack of relevant optical materials data, or the search for sources of relevant data being time consuming, might explain why this methodology is not widely used. As the purpose of this study is to examine the hypothesis of the suggested glazing system using relevant basic materials the use of Fresnel formulas to simulate solar radiation transfer across the systems was considered appropriate, particularly if it is be associated with other platforms that could simulate the other modes of heat transfer.

References:

1. Agnihotri O.P, solar selective surfaces. In: Gupta B.K, editor. Alternate energy series. New York: John Wiley & sons Inc. 1981; p145-160.

2. Balcomb J. D, Passive solar buildings. Massachusetts: MIT Press. 1992

3. Blinn J. F. and Newell M. E. Texture and reflection in computer generated images CACM 1976;19(October): 542-547.

4. CG. Granqvist. Smart glazing. Solid State Materials Science1990;16(291).

5. Corlett R.C. Direct Monte Carlo calculation of radiative heat transfer in a vacuum. Heat transfer 1966; 88: 376-382.

6. Ćurčija C. Component Performance Assessment Methodology (CPAM), Part 1: Issues and research needs. Report of IEA task 27, for the International Energy Agency, Solar heating and cooling programme, Centre for Energy Efficiency and renewable Energy, Massachusetts USA, 2002.

7. Digital Library and Archives, University Libraries, Virginia Tech, USA, 2002. See also:
www.scholar.lib.vt.edu/theses/available/etd-12062002-211117/unrestricted/ch2.pdf

8. Eames P.C. & Norton B. A window Blind Reflector System for the deeper penetration of Daylight in the rooms without glare. International journal of Ambient Energy 1994; 15(2) April.

9. Efficient Window Collaboration Program, Manager Alliance to Save Energy 1200. Washington, D.C. 20036: Efficient windows organisation, 2001. See also: http://www.efficientwindows.org/contact.html.

10. Furler, R.A.. Angular dependence of optical properties of homogeneous glasses. ASHRAE Transactions. 1991; 97:1129-1133.

11. Gombert A., Glaubitt W. *et al*, Glazing with very high solar transmittance. Solar energy 1998; 62 (3): 177-188.

12. Haines E. Computer graphics rendering. Rep.: FAQ [part 1/2]. Florida, Ray tracing magazine, AMC group, August 1996.

13. Holland L. Vacuum deposition of thin films, New York: John Wiley & sons publications, 1958.

14. Howell R. J. and Perlmutter C. Monte Carlo solution of thermal transfer through radiant media between grey walls. Heat transfer 1964; 70: 320-330.

15. Howell R. J. the Monte Carlo method in radiative heat transfer. Heat transfer1998; 120: 547-599.

16. International standard, ISO 9050, 1990.

17. Karlsson J. Windows-optical performance and energy efficiency. Report in: Solid state physics, Uppsala, Uppsala university: the Angstrom laboratory, 2000.

18. Karlsson J., Ross A. Modelling the angular behaviour of the total solar energy transmittance of windows. Solar energy 1999; 69(4): 321-329.

19. Lafortune E, Willems D, A 5D Tree to Reduce the Variance of Monte Carlo Ray Tracing, Department of Computer Science Katholieke Universiteit, Belgium. A Conference Paper In: the 6th Eurographics Workshop on Rendering, Dublin-Ireland, June 12-14, 1998.

20. Maekawa Z and Lord P., Environmental and Architectural Acoustics. London: E & FN SPON, 1994. p.260-265.

21. Maltby J. D & Burns J. P, performance, accuracy, and convergence in three-dimensional Monte Carlo radiative heat transfer simulation. Numerical heat transfer1991; part 19(B): 191-209.

22. March A, Thermal performance-shading coefficients. The fridge/ architectural science Lab/ School of Architecture and fine Arts. The University of Western Australia, 1999. See also:

23. McCluney R, fenestration solar energy gain analysis, Rep. no. FSEC-GP-65, cocoa, FL, Florida solar energy centre, 10 October 1996.

24. McCluney R. Angle of incidence and diffused radiation influence on glazing system solar gain, Solar Boulder. Proceedings for the American solar Energy Society, Colorado, USA, 1994.

25. McCluney R. sensitivity of fenestration solar gain to source spectrum and angle of incidence, ASHRAE Transactions- research 1996; 3991:112-122.

26. Montechi M., Nichelatti E & Polatto P., Equivalent models for the prediction of angular glazing properties. Rivista Della. Stazione Sperimentale. Del Vitro1999; 5:225-236.

27. Roos A, Optical properties of Pyrolytic tin Oxide on aluminium, Thin Solid Films 1991; 203: 41-48.

28. Rubin M, Optical Constants and Bulk Optical Properties of Soda Lime Silica Glasses for Windows. Solar Energy Materials1985; 12(4)-: 275-288.

29. Rubin M., International Glazing Data Library; the International fenestration rating council. Sliver Spring, MD: LBNL 2003, See also: http://Windows.lbl.gov./materials/optical_data

30. Rubin M., Powles R. and von Rottkay K., Models for the Angle-Dependent Optical Properties of Coated Glazing Materials. Solar Energy1999; 66(4) 267-276.

31. SBIC guideline and software. Washington DC: Sustainable building Industry council, 2003. See also: http://www.sbicouncil.org/soft/index.html

32. Smith G. B. et al., Thin film angular selective glazing. Solar Energy1998; 62(3):229-244.

33. Smith G. B., Dligatch S., and Ng M. W., process in window innovations "A World Conference on State-of-Art Window Technologies for Energy Efficiency in Buildings", In: Canadian Government, publisher. ISBN 0-660-16085-4 1995 Toronto: Canada, 1995. p598-605.

34. Smith G. B., Dligatch S., IEA TASK 18, Advanced Glazing. Report no.: T18/B7/AUS96-project B7. The international Ergonomics association, 1996

35. Smith G. B., Ng M. W., Ditchburn R. J., Martin P. J., and Netterfiled R. P., cermets for angular selective transmittance. Solar energy materials 1992; 25: 149-167.

36. Sutherland, I. E., Sproull, R. F. and Schumacker, R. A. a characterisation of ten hidden-surface algorithms. Computer survey 1974; 6(1): 1-55.

37. Tabor H., Use of Solar Energy, In: ASHRAE Transactions Conference, Tucson, AZ October 1955. V. 2: p24.

38. Tanda G, Application of the schlieren technique to convective heat transfer measurements, applied optics group, a paper conference for the University of L'Aquila, Italy. 1999. See also:www.dau.ing.univaq.it/omhat/Papers/sch.pdf

39. Thermal properties, shading index. The Fridge Architectural science lab. Ontario, Canada 2002. See also:

http://fridge.arch.uwa.edu.au/topics/thermal/shading/index.html

40. Veach E, robust Monte Carlo methods for light transport simulation, A PhD. Thesis. Department of computer science and the committee on graduate studies of Stanford University, USA 1997.

41. Watt A., Watt M. Advanced Animation and Rendering Techniques In: Theory and Practice, Atlanta: John Wiley & sons Inc. 1994. Chapter 8.

42. WINDOW program versions, technical questions. Berkeley, CA: Lawrence Berkeley Laboratory, 2003. See also:
http://www.eren.doe.gov/erec/factsheets/sunspace.html.

43. Wojciech T. Konka. Simple visualisation methods to support "conventional" investigation of natural convection heat transfer, report no.: 2, Lodz, Poland: Institute of Thermal Technology and Refrigeration, Technical University of Lodz, 1996.

44. Zeegers J., van Dijk H.A.L., A note on the net radiation method applied to a system composed of a semitransparent film between two glazing. Solar Energy Materials and Solar Cells 1994; 33 (4): 23-30.

CHAPTER FOUR

MODELING AND SOFTWARE DEVELOPMENT

Introduction

An important concern for this research was to set up a model that would examine the behaviour of the suggested glazing system in relation to its geometry and in response to the incident solar radiation and heat transfer mechanisms, to and from the adjacent indoor and ambient environments. *Fig 4.01* shows the interaction of the different components of the algorithm/model. Accurate determination of the hourly solar radiation received during an average day per month was considered to be a prerequisite when modeling the solar energy behavior.

In general, the thermal transmittance of a fenestration product is (ISO/DIN 15099 2003):

$$U_{total} = \frac{\sum A_g U_g + \sum A_f U_f + \sum l_\psi \psi}{A_{total}} \qquad (4.001)$$

Where, A_g and A_f are the projected vision area (i.e. of the glass pane) and frame area, respectively. The length of the vision area perimeter (l_ψ) and (Ψ) is the linear thermal transmittance (W/m.K) and can account for the interaction between frame and glazing or the interaction between frame and an opaque panel. However, the research objectives are to deal with the new glazing suggestion where the frame material and geometry parameters would be assumed as constants at this stage of research, hence not be included in the simulation, i.e. the research would account for centre of glazing calculation only. Assuming an environment's scenario involving indoor/outdoor temperature differences, with incident solar radiation in this case, the thermal transmittance U_i can be simulated and would be the reciprocal of the thermal resistance R_i of the system for the i^{th} glazing.

$$U_{total} = \frac{1}{\sum_{i=1}^{n+1} R_i + \sum_{i=1}^{n} R_{g.i}} \qquad (4.002)$$

R_g is the thermal resistance of the projected vision area, of glass, for the i^{th} space where the 1st space is the outdoor environment and the last space is the indoor environment and the spaces between the glazings cavities would be:

$$R_i = \frac{T_{ni} - T_{ne}}{q_i} \qquad (4.003)$$

Where q_i is the transmitted energy for the i^{th} space, the environment temperature T_{ne} is the weighted average of the ambient environment temperature, T_{rm} is the mean radiant temperature, which is determined for outdoor and indoor environment in boundary

condition. Both temperatures are respectively calculated, according to the relative magnitudes of the convective and radiative heat transfer coefficients (h_c and h_r) that exist between the surfaces of the fenestration system and the environment. Thus, T_{ne} is:

$$T_{ne} = \frac{h_c T_{air} - h_r T_{rm}}{h_c + h_r} \tag{4.004}$$

As shown in *chapter 3*, most of the current algorithms, which simulate radiative heat transfer in glazing, tend to simplify the modelling environment. Justification is given by assuming a small role for this component, compared to other contributors to heat transfer processes, e.g. convectional heat losses through the glazing surface, window frame and thermal bridging heat losses. It was also shown that most of the net radiation algorithms, which are commonly used, could return error results when dealing with complex glazing environments, or with system with multiple coating; as those algorithms usually assume that the glass is opaque to radiation. Thus, a raytracing algorithm is proposed to address these issues:

4.1 PROPOSED RAYTRACING ALGORITHM FOR THE GLAZING SYSTEM:

The following algorithm assumes the outer vertical pane surface of the suggested multiple glazing system as its origin; with the vector input values transferred manually from SMARTS2 output file, e.g. those of the direct beam, the sky diffused and ground diffused components.

As the rays would pass through a first Fresnel glazing interface; the corresponding angle of refraction is calculated to trace the path of rays passing across the thickness of the glass layer. Capture surfaces and planes are then created for these rays, in the two dimensional glazing model, *see fig 4.01(i)*, to emulate the optical behaviour of the relevant surfaces to the passing irradiation:

Capture planes:

Planes defined by raytracing algorithms (2D & 3D) to Find the intersection of a ray and an object or plane and requires solving an equation. The exact form of the equation depends on the type of plane or surface. For all intersection tests, the ray in vector form is represented as (Wyvill 1998):

$$\mathbf{p} = \mathbf{u} + \mathbf{v}t \tag{4.005}$$

u is the starting point and **v** is the direction of the ray. The variable **t** indicates how far down the ray the intersection point **p** is. To create a capture plane of a triangle in a two dimensional model, e.g. as the ones formed in the second and fourth zone respectively, three vertices ($\mathbf{a}_i$, $\mathbf{b}_i$, $\mathbf{c}_i$) are assumed to describe the triangle in a plane, where the cross product of those vectors $(\mathbf{b}_i\text{-}\mathbf{a}_i)\times(\mathbf{b}_i\text{-}\mathbf{c}_i)$ is normal to this plane, $(\mathbf{b}_2\text{-}\mathbf{a}_2)\times(\mathbf{b}_2\text{-}\mathbf{c}_2)$; $(\mathbf{b}_4\text{-}\mathbf{a}_4)\times(\mathbf{b}_4\text{-}\mathbf{c}_4)$ for the second and fourth zone, respectively. (*i*) identifies the plane of relevant vertices

$$\mathbf{n} = (\mathbf{b}_i - \mathbf{a}_i) \times (\mathbf{b}_i - \mathbf{c}_i) \tag{4.006}$$

For any point **p** in the plane:

$$\mathbf{n}\times(\mathbf{p}-\mathbf{b}_i)=(\mathbf{b}_i-\mathbf{a}_i)\times(\mathbf{b}_i-\mathbf{c}_i)\times(\mathbf{p}-\mathbf{b}_i)=0 \qquad (4.007)$$

This is the equation of the plane. Where the ray meets the plane $\mathbf{p}=\mathbf{u}+\mathbf{vt}$, so satisfies (4.005) and:

$$\mathbf{n}\times(\mathbf{u}+\mathbf{vt}-\mathbf{b}_i)=0$$
$$\mathbf{t}=\mathbf{n}\times(\mathbf{u}-\mathbf{b}_i)/\mathbf{n}\times\mathbf{v} \qquad (4.008)$$

If ($\mathbf{n}\times\mathbf{v}=0$), it can not be realised and there is no intersection, otherwise there would be single intersection with the plane ($\mathbf{p}=\mathbf{u}+\mathbf{vt}$) and the surface normal is **n**, still **p** would be outside the triangle. If there are three products which are described as:

$$(\mathbf{b}_i-\mathbf{a}_i)\times(\mathbf{p}-\mathbf{a}_i).\mathbf{n},(\mathbf{c}_i-\mathbf{b}_i)\times(\mathbf{p}-\mathbf{b}_i).\mathbf{n},(\mathbf{a}_i-\mathbf{c}_i)\times(\mathbf{p}-\mathbf{c}_i).\mathbf{n}\,. \qquad (4.009)$$

Then, whenever the expressions have the same sign, then the (**p**) "intersection" is inside the triangle, being with different sign means the vector products would be either to the left or the right of the triangle. Following that, several capture zones were created for the glazing model to represent the different planes, which the radiation component would pass through, *see fig 4.01(ii)*:

- In the First zone: representing the outer vertical surface of the outer glazing pane.
- In the Second Zone; which included:

(i) The lower horizontal surface of the separating cavity spacer-frame.

(ii) The inner vertical surface of the outer glazing pane.

(iii) The outer layer of the angle-inserted element.

- In the Fourth zone included;

(i) The upper horizontal surface of the separating cavity spacer frame.

(ii) The inner vertical surface of the inner glazing pane.

(iii) The inner layer of the angle inserted element.

All the other surfaces within the other zones were treated only according to Fresnel formulas, and as follows:

First zone: upon propagation from the point of origin (i.e. where incident ray would hit the surface at: $\mathbf{0°\leq\theta_1\leq 90°}$

Where $\theta_1=\theta_{incidence}$ and $\theta_2=\theta_{refracted}$, using Snell 2nd law, assuming $\mathbf{n_1}=\mathbf{n}_{air}$, $\mathbf{n_2}=\mathbf{n}_{glass}$

$$\frac{n_1}{n_2}=\frac{\theta_2}{\theta_1} \qquad (4.010)$$

For a single glass pane, the extinction coefficient is very small, so the expressions for a perfect dielectric (Siegel, 1992a) can be used to obtain the interface reflectivity.

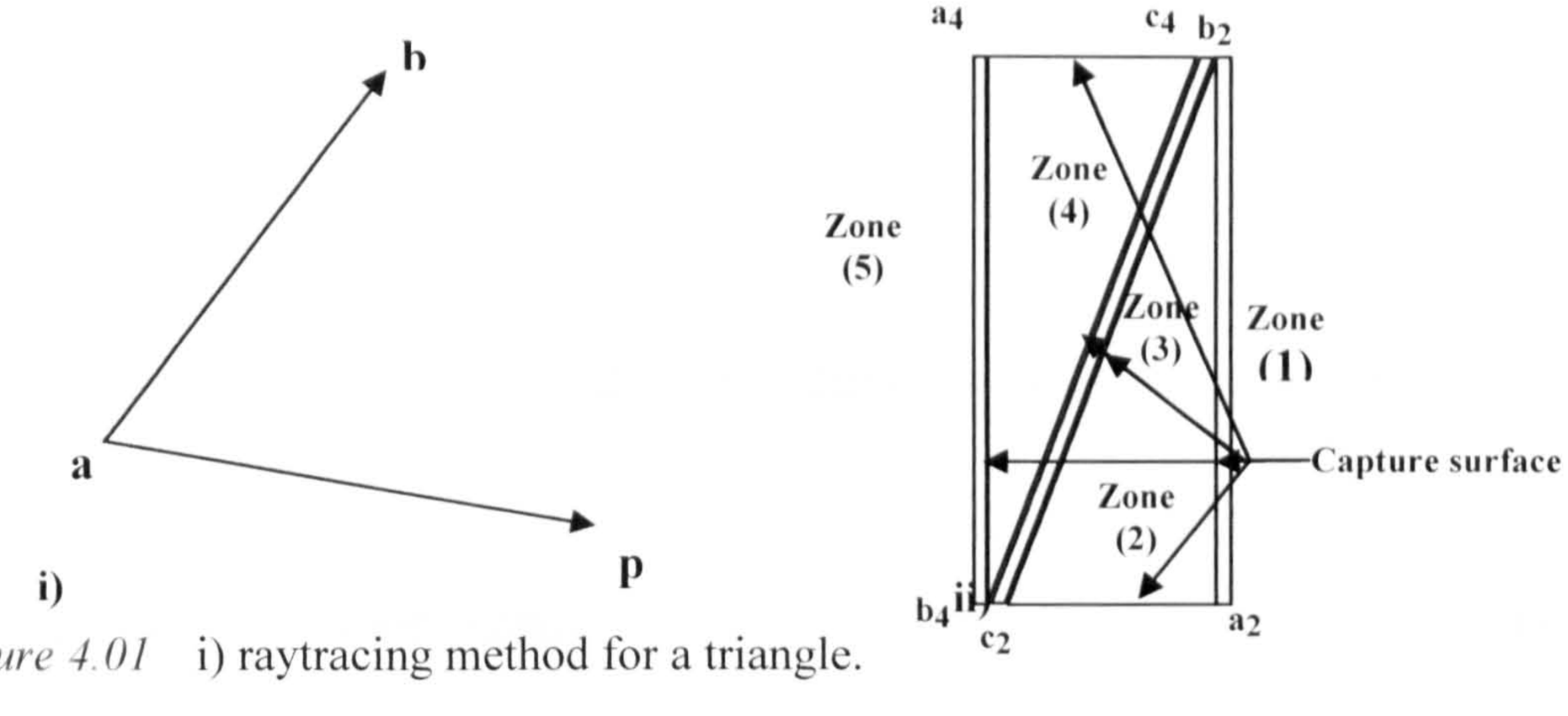

Figure 4.01 i) raytracing method for a triangle.

ii) Schematic of the zones and capture surfaces in the model.

A constant absorption coefficient is assumed and both polarization components, a parallel (r_{II}) and a perpendicular ($r_{\perp}$) planes are taken into account; *see fig 4.02*, where $\boldsymbol{n_{1,2,3}}$ is the refractive for corresponding material and $\boldsymbol{K_{1,2,3}}$ is the extinction coefficient .of glass.

Second zone: Upon emerging through the first layer of glass pane, the transmitted ray angle will be in a range of $\mathbf{0°} \leq \theta_i \leq \mathbf{90°}$ so if:

θ_i=0°→then $\boldsymbol{X}=\boldsymbol{Y}/\tan\beta$, accordingly in case of a maximum incident angle on the lower spacer surface where $0<\theta_1<90$ when X=Δ.

Then, while max point ***B*** in (X, Y coordinates), *see fig 4.03*, a first reflection will be at:

$\boldsymbol{B^1}=(\boldsymbol{Y^1})^2+(\boldsymbol{X^1})^2$ and θ_f is the inclination angle of the film in the cavity, and $\theta_i = 90-\phi$

In a second reflection, three possibilities would emerge:

- If θ_{Ri}=0 where θ_{Ri} is the angle of reflection and so $X=\Delta$, $Y=L$; *see fig 4.03, b.*

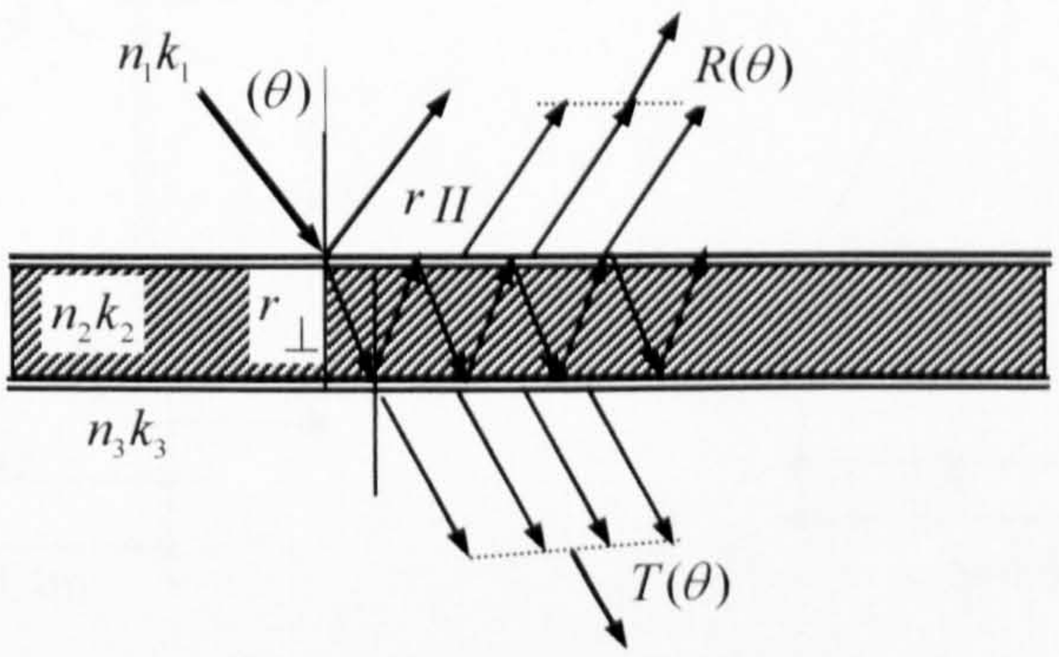

Figure 4.02 Showing multiple reflections and transmittance inside a Fresnel pane of glazing.

- If θ_{Ri}=90 then there will be no reflection as angle θ_f will be zero then.
- This assumption also valid in those simulations where there is no inserted film.
- If $0<\theta_{Ri}<90$ then $\phi = \tan^{-1}\frac{(\Delta - X)}{Y}$

Assuming ψ is the max angle of reflection in this mode, it will be: $\psi=\theta_f-\varphi$

$0<\theta_{Ri}<\psi$ so in this case:

$X=\Delta$, $Y=(\psi-\theta_{Ri})\sqrt{D}/\sin(90+2\theta_{Ri})$ (4.011)

$\psi<\theta_{Ri}<90$, and consequently:

$X=(\theta_{Ri}-90)\sqrt{\theta_f}/\sin(90+\theta_{Ri}-\theta_f)$, $Y=0$ (4.012)

In this case ; $\theta_{R_i} = 90 - \theta_i$ (i.e. $\theta_i<\theta_f$) Also

$w = X\tan\theta_f$,and, $\sin\theta_{R_i} = \frac{Y}{X\tan\beta}$ *(See (a) in fig 4.04)*

Therefore coordinates would be:

$Y = (X\tan\theta_f + \sin\theta_{R_i})$, while $X=\tan^{-1}Y$, (4.013)

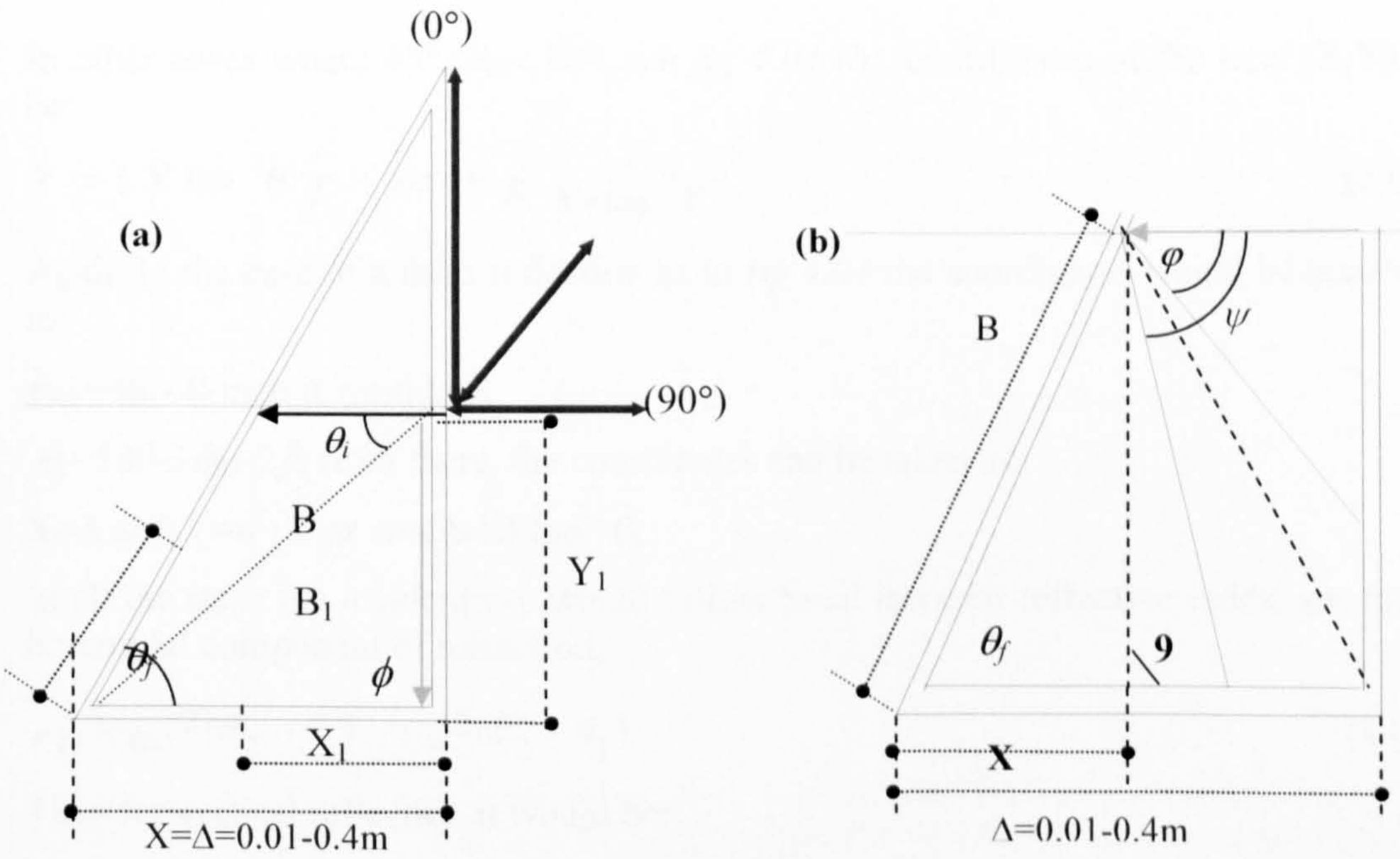

Figure 4.03 showing a) the possibilities of the first zone capturing surfaces.
b) Different possibilities of first reflection.

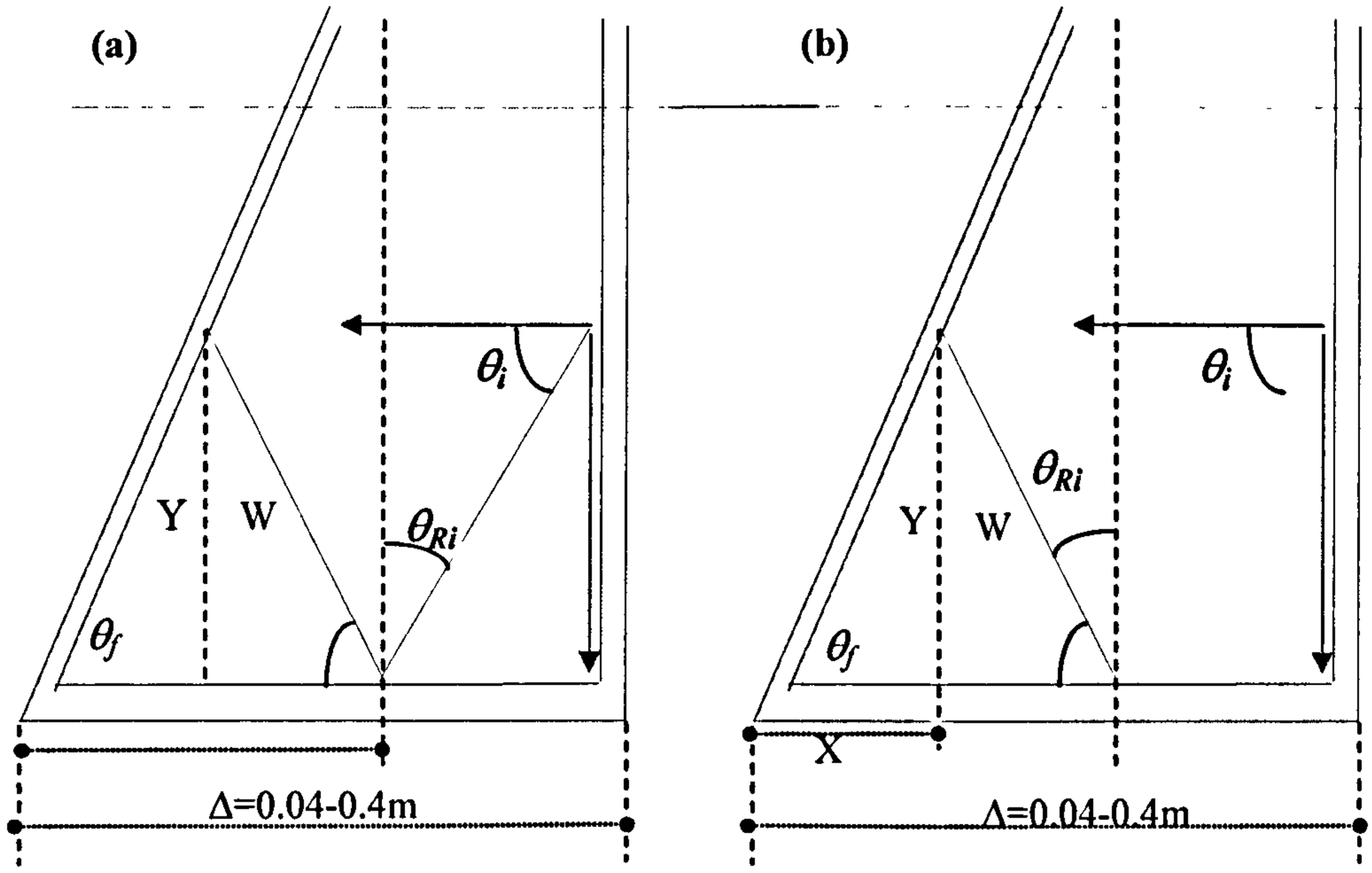

Figure 4.04 showing the possibilities of the second and third reflection (a, b) respectively.

This possibility could also present another first reflection, which would be projected on the "spacer" (capture edge) in the second zone and not on the "film" capture edge, as seen before.

With this possibility, the second reflection would be when $\theta_{RI}=\theta_f=45°$, this latter is the angle of reflection in which the 3rd reflection would be **90°.**

In other cases where $45°<\theta_{Ri}<90°$, *see fig 4.04 (b)*, coordinates of the new (X,Y) can be:

$$Y = (X \tan \theta_f + \sin \theta_R \quad X=\tan^{-1}Y \tag{4.014}$$

Again In the case of a third reflection as in *fig 4.04* the coordinates would be according to:

$\theta_{R2}=\theta_{R1}-\theta_f$ then it would be:

$\theta_I=180-3\theta_{R1}-2\beta$, from there, the coordinates can be taken as:

X=Δ and **Y=w+Y** as **w=(Δ-X) tan$^{-1}\theta_i$.**

In all the steps the incident ray would follow Snell laws for refractive index, so: for the horizontal component of refraction,

$$r_{II} = \tan^2(\theta_2 - \theta_1) \,/\, \tan^2(\theta_2 + \theta_1) \tag{4.015}$$

Then for vertical reflection it would be:

$$r_{\perp} = \sin^2(\theta_2 - \theta_1) \,/\, \sin^2(\theta_2 + \theta_1) \tag{4.016}$$

Hence, for multiple reflective, total transmissivity of the refracted rays would be:

$$\overline{\tau_r} = 1/2 \times \left[\frac{1 - r_{\perp}}{1 + r_{\perp}} + \frac{1 - r_{II}}{1 + r_{II}} \right] \tag{4.017}$$

Assuming that (I) is the intensity of the incident solar energy:

$$dI = -IKdx \tag{4.018}$$

Where (dI) is the *change in incident solar energy after attenuation by* the extinction coefficient, (K). Thus, transmissivity, could be defined by the expression:

$$\tau_a = e^{-kl/\cos\vartheta} \tag{4.019}$$

Where τ_a is the *portion of transmissivity* that relates to *absorption of the incident light* with the *subscript (a)* and (KL) is determined by the glass type, i.e. K= the extinction factor, L= the path of the refracted light beam in medium in meters), while ($\cos\theta_l$) is the angle of incidence, and so the *mean value of transmissivity* would be:

$$\overline{\tau_m} = \tau_a + \overline{\tau_r} - 1 \tag{4.020}$$

And as for absorbitvity:

$$\alpha \approx 1 - \tau_a \tag{4.021}$$

Also:

$$\rho = \tau_a - \bar{\tau}_m \tag{4.022}$$

Dividing the incident solar intensity over the module surface area of (1.0m× unit length of the window width), $dI_D = I_0 / dx\, y$ as (I_D) is the direct intensity per unit length along the height of the glazing.

$$I_{transmit} = I_D(\bar{\tau}_m)_{S1} \tag{4.023}$$

Where ($I_{transmit}$) is the direct transmitted radiation intensity and ($\bar{\tau}_m$) is the mean transmissivity of first surface designated ($S1$). If the emerging radiation were incident on a semitransparent surface then, again there would be another refraction, reflection and absorption where the emerging intensity would be:

$$I_{transmit} = I_D(\bar{\tau}_m)_{S1}(\bar{\tau}_m)_{S2} \tag{4.024}$$

While, some of the radiation would reflect either from the inner glazing surface or from a non-transparent reflecting surfaces (i.e. like the spacers) then:

$$I_{transmit} = I_D(\bar{\tau}_m)_{S1}\rho_{S2},\rho_{S3} \tag{4.025}$$

(ρ) is the reflectivity of (S) at the end, by integrating for all the emerging intensities from the first zone (up to three reflections per radiation unit).

Third zone: all residual/ incident radiation that would go into the film layer would emerge to the next cavity, similar in environment and geometry to that of the first cavity layer apart from the switching of co-ordinates, i.e. upside down and right to left.

Fourth zone: a simplified alternative is proposed to model the behaviour of the transmitted energy emerging to this zone (i.e. to minimise CPU time) depending on assuming similar geometry and optical properties of the second zone and by using a fitting curve; it could be said that:

$$I_{totaltransmit} = \sum_{i=1}^{n=3} \left| I_{filmlayer} \times (I_{firstlayer} / I_{Incident}) \right|_{transmit} \quad (4.026)$$

Where n= is again the maximum number of expected reflections (up to 3), *see appendix ii.2.*

Fifth zone: a similar approach to the first zone was used for this zone. In summary, the total transmitted radiative solar intensity would be:

$$I_{transmit} = I_D \sum_{S=i+1}^{n=3} (\bar{\tau}_m)_S \cdot \sum_{S=i+1}^{n=2} \rho_S \quad (4.027)$$

While for the total absorbed energy:

$$I_{absorbed} = I_D \sum_{S=i+1}^{n=3} (\bar{\tau}_m)_S \sum_{S=i+1}^{n=2} \alpha_S \quad (4.028)$$

(n) here is total the number of reflections; (i) refers to the number of a surface S. The algorithm also accounted for the remaining absorbed energy that is a product of each reflection and refraction.

In summary, the method calculated the residual transmitted insolation after each reflection and absorption. While the re-emitted radiation as a long wave radiation was accounted for in the forthcoming CFD simulation. While, the option of writing the current algorithm as an added code for CFD software would take a considerable CPU time, and raise the need to parallel processors to finish the simulation. Consequently, two types of output results are carried over manually, i.e. as a file, to the next stage:

- The total transmitted intensity ($I_{totaltransmit}$), which will be added to the final counter.
- The total absorbed intensity ($I_{totaabsorbed}$), which will be considered as embedded fixed heat flux (W/m^2) for convection and conduction calculations, added as long wave radiation at the start of the CFD simulation.

Hence, in accordance with the objectives and methodology of the research (*see 1.8.i and 1.8.ii*), the research chose: the following modelling techniques:

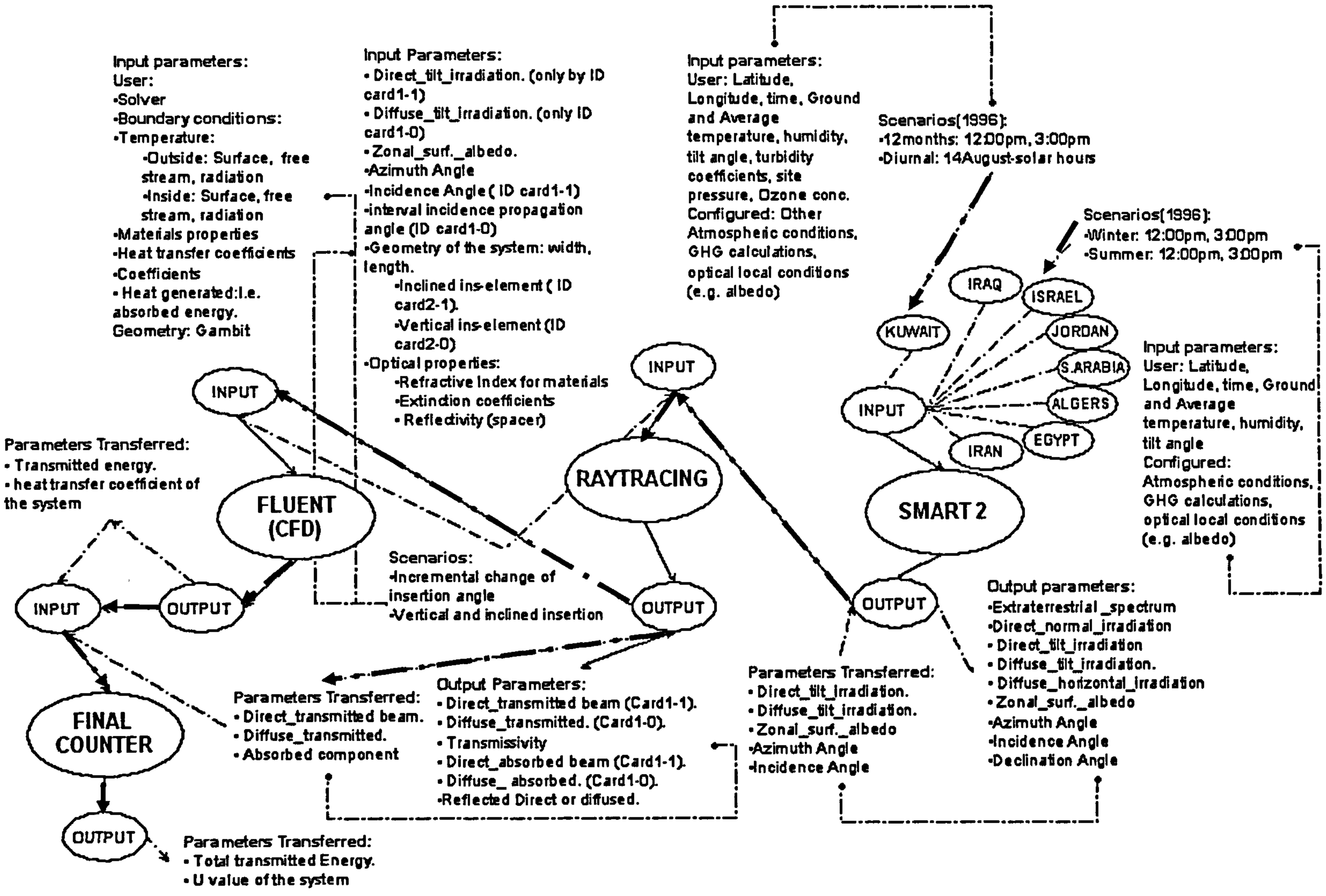

Figure4.05 a flow diagram of the different components of the software tiers

- **Gueymard model**, which is an algorithm to calculate the amount of the insolation relevant to the diurnal/annual cycles and parameters of the chosen latitudes, *see chapter 3, conclusion.* SMARTS2 (*Simple Model of the Atmospheric Radiative Transfer of Sunshine*) version 2.8 was chosen for the research. This uses the same algorithm that was developed by Florida solar center, N. Berkley Labs/USA.
- **A *novel* Raytracing modeling technique** developed by the research to model the radiative component of the heat transfer through the glazing; with a relevant suggested code that could account for changes of parameters in a multiple glazing geometry, materials specifications and optical properties with regard to insolation components, i.e. direct, diffused and albedo.
- **Convection and conduction modeling;** those two components of heat transfer, had to be calculated separately from the radiative component, through the use of an available CFD software (i.e. computational fluid dynamics) tool. Fluent 5.3 & 5.4 were used for this purpose.

Figure 4.05 shows a flow diagram of how the chosen models were compiled to verify the hypothesis for the suggested system; it shows how the different outputs of one stage are used as inputs for the next one, i.e. SMARTS2 output results are input to the raytracing algorithm and the latter results are used as inputs for both of the CFD and the final counter.

A main disadvantage of having three such platforms, linked with a code to perform the simulation, is the expected long CPU time. This issue is usually addressed through distributing the bulk of simulation into batches handled by parallel processors simultaneously, i.e. that of a network or several terminals. However such an approach is not user friendly for researchers, as it requires the user to have continual access to those facilities. Consequently, it was decided to process results from each model in an OUTPUT file fed manually into the input of the next simulation platform. The latter approach, though not attractive, was favored as it offered the user the option of performing the calculations on serial processors as in individual desktop facilities.

4.2 INSOLATION MODELING USING SMARTS2

SMARTS2 is a spectral model in FORTRAN 77 code that calculates direct beam, diffuse and global irradiance incident on the surfaces of any geometry at the Earth's surface. Covering the whole short-wave solar spectrum (280 to 4000 nm), it includes the UVA, UVB, Visible and Near-Infrared bands. Besides the regular irradiance predictions needed for many possible applications, it can also simulate the spectral or broadband irradiance that could be measured by a radiometer, such as, a spectroradiometer, a pyranometer, or a pyrheliometer. It can predict the illuminance on any surface, the luminous efficacy of direct, diffuse, and global radiation, the UV index, as well as various UV action weighted spectra. (Gueymard C. 2002). The first version of SMARTS2 was released in 1994 and was described in available literature (Gueymard, 1994b, 1995).

A peer-reviewed journal paper (Gueymard, 2002) also gives a partial but updated description of the model version 2.8; which is still currently used since November 1996. As a software structure, program files and sub-folders need to be correctly located in a

main SMARTS2 folder/directory. The program uses a generated input file (e.g., 'SMARTS2.INP' or 'Test_for_July.INP') that contains a multiple input data set in a number of CARDS that are linked to several subroutines and backup data files. Two types of cards are used; main cards that are obligatory for general input and optional cards whose presence and contents depend on the options selected on the preceding Main Card. *See appendix i.1, i.2, i.3 for details of the associated CARDS and data sources.*

An executable file ('SMARTS_291.EXE') is then used to start the processing. A window would appear immediately to ask if working in batch mode is what is required. Upon confirmation execution would resume, using the existing default input file. If a different input file was to be used, (i.e. a differently named input file), then typing "**n**" would prompt a new question about the desired input and output filenames.

I. The parameters of interest in SMARTS2 model's cards are categorized into "inputs" and datafiles "outputs", for the inputs:

- **Latitude and longitude** for the site.
- **Atmospheric card**, for ground level temperature, humidity, average daily temperature, season
- **Water vapour,** information calculated from the previous card.
- **Ozone** was taken locally for the specified band from NASA website.
- **Level of pollution,** which was taken as low, according to the guideline.
- **Carbon dioxide concentration** used from files.
- **Extraterrestrial spectrum**, synthetic Gueymard's was used as it is updated according to the NFRC, i.e. the National Fenestration Rating Council, US.
- **Aerosol model**: the local code was *rewritten* and was used: for Alpha1, Alpha2, Beta, schuep, *see chapter 3 conclusion.*
- **Turbidity value** was calculated from the relevant equation and was introduced as user input.
- **Albedo type**: dry sand was used.
- **Tilted surface and local albedo**: for this setting a tilt of 90° was used and different settings for the local surface azimuth were used, (90, 180, 270°) to account for the different orientation, also dry sand files were used.
- **Spectral range**: 280-4000nm and the solar constant is: 1367.0 W/m^2.
- **Out put type of range**: 280-4000nm.
- **Circumsolar calculation** was by passed; this type of calculation is experimental and based on the same approach that has been used for years for the illuminance. Usually, the results generated in the output file are for direct, diffused ground albedo, and the circumsolar component. Still, there is evidence that this circumsolar output is not accurate as it assumes a static value to the site humidity, which makes the calculation of lower solar angles not accurate and exaggerated, i.e. in real time calculation, humidity changes with the air mass.

Another factor, which supports such decision, is that the ray tracing software would calculate the diffused factor at a one angle per rotating calculation, to give more accurate results. For such cases, more consideration should be given to the input values if the circumsolar, which is a non- scalar quantity, is to be used.

- **Smoothing factor** was used to get a uniform insolation wavelength band.
- **Illuminance card** was by passed for not being relevant to the research's objectives.
- **UV calculations** were bypassed for the same reason.
- **Solar Geometry card**: year, month, day, hour, longitude, latitude, Local Standard Time, and time zone difference.

II. Output results: these could delivered of up to 32 combination files, the ones chosen would include:

- **Solar position:** zenith angle, solar azimuth angle (from North).
- **Relative optical masses:** Raleigh air mass.
- **Specific day details:** (modified as to solar time, Julian day, etc.).
- **CO_2 mixing**; to take pollution turbidity into consideration.
- **Relative gases mixture.**
- **Specific surface calculation**; tilt, surface azimuth, angle of incidence.
- **Diffuse irradiance ratios** (for conversion to Isotropic or anisotropic model (i.e. using Gueymard's built in formulas).
- **List of irradiance per wavelength,** depending on the type of output sought.
- **Broadband irradiance** (W/m^2): for the extraterrestrial, horizontal plan, tilted plane e.g. the relevant case of setting, experimental with circumsolar correction. For all of these there would be direct, diffused and albedo factors.

4.3 MODELING OF THE GLAZING

Modeling of the heat transfer modes across the glazing had to be carried out on two platforms, one for radiation calculations and the other for the combined convection and conduction calculation.

4.3.1 Raytracing Modeling

The research used the relevant developed algorithm, to simulate the radiative component of heat transfer. Nonsequential raytracing methodology was favoured; *see chapter 3 conclusions*, as the simulation tool.

The next decision was to assess how the written code would handle the different components of insolation, i.e. the direct beam, sky diffused and albedo components. A code that manages the three components simultaneously would increase the software complexity; alternatively, an option that deals with them consecutively would increase

the needed CPU time. Finally the latter decision was favoured due to the followings reasons:

(i) It is only part of a larger and extended tool to simulate heat transfer across the glazing system, so it should be simple to use.

(ii) It also should be flexible to account for any relevant changes in the system's geometry, materials properties, and type of insertion of the suggested element.

(iii) It is able to simulate both the direct beam and diffused components of the insolation, with a lesser possibility of facing problems associated with running such code/ software and would also generate simpler type of output files that could be used as inputs for the next level of calculation.

(iv) Minimising distortion when simulating the diffused component.

(v) The objective of having this calculation is to simulate radiative heat transfer; using more complicated methods for raytracing would not improve results substantially, and the nominal difference could be marginal, e.g. works of McCluney 2004, Florida Centre.

(vi) The type of output data expected should be concise and easy to process to the other levels of the algorithm. As such, it would easier to isolate those components of output that are of interest to the next level of simulation.

The flow diagram in *fig. 4.06* shows how the raytracing code would deal with the insolation. The strategy was to divide the model into zones that would have the flexibility to account for any changes in the geometry parameters and tilt angle of the inserted element, it would also have to account for other simulation scenarios with changes to the optical properties, or comparing results with those of a vertical insertion setting or without an inserted element.

A separation between the optical mechanism of the raytracing and any relevant calculation of heat transfer was suggested to reduce CPU time, *see chapter 2*.

Consequently, the developed code was structured as to have generic subroutines, for optical, and for heat transfer calculations approached and managed separately along the flow of the data, *see fig 4.07*.

Consequently, it was decided to arrange the code into three main modules:

- Subroutine for the raytracing mechanism, main decision making modules.
- Subroutines for optical calculation, i.e. relevant to Fresnel formulas.
- Subroutines, which would facilitate the calculations, either, as capture surfaces, identifying/selecting type of radiative components, geometry parameters, decision-making gates, and counters to accumulate results.

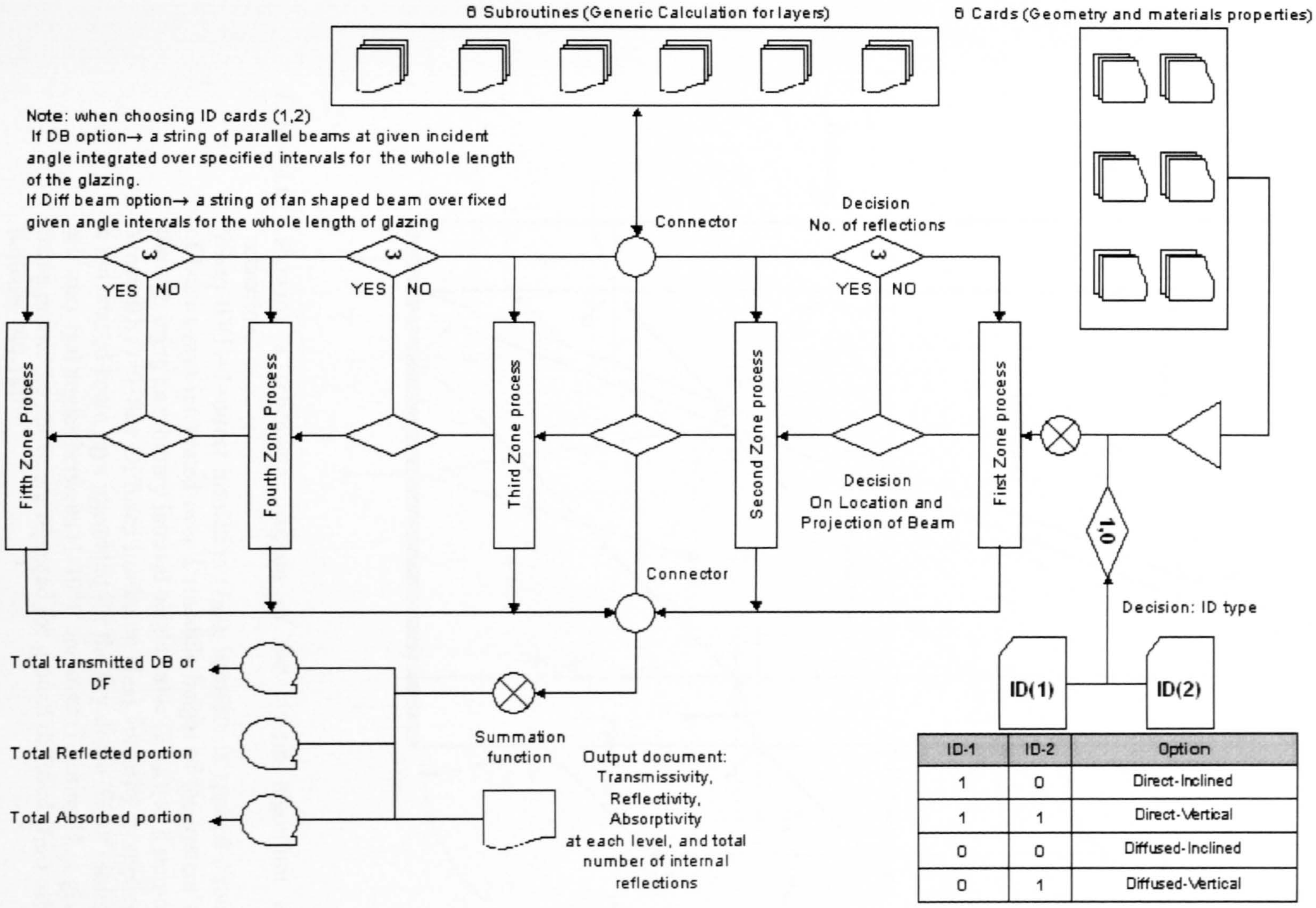

ID-1	ID-2	Option
1	0	Direct-Inclined
1	1	Direct-Vertical
0	0	Diffused-Inclined
0	1	Diffused-Vertical

Figure 4.06 showing a flow diagram of the raytracing algorithm

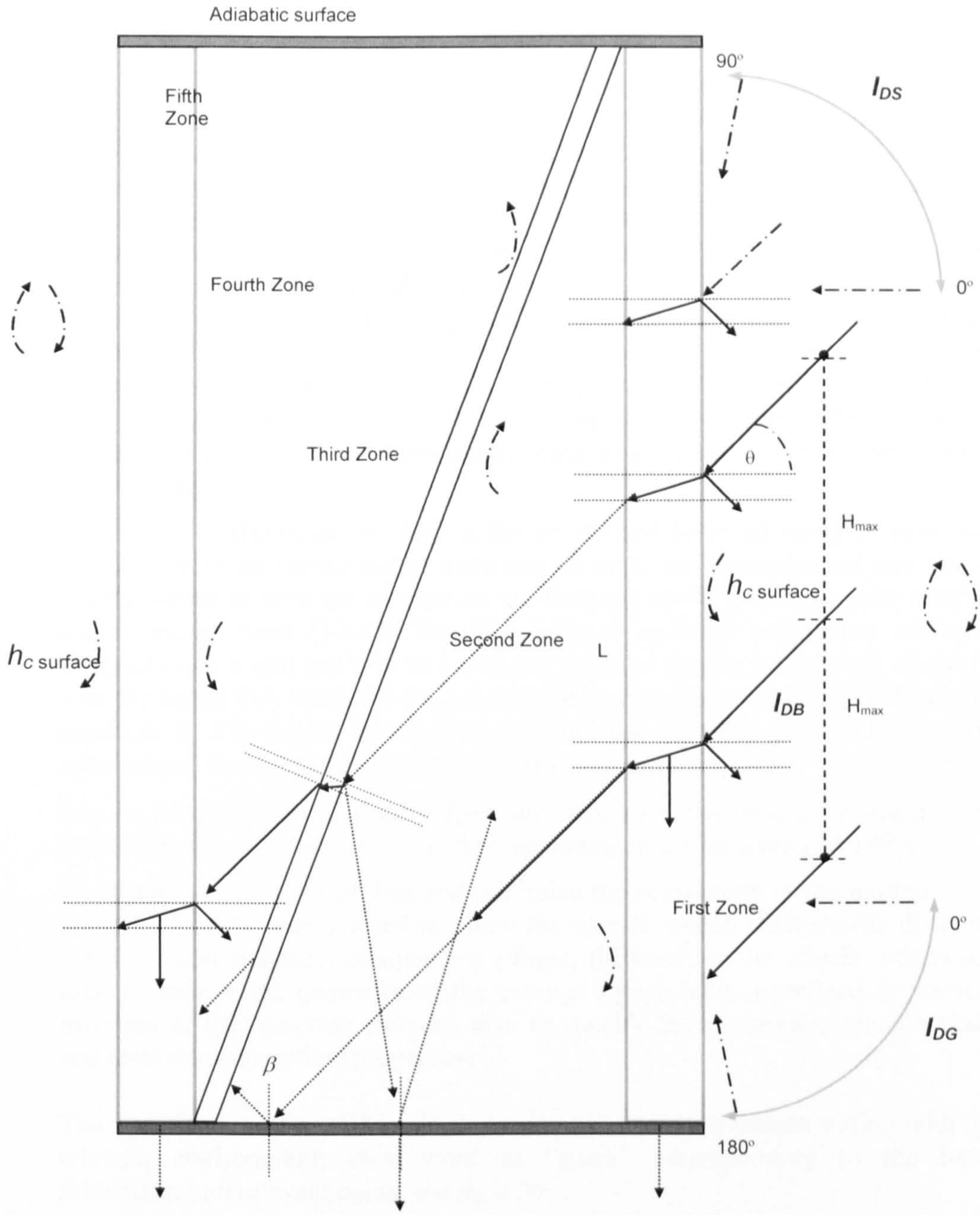

Figure 4.07 showing a schematic diagram of the system algorithm raytracing scenarios.

- When ID(1)=1=direct insolation (I_{DB}), intensity is applied through string of beams-rays integrated over L (module height of the system's glazing) through using an arbitrary interval height value (H_{max}), as a step-counter.
- When ID(1)=0=Sky Diffused insolation (I_{DS}), intensity is applied through a fan shaped beam rays integrated for the sky dome (90-0°) using interval arbitrary real angles between (1-10°)° and over (L) using H_{max} given value
- Same procedure above are repeated for ground diffused (I_{DG}) using angles between (90-180)°

NB: Reflections and absorption are calculated up to the third reflection.

The proposed algorithm maps a modular 2D unit/slice of the suggested glazing, through the following steps:

- For the direct beam calculation (I_{DB}): a string of parallel single beams was assumed to propagate from distant source, i.e. the sun, and is received at any given incidence angle (0-90°), which is provided by the solar model SMARTS2. The direct-beam radiation intensity was then changed from a unit per modular area to a unit per modular length to account for the 2D environment. Then it was integrated over the given height of the modular glazing (L). This is done by dividing (L) into given equal height-interval components (H_{max}), *see fig 4.07*. Built-in counters and relevant algorithms (subroutines) would be used to trace the path of each single ray and its subsequent "ray tree-simulation" pattern through the glazing system zones, by corresponding to the optical properties of each zone's *capture surface* materials, i.e. up to 3 reflections; after which the diminished intensity of the transmitted beam would have minimal effect on the total outcome.
- For the sky diffused beam (I_{DS}): a fan-arc shaped beam of string of rays was assumed, with no source point, depicting an artificial hemispherical sky dome. All the string of rays are to span an arc between (0-90°), at any given interval angle ranging from (1-10°). The Sky-diffused intensity component was also changed from a unit per area to a unit per modular length; integration would be over the height (L), using the (H_{max}), and the assumed interval angle (TH_{max}), *see appendix ii*. The follow up calculation would use the same path of the generic subroutines, this time to account for the sky diffused component.
- For the ground diffused albedo (I_{DG}): the same previous procedure was used to depict the albedo component, this time spanning an arc between (90-180°).
- To ensure an easy flow of data and minimize the complexity of the written code, several ID cards were created to allow the user to switch between the different types of solar radiation components (direct, diffused) or the albedo; others are used to change the geometry of the setting, e.g. to have a inclined or vertical insertion of the bisecting element, also to specify the materials of each surface and their relevant optical properties.

  The combination of the ID cards sets are used to create a certain setting with the relevant environment; they work as "gates" corresponding to the input information on relevant cards, *see fig 4.06*.

- Counters were created for the accumulated reflected and absorbed intensities, for each surface, while another counter would account for the overall transmitted solar intensity.

In summary, the model used Fresnel formulas as part of an explicit method approach (*see chapter 3*). Written code worked at two levels; a collective level, which followed the path of the incident rays, through the glazing environment and a quantitive level that measures the intensity of the emerging rays from the other side of the glazing environment.

4.3.2 Convection & conduction modeling using Fluent

The CFD Software FLUENT was used for modelling the fluid (air in this instance) convectional flow behaviour and the remaining heat transfer modes in the cavities of the glazing system.

The program provides the complete mesh flexibility that was necessary in this case as the suggested geometry involves considerable variations in dimensions used (i.e. range of dimensions is between meters and microns).

In addition, the sharp set angles of the inserted element would need the use of 2D-triangular/ quadrilateral/ wedge or hybrid mixed meshing. The program is written in C language. The computational mesh for the cavity space could be generated in several ways (e.g. using the proprietary software GAMBIT).

The generated meshed model was transferred to the CFD software FLUENT and all the remaining calculation operations were performed within this solver.

The relationship between the various CFD software components is shown in *fig 4.08.* These include setting boundary conditions, defining fluid properties, executing the solution, refining the grid, viewing and post-processing the results.

4.3.2.1 GAMBIT

GAMBIT is a Fluent pre-processor that was used to generate the mesh and grid. The grid/mesh files generated by GAMBIT contained the coordinates of all the nodes in relation to the geometry of the cavity. It also contained information about connectivity i.e. how the nodes are connected to one another to form faces and cells, and the zone types and numbers (e.g., wall-1, pressure-inlet-5, and symmetry-2) of all the faces of the cells.

The first task was to generate three "2D-meshed" models that had the flexibility to be scaled extensively to account for the changes in the cavity width (e.g. of 0.02, 0.04, 0.05, 0.06, 0.07, 0.08, 0.1 and 0.12m), which would affect, in turn, the angle of the internal reflecting element in the cavity, while maintaining the same dimensions for the other different components and materials of the model, three scenarios were investigated:

- A model with an inclined inserted element, which used a hybrid of quad lateral/ triangular meshing regime using the unstructured option.
- A model with a vertical insertion, which used a quad lateral/meshing regime using the structured "pave" option.
- A model with no insertion. Same as above.

For boundary layers, the developed meshed models maintained the same zoning method developed for the raytracing model, i.e. zone 1-5, with respect to the different scenarios.

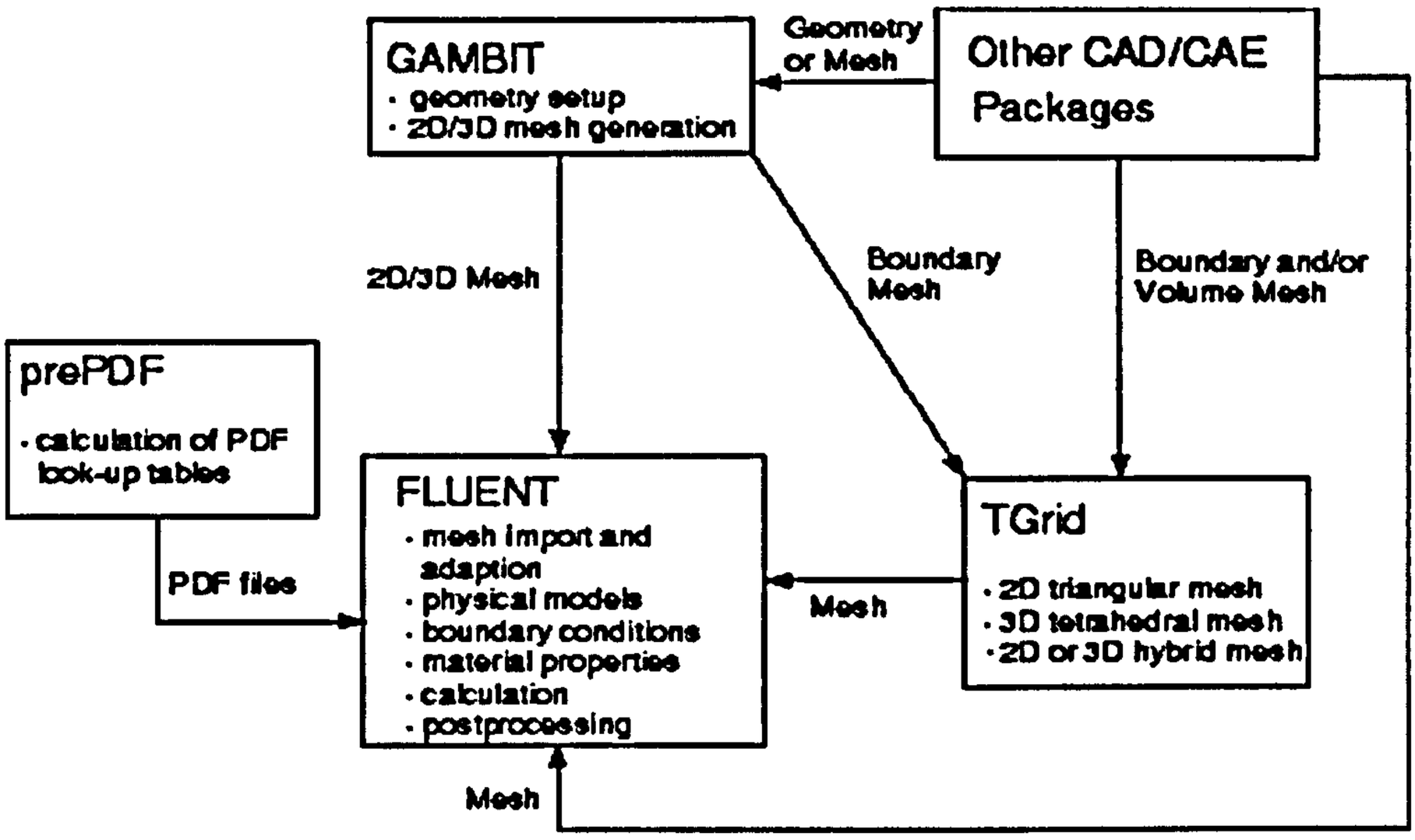

Figure 4.08 showing basic program structure (figure from Fluent5 documentation).

Before exporting to the solver, two main entities were created, within the zones, for the three meshed scenarios:

- A "Solid" entity: for glass, polystyrene and aluminium spacers.
- A "fluid-continuum" entity: for air or any other gas used to fill the system's cavity

Subsequently, Gambit's quality checking procedures were administered to the resolution and density of cells, special care was required for awkward and skewed points in the meshing process and boundary walls formations near the shear walls of the entity (i.e. geometry).

This factor is important for preventing any overlapping of nodes and assuring a smooth conversion during and post processing. Generated mesh files were then exported using Fluent 5/6 as solver. *Fig 4.09* shows a sample of the mesh generation quality; *see Fluent 6 manual.*

4.3.2.2 Solver

FLUENT provides three different solver formulations: segregated, coupled implicit and coupled explicit. All three of the solver formulations provide accurate results for a broad range of flows, though in some cases one formulation may be more appropriate than the others (e.g., it may yield a solution more quickly). The segregated and coupled approaches differ in the way that the continuity, momentum, and (where appropriate) energy and species equations are solved: the segregated solver solves these equations sequentially (i.e., segregated from one another), while the coupled solver solves them simultaneously (i.e., coupled together). Both formulations solve the equations for additional scalars (e.g., turbulence or radiation quantities) sequentially. The implicit and explicit coupled solvers differ in the way that they linearize the coupled equations.

The choice of the appropriate solver for the simulation is dependent on the type and complexity of the model and on the expected CPU-time.

2DDP (two dimensional double precision panel) was chosen as the version solver, as:

- The meshed geometry of the models has features of very disparate length scales (e.g. a 1m modular height of the glazing compared to 0.0001m of width for the polystyrene inserted element; *see Fluent 5 manual*.
- Having high-aspect-ratio grids, which would have been impaired with the single-precision solver, due to inefficient transfer of boundary information.

The Segregated option formulation was chosen. This option was favoured on the base that it would require less memory to run. On the control panel; a steady time factor and absolute velocity formulation were chosen (i.e. relative option is applied in moving grid scenarios).

Imported grid files, from Gambit, were then processed, assigned relevant operating conditions. Solution controls were assumed with default setting when started (e.g. Pressure: standard, Pressure-velocity coupling: simple, momentum: first order upwind and Energy: first order upwind (relevant to buoyancy).

4.4 VERIFICATION OF THE WRITTEN CODE:

One of the tasks of the research involved in writing a code is verifying it. *Software inspection* is usually used as one method for the early detection and removal of existing defects. The value of an inspection stems from the fact that it improves quality and saves defect costs, since it minimizes the time between insertion of a defect and its discovery.

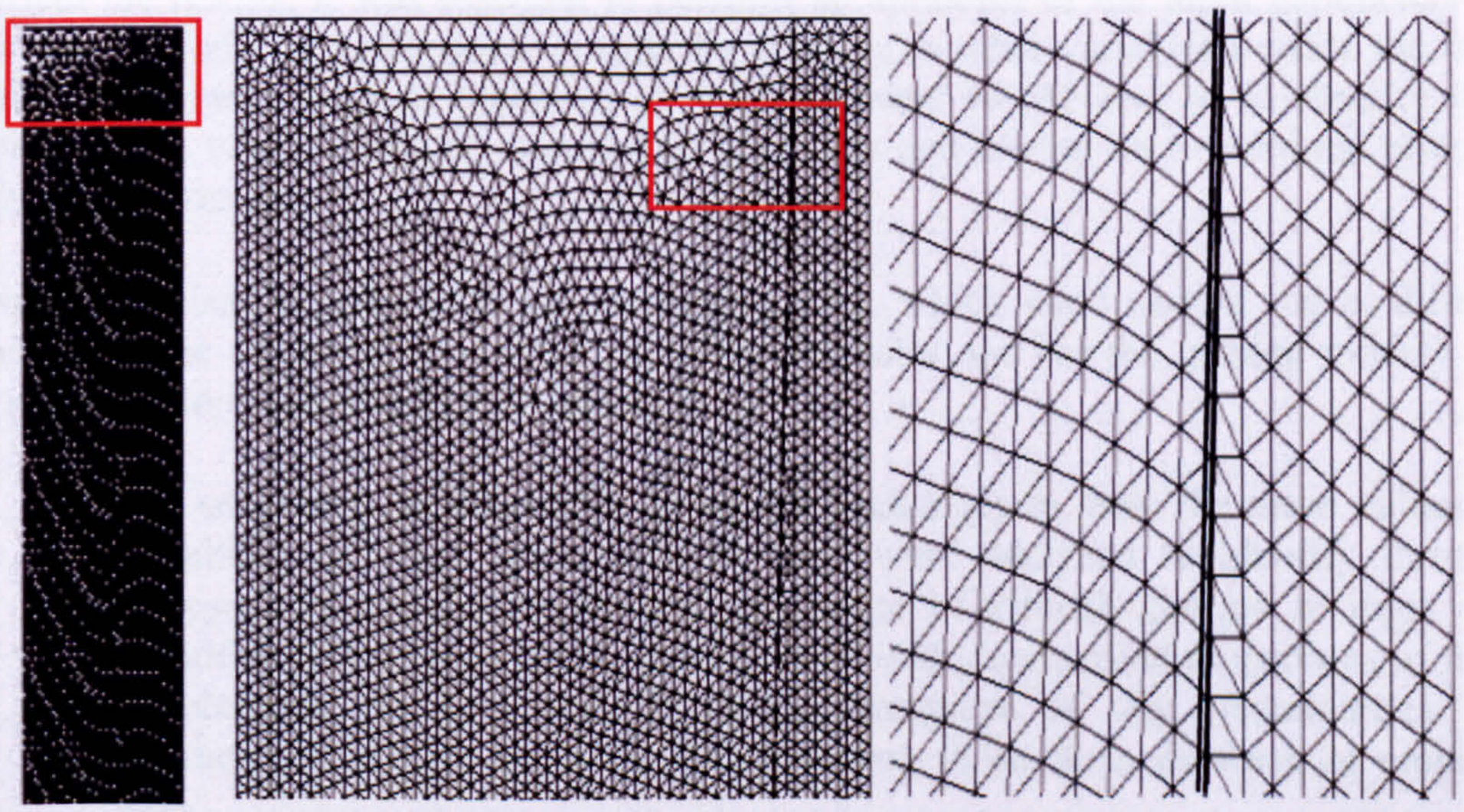

Figure 4.09 3 detailed shots of a meshed geometry of 0.04m cavity width, showing the range of dimensions used and the hybrid types of mesh generated.

This is important because the cost of finding and fixing a defect increases significantly each time it propagates to the next development phase. (Laitenberger 2001).

Software engineering verification principles are a list of steps used through developing a computer *software system* to produce activities, tasks, and procedures, those can be categorised in five main functions of system engineering that were investigated for quality assurance of the computer code:

(i) *Requirement analysis*; by establishing the need for having the software and ensuring that it provides the output that it was built for. *See sensitivity tests, raytracing.*

(ii) *Software design*; choosing the right language that is one that would not create difficulties when transferring the output to another parallel tool; *see 4.1.*

(iii) *Process planning*; to ensure that the different input and output blocks (i.e. subroutines, data, etc.) within the software can be assessed easily on command and without any blockage or crash occurring as the program runs.

(iv) *Process control and verification*: to ensure that software would respond properly in regard to logical input and the flow of that input.

(v) *Validation and testing*: this requires an examination of the different approaches to validation of results and performance;

The latter category, (v), included carrying out *sensitivity tests* for the input parameters that are discussed in the next section. Comparative tool checking is investigated in *chapter 7*. (Thayer H, 2002).

4.5 SENSITIVITY TESTS

As the developed model involves the inclusion of multiple parameters, which would affect the results, it was essential to perform an appraisal of the input parameters that would normally be influenced, in turn, by changes in other variables outside the frame of the program. Another objective of such appraisal would also be to identify those parameters, which could be assumed as constants and having no or minimal effect on the overall results.

Such appraisal is referred to as, sensitivity tests, which were carried out at different levels of the compiled model (i.e. both for the solar and for the glazing model). The criteria set to those tests were to check:

(i) The sensitivity of the models involved to changes in, both the mean values and variability of input parameters as they were analyzed to identify threshold responses. Once the magnitude and nature of critical changes in input were identified, the models could then be tested with downscaled projections of future simulations. At each step in any assessment of any uncertainties their interactions have to be evaluated, including those from database or empirical data.

(ii) The effect that the lack of available empirical data would have on the results expected and, if using a mixture of empirical and built-in input variables in the model, would affect its performance or that of the software developed afterwards.

(iii) A proper method to set up a cross check across the different levels of the compiled model, so as to eliminate repetition or replica scenarios of input parameters, under different names or runs, thus reducing the number of simulations needed to check the hypothesis.

Accordingly, the research used the above-mentioned criteria in identifying those input parameters that would need sensitivity assessment throughout the model:

- In the solar model (SMARTS2); tests were performed to check the validity of the built-in values quoted for the turbidity factors. Another test was performed to check the effect of changing the physical orientation of the glazing system, relevant to the principal coordinates on results.
- In the raytracing model; tests were performed to check the effects of;
  - Changing the optical properties of suggested materials, the effect of polarization and the effects of deflection at the edges of the glazing on the overall results.
  - Level of detail of the raytracing code; i.e. recommended number of projected rays per simulation.
  - Geometry of the suggestion; 2D or 3D setting.
- In the CFD model, tests were performed to check the effects of;
  - Adding the radiation option in the software turned off and on during the simulation to check its impact on the reported heat transfer coefficient.
  - The effect of changing the principal coordinates orientation of the glazing on the external surface system's resistivity, relevant to the change in the wind orientation.

SMARTS2

Lately, much work has been done to assess the performance of SMARTS2 (Gueymard 2001) in relation to empirical data that might be used as input data at different levels of the model. However, as in most of broadband mixed models, a need always exists to check the effect of the high level of *turbidity factors* (i.e. type of the dust, particle sizes, concentration, and their relation to the relative humidity of the considered air mass), in the atmosphere, at the relevant latitudes of interest.

SMARTS2 has several registered limitations, especially in the way it calculates the Albedo, e.g. it returns fixed values outside certain wavelength band, other limitations relate to the values of turbidity assumed in the algorithm.

In order to compensate for the lack of empirical data, most models (i.e. as in SMARTS2) use a modified Ångstrom approach to calculate the turbidity factors, as suggested by (Bird 1984). Thus, it was considered worthwhile to check the viability of the model by comparing its output to that provided by empirical turbidity data when it is available. The SMARTS 2-model output could be compared when implementing the empirical data as against the built-in algorithms used in the model. Data supplied by the Kuwaiti Institute for Scientific Research, energy department, for 1996 were used for this purpose. Calculations for the effect of the dust particles in the air at the specific latitudes; were carried out as follows:

Particle sizes and correspondence to correlation:

The research checked the viability of values of the turbidity coefficient β suggested by Gueymard's model and the α coefficient related to the optical depth of λ_1 wave length. It included checking the coefficients against the gathered data of concentration of dust as the dominant aerosol.

The model used the set of equations of Rayleigh,(Angstrom A. 1929) which states:

$$Q = Q_o \lambda e^{-k\lambda} \tag{4.029}$$

Where:

$$k = \frac{32\,\pi^3 (\mu - 1)^2}{3\,N\,\lambda^4} \tag{4.030}$$

Where, (μ= Index of refraction of particles in the air mass, λ= wave length of incident radiation, and N= number of molecules per cubic centimeter). In the case of the solar radiation passing through the atmosphere in a vertical direction the equation will take the form:

$$Q = Q_{o\lambda} e^{-\frac{\alpha}{\lambda^4}} \tag{4.031}$$

Where:

$$\alpha = \frac{32\pi^3 (\mu - 1)^2 Hp}{3N_0 \times 760} \tag{4.032}$$

Here the H is the height of the homogenous atmosphere in meters at 1013 *hpa* of mercury, temperature of 0°C, Q_0, Q= intensity of attenuated and unattenuated insolation respectively and N_o is the number of the dust particles in a cubic centimeter set at the standard pressure and temperature. As a result the absorption coefficient of the dust will be:

$$\tau = \frac{\beta}{\lambda^{\alpha}} \tag{4.033}$$

Where τ_5 (i.e. the optical thickness at limiting wavelength λ_0=500nm) is expressed here by Ångström coefficient β and Ångström wavelength exponent α_2 for $\lambda > \lambda_0$. In order to check the validity of values of the turbidity coefficient β, as utilised in Gueymard's model, the assumption was made that dust is the main dominant aerosol to be used in the calculations.

Also, as most of the surfaces at the latitudes considered in this research are covered with quartz sand (i.e. SiO_2), another assumption was made that the suspended particles were of quartz and spherical in shape and nature. Accordingly, as base for subsequent calculations, the size and the bulk density of these particles were assumed to be, (Volf Milos B. 1988):

- Bulk density: 2,650 kgm^{-3}.

- For simplicity of the calculations, the shape of the oxide particles (i.e. dust particles) was assumed to be spherical, and sizes similar with diameters of ≈2.6 μm. This diameter was chosen as an acceptable mean size for dust particles, i.e. for those particles staying suspended in the air without sedimentation effect, also relevant to available dust concentration data (Kuwait 1996).

By taking random samples of dust concentration per month or per day from the available empirical data, it was found that the calculated value of α, *see equation 4.031*, could be outside of the range acknowledged in Gueymard's model (i.e. between 0-4). However, in reality the size of the particles will not be uniform, with smaller sizes than those given in the assumption being present, i.e. relevant to Angstrom coefficients, *see definition of Angstrom Coefficients in glossary*. Therefore it is suggested that the current values for α and β, found in the model, were adequate for the purposes of this research.

However it is worth mentioning that the newer version (i.e. SMARTS2 2.9) now uses a revised equation for the turbidity factor calculation in the model (Miskolczi. *et al* 1990), it reads now as:

$$\beta = (0.55^{\alpha 2})\,[0.77682\,(VR^{-1} - 0.00293384)^{0.48896} + 4.1627\,(VR^{-1} - 0.00293384)] \quad (4.034)$$

Where *VR* is the metrological range (km) for visibility.

Dust concentration and relation to diffused component and humidity:

The gathered data of the diffused and direct components of the insolation were checked against dust concentration and relative humidity levels to assess the effect of variations of dust concentration on the magnitude of the diffused component of the insolation in relation to the direct component. This comparison included the effect of changes of relative humidity on the calculations. The method by which the effects of the various parameters were assessed was as follows:

(i) The relative portion of the diffused component of insolation was checked (as a percentage) against the whole incident net global solar gain for the same period, to show the effect of dust concentration on the amount of diffused component obtained.

(ii) Humidity levels were checked for the same period

(iii) Trend lines were drawn to understand the fluctuating behaviour of the diffused component of insolation in relation to the effect of humidity and dust concentration on the results achieved.

(iv) For the sensitivity check, data for dust concentration was taken for the 24-hour period of the 14th day for each month respectively. A relation between the available empirical dust concentration data and the turbidity optical thickness was derived using the following formula:

$$\tau_5 = 2^{\alpha 2}\,\beta \quad (4.035)$$

Where τ_5 (i.e. the optical thickness) is expressed here by Angstrom coefficient β and Angstrom aerosol $\alpha 2$, thus reflecting the increasing contribution to this turbidity coefficient.

A curve fit was then generated by calculating the dust concentrations at 12:00 noon for the 14th day of the month for the year, i.e. Kuwait dust data 1996, then to its relation to the average at that day. Results were then compared to the annual average dust concentration for the 14th day/ month of that year.

Additionally, trial runs were made using SMARTS2 by utilising the empirical solar, humidity and dust data.
The optimum average dust result/ month that provided the best result for the software: 1.0625/1.033889, i.e. here June, in relation to the mean average dust concentration throughout the year was selected to normalise the rest of data, *see table 4.01*. The results were then used to normalise the model inputs for the remaining months.

Consequently a profile was drawn for ($\alpha 1$,$\alpha 2$), using wavelength exponents; *see table 4.02*, for different aerosol models (Shettle and Fenn, 1979) and eventually β was recalculated, as either average or hazy, depending on size and concentration of aerosols, using Angstrom's definition (Angstrom A. 1929), while the previous method used to represent Angstrom's coefficient of $\alpha 2$ as 0.085 as a pretext value taken for rural conditions and is built-in into SMARTS2.

Table 4.02, shows those results, where τ_5 could be calculated from either of two types of β depending on the corresponding value of ($\alpha 1$,$\alpha 2$) and relative humidity.

Upon checking the relation between the dust concentration at certain times (daily) and the relative humidity concentration for the same period against recorded amounts of the diffused component of the insolation for that period; it was found that there was an evident link that might already affect the turbidity factors used in Gueymard's model; this might be due to the effect of humidity on the size of dust particles.

However, for the purpose of generating input data only for the ray-tracing model, it was considered that there would not be a need to re-evaluate the obtained results against any refined formula for the turbidity factors.

Table 4.01 Average dust concentration (Kuwait 1996)

Average dust concentration 14th/month/year	Month	Dust concentration for 12h/14th/month mg/cm^3	Average value mg/cm^3
	January	0.03	0.022083
	February	0.14	0.130833
	March	0.62	1.105417
	April	0.78	1.467083
	May	1.49	1.427917
1.033889	June	0.74	1.0625
	July	1.51	1.761667
	August	0.11	0.405833
	September	1.14	1.610417
	October	1.06	1.557917
	November	1.59	1.477083
	December	0.32	0.377917

Table 4.02 values of wavelength exponents for different aerosol models (Gueymard 2001)
NB α_1 is Ångström wavelength exponent for $\lambda < \lambda_0$, α_2 is for $\lambda > \lambda_0$

Relative Humidity		**0%**	**50%**	**70%**	**80%**	**90%**	**95%**	**98%**	**99%**
Rural	α1	0.933	0.932	0.928	0.902	0.844	0.804	0.721	0.659
	α2	1.444	1.441	1.428	1.376	1.377	1.371	1.205	1.134
Urban	α1	0.822	0.827	0.838	0.829	0.779	0.705	0.583	0.492
	α2	1.167	1.171	1.186	1.229	1.256	1.252	1.197	1.127
Maritime	α1	0.468	0.449	0.378	0.226	0.232	0.195	0.141	0.107
	α2	0.626	0.598	0.508	0.286	0.246	0.175	0.098	0.053
Tropospheric	α1	1.01	1.008	1.005	0.98	0.911	0.864	0.797	0.736
	α2	2.389	2.379	2.357	2.262	2.13	2.058	1.962	1.881

Effect of the orientation;

The placement of windows/openings in buildings envelope, relative to walls facing any of the four principal orientations, affects the amount of day lighting and energy entering the building spaces. Thus, the effect of the orientation, as a parameter on the suggested glazing, was investigated, to verify its effect. Several scenarios, accounting for changes in the orientation setting and season were tested for Kuwait.

An orientation parameter would usually affect the heat transfer through system in two aspects:

(i) By influencing the amount of insolation received, i.e. of the direct beam component, with relevance to the solar azimuth angle, solar inclination angle and the tilt of the system. Those usually govern the corresponding view factors of the glazing system surfaces. View factors are also controlled by the ensuing geometry (i.e. of both the solar position and the glazing system). However, it was found that such effect would only start to be noticeable within a solar inclination angle of +40~45 degrees (i.e. works of Kurata K. *et al* 1998, Bodart M. 2002).

In order to test the effect of this parameter on the amount of insolation received, several runs were carried out on SMARTS2 and the raytracing code using empirical data of Kuwait 1996; and assuming seasonal scenarios (14 August/summer, 14 January/winter), which were tested for several insertion angles of the proposed element. Scenarios also assumed changes in the surface azimuth angle (e.g. 90, 180, and 270°) to account for East, South and West orientations respectively. *See fig. 4.10*

(ii) The local effect of the system's surface resistivity (i.e. relevant to the local ensuing convection regime), this parameter is governed by the local surface heat transfer coefficient of the system, which in turn is affected by location of the glazing system and the glazing surface wind correction factor, relevant to the orientation and the prevailing wind (windward or leeward) ISO 15099. This aspect would be further investigated in detail in another section.

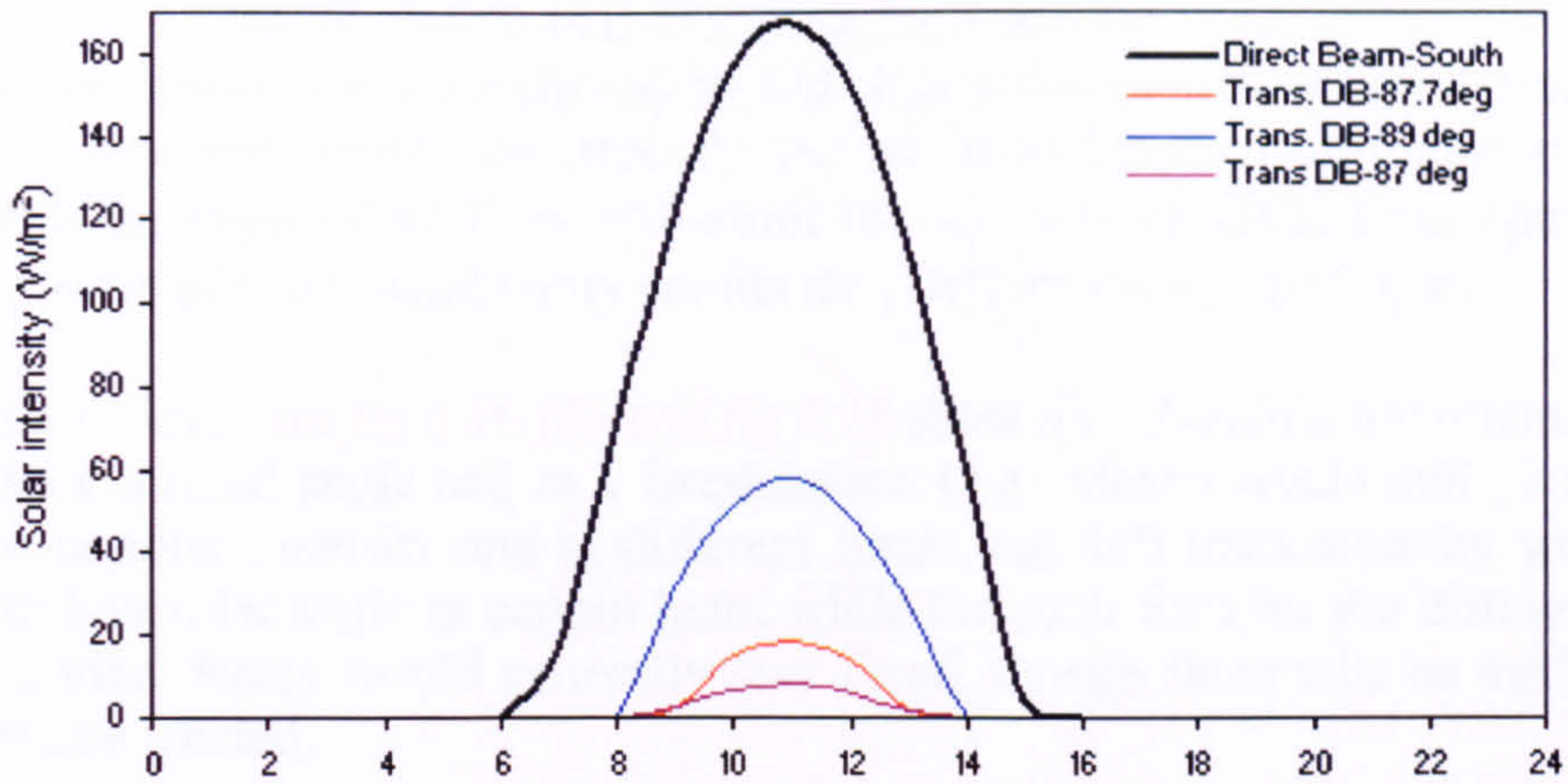

A)

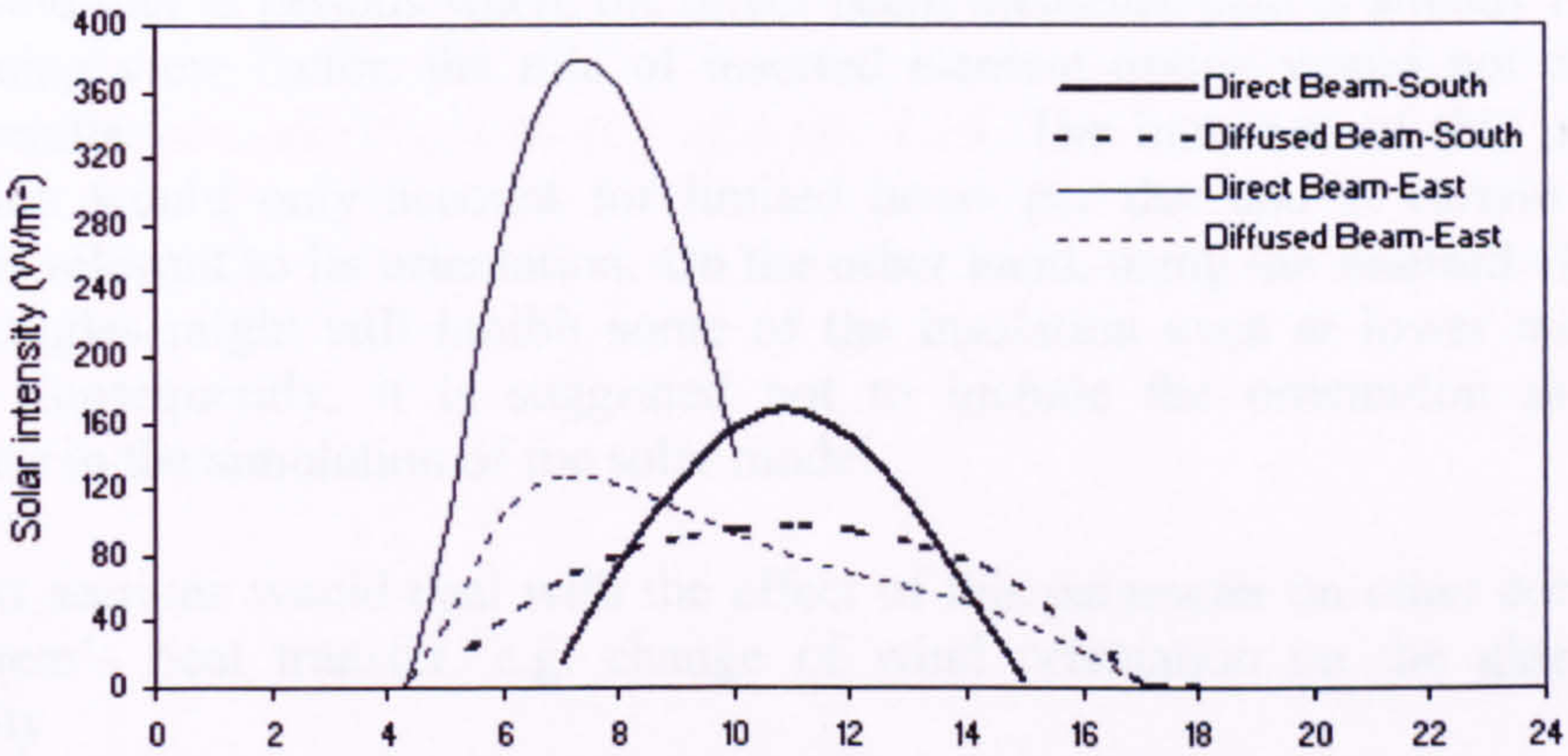

B)

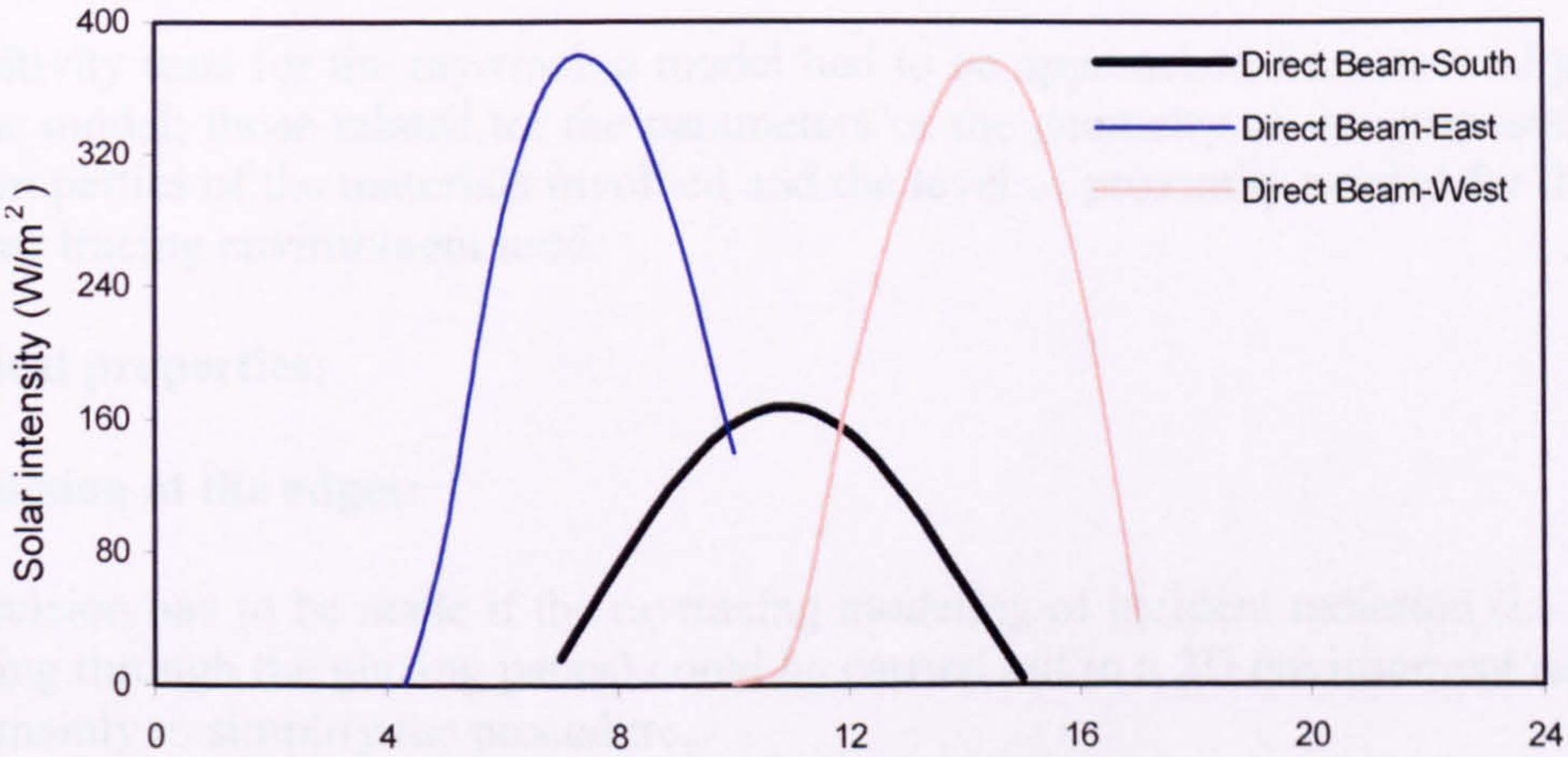

C)

Figure 4.10 showing three simulation tests to the parameter sensitivity:
A) Transmissivity values of the system for several insertion angles of the element- Kuwait 14th August- South Orientation
B) Transmissivity values of the direct and diffused beam for the South and East orientation respectively - Kuwait 14th August
C) Transmissivity values for a vertical system with no element for the Southern, Western and Eastern orientation-Kuwait 14th August.

Figure 4.10 (A) shows clearly that changing the insertion angle of the element during the solar time (hours) of a certain day would change the amount of direct beam admitted into the system and would also affect the periods in which such admission starts to take effect. E.g. an angle of 87.7° would admit the direct beam (DB) from 6am-15: 45pm while an angle of 89.0° would only admits the (DB), from 8am-14:00pm.

Other simulations, *see fig 4.10 (B) and fig 1.15* show that changing the orientation while maintaining a fixed angle and in a fixed season (e.g. winter) would still yield different variation in solar intensity and at different times, e.g. DB transmissivity would fall to zero with low solar angle at certain hour, while the solar time for the diffused beam, of the same view factor would generally stay fixed, though there will be variation in its intensity as expected.

Changing this parameter *does* affect insolation results, however from a practical point; it can be said that in periods where the direct beam incidence path is already restricted by the ensuing view factor, the role of inserted element option would not considerably affect results, *see also fig 4.10 (C) and fig. 1.16*. The inclusion of this parameter in simulation would only account for limited hours per day and at certain settings of windows relevant to its orientation. On the other hand, using the inserted element even at low angles might still inhibit some of the insolation even at lower sun incidence angles. Consequently, it is suggested not to include the orientation as a feasible parameter in the simulation of the solar model.

The next sections would deal with the effect of this parameter on other contributors to the system's heat transfer, e.g. change of wind orientation on the glazing surface resistivity

RAY-TRACING MODEL

Sensitivity tests for the ray-tracing model had to be approached from several platforms in the model; those related to: the parameters of the geometry of the proposed system, the properties of the materials involved and the level of proximity needed for the sort of the ray tracing environment used:

Optical properties:

Deflection at the edges:

A decision had to be made if the raytracing modeling of incident radiation (i.e. upon its passing through the glazing panes) could be carried out in a 2D environment rather than 3D, mainly to simplify the procedure.

There was a concern that using a 2D technique would lead to the neglect of other deflections of insolation that are only shown in 3D environment, e.g. the multiple reflections at the edges of the panes of glazing or from the reflective material of the separators that form the edge boundaries of the glazing cavity, thus affecting the result accuracy. Accordingly a sensitivity test was also carried out using a 3D a single glass pane unit sample with dimensions of (Δx, Δy=1, Δz=0.006m), to work as small square *parallelepipeds*, *see fig 4.11*. Assuming a fraction of the incident light (I_D) on the slice at the same given incident angle (θ_I), in which the deflection took place; a fraction (f) is

deflected through the angle ($2\theta_1$) while the remainder (1-f) is transmitted un-deflected. Following the simple laws of the optics, it can be said that:

$$f = (W/D)\tan r \quad (\theta_1 < \theta_0) \tag{4.036}$$

$$f = 2-(W/D)\tan r \quad (\theta_1 > \theta_0) \tag{4.037}$$

Where (θ_0) is the refraction angle in the glass, and (W/D) here is the ratio of the cut depth to the cut spacing of the slice or ($W/\Delta x$), where (Δx) could be assumed here as 1 cm in this case so the equations would become:

$$f = (W/0.01)\tan r \quad (\theta_1 < \theta_0) \tag{4.038}$$

$$f = 2-(W/0.01)\tan r \quad (\theta_1 > \theta_0) \tag{4.039}$$

For one side edge slice and (**1-2f**) for two sided edge slice, i.e. as in the corners. Substituting the amount of the original incident (I_D) for the fraction incident, I_D (**1-2f**) for the corner slices and I_D (**1-f**) for the edge border slices. These two values are the transmitted fraction of the insolar before attenuated by the glass refraction index. Thus after attenuation it would be:

$$I_{transmit} = I_D(1-f)(\bar{\tau}_m) \tag{4.040}$$

Or for corners:

$$I_{transmit} = I_D(1-2f)(\bar{\tau}_m) \tag{4.041}$$

An important aspect of this correlation is that the deflection has little effect for the incident insolar with an inclination of less than (+30), and it doesn't start to have a notable effect till the angles exceed (+45).

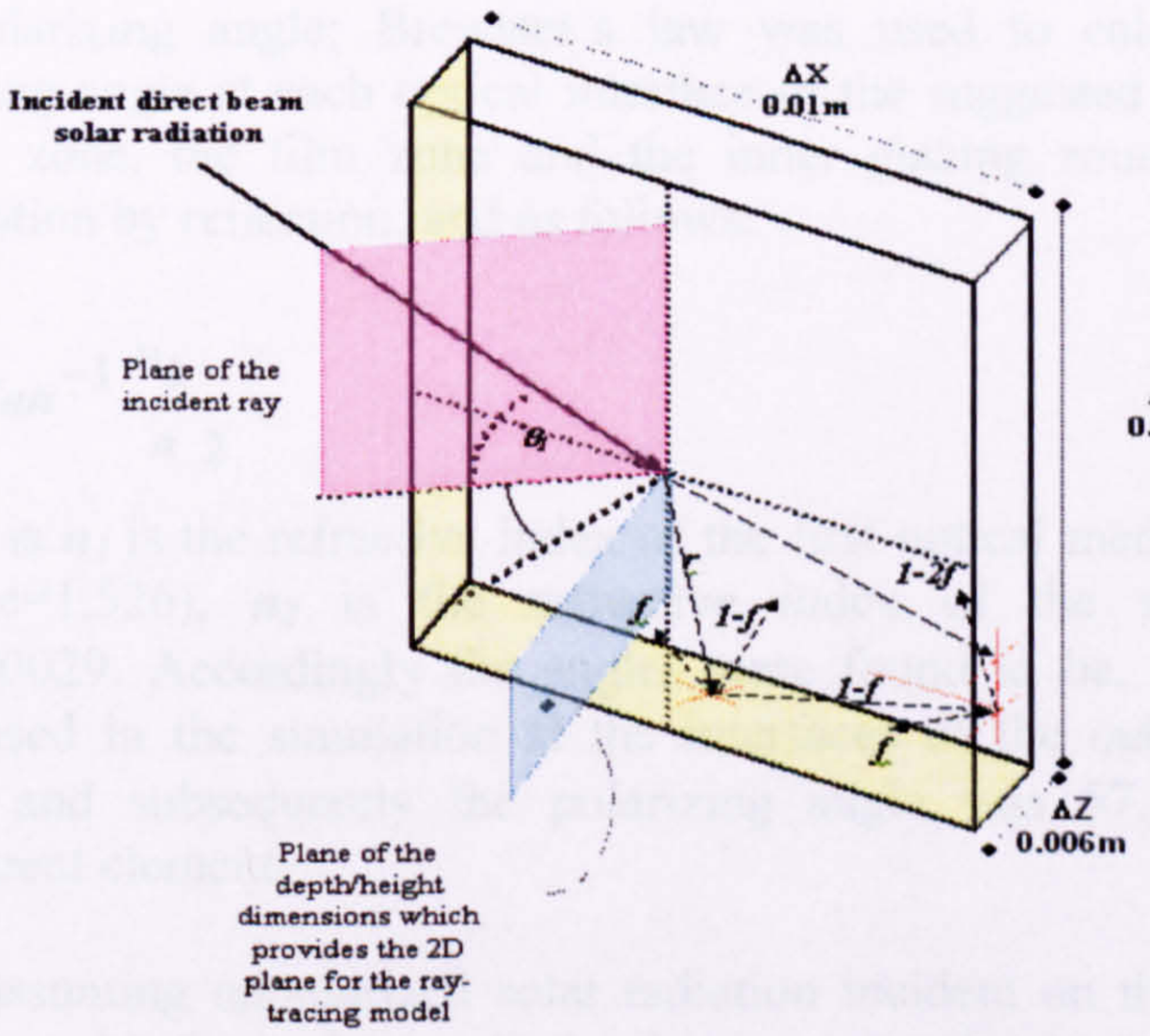

Figure.4.11 showing the principle of reflection at the edges

It can be seen that the proportion of this "*edge*" transmittance and reflection is relatively small (i.e. one to two sides only of an imaginary slice that has four sides and which measured at 1/10 of a unit column of vertical or horizontal slices). Thus, the effect of the internal reflection at the edges could be neglected in the total calculations.

Effect of Polarization:

Light from natural and incoherent artificial sources is often slightly polarized; e.g. the degree of polarization is usually small enough to be negligible. Still, any assumption that the incident solar radiation, upon passing the system, would emerge unpolarized could be oversimplified. Polarization usually occurs at the interface between two different mediums, which vary in their optical density thus their refractive indices, e.g. as in gas and solid; by transmission, reflection, refraction and scattering.

Generally, upon carrying out sensitivity tests for the effect of polarization, on the transmitted insolation; the following factors have to be taken into consideration and the effect on the total output, i.e. the intensity of the transmitted light (Greenhalgh D 1982):

- Type of the optical mediums; i.e. a normal float glass and polystyrene sheet insertion were used in the suggested proposal; such materials have one refractive index, thus no double refraction (Birefringence) effect is expected from such system. (Oriel 2004).
- Spectra polarization; e.g. the level of change in polarization, relevant to the wavelengths of spectra insolation, i.e. those taken within the visible band. The change was found out to be minimal within this range of the simulation.
- Number and type of added interfaces; if substrates or coatings are used, condition of interface surfaces used; i.e. to cause reduction in transmission, increase or decrease in reflection through destructive interference.
- The polarizing angle; Brewster's law was used to calculate the maximum polarizing angle at each optical interface of the suggested system, i.e. the outer glazing zone, the film zone and the inner glazing zone, to account for the polarization by reflection; and as follows:

$$\phi_B = Tan^{-1}\frac{n_1}{n_2} \qquad (4.042)$$

Where is n_1 is the refractive index of the first optical medium, i.e. glass in this instance=1.526), n_2 is the refractive index of the second medium, i.e. air=1.00029. Accordingly the angles were found to be, 56.7° for the normal glass used in the simulation at the interfaces of the outer and inner glazing zones; and subsequently the polarizing angle was 57.163° at the inserted transparent element.

Thus, assuming unpolarized solar radiation incident on the surface of the first zone, i.e. with 50% of the radiation having (o) orthogonal polarization and 50% (p) parallel polarization; such radiation would eventually leave the interface zones of the system, using Fresnel formulas to account for (o) and (p) transmittance, and as follows:

The outer zone: 43.89% (**o**) and 56.11% (**p**). This was then calculated to the last zone leading to 32.1% of (**o**) transmitted light and 67.9% of (**p**) transmitted light. Alternatively, a complete internal deflection of the reflected light would happen at an internal critical angle of 42.6°, i.e. from glass to air.

Still, it can be said that, even in best scenarios, the emerging light, i.e. after passing though the system, would still be partially polarized, thus minimizing its effect on the overall transmissivity and reflectivity of the system. (Project#6 2004).

Consequently, a decision was made not to include the polarization effect into calculation, though such statements might differ, if more glazing layers and/or enhanced materials are to be used in the proposed system, i.e. dielectric coatings. In the latter case, the intensity of emerging light would depend on the rotation angle of polarizing layer, i.e. affecting the (**o**) and (**p**) planes of insolation, using Malus's Law:

$$I_\theta = I_0 \cos^2 \theta \qquad (4.043)$$

Where I_θ= the intensity of the emerging polarized light, I_0= the intensity of the incident light and θ= is the rotation angle of the dielectric coating or the selective angle of coating. Alternatively, an increasing plane polarization of the (**p**) reflected light would also increase its intensity. Such effect must be taken into consideration throughout any future design process of the system as it causes harmful glare.

Refractive index and Extinction Coefficient:

Refractive indices in glazing systems change with changing the materials and/ or their physical layout within the systems; *see chapter 3*. They also respond to changes in the operating conditions, e.g. that of temperature and solar geometry.

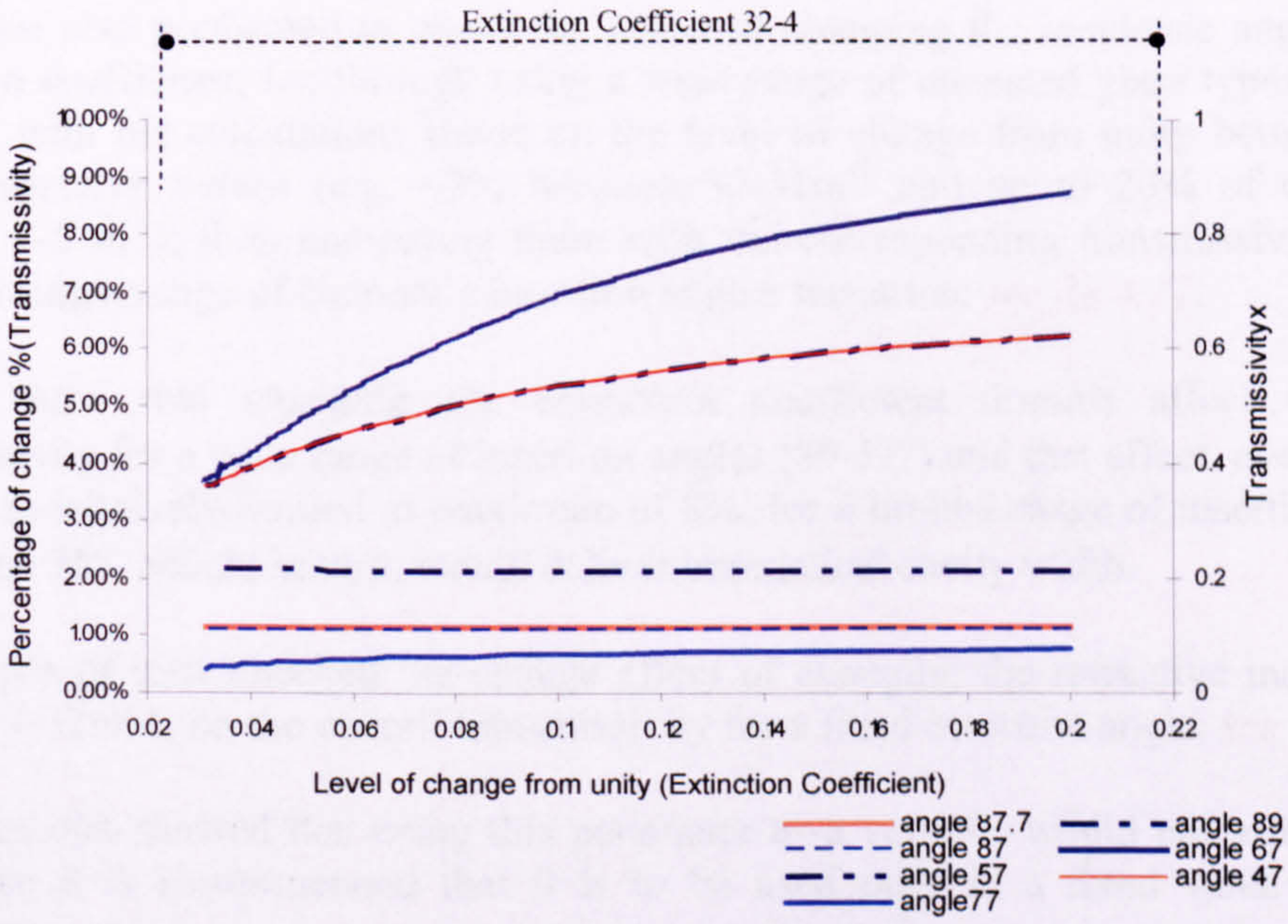

Figure 4.12 shows change of extinction coefficient with the changes in incidence angle and the relevant transmissivity.

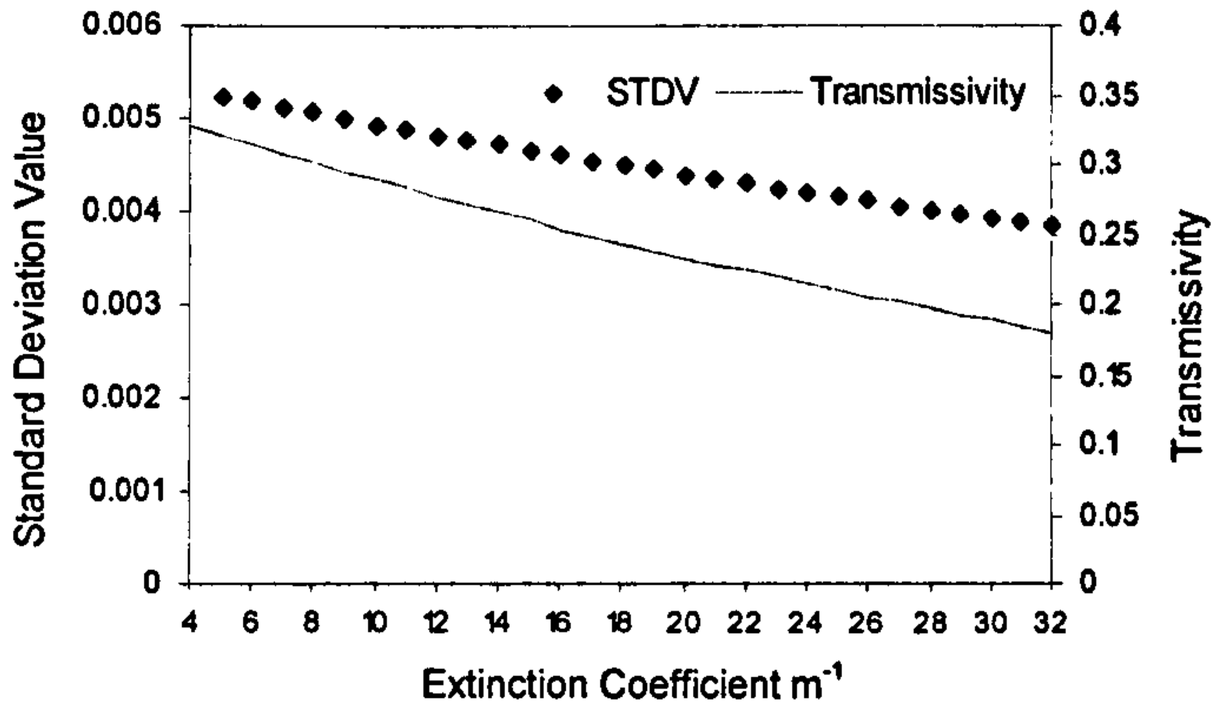

Figure 4.13 shows the level of change in a "fixed angle insertion" element's transmissivity with the value of extinction coefficient, i.e. with change of glazing material. NB: STDEV refers to standard deviation value.

However, temperature here is not a major factor; the statement is valid when working in ambient conditions (i.e. of temperature and pressure, and in which the refractive index is normally measured and specified). Real change in refractive index doesn't occur till after a relative high band of temperatures exceeding 100°C, thus it was decided not include the temperature as a variable in calculation of refractive indices (Ranzon 1980).

Refractive indices of optical materials are usually calculated through analyzing bulk samples and at normal incidence angles. To simplify calculations, results are then normalized for the range of incidence angles between 0-90°.

Tests were also performed to check the effect of changing the incidence angle on the extinction coefficient, i.e. through using a wide range of uncoated glass types between 32-4m^{-1}, with the calculations based on the level of change from unity between each two consecutive values (e.g. ~2% between 32-31m^{-1} and up to 20% of difference between 4-5 m^{-1}); then comparing them with the corresponding transmissivity of the system, using a range of element's insertion angles scenarios; *see fig 4.12*.

Results show that changing the extinction coefficient doesn't affect the glass transmissivity for a wide range of insertion angles (89-77°) and that effect, even when it happens is relatively limited to maximum of 8%; for a limited range of insertion angles lower than 75°, which, in turn, would deliver impractical cavity width.

Other types of tests checked the change effect of changing the refractive indices, e.g. between 4-32m˜1, on the overall transmissivity for a fixed insertion angle, *see fig 4.13*.

Overall results showed that using this parameter as a variable would not affect results and hence it is recommended that it is to be used only as a fixed value in future calculations.

Decision on the coordinates and setting of the simulation environment:

Changing the primary coordinates would affect the amount of solar radiation incident on the glazing surface. It would also affect the angle of incidence and the view factor of the insolation. The account of multiple reflections in 2D environment could still be traced in the approach adopted for the raytracing calculations, as can be shown:

- Stating the facts and background; two types of raytracing exist; sequential where the intersection point is known and required (for image forming) and non sequential where intersection are not mandatory as results are calculated through probabilities using capture surfaces, for heat transfer applications (as in solar collectors, fiber optics, light pipes and glazing). This is not to say that the calculation are not assuming vector quantities, its main advantage is in minimising CPU time.

- Most of the current software used nowadays to simulate radiative calculation and not, just the lighting simulation aspect, would use 2D simulation environments to minimise the CPU time. However, 3D environment modelling is used extensively in simulating certain multiple slats or Venetian blinds insertions in the cavity. Such software would only be able to illuminate and visualise the objects or surfaces in the environment by intersecting the incident lighting.

  Examples of the latter cases are shown in quite recent works of (McCluney 2004, IES Task 2004), or the new versions of WINDOW. Even in the latter 3D types, specular radiation simulations are simplified to opaque calculations.

- As shown capture surfaces, use simple equations to describe the light intersection with the surrounding environment, e.g. with a sphere, cube, triangle (for 2D surface) etc.; once a relationship is established to decide if the ray was intersected by the object or surface, then it would change into a scalar quantity as in radiation intensity.

- To establish if a 3D environment model is necessary for raytracing accuracy, a simple assumption was made that, once a master ray e.g. (**T1**) passes the first layer of system's glazing, it would be captured either by the inserted element surface, or by one of 3 (capture) spacer surfaces; (i) the lower spacer, which is already used in the 2D calculations, (ii) the side spacers, relevant to a 3D calculation. Thus, in 3D assumption 4 capture surfaces are needed, while in 2D only two are needed; the lower spacer and the inserted element; *see fig. 4.14.*

  After first reflection, a slave ray (**R1**) would again hit either of 3 spacers surfaces or the inserted element, and so on, e.g. **R2**, **R3**, etc.

Probabilities of intersection for these rays with the surfaces are dependant on the view factors and solar geometry only once, then after first reflection it would be dependant on the view factor of the surface and geometry of the setup only. It was also established that the effect on transmissivity of rays falling on the side edges of the system are much less due to the proportion of the view factor of the side spacers to that of other surfaces e.g. that of the inserted element, outdoor or indoor glass layers.

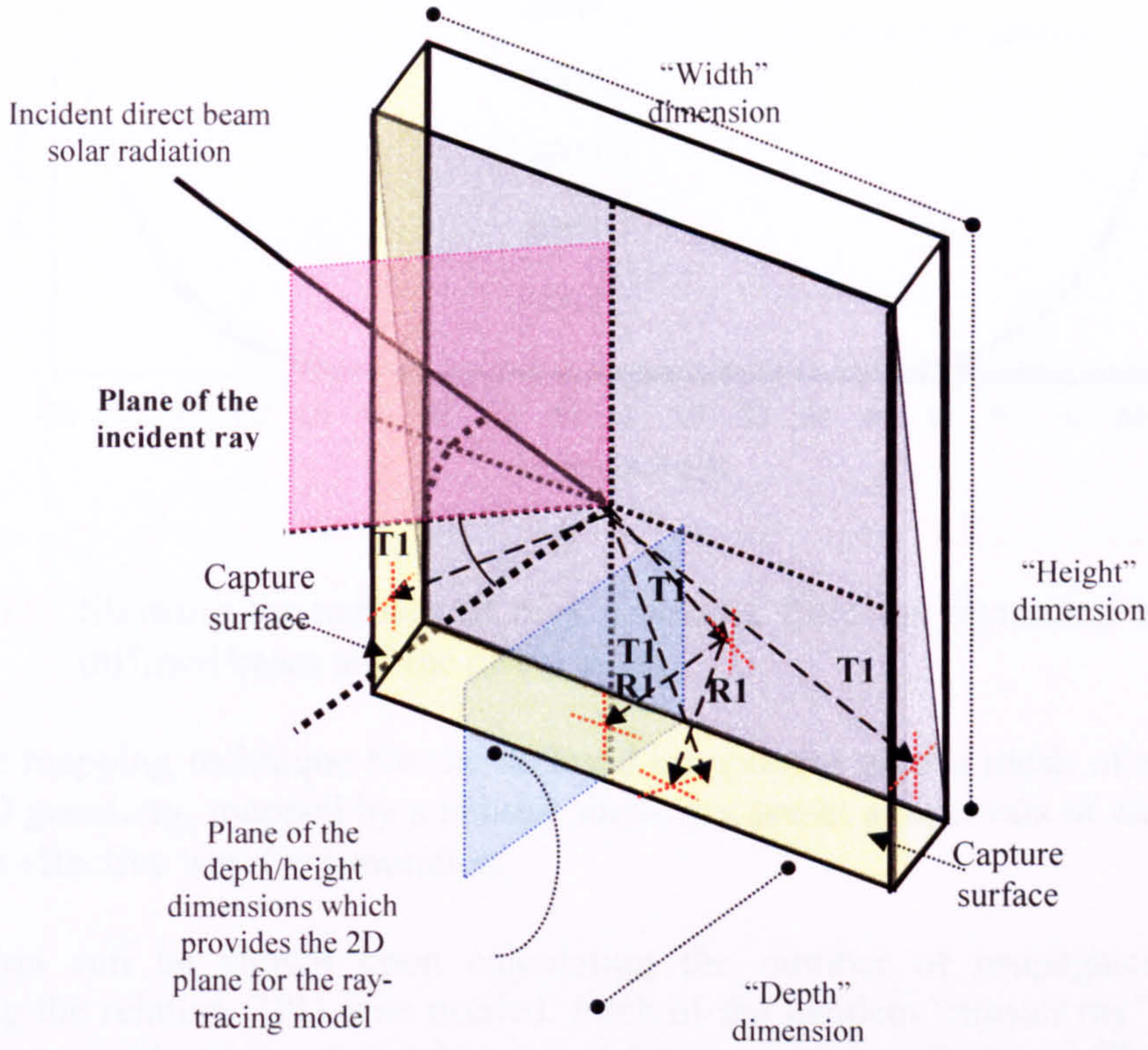

Figure.4.14 showing probabilities of reflection at assumed 3D capture surfaces model.

The relationship between the two types of view factors i.e. that of the lower spacer and the inserted element is constant. While it is in favour of the inserted element, with the change of insertion angle, when compared with the side spacers surfaces, i.e. in 3D environment, thus suggesting a logical decision of excluding the side faces on probability and adopting a 2D raytracing environment.

Acceptable number of raytracing rays:

Different types of raytracing techniques were evaluated in order to determine which should be used in the simulation; *see chapter 3*. The objective was to select a technique that maintained a balance between accuracy of results and the expected CPU time. Some techniques (e.g. sequential types), being visually oriented as shown, could be more accurate and would yield less number of rays and probabilities compared to the suggested non-sequential method.

However, the latter is the only one recommended to deliver radiative heat transfer calculation. Thus, an evaluation was made to balance accuracy with increasing the simulation time and requiring parallel servers running concurrently to handle several batches for each simulation (run).

The decision was also made to use the nonsequential *forward method* with single pencil array for each degree angle of the direct beam simulation passing through the geometry environment.

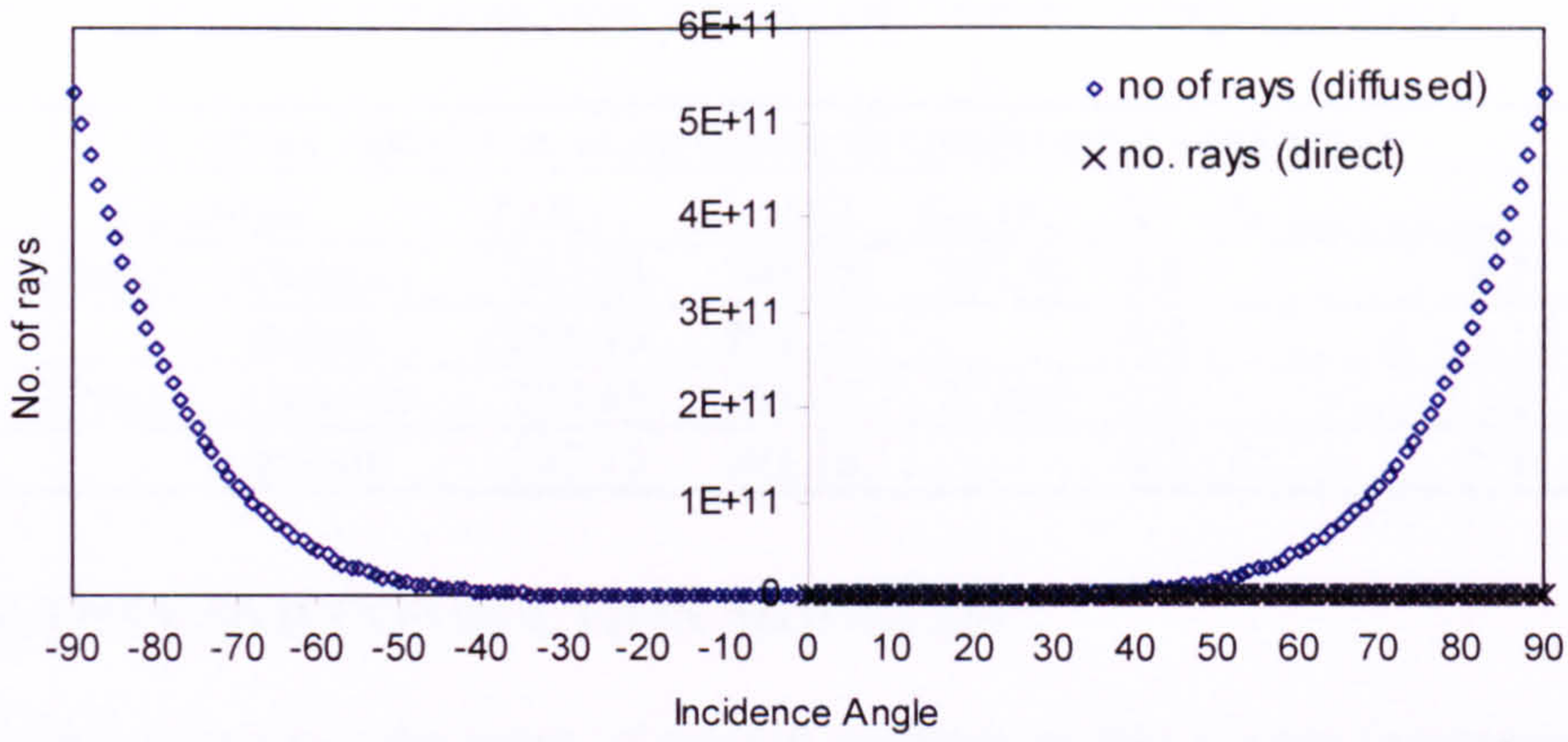

Figure 4.15 Showing the number of rays generated from the raytracing code for the diffused beam and the direct beam.

While the mapping technique for the diffused component used a mesh of square units for the 2D geometry, mapped by a similar single ray preset at intervals of an arc of total 90°) as an effective way for simulation.

Justification can be shown upon calculating the number of propagated rays and calculating the relative CPU time needed. Each of the incident "master ray" projection, *see fig. 4.14*, could yield up to 3 "slave rays" due to multiple reflections. The number of rays simulating the diffused components, in each run, would increase in a parabolic pattern for angles between 0-90° for the sky diffused and -90-0° for the albedo, *see fig. 4.15.*

However, this fact is less apparent in the simulation of the direct beam component, where the increase in number of rays per simulation/run is linear regardless of the incidence angle.

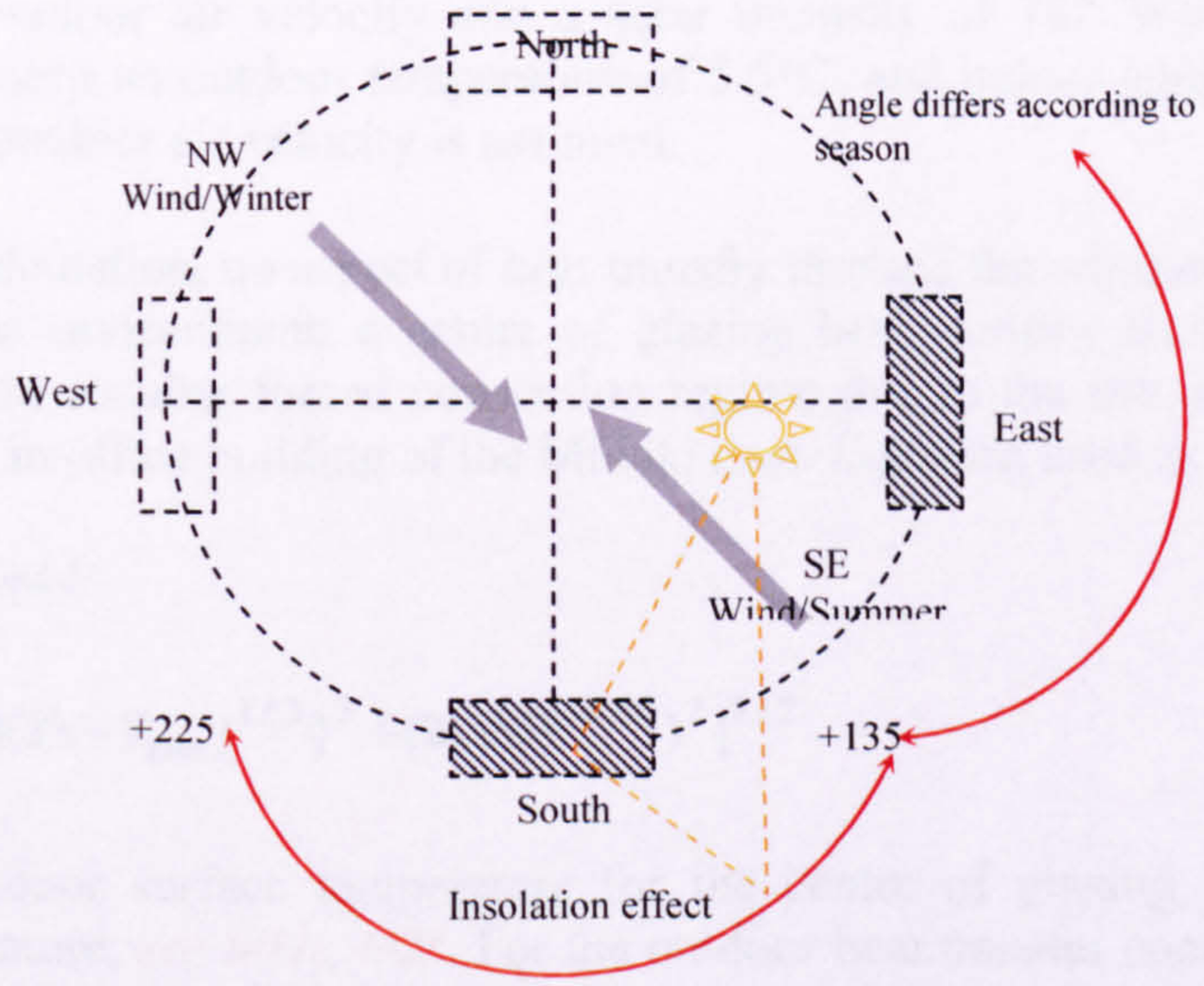

Figure 4.16 sketch, showing several layout scenarios of the system and the effect of changing the orientation on the wind direction with relevance to openings.

Table 4.03 showing the indoor heat transfer coefficient –office buildings

h_c indoor calculation using indoor air conditioning wind action						
Condition		T_S(K)	T_{env} (K)	T_{sky} (K)	V	$h_{c(glazing\ surface)}$
Summer	Outdoor	304.65	309.95	303.95	4.8	9.73
	Indoor	295.15	291.15		0.2	5.14
Winter	Outdoor	288.65	285.65	279.65	3.7	7.67
	Indoor	287.15	291.15		0.2	5.14

CONVECTION AND CONDUCTION MODELING

CFD simulation involves the input of several parameters that govern the process. Still, Two main solver parameters had to be tested, to decide if their results showed differences, which would justify considering them as variables, hence change the solver option. Those relate to the change of wind direction and orientation, and effect of turning on/off the radiation option in the simulation, on a collective heat transfer coefficient for the system.

Effect of orientation and wind on surface resistance:

The forced convection method, (ISO/DIN 15099) was used to calculate the effect of convectional forces caused by the ensuing wind action relative to orientation. Other Environment parameters, e.g. temperature, wind velocity, were based on a balance between the National Fenestration Rating Council method and European U-value formerly "K value" (ISO-DP10292 draft standard conditions); *see fig. 4.16.* Calculations were performed for seasonal changes e.g. August/summer and January/winter using (Kuwait 1996 weather data).

The latter data was then compared with both of the European code and NFRC database for standardised U-values for glazing systems, e.g. the latter summer daytime data: is based on an outdoor temperature of 32°C, an indoor temperature of 24°C, a 6.2 mph (10.1 km/h) outdoor air velocity and a solar intensity of 782 W/m^2). While, in the European standard an outdoor temperature of 5.5°C, and indoor temperature of 20.5°C and a 4.8 m/s outdoor air velocity is assumed.

To simplify calculation, no aspect of heat transfer through the window frame was taken. For the indoor environment; a centre of glazing heat transfer coefficient $h_{c(indoor)}$ is assumed and an ensuing forced convection regime due to the use of air conditioning, e.g. especially in office building of the Middle East. Equation used is:

$$h_{c,ind\ (Surface)}=4+4V \tag{4.044}$$

$$h_{c,ind}=[\{0.84(Ts-T_{env})^{1/3}\}^2+(2.381V^{0.89})^2]^{1/2} \tag{4.045}$$

Where T_s= indoor surface temperature for the centre of glazing, T_{env}= indoor free stream temperature; *see table 4.03*. For the outdoor heat transfer coefficient $h_{c(outdoor)}$, a forced convection regime was assumed due to the effect of wind on the outer building skin, e.g. in multi-story offices, as investigated in works of Loveday 1996-1998.

Table 4.04 calculation of the outdoor heat transfer coefficient-in office buildings

h_c outdoor calculation according to the wind									
Condition		ϕ	ε	y	{y}	υ windward	υ leeward	$h_{c\,(conv)}$	$h_{c\,(conv+rad)}$
Summer	South	135	0	45	45	1.2		13.82	20.57
	North	135	180	225	135		0.54	8.804	15.55
	East	135	-90	-45	-45	1.2		13.82	20.57
	West	135	90	135	135		0.54	8.804	15.56
Winter	South	315	0	-135	-135		0.54	8.804	14.08
	North	315	180	45	45		0.54	8.804	14.09
	East	315	-90	-225	135	1.2		13.82	19.106
	West	315	90	-45	-45		0.54	8.804	14.09

$y=\varepsilon+180-\phi$, $\{y\}>180$, then **$y=360-\{y\}$**. If **$-45\leq\{y\}\geq45$,** surface is windward, else leeward.

Here **V**=wind velocity in m/s, ϕ= wind direction, ε= wall azimuth angle, positive degrees westward from south and negative eastwards, v= surface air velocity near the outer building surface.

Air velocity near the surface (v) if windward: **$v=0.25V$** if **$V>2$** or **$v=0.5V$** if **$V\leq2$**

Air velocity near the surface if leeward u: **$v=0.3+0.05V$**

$h_{c(outdoor)}=4.7+7.6v$ would be the outdoor centre of glazing heat transfer coefficient.

Accounting for wind correction factors, table 4.04 shows the results of outdoor heat transfer coefficients for the system taking into consideration seasonal differences and windward/leeward directions; *see fig. 4.16*. The last column in the table presents collective heat transfer coefficient accounting for convective/conductive and radiative flux forces. The latter is calculated from the following equation:

$$h_{rad}=4\sigma(T_m)^3 \qquad (4.046)$$

Where σ is Stephan Boltzmann constant ($5.6697\text{x}10^{-8}$ W/m^2K^4), T_m (Kelvin) is the mean monthly temperature, i.e. for January and August respectively, calculated from i.e. the weather files of Kuwait for the last ten years, (RET screen Program 2003).

Using two sets of scenarios, i.e. for summer and winter, with a relevant wind orientations, it was found that the surface heat transfer coefficient, at e.g. one of the inserted film faces in the cavity, with a width e.g. of 0.05m, would return a rate correspondent to specific orientation. This relationship would stay reasonably constant, if the radiation contribution component was fixed at certain rate while changing the cavity width itself; *see* (4.004). Consequently, A relationship between the inserted element's surface resistivity values and the prevailing wind orientation could be established and would stay proportional to the change in the cavity's width, only if other parameters were to stay constant, e.g. those of temperature and insolation fluxes; *see chapter 5*.

Subsequently, effect of wind orientation though important in calculating the outer system's glazing surface resistivity; still, it would not be used a variable parameter in the system's set up scenarios as it would deliver a proportional correlation that once is established could be extrapolated to fixed orientation scenarios.

Effect of the radiation option on the overall heat transfer coefficient:

Another tested parameter was the effect of activating the radiation option in "Fluent" simulation controls options panel; *see Fluent 5 manuals.*

"Fluent" deals with the radiation effect through several built in algorithms; *see chapter 3.* A control panel provides the user of choosing to activate the radiation solver option and the type of that solver.

However, not activating the radiation option doesn't mean necessarily that radiation heat fluxes would not be included in simulations; it would only assume that heat fluxes contribution would be only through thermal longwave radiation added through absorption and emittance.

Consequently, two sets of simulations were carried out; with the radiation option turned on/off. A constant insolation "heat flux" was assumed with a relevant solar incidence angle and fixed view factor, while a small internal constant generated heat flux was assumed to account for the contribution of remitted longwave radiation from absorption. Tests showed that activating the radiation solver throughout the simulation could have a considerable effect on the whole convergence of the simulation.

However, it was decided to exclude this option from the control solver, as the heat flux resulting from the incident radiation would be addressed in the raytracing code.

Finally, the effect of increasing the number of nodes (cells) were checked, by refining the mesh laterally in the thin film itself to achieve a better understanding of the optical properties of the element investigated. The results showed that any refinement in the mesh generated (i.e. beyond a critical threshold dimension of 0.0001m taken as the used width) would have negligible effect on the calculation.

As the element, with the radiation turned off, would perform only as an inhibitor to the convectional currents in the cavity with a limited effect on the conduction mode due to the minimal width of the film used.

Reference:

1. Anderson M, Rubin M and Scartezzini JL. Comparison between ray-tracing simulations and bi-directional transmission measurements on prismatic glazing. Solar Energy 2003; 74(2): 157-173.
2. Angstrom A, on the atmospheric transmission of sun radiation on dust in the air, Geografiska Annaler 1929. 2:156-165.
3. Bird R. E. A simple, solar spectral model for direct normal and diffuse horizontal irradiance. Solar Energy 1984; 32(4): 461–471.
4. Bodart M. and De Herde A, Global energy Savings in offices buildings by the use of daylighting. Energy and Buildings 2002; (34): 421-429.
5. Fluent 5 online index manual Apache Web server Fluent incorporated 2003. See also: http://lis.dvo.ru/fluent/ug/node16.htm#4088

6. Foundation for Alternative Energy (FAE), Slovakia 2005, "Solar Energy" Dieret-website. See also: http://www.fae.sk/Dieret/Solar/solar.html
7. Greenhalgh D. A., Sarkies P. H, Novel geometry for simple accurate tuning of lasers. Novel geometry for simple accurate tuning of lasers. Applied Optics 1982; 21(18) 3234-.
8. Gueymard C. A, Parameterized Transmittance Model for Direct Beam and Circumsolar Spectral Radiance, Solar Energy 2001; 71(5): 325–346.
9. Gueymard C. A, SMARTS code version 2.9, user manual, Cocoa: Bailey US, February 2002 revised May 2002. pp1-36.
10. Jenkins F. and White H., Fundamentals of optics. Third edition, London: McGraw hill Book Co. 1957. Chapter 24,.Page 118
11. ISO/DIN 15099, Thermal Performance of Windows, Doors and Shading Devices — Detailed Calculations, ISO Central Secretariat, Geneva, Switzerland 2003.
12. Kurata; K. Li. and Takakura T., Solar Radiation Enhancement in a Lean-to Greenhouse by Use of Reflection. Journal of agricultural. Engineering Research. 1998, 71: 157-165, Article No. ag. 980311.
13. Laitenberger O., Cost-effective Detection of Software Defects through Perspective-based Inspections. Empirical Software Engineering 2001; 6: 81–84.
14. Loveday D. L, Taki H., Convective heat transfer coefficients at a plane surface on a full-scale building façade. International journal of Heat Mass transfer 1995; 39(8): 1729-1742.
15. McCluneyFSEC Fenestration; Raytracing subtask an interim progress report for TaskDOE BAIHP Project, Florida Solar Energy Center, Florida USA. 2004.
16. Miskolczi F. M. et al., High-resolution atmospheric radiance-transmittance code (HARTCODE). In: Meteorology and Environmental Sciences. Singapore: World Scientific1990. p. 770.
17. Nagtegaal M., Optical method for temperature profile measurements in glass melts, a research in: CIP-data library Eindhoven Technische Universiteit Eindhoven, Germany 2002.
18. Oriel instruments. Metrology Research Institute. In: Helsinki University of Technology, Hut, Finland: Department of Electrical and Communications Engineering 2004.

    See also: http://metrology.hut.fi/courses/s108-199/PolarizingOptics.pdf

19. Pajonk G., Elaloui E., Acard P, Chevalier B, Chevalier J and Durant M, Physical properties of Silica gels and Areogels prepared with new polymeric precursors. journal of Non-crystalline solids 1995; 186:1-8.
20. The Physics Classroom; Studyworks online: The Physics Classroom and Mathsoft Engineering & Education, Inc. 2004. See also:

    http://www.phy.ntnu.edu.

21. Project#6, Optical and Circular Experiments, Optics Quantum Mechanics. Michigan technological university, Department of Physics: PH3480 Modern Physics Laboratory 2004.

    See also: http://www.phy.mtu.edu/~nadgorny/manual_optics.pdf.

22. Rantala, M. and Karvinen R., Treatment of transient radiative heat transfer in glass tempering process Energy and process engineering Dept. Tampere University of technology, Tampere, Finland. International Center for Heat and Mass transfer. See also: www.ichmt.org/abstracts/RAD-01/posters/PS-8.pdf
23. Ranzon H., Properties and Applications of Glass, Amsterdam- Oxford-New York: Elsevier Science publishing Co. 1980
24. Rubin M., Optical properties of soda lime silica glasses. Solar Energy Materials Journal. 1985; 12: 275–288.
25. RET Screen PV2004 software, managed by CETC Canmet Energy Technology centre, Varness
26. Shettle E. P. and Fenn R.W. Models for the aerosols of the lower atmosphere and the effects of humidity variations on their optical properties. In Report no.: AFGL-*TR*- 79- 0214, Hanscom, MA: Air Force Geophysics Laboratory, 1979.
27. Thayer H., Richard H, Software system engineering: A tutorial, COMPUTER 2002; 35(4): 68-73.
28. Viracon, Inc. Viracon-consulting Glass data. USA 2002. See also: http://www.viracon.com
29. Volf Milos B., Mathematical approach to glass. Prague: Elsevier Science publishing Co. 1988. Table 5-1, p46.
30. Watt A., Watt M. Advanced Animation and Rendering Techniques Theory and Practice, chapter 8, Atlanta, 1994
31. Wojciech T. Konka. Simple visualisation methods to support "conventional" investigation of natural convection heat transfer, report no.: 2, Lodz, Poland: Institute of Thermal Technology and Refrigeration, Technical University of Lodz, 1996.
32. Y Fang, Eames P., Hyde T and Norton B, Complex multi-material insulating frames for windows with evacuated glazing. Solar Energy Journal. 2005; 79(3): 245-261.

CHAPTER FIVE

ASSUMPTIONS AND PARAMETERS OF SIMULATIONS

Introduction

Prior to setting the computer simulations that are needed to check the hypothesis, *see chapter 1 and 3*, put forward in this thesis, it is necessary to layout the objectives sought from such simulations and so to decide which parameters are to be involved and the number of simulations needed.

Such decision-making is usually associated with simulations that are conducted over different platforms, use a relatively large numbers of input data and involve dealing with different tools/software.

Apart from cutting down on the CPU time, laying out the objectives would also ensure that the bulk of the results obtained would not overlap each other causing an excess number of unnecessary simulations.

Also it is important to be able to understand and justify simulation outputs where a lack of available empirical data for some parameters has led to the use of assumed or generic data values for program inputs. This approach would enable a general trend of the output values to ensue.

Hence, several objectives were highlighted as baseline, upon which the simulation process should be devised and evaluated:

(i) As the hypothesis of the system depends on its geometry, rather than introducing new glazing materials. The simulation should test the effect of changing the parameters of that geometry on insolation (direct, diffused and albedo) passing through the system.

(ii) To check the effect that the angle at which the inserted cavity element has on the amount of insolation transmitted with regard to variations of latitude, and thus determine a mean angle of optimal behaviour for a system operating in those latitudes.

(iii) As the idea of inserting a suspended transparent thin element in multiple cavities glazing is not new, so another objective of the research is to check the enhancement in performance, if any, which tilting the inserted element would bring compared to a vertical setting and check the two results with those obtained from not having a suspended element at all.

(iv) To ascertain the effects of the changing geometries of the bisected cavities on the convection regimes within those cavities.

(v) The geometry parameters should be limited to comply with practical dimensions for normal building façade constructions and similar glazing systems.

(vi) The performance of the calculation methodology suggested within this research should be verified as far as is possible.

5.1 PARAMETERS OF (SMARTS2)

As discussed in *chapter 4*, one of the main aspects of the solar model (SMARTS2) is the broad band of input data needed at its different levels. These inputs are either derived from direct empirical/measured data (to assume accurate predictions), or as generalised correlations from the available weather files that exist for locations at the latitudes involved, which are built-into the program; *see appendix i.1, i.2, and i.3 for details of the associated CARDS and data sources.*

Such information is usually obtained through a variety of methods that include collecting data via satellites, weather stations, and high altitude balloons.

The level of accuracy of the SMARTS2 model is subjected to the availability of such input data (Gueymard C, 1994) This usually must include, diurnal, seasonal weather data and: solar profile, temperature, ambient atmospheric conditions, turbidity, concentration of major gases in the atmosphere, type of sun tracking devices used (to account for deviation factors), and geographical definition data of the surrounding surfaces, etc (Gueymard C, 1996).

In most cases and in this research particularly, difficulties exist in acquiring detailed information regarding all the individual data categories described. Thus it was decided that solar data from Kuwait that was available for this research should be used, *see appendix iii.1 for details of* kw1996, with ambient temperature files, humidity, and concentration of dust; *see appendix iii.2 for details Dust1996.* Such data were recorded at hourly intervals. However, for the remaining data input required by the program, the research used the generalised files available in SMARTS2.

Every effort was made to ensure the accuracy of solar model input data, and consequently the output data obtained, which were used in turn for the Ray tracing algorithm.

A key objective of the research was to validate the hypothesis regarding the behaviours of the suggested glazing system through computer modeling and simulation. It was considered that the SMARTS2 model, used with as much measured input data for the particular latitudes as possible, provided a good compromise in ensuring the quality of the values of solar parameters used.

More accurate results for the solar model could be achieved in future if more measured weather data inputs become available.

The input parameters that were used are:

(i) Location: latitude and longitude positions of 8 countries were taken using the NASA meteorological site, indicating, when available, the location of the source weather station; *see appendices iv.1-8.*

(ii) A solar almanac was obtained through ASTRONOM 8.1 software and was utilised to derive the seasonal and diurnal variations of solar geometry .

(iii) General weather files of the chosen countries, apart from Kuwait, were obtained through the NASA meteorological site.

(iv) The year set for the simulation, for all the countries was chosen as 1996 to account for the available empirical data from Kuwait for that year.

(v) Clear weather sky conditions were assumed for all calculations.

(vi) Sea level was assumed as the base for temperature, wind profile, and turbidity inputs.

(vii) Gaseous absorption was taken from files, e.g. CO_2 concentration was assumed at 370 ppmv.

(viii) Ozone concentration, Angstrom constants and aerosol conditions were obtained from standard built-in files of the SMARTS2 software indicating those of ASTM E891-87 (i.e. American terrestrial conditions), due to lack of empirical data, Alternatively, for Kuwait data the followings were assumed

For Kuwait data, ozone concentration of "0.3 atom-cm" was assumed as a mean value, using the metrological data of Kuwait International airport weather station (RET screen 2003).
While, for the turbidity factors and Angstrom constants a normalised formula was derived from measured data, *see chapter 3 and 5.1.1.* Results were used, to generate a more realistic profile by using the available empirical dust concentration.

(ix) Dry sand albedo profile was used to simulate the ground reflectivity for all simulations.

(x) Having established that using the global coordinates as a variable parameter for the system's orientation would not enhance results; the method of tracking solar elevation embedded in SMARTS2 was used as an input for the mean insolation profile given on tilted surfaces. This also meant that wall azimuth option was deactivated and the tilt angle of the system was 90°.

(xi) Solar elevation at local time of 3.00pm was used to compare the glazing behaviour for all the weather files to check the system's sensitivity at relatively low sun angles. Other sets of runs were selected for Kuwait; using a solar elevation at local time of 12.00am to check the seasonal changes and a separate set for the diurnal behaviour of the system.

5.1.1 Turbidity calculation

The software was used to predict the solar profiles for the countries lying within the chosen band of latitudes. Two sets of runs were applied to seven of those countries (at 3:00pm of 14th January and 14th of August respectively) so as to provide the required solar radiation data and allow an examination of the effects of seasonal changes; *see appendices vi.1-7 SMARTS2 results 7 countries.*

Additionally, two separate solar data sets were used to predict; (i) the insolation patterns in Kuwait at 12:00am of the 14th of each calendar month of a particular year i.e.1996; *see appendices vii: vii.1.a-b to vii.12.a-b for Kuwait*, and; (ii) the diurnal solar pattern by choosing 14th of August as representative of the "day of the year"; *see appendices viii-Kuwait 6am-18pm.* More accurate results were expected from the Kuwait simulations.

Table 5.01 modified turbidity factors relevant to ambient atmospherical conditions in Kuwait 1996. (Numbers in cells with bold edges are threshold values upon which a normalized fitting curve was used).

Month	$\tau 5$	$\alpha 2$	**RH**	β average	β hazy
January	0.272	1.43	53	0.101	0.536
February	2.228	1.442	39.4	0.101	0.541
March	0.264	1.442	39.4	0.1001	0.541
April	1.101	1.4435	27.4	0.101	0.41
May	1.141	1.444	24.8	0.101	0.419
June	0.27	1.444	24.8	0.101	0.56
July	0.921	1.441	19.4	0.101	0.339
August	0.72	1.441	43.2	0.1001	1.472
September	1.0071	1.441	39.8	0.101	0.371
October	1.376	1.438	51.8	0.1001	0.508
November	1.412	1.438	53	0.101	0.52
December	0.771	1.441	48.6	0.101	1.519

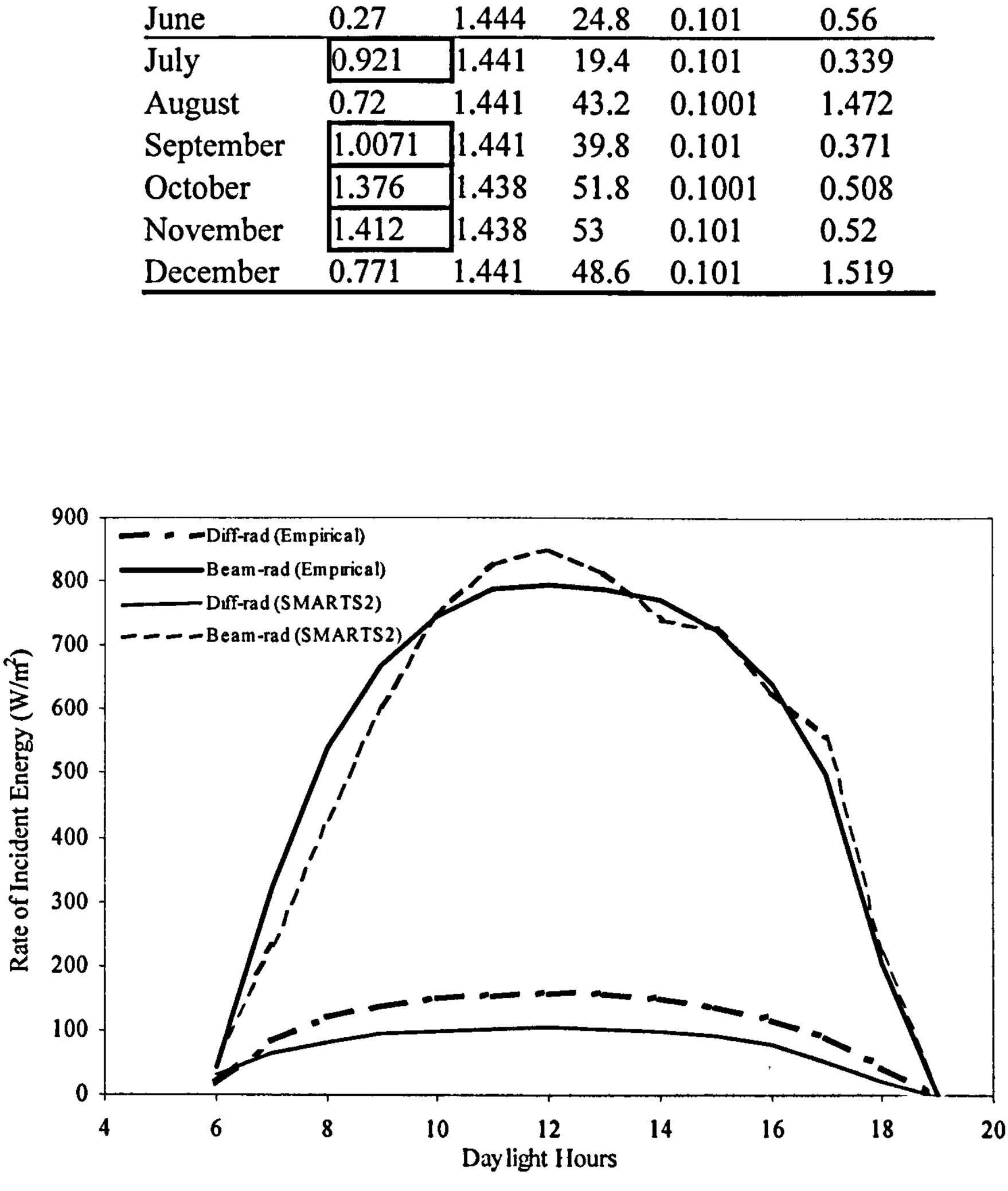

Figure 5.01 Diurnal insolation behaviour as predicted by (SMARTS2)-for 14.08. 1996/ Kuwait

Modified turbidity data, were applied in the case of the Kuwait data allowing the depiction of more hazy atmospheric conditions than those usually assumed by the SMARTS2 software.

Table 5.01 shows a suggested local code for Kuwait, highlighted in two sets of those turbidity factors that were used in the local climate simulations, i.e. the average and hazy conditions for each month.

Analysis of Kuwait output files shows two levels of accuracy in the results, depending on the precision of the turbidity factor used in the SMARTS2 simulation; *see figs 5.01 and 5.02*. Results show larger discrepancies in the direct component output calculated through the empirical dust data, once compared with SMARTS2 results while the diffused beam results data are more in accord with the ones obtained through using SMARTS2 built-in data base.

The diurnal insolation predictions were also more accurate during those days where a precise record of turbidity concentration was available and humidity levels were relatively low. On the other hand, the level of accuracy would drop upon comparing the insolation behaviour of a certain day of the month, throughout the year, because humidity levels would vary and so influence results; *see fig. 5.01*.

Figure 5.03 demonstrates the link between turbidity and the diffused component of insolation in the designated latitudes, with regard to humidity levels. Accuracy ranges between 180~65% with poor expected behaviour for those months with high humidity levels (i.e. above 50%).

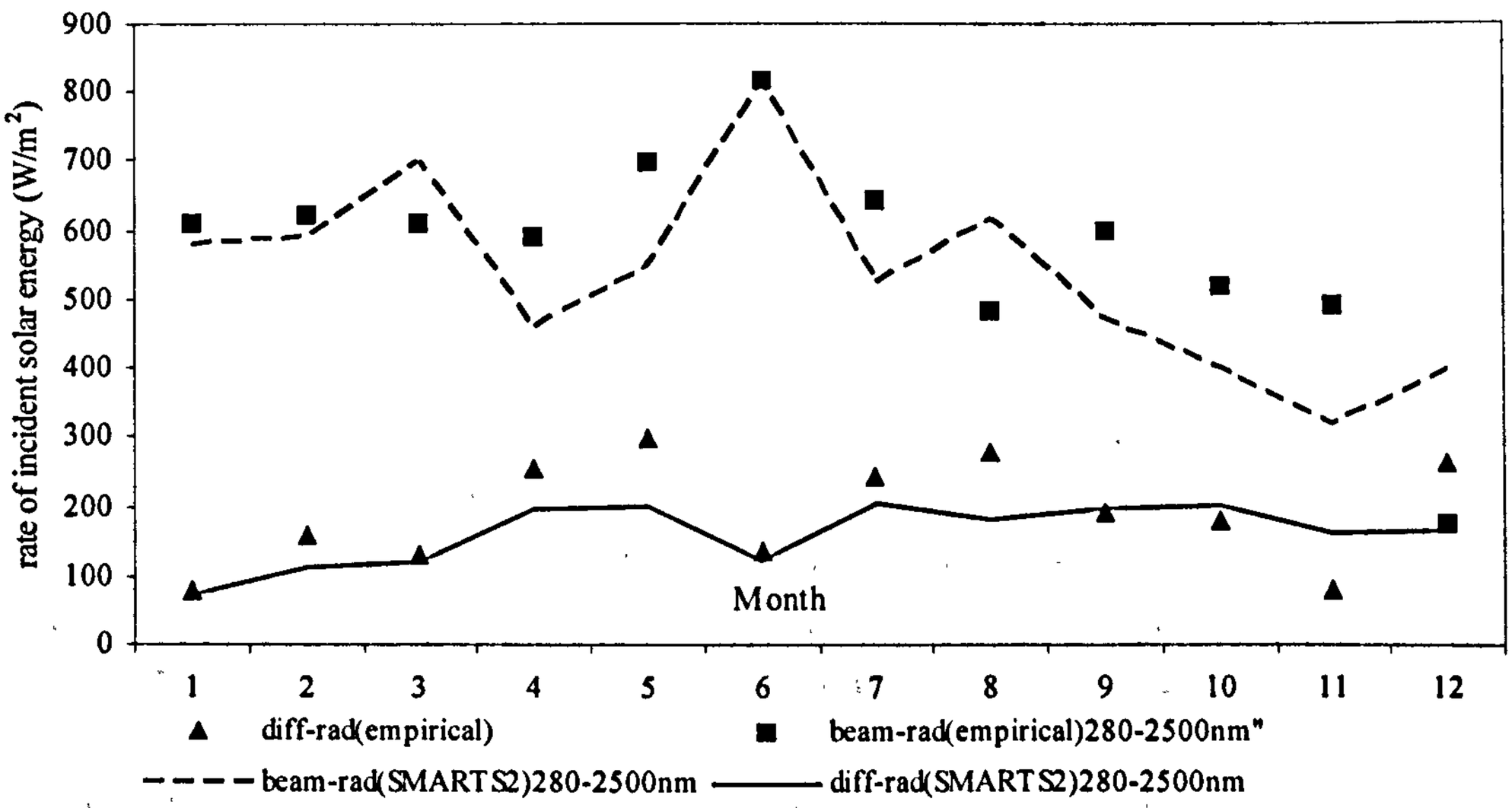

Figure 5.02 Comparison of results of insolation between (SMARTS2) and recorded empirical data calculated at 14H:14D:M:1996 for each month. Kuwait 1996 (Nadia 1996)

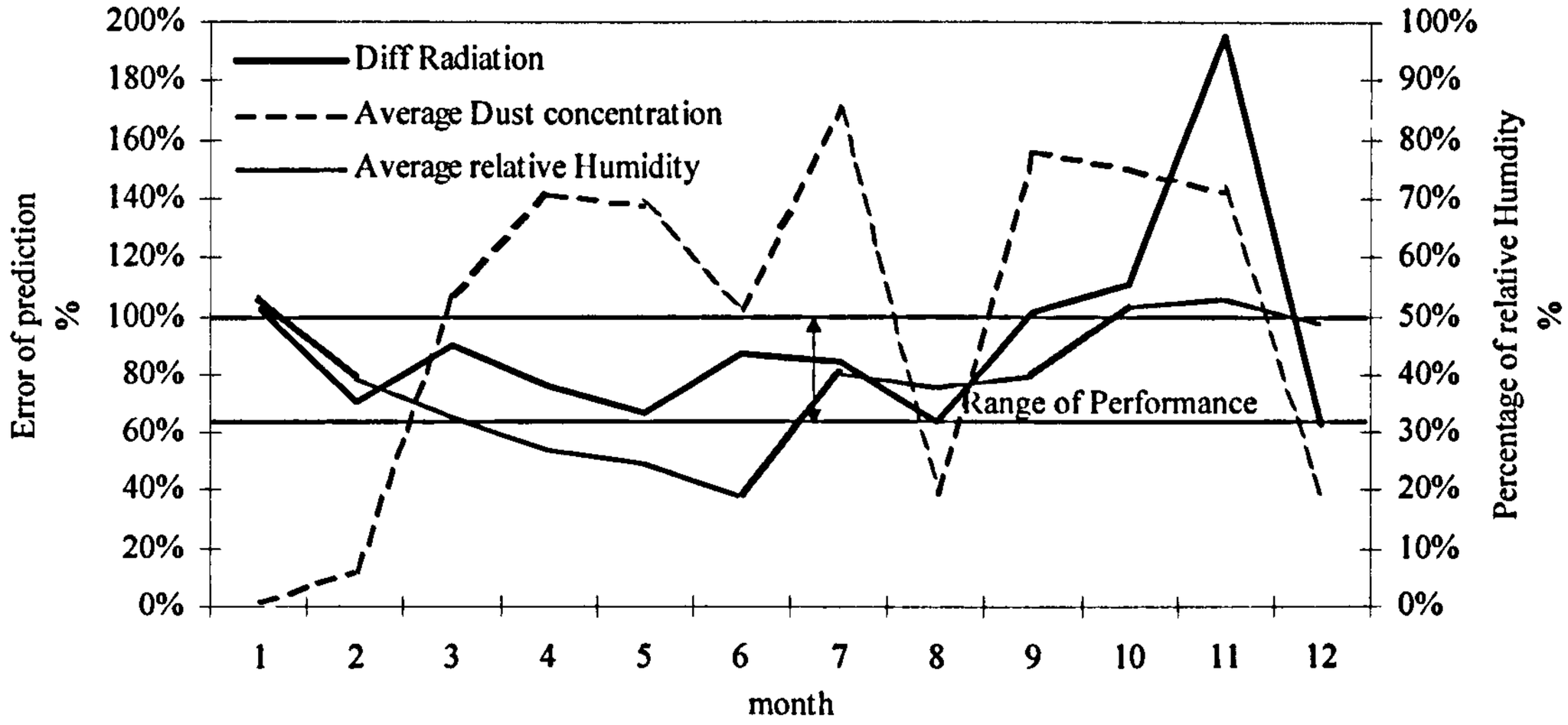

Figure 5.03 Effect of dust concentration and humidity on the accuracy of results of diffused radiation predicted by SMARTS2, when compared to empirical data, for the 14th of each calendar month.

5.2 PARAMETERS OF THE RAY TRACING MODEL:

The following parameters were suggested for the ray-tracing model as part of the assumed glazing system, within the main frame of the model, *see figs. 4.05 and 4.06*:

Environment of simulation:

(i) The non sequential raytracing method was used for simulations,

(ii) For the direct component insolation input, a single ray was assumed incident, at the outer layer of the glazing, at an angle corresponding to the direct beam incidence angle at certain latitude and a Julian day.

(iii) For the diffuse component insolation input, a perpetual chain of single rays was assumed incident at the outer layer of the glazing with an interval/unit angle spanning 0~90° arc, for sky diffused radiation.

(iv) For the albedo input, the same method as that used for the diffused component was applied, spanning 91~180°.

(v) Global coordinates of the X, Y directions were assumed.

(vi) A modular slice of the glazing system was assumed. The local X, Y co-ordinates have variable inputs, thus dealing with the set inclination of the inserted element in the cavity.

(vii) The model is orientated normal to the line of the horizon, i.e. tilt angle is 90°, sitting directly on the ground level.

(viii) Simulations are conducted at daytime and on a clear day.

(ix) "Deterioration of transmissivity" effect due to dust accumulation on glazing was neglected.

(x) The model calculates reflectivity from different surfaces up to 3 reflections.

(xi) The model did not address the long wave radiation from the indoor environment as it was calculated within the CFD simulation.

(xii) All re-emitted absorbed radiation is considered as uniformly grey body diffused

5.3 GEOMETRY AND MATERIALS PARAMETERS:

(i) The system was divided into several physical zones, which were used in both the raytracing and the CFD simulation, *see chapter 4*. Those zones are: *outer conditions "first zone", second zone, third zone, fourth zone, indoor glazing "fifth zone"*, for the both of the options, i.e. vertical and inclined insertion of the element.
For the no insertion element setting: *outer conditions zone, first zone, second zone, fourth zone and fifth zone.*

(ii) The model assumes a minimum width of 0.02 m of gaseous cavity thickness at the start of simulation, i.e. this would mean having a minimal thickness of about 0.01m on each side of the inserted element, to ensure invoking convection in the cavity.

Also a minimum length of 1.00 m in the Y direction was assumed to maintain a workable set angle for the element, *see fig 4.02*. Such parameters can be modified, if necessary, to account for dimensions used in commercial glazing applications.

(iii) The width of the cavity (Δx) is a variable sum correspondent to the element's insertion angle $\tan\beta$ given in a range between (~88.85-65.77°), thus covering a range of cavity width between (0.02-0.45m) respectively. The latter figure was taken to check the sensitivity of the suggested glazing system.

(iv) The type of glazing used in the calculations is of clear ordinary type of Silica glass normally used for windows. Panes on both sides of the model have a standard thickness of 0.006m and a refractive index of 1.526.

(v) Material used for the inserted element is an ordinary transparent polystyrene sheet of medium thickness of 0.0001 m. refraction index of 1.55, tensile strength 66 ($10N^6/m^2$), Mpa, thermal expansion coefficient $27\times10^{-4}1/K$, density is 0.034 g/cm^3, solar transmission at normal incidence angles 85%.

(vi) The type of spacers assumed for the glass panes were standard aluminium with a grated or un-polished surface; (special types of spacers, i.e. foam types, or black thermo-painted were not used as these might affect results).

Reflectivity of the spacers is set at 0.99. In further simulations a less reflective spacer was also assumed to compare the effect of the reflectivity of the spacer on the system behaviour.

(vii) No frame setting was assumed for the model, so no "edge of the glazing" effect was presumed for calculation.

(viii) The model is in adiabatic conditions regarding heat transfer, (i.e. total insulation with no lateral transfer or losses to both of the horizontal top and bottom of the "model". (I.e. only 1 dimensional horizontal heat transfer regimes ensue through the system).

(ix) The cavity's gas filling will be normal dry air with refraction index of 1.00029 at standard temperature and pressure, i.e. dry air at 15°C and 1.0032Pa at sea level.

(x) No substrates or filler coatings were used in the glass layer. Having investigated the effect of refractive index as a variable, the coefficient of extinction calculated was assumed to be=32m¯1 of clear low quality green glass, rather the clear white ordinary window glass to verify the optical sensitivity of the inserted element.

(xi) Gaseous pressure in the cavity is constant and assumed homogeneous through the modeling (i.e. no escape of gas particles through the pores or the molecular structure of the glass.

5.4 SIMULATION OF CONVECTION AND CONDUCTION:

The next step of calculation is of convection and conduction, and was conducted using:

- Gambit (i.e. software for unstructured mesh generation) for the built model/slice.
- FLUENT V5.4 computational fluid dynamics software.

5.4.1 GAMBIT model:

As shown there was considerable range in the geometry limits taken for the sample, *see fig 4.07*, there was also another difficulty related to the set angle of the inserted element; as changing it should be carried out with special attention to avoid mesh overlapping of different zones, thus minimising accuracy.

It also meant that a suitable mesh generator was needed to model the unstructured meshing qualities of the sample.

(i) Three types of generic modules were built in GAMBIT. One with an internal inserted element at an inclined angle, the second module with a vertical insertion and a third without an element.

(ii) The variations in geometry were constrained in relation to changing the width of the cavity only and its fluctuation, which in return would change the set angle of the inserted element, *see 5.3*.

(iii) Five zones were created in two modules (i.e. the ones with the element), and three zones in the module with no element, *see table 5.02*.

Lateral faces of each module were considered to be symmetrical, (i.e. with no zonal reference) to model the sample as part of continuous section of glazing.

(iv) Preset boundary layers meshing were created in two zones; the internal surface of the outer glazing, i.e. in the second zone, and the internal surface of the fourth zone. Meshing grade taken was: 1:5 facing the inside of the cavity to increase accuracy of results.

Table 5.02 shows list and type of modules created in GAMBIT

Type of model	Number & list of entities		Zones Limits	Generic entity (material)
Inclined insertion 	5 entities	First zone	1.0m, 0.006m	Solid (glass)
		Second zone	1.0m,variable	Fluid (air)
		Third zone	Variable, 0.0001m	Solid (polystyrene)
		Fourth zone	1.0m, variable	Fluid (air)
		Fifth zone	1.0m, 0.006m	Solid (glass)
No element 	3 entities	Outer glass	1.0m, 0.006m	Solid (glass)
		Cavity	1.0, variable	Fluid (air)
		Inner glass	1.0m, 0.006m	Solid (glass)
Vertical insertion 	5 entities	First zone	1.0m, 0.006m	Solid (glass)
		Second zone	1.0m, variable	Fluid (air)
		Third zone	Variable, 0.0001m	Solid (polystyrene)
		Fourth zone	1.0m, variable	Fluid (air)
			1.0m, 0.006m	Solid (glass)

(v) Also triangular/ quadrilateral/ wedge meshing was used in areas where zonal edges would meet at inclined angles.

5.4.2 FLUENT 5.4 MODEL:

(i) The upper and lower edges of the model are in an adiabatic condition with its environment.

(ii) A 2ddp solver was chosen for the simulations, due to the type of mesh chosen and the association of energy transfer with the natural convection regime and large numbers of multi-head mesh cells, so as to ensure acceptable results and a CPU time; *see fig 4.06*.

(iii) The option of the Solver is the *explicit* method (i.e. equations of convergence are calculated separately), the time factor used for simulation is *steady state* and the velocity formulation of calculation is set for *absolute setting* (i.e. no change over time). Other options used included; the *Energy* option that enabled calculations to account for energy convergence over time and the *viscous model* was set to

laminar, i.e. no change in the viscosity of the gas within the cavity during the simulation.

Additionally, the following models were turned off during simulations: *(Species, Radiation, discrete phase, multiphase)* options, as they weren't relevant to the simulation environment.

(iv) Materials used for the different zones are:

(v) *Fluids*: air is used

Solids: are glass (for two zones), polystyrene (one zone) and aluminum (for spacers); *see appendix v* for materials properties.

(vi) Operating conditions are: *Pressure*: 101325 Pascal, *Gravitational acceleration:* is –9.81 m/S^2 in the Y co-ordinate. *Boussinesq model*: is used for buoyancy flow, with operating temperature of 288.16 k and changing specified density for the air.

(vii) *Boundary conditions*: mixed modes of boundary conditions, i.e. relevant to changing the surfaces resistance to wind convectional forces, were used in the simulation; *see chapter 4*. Consequently, heat transfer coefficients for both the ambient air, and for indoor conditions, next to surface glazing, were calculated using the thermal resistance in windows and glazing equations (ISO/DIN 15099):

Ambient, ground and sky temperature, local wind velocity values of the surrounding were taken using data from NASA website and then adjusted to the local glass surface respectively, e.g. the local wind V was taken as 4.3m/s; an average in the Kuwait area; *see chapter 4*. (NASA interactive Surface meteorology and Solar Energy Data Set/ Kuwait annual data 1996).

As shown, changing the wall azimuth angle of the system would have an effect on the system's surface thermal resistance due to the change in the prevailing wind direction and relevant convectional forces; *see chapter 4*.

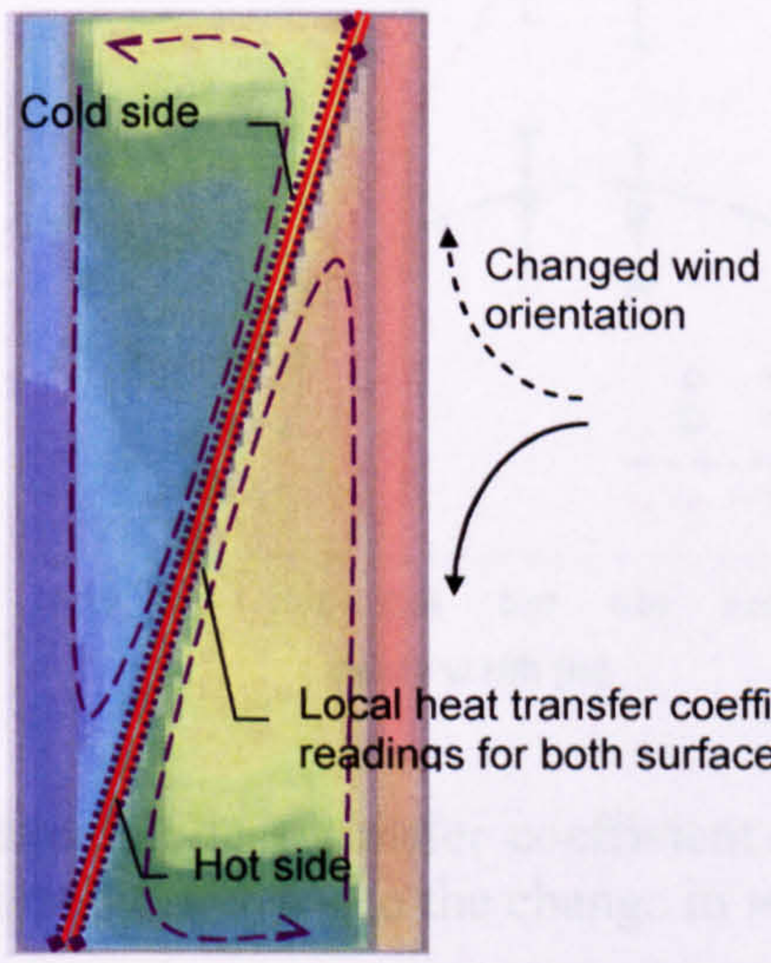

Figure 5.04 schematic of the scenario assumed (in Summer).

The effect of the change in principal orientation was analyzed through a set of scenarios of varying cavity widths, and seasonal changes. The thermal resistance of the inserted elements surfaces, i.e. (***1/hc***) was selected as a test sample for this effect, being a decisive element in the suggestion and as follows

- Seasonal changes were included, i.e. 14th January-for winter and 14th August-for summer were selected using Kuwait weather data files.
- Tests were conducted for a variety of changes in the width cavity (0.02~0.12).
- To deactivate the effect of the radiative heat flux on the simulation a constant heat flux was assumed for all the simulations scenarios.
- For each cavity width, a mean heat transfer coefficient was calculated from the local surface heat transfer coefficient by taking several hundred-sample points on both of the outer and inner surfaces of the inserted element; *see fig. 5.04*.

  As the thickness of the element is too small, marginal differences in results were recorded on both sides of the element.

- Such scenarios were repeated for different wind orientations.
- Results were then plotted; and polynomial trend curves were drawn, which showed similar representative curve equations. Consequently, a weighing factor of 1.0599 was achieved by dividing those set of equations; *see fig 5.05*.
- Such factor could be used as constant value that could be used to account for the change in wind orientation for the local weather conditions of Kuwait. Still, more simulations are needed to verify this assumption and for different latitudes.

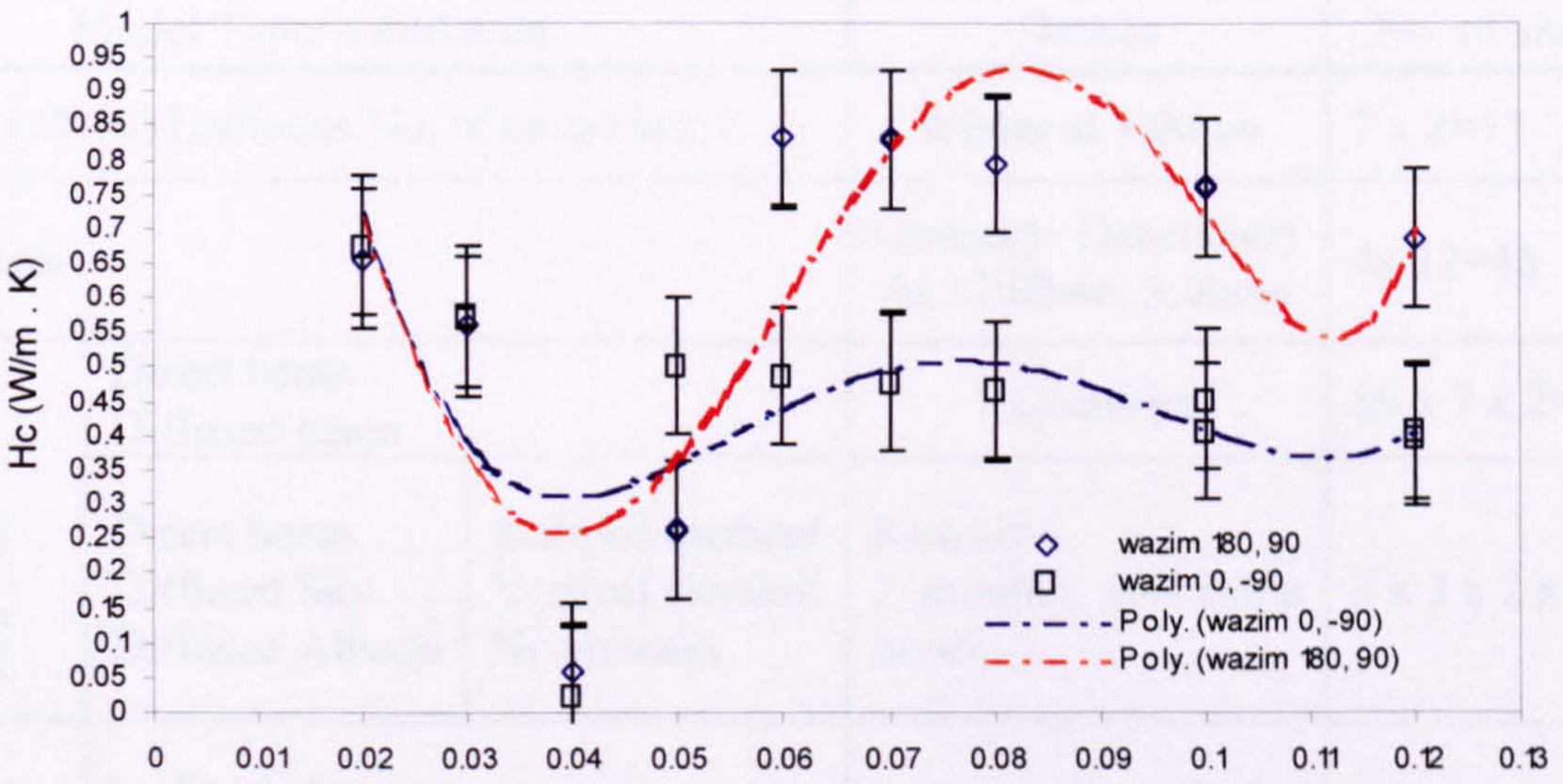

Figure 5.05 showing the average heat transfer coefficient on both of the surfaces of the inserted element relevant to the change in *wazim*=wall azimuth angle.

NB wall azimuth angle is: 0° for South, 180° for North, -90° for East, 90° for West.

- Calculated STDEV, standard deviation values were 0.271 and 0.179 for the South-North, West-East and the Summer-winter respectively.

(viii) In the raytracing method applied, *see chapter 4*, and after multiple reflections of the incident radiation, the film and the glass panes would continually absorb a portion of the propagated rays. The amount of this absorption would depend, however, on the optical properties of the materials themselves.

In real time, the emittance of the absorbed portion would happen not simultaneously with the rest of energy transmission (i.e. as in gray objects radiation diffusion/scattering assumptions), but would take place in a very small time lag of Δt depending on the thermal properties of the materials.

Isolating the effect of such absorption in the CFD simulations is not possible; as such a process would need special arrangement to write a code for this purpose only.

A decision was made to add this portion of absorption carried over from the "storage units" in each zone and reported in the raytracing output files to their correspondent zones in the CFD model at the beginning of the simulation; *see fig. 4.06*. As the written code of the current radiation models used in the CFD doesn't include a variable time factor when working with radiation algorithms, therefore

Table 5.03 shows details and number of simulations taken for each stage of the software, *see appendices III-IX*.

Model Type/ simulation				Details	No. of simulations
SMARTS2	(30-40) Latitudes No. of countries: 7			Winter at 3:00pm	7 x 2=14
	Kuwait			(January- December) At 12:00am, 3:00pm	4x 12=48
Raytracing	0.02-1 m	Direct beam Diffused beam		7 Countries	89 x 7 x 2= 1246
		Direct beam Diffused Sky Diffused Albedo	Inclined element Vertical element No element	Kuwait: 2 months, sun shine hours	3 x 3 x 2 x 8= 144
CFD	0.02-0.12m	Inclined element No element Vertical element		Kuwait: Summer, Winter	2x 3x 8= 48
Total number of simulations					1500

(ix) For solution controls; only the flow was activated as part of the coupled alternative. The relaxation factor was taken first as default value of 1 and then reduced to 0.5 in some runs after not achieving convergence of several hundred runs, (as a recommended value for small temperature differences calculations) to ensure solution convergence.

The flow regime was calculated utilising the *first order upwind* then switched to the *second order upwind solver*.

A varying number of iterations were selected for each "run" varying between 60-800 to achieve acceptable convergence for the regime flow.

5.5 SETTING THE BOUNDARIES OF SIMULATION:

The next step was to set the boundary limits to each stage of the simulations; such a step would then indicate the required number of runs necessary in each stage of the collective model; *see fig 5.06*:

Stage one (Solar model)

(i) Weather files of 8 countries (i.e. of latitudes between 30-40°) were used, ranging between Iran at the eastern and Algeria at the western edges of the band.

(ii) The mid day of each month (i.e. 3:00pm 14th of January/August 1996) was taken as representing the change of seasons (i.e. winter and summer) respectively, for 7 different countries so as to show solar geometry sensitivity.

A larger number of simulations, i.e. 12:00pm and 3:00pm the 14th of each calendar month of 1996, were completed for Kuwait for the purpose of validating the accuracy of the solar model against the collected empirical data.

(iii) A set of simulation for Kuwait (i.e. diurnal profile of the 14th August 1996, local solar hours) was chosen to check the sensitivity of the suggested glazing system with regard to daily change of incidence angles.

Stage two (Raytracing model)

(i) The glazing geometry utilising the inclined element was applied to the INPUT files of all 7 countries. Two additional geometries were applied to simulations of Kuwait files, i.e. the inserted element is vertical and no element in cavity.

(ii) A fixed width of cavity, i.e. 0.04m, was used for simulations of the 7 countries. While a flexible and incremental range of widths, i.e. 0.02-0.45m, were used to calibrate the sensitivity of the element upon change of tilting angle.

(iii) Simulations of both the direct beam and the diffused components of the solar radiation were used in simulations for all 7 countries.

In the case of Kuwait, a more detailed simulation for the diffused component was also used, i.e. both ground albedo & sky diffused.

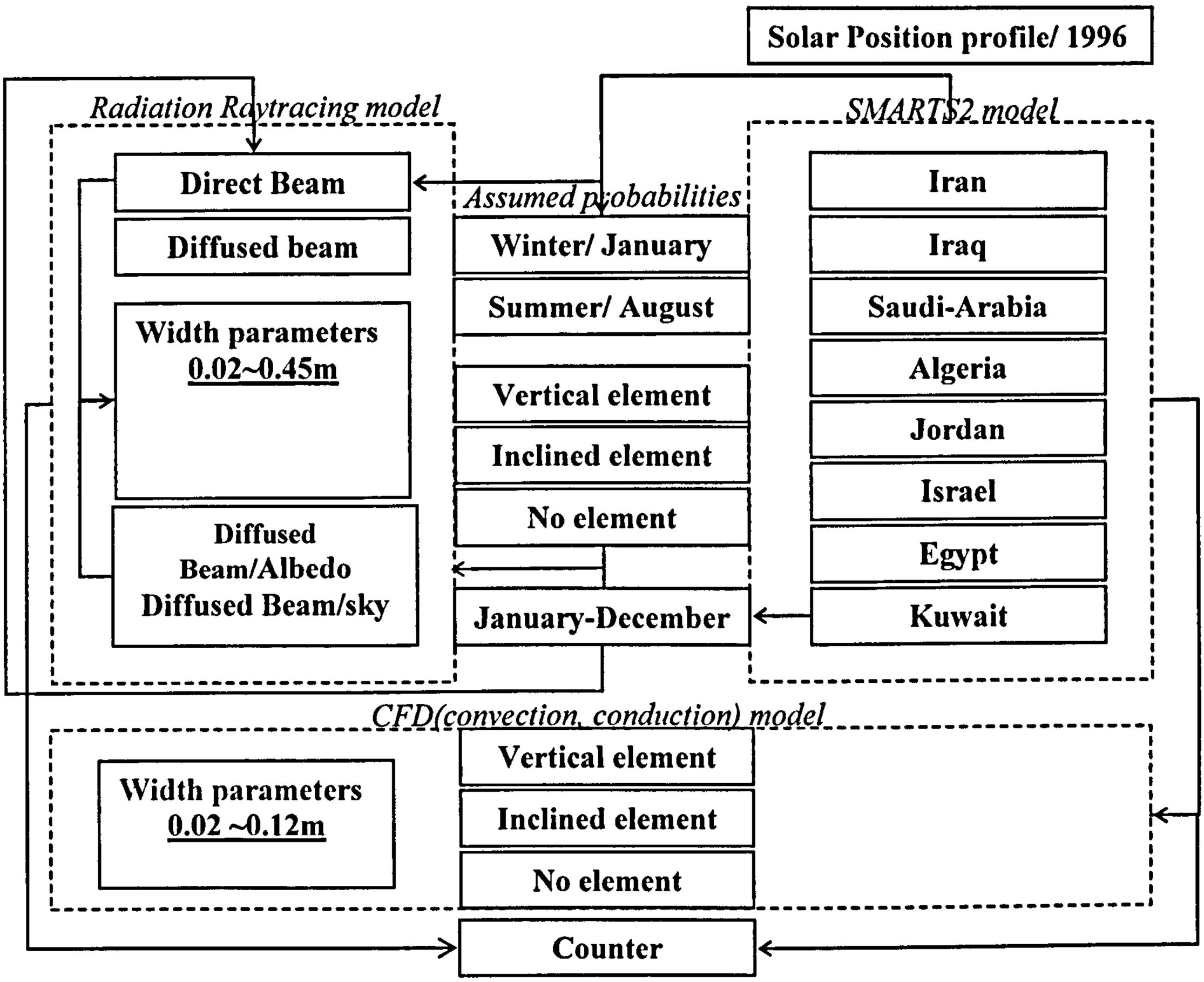

Figure5.06 showing extent of probabilities taken of simulation for each part of the software; please note that width parameters in Raytracing model aren't wholly reflected in the CFD model.

Stage three (CFD)

(i) In the Computational fluid dynamic model, several different width parameters were used to check the change of convection behaviour in the cavities vortices created by the insertion of the element in the normally rectangular (0.02-0.12m) cavity.

(ii) Two seasonal sets of simulation were used in at this stage, i.e. Kuwait at summer/winter time, to check convectional forces behaviour against change in temperature and wind profile.

Finally a counter is set to gather manually, at this stage of research, all the obtained outputs, to create a total energy transfer profile, *see table 5.03*.

Reference:

1. Alamdari F, Hammond G.P. Improved data correlation for buoyancy-driven convection in rooms, Building services Engineering. Res. Technology 1983;4 (3):106-112.
2. ASTRONOM 8.1, Manual. USA: Wageningen Co.; September 2000.
3. Nadia. Provider of Dust data. Kuwait: Institute for Scientific Research; 1996.
4. NASA, surface meteorology and Solar Energy Data Set. CANMET Energy Technology Centre and CETC-Varennes. Sponsored by NASA and Earth Science Program 2005. See also; http://eosweb.larc.nasa.gov/sse/RETScreen/
5. Fluent documentation, Fluent Version 6.1, San Jose, California, USA: Globetrotter software 1996-1998. See also: http://www.globetrotter.com
6. Gueymard C., Turbidity determination from broadband irradiance measurements: a detailed multi-coefficient approach. Report no.: FSEC-PF-311-96. USA: Florida Solar Energy Center; September 1996.
7. Gueymard C., Simple Model of the Atmospheric Radiative Transfer of Sunshine (SMART2): algorithms and performance assessment. Report no.: FSEC-PF-270-94. Cocoa (FL): Florida Solar Energy Center, 1994.
8. Gueymard C. SMARTS2, a Simple Model of the Atmospheric Radiative Transfer of Sunshine: algorithms and performance assessment. Rep. FSEC-PF-270-95. USA: Florida Solar Energy Center; 1995.
9. Hammond G.P. Thermal performance of advanced glazing systems, Journal of institute of Energy 2001; 74 (March):2-10.
10. Kuwait annual weather data, NASA Surface meteorology and Solar Energy Data. USA 2001. See also: http://eosweb.larc.nasa.gov/sse/RETScreen/
11. Mahmoud Eid. Provider of Kuwait solar data (kw96). Kuwait: New Horizon Company; 1996.

CHAPTER SIX

RESULTS AND ANALYSIS

Introduction

The considerable amount of and nature of the data generated from each stage of the simulation process meant that not all the output results from one stage could be automatically processed to the next one. Consequently the processed output data from one stage was transferred manually to the input files of next process stage rather than through an assigned written protocol within the software.

This strategy was adopted to minimise CPU time and to reduce the probability of computer system crashes. The accumulated data was then processed and written as input to the next stage. Results were obtained and analysed at each of the following layers and as a collective output:

- SMARTS2 results.
- Raytracing results
- Computational fluid dynamics results; i.e. Fluent 5.4, 6.
- Final outcome (i.e. counter).

6.1 SMART2 RESULTS

The software was used to predict the solar profiles for the countries lying within the chosen band of latitudes. Two sets of runs were applied to seven of those countries (at 3:00pm of 14th January and 14th of August respectively) so as to provide the required solar radiation data and allow an examination of the effects of seasonal changes; *see 5.1, also appendices vi.1-7* for SMARTS2 results 7 countries.

Additionally, two separate solar data sets were used to predict; (i) the insolation patterns in Kuwait at 3:00pm of the 14th of each calendar month of a particular year i.e.1996; *see appendices vii: vii.1.a-b to vii.12.a-b*, and; (ii) the diurnal solar pattern by choosing 14th of August as representative of the "day of the year". *See appendices viii-Kuwait 6am-18pm.*

The wall azimuth angle calculation option was deactivated in the software for those set of simulations, *chapter 4, and figure 4.10(A, B, C)*, and a tracking system with fixed tilt angle of 90° was chosen for the glazing; thus the software would return results of solar incidence angles for a relevant vertical system with no specific orientation.

In general, ascertained results for Kuwait, through using the modified turbidity factors make it obvious that though they are not totally in accord with the empirical data obtained, still they show more acceptable level of accuracy than those obtained for the remaining other countries that used the built-in turbidity constants of the software.

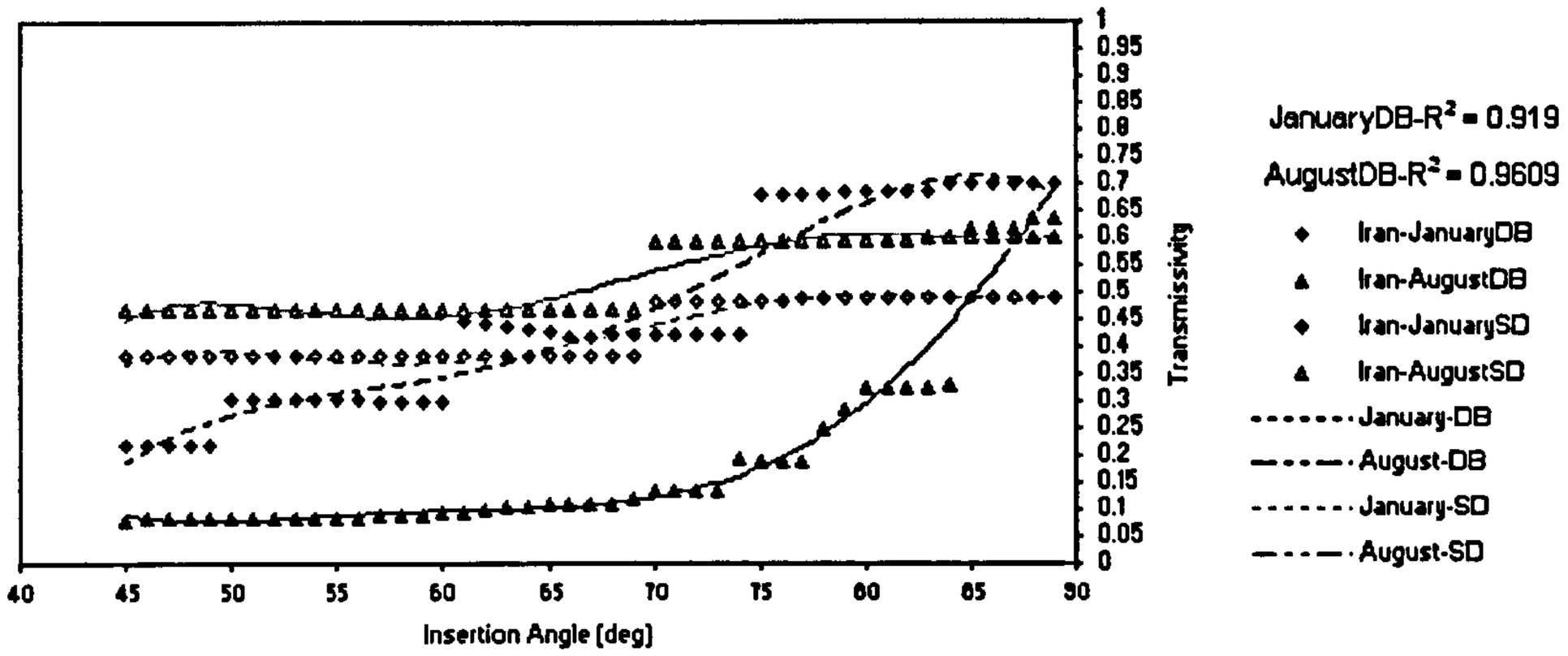

Figure 6.01 Seasonal transmissivity of the suggested system in Iran- 14th January/ August, 3:00PM, DB=direct beam, SD=sky diffused.

6.2 RAY TRACING RESULTS

Insolation data outputs from the SMARTS2 software were used as inputs to the raytracing algorithm; which was used to predict the behaviours of the solar radiation components as they were transmitted through the glazing system.

Objectives sought in this stage were to predict a behaviour pattern with regard to the bulk optical properties of the new system through changing the insertion angle of the element and the latitude of the location.

Hence, the following steps were used to calculate the system total optical behaviour:

(i) The transmissivity of the direct beam, the diffused and the ground albedo components were realized by comparing the values of the incident solar radiation with those of the output obtained from the raytracing algorithm after accounting for the components of the solar radiation passing through the glazing system, *see appendices ix.1-7 for Raytracing results of the 7 countries.*

(ii) Transmissivity results of up to 90 runs for each of the seven countries studied were processed to evaluate the variations in seasonal behaviour, 540 runs, in the case of Kuwait, to cover the annual behaviour.

Separate 91 runs were also needed to evaluate the annual behaviour of the system by running the simulations for a specific hour/ day through 12 months, using Kuwait atmospherical data. (Nadia 1996).

(iii) Transmissivity results for the diurnal behaviour were calculated per solar hour for a particular day of the month/ 14th August. (Nadia 1996). Several bands of insertion angles were used to test the change in transmissivity with that of the cavity width.

(iv) Transmissivity profiles for a set of insertion angles between (45-89°) degrees were calculated at a one-degree interval; this approach insured that any

incremental change in transmissivity, corresponding to change in the cavity width, would be ascertained.

Assuming that not all the incremental changes in the angle of the inserted element could be assigned to a workable cavity width due to manufacturing limitations in cavity spacers grading; results were compared with each corresponding cavity width (between 0.02-1m) to ensure a practical grading of the cavity space by assuming a modular height of 1m, *see chapter four*.

(v) Consequently trend lines were drawn, both for the direct beam and the diffused component; so as to specify the system's transmissivity trend behaviour. The objective was to verify the assumption that there could be an ensuing correlation governing the relationship between the solar incidence angle, the latitude and a relevant optimum cavity width, while taking into account the change in solar geometry with seasons; *see figs 6.01-6.07.*

(vi) R-square values were ascertained for all the produced trend lines to check, the level of variance in results, and confidence levels of the regressions produced. R-square values varied between (r^2=0.92-0.96) for the transmissivity of both of the direct beam and diffused components.

The graphs showed reduction in the overall transmissivity values for the diffused and direct solar insolation components when passing through the system, *see figs 6.01-6.07*.

This pattern was more obvious upon accessing the annual transmissivity of the system, which was calculated at 3:00pm on the 14th of each month; *see fig 6.08*. Those results could be explained by the fact that the "monthly" simulations were carried out for a system operating from in fixed position, i.e. of latitude and longitude, and the only changes to the solar geometry were those due to seasonal changes in the sun position.

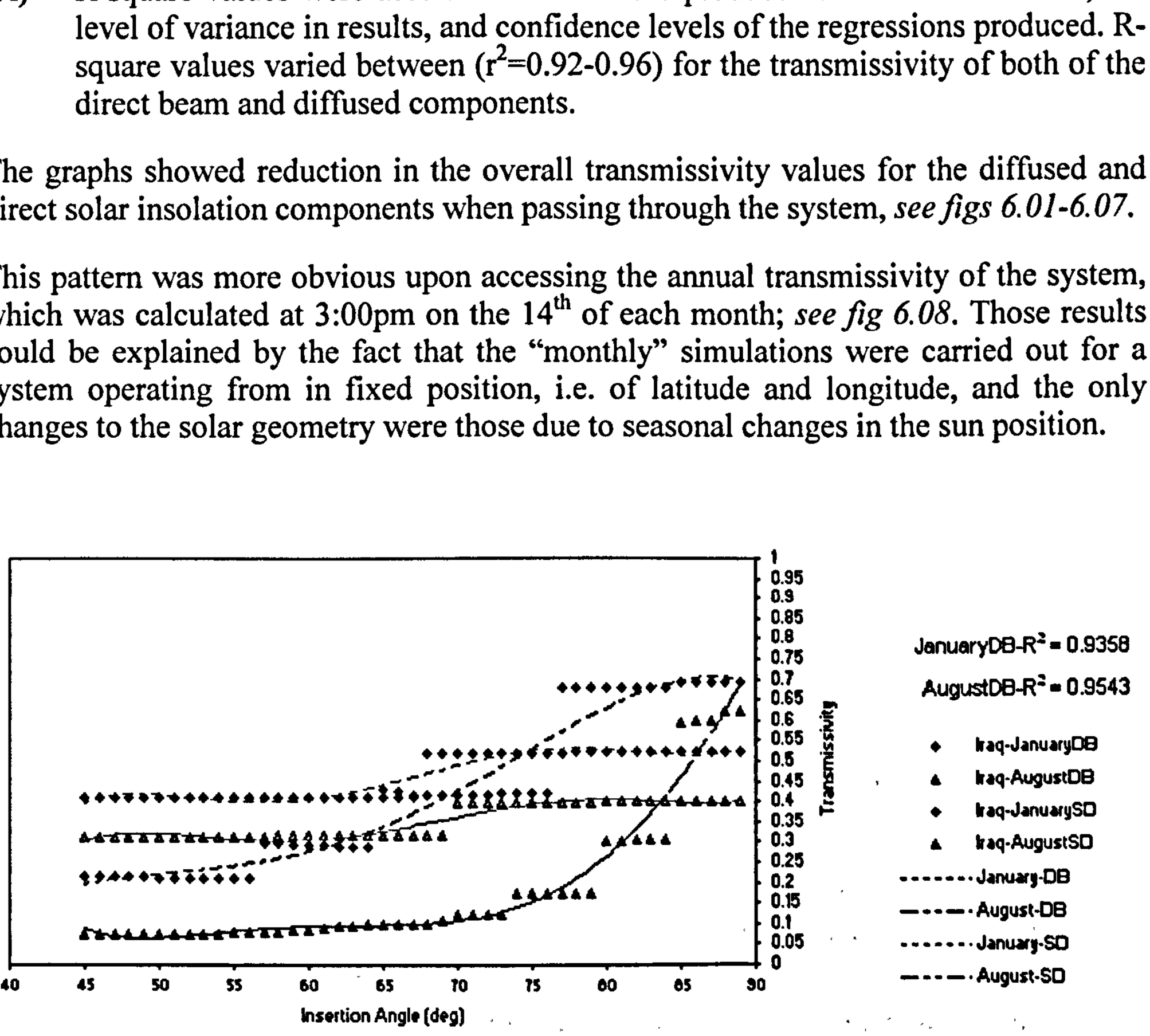

Figure 6.02 Seasonal transmissivity of the suggested system in Iraq- 14th January/ August, 3:00PM

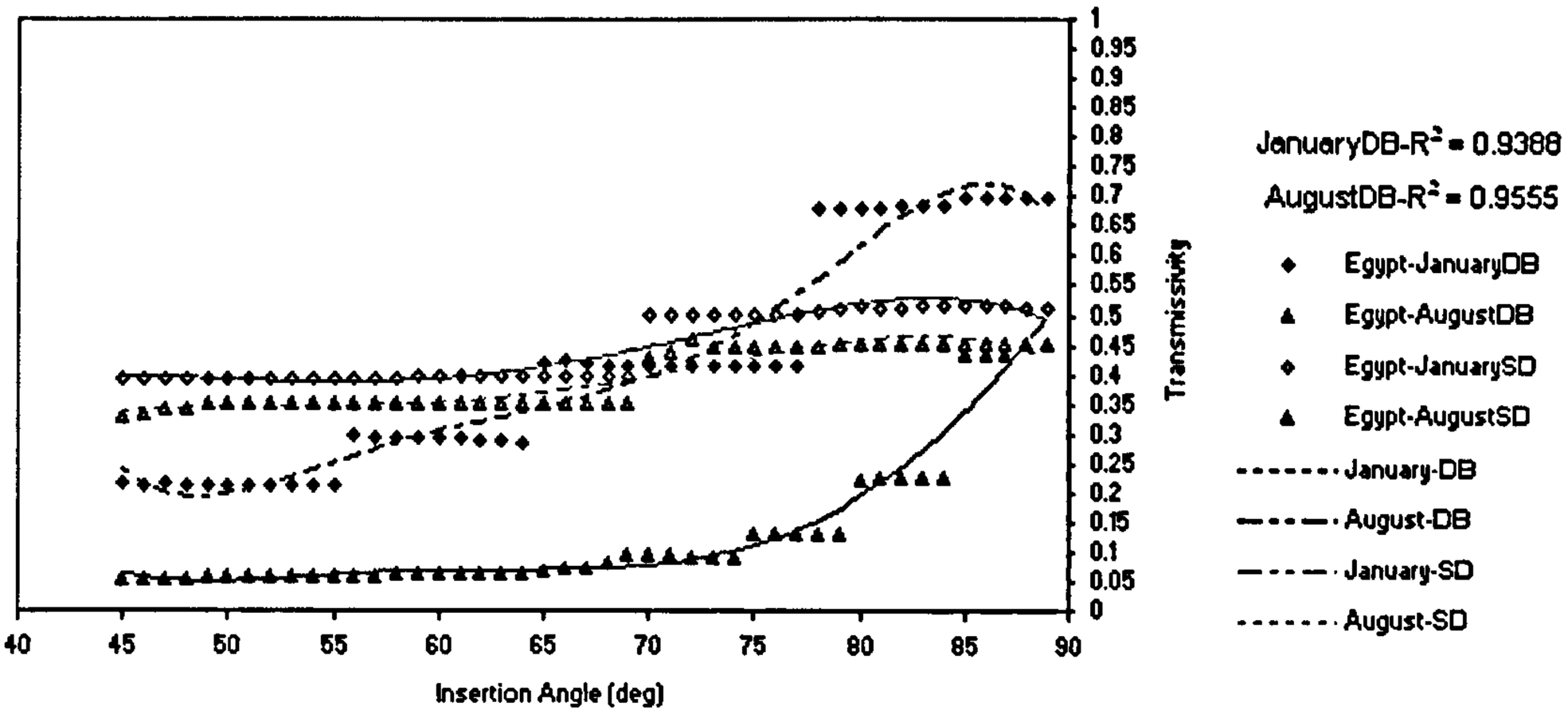

Figure 6.03 Seasonal transmissivity of the suggested system in Egypt-14th January/ August, 3:00PM.

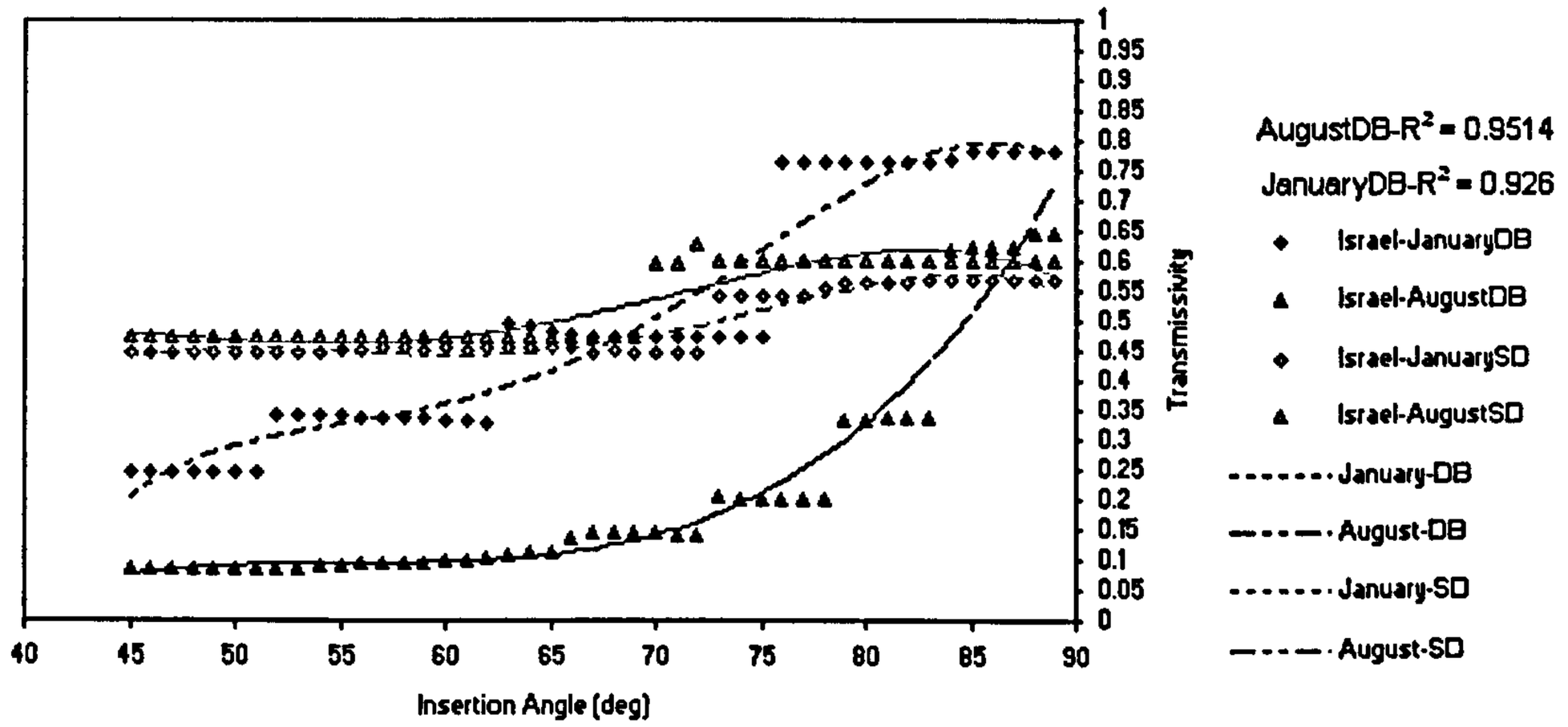

Figure 6.04 Seasonal transmissivity of the suggested system in Israel-14th January/ August, 3:00PM.

The results also showed that the pattern of steady fall in the system's transmissivity is associated with a decrease in the insertion element's angle.

This trend of overall reduction was also more associated with the transmissivity results of the direct beam than those of the diffused. It was expected that the latter would stay generally stable throughout the simulation.

An advantage of using relatively low sun incidence angles in simulations, e.g. at 3:00pm throughout the seasons, was to check the suggestion's sensitivity. Results showed that a considerable reduction in the direct and diffused beam transmissivity is achieved when using relatively small insertion angle (θ), e.g. below 70° degrees due to the restricted view factor caused by the inclined inserted element; *see fig 6.13*.

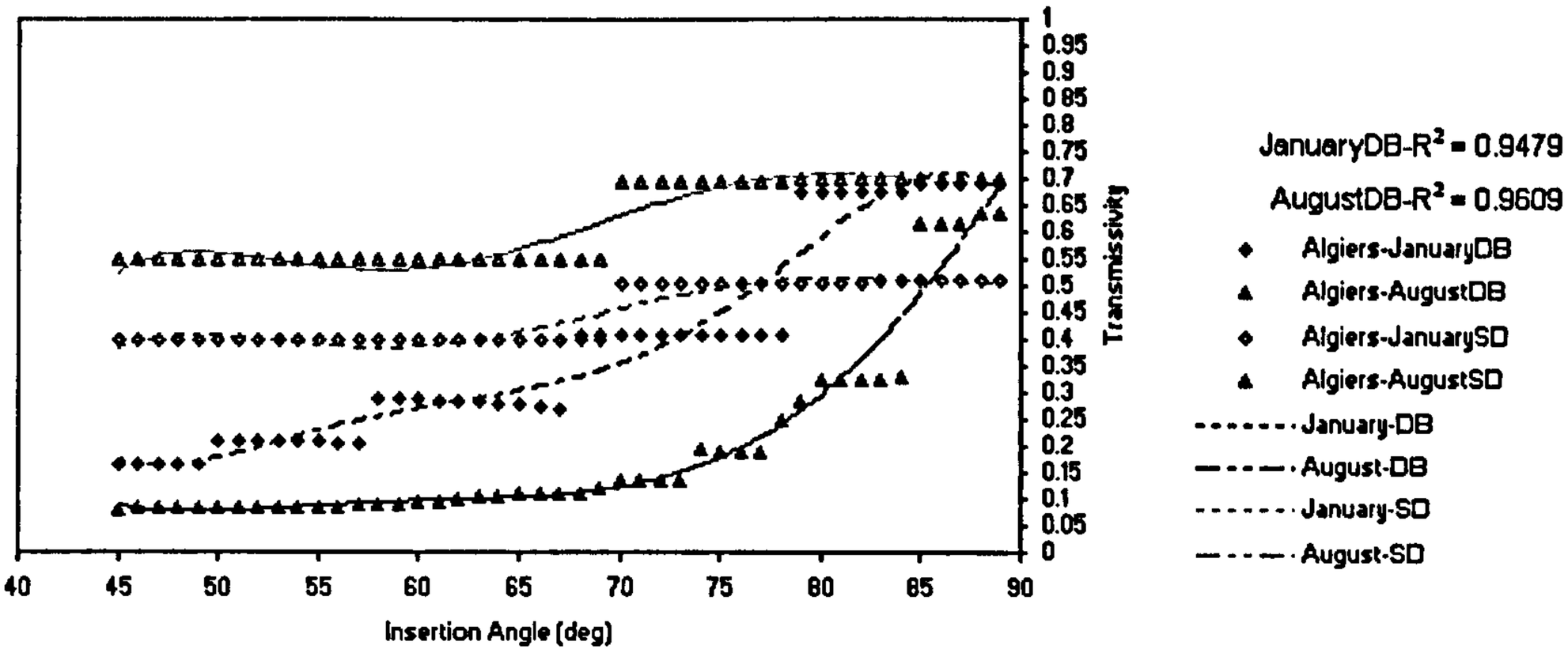

Figure 6.05 Seasonal transmissivity of the suggested system in Algers-14th January/ August, 3:00PM

Looking at the pattern demonstrated in *figs 6.01-6.07*, it can also be noticed that there was also an incremental unsteady variation, e.g. noise, in the reported direct beam transmissivity data results associated with a slight decrease at certain angles bands followed by a perpetual fall in the transmissivity curve at a specific angles, then to have another band of steady decrease in transmissivity. The same trend of results, *see fig 6.08(A)* could also be noticed upon inspecting the monthly behaviour of the system using Kuwait 1996 results.

Figure 6.08 (A&B) shows that those identified "falls" in the monthly transmissivity pattern tend to be more frequent and closer to each other, at those months associated with relatively high sun angles (i.e. between June-August), while low sun angles in the months of (November-February) would yield more stable behaviour and is more associated of what it is expected from the system when dealing with the diffused component.

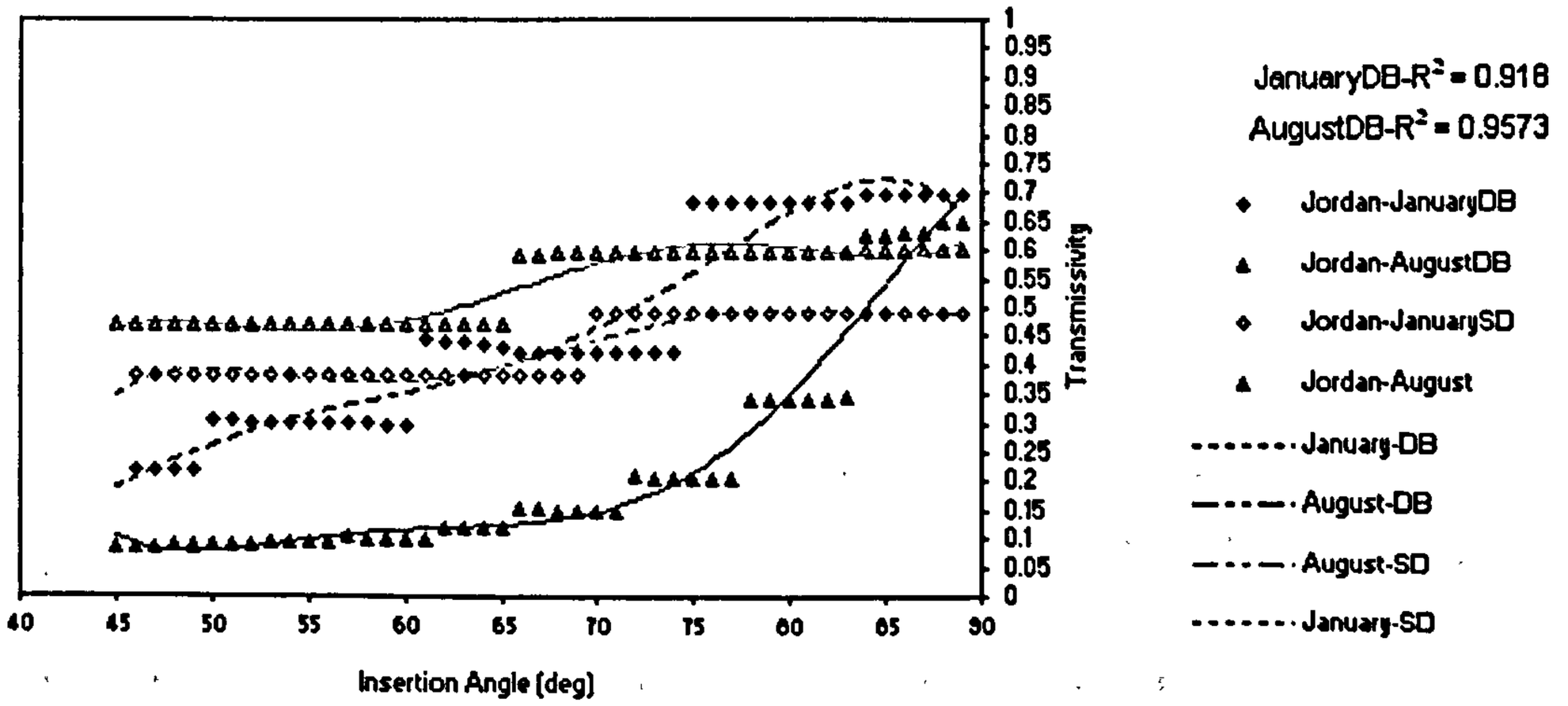

Figure 6.06 Seasonal transmissivity of the suggested system in Jordan-14th January/ August, 3:00PM.

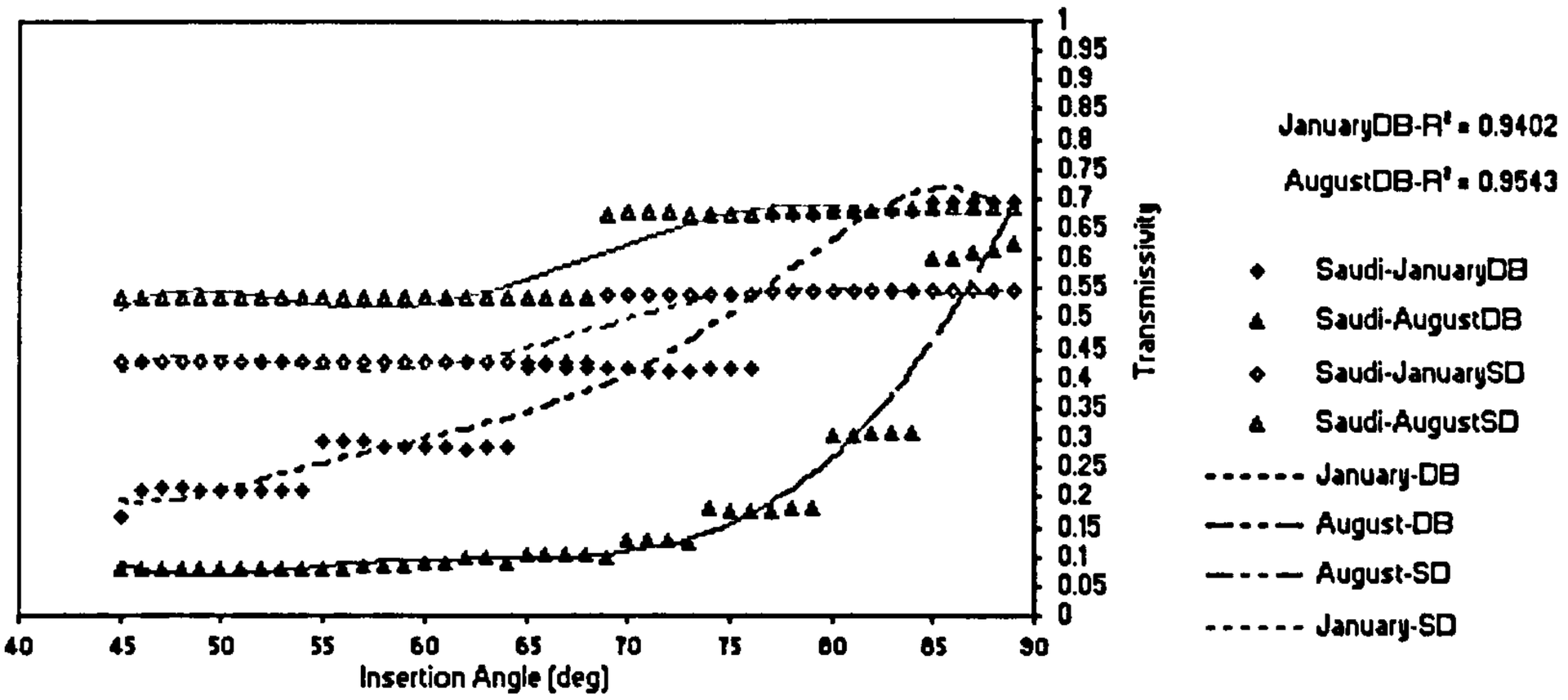

Figure 6.07 Seasonal transmissivity of suggested system in Saudi Arabia-14th January/ August, 3:00PM

Alternatively the purpose of running simulations, based on the diurnal behaviour of the system, was to assess the effect of changing the solar geometry throughout a certain day, on a system with a fixed insertion element's angle; *see fig 6.09*.

4 sets of fixed insertion angles with wide band of intervals were selected (i.e. 89, 80, 70, 60°) respectively; runs were performed for the solar sunshine hours of e.g. 14th August 1996 in Kuwait between (5:30AM-18:30 PM).

A considerable reduction in the direct beam (DB) transmissivity was evident at noon with high sun angles of (70-74°), while the system allowed more direct radiation to pass through at lower sun angles as expected.

More uniform gradient pattern in (DB) transmissivity was evident in the behaviour of a system with relatively low insertion angles.

Alternatively, when the insertion element's angle was near normal e.g. 89°, steep decrease in the transmissivity profile was noted near noon, compared to a lesser behaviour in inhibiting insolation at low sun angles.

No fluctuation in transmissivity results was noted in the "diurnal sets" as the simulation allowed a wider incremental step-change of the cavity width from that sought in the "monthly sets", *see figs 6.08, 6.09*, for comparison respectively.

Trend lines of *fig. 6.08(B)* also predict a stable transmissivity pattern for the direct beam corresponding to certain insertion element's angle, incidence angle throughout the year for the seven countries.

R^2 value for all trend lines generated had acceptable accuracy of minimum of 0.92; *see Glossary for definition.*

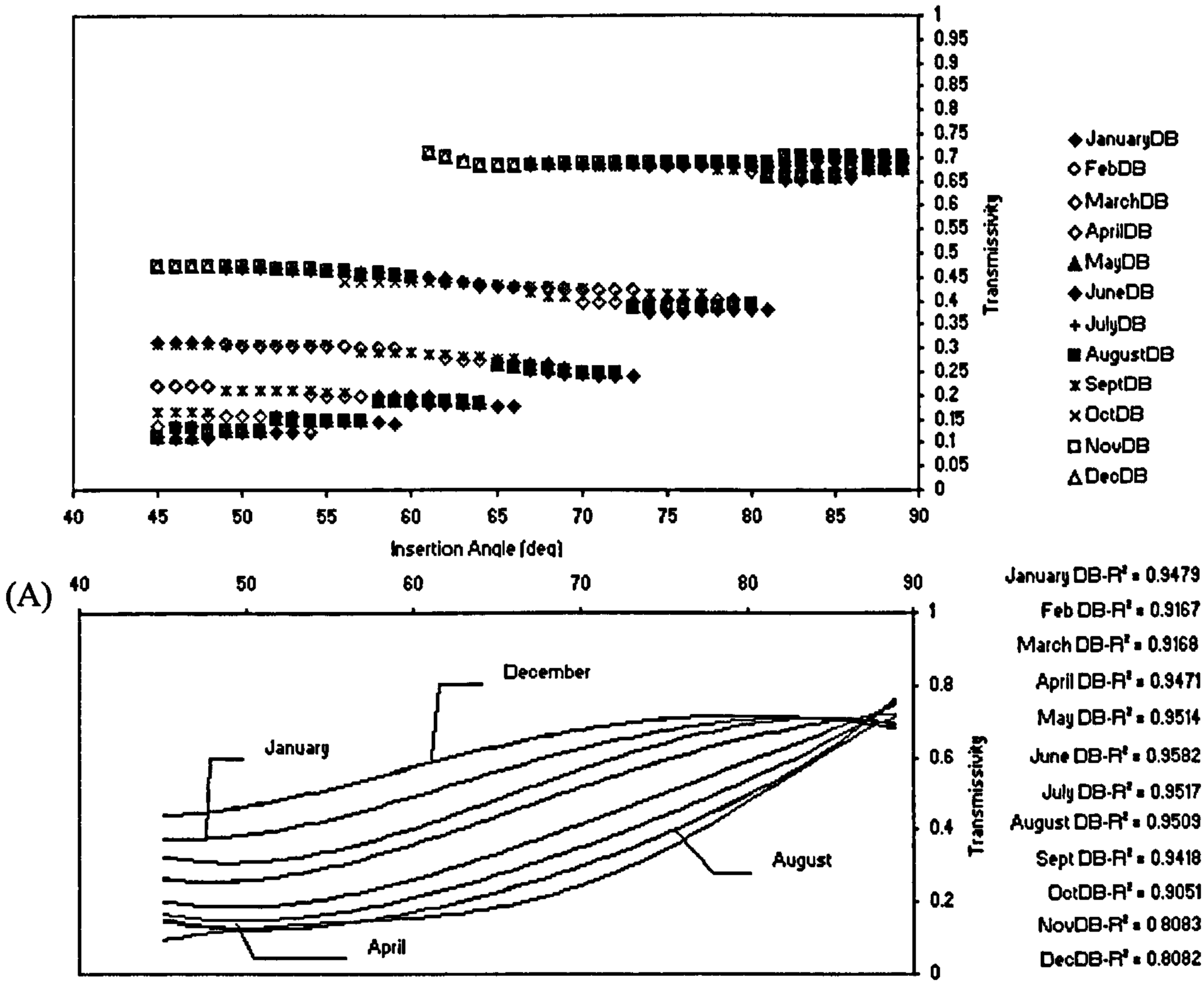

(B)

Figure 6.08 Showing monthly transmissivity of the direct beam transmissivity for the suggested system in Kuwait-14th of the month, 3:00PM
A-Direct beam transmissivity, calculated by degree angle.
B-Trend line behaviours

6.2.1 Understanding raytracing results

While analysing results, a small fluctuating stepping down pattern associated with falls was noticed in the (DB) transmissivity curve, especially at certain insertion angles and cavity widths, though the overall trend-line referred to continuous and steady overall decrease in the transmissivity.

Mitigation of the small-recorded variation in data results could be due to a product of raytracing algorithm called "Aliasing"; *see chapter three and definition in nomenclature*. Aliasing usually differs from other types of noise, e.g. disturbance data generated, in that its pitch would change radically when the level of the intended ray changes, i.e., as in cases when received insolation intensity changes with solar geometry (PRQC 2005). While the periodical stepping falls in graphs are a product of the method used in compiling the raytracing software due to the discriterization of data, i.e. the propagated beams are projected successively at assumed intervals of 0.10m length segments of the modular 1.00m height of the system. This could also explain the semi stable frequency of these signals/"falls" in transmissivity curve, e.g. at 10 degrees intervals.

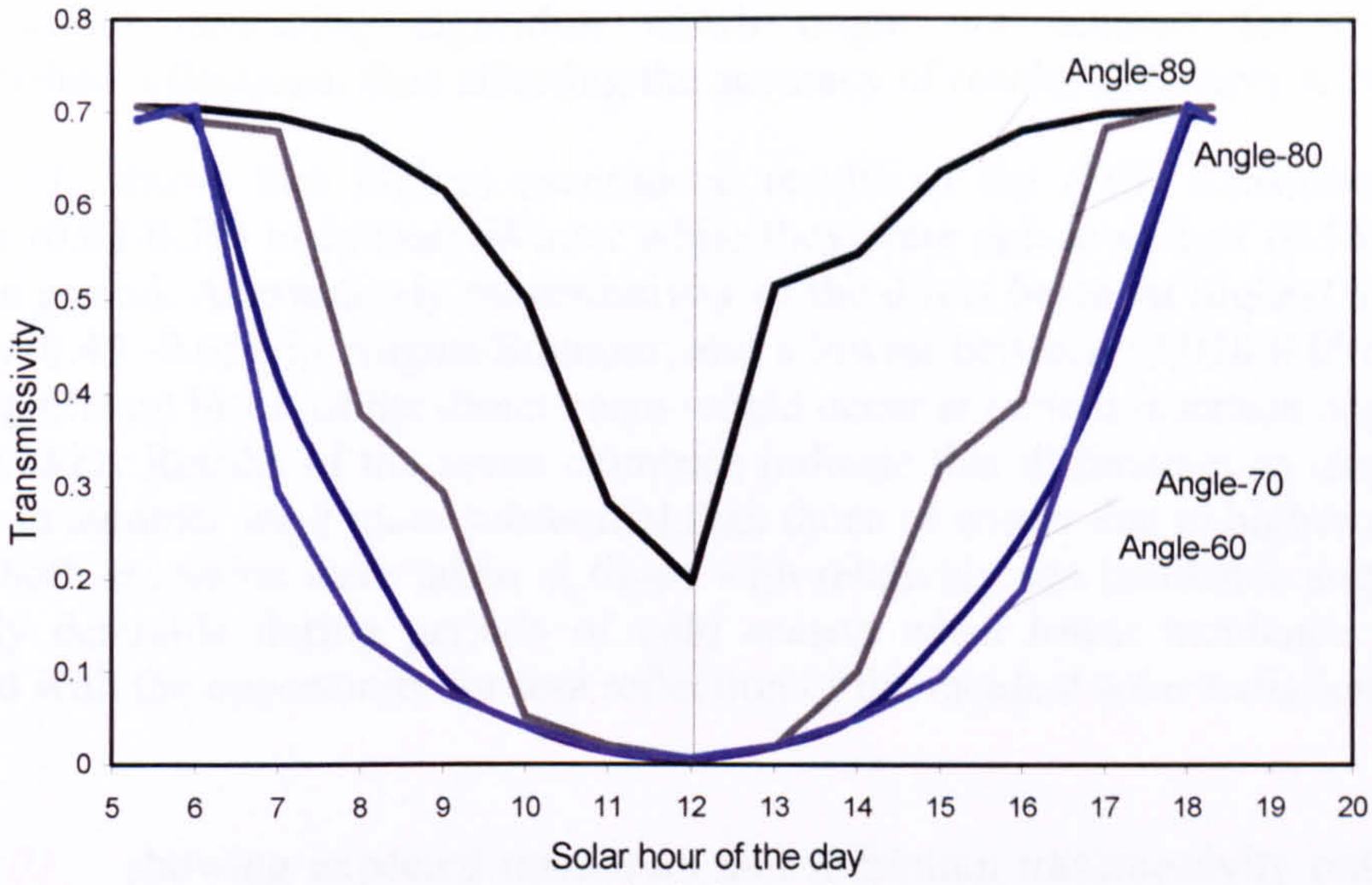

Figure 6.09 Showing diurnal transmissivity of the direct beam for the suggested system in Kuwait-14th of August, at 3:00PM,
NB element's insertion angles used are (89, 80, 70, 60°)

The system's transmissivity corresponded to the various insertion angles used and also to the solar geometry with seasonal and latitude changes.

In general, raytracing presentation and accuracy could be improved by filling or averaging the gaps in those falls by increasing the pixel intensity (points) of calculation; either through:

(i) Increase the number of runs per/ an incremental change of the insertion angle, or (ii) use a smoothing curve technique. Accuracy could also be improved by (iii) increasing the number of raytracing arrays per each calculation, i.e. either by increasing the number of segments mapped by the rays per unit length or (iv) directing more than one ray at a segment per unit time, though leading to an increased CPU time (Rayica 2005).

However, it was felt that implementing any of the suggested changes to the current software would not improve the results substantially and would increase the CPU time. The level of change in transmissivity was more noticeable within a small band of angles within the high or near normal insertion setting (e.g. 78-89°). The level of fall in transmissivity and its frequency were less obvious as the cavity width increased leading to an incremental and semi stable behaviour and suggesting that efficiency of the system in controlling transmissivity has reached its optimum; *see figs 6.01-6.08*.

Several hundred runs of the software were used to analyse the optical behaviour of the system and yielded huge amounts of data. In general, the behaviour of the glazing system was evaluated, in the light of two factors:

- Time related (i.e. hourly, daily, monthly and seasonally)
- Type of insolation component (i.e. direct and/or diffused).

The analysis has also to take account the conditions of the simulation environment i.e;

(i) Working within a wide range of insertion angles and using an incremental step change of one-degree angle per simulation and, (ii) The effect of using the developed

non-sequential raytracing algorithm which might not account for all multiple undiminished reflections, thus affecting the accuracy of results. (Pfisterer R 2003).

Table 6.01; shows that highest ascertained results of the (DB) transmissivity were between (0.69-0.78) in January/Winter while they were at a lowest of (0.163-0.24) for the same period. Alternatively transmissivity of the direct beam, at highest levels, were between (0.45 -0.65), in August/Summer, and a lowest between (0.058-0.09) indicating that a significant block of the direct beam would occur at certain insertion angles and so cavity widths. Results of the seven countries indicate that differences in transmissivity patterns in summer were more substantial than those of winter due to higher sun angles, though both scenarios were taken at times with relatively sun incidence angles This is generally desirable during periods of cold season when lower incidence angles are expected with the opportunity for less reflection of the incident solar radiation.

Table 6.01 showing expected maximum and minimum transmissivity output results for the participated countries (based on running simulations for the chosen cavity widths on the 14th January/ August, i.e. chosen day of the year, 3:00PM).

Countries	Season	Max. trans. Value	Type of the Insolation Component	Min. trans. value
ALGIERS	January	0.69	Direct beam	0.163
	August	0.57		0.058
	January	0.51	Sky Diff	0.4
	August	0.7		0.55
IRAQ	January	0.7	Direct beam	0.21
	August	0.62		0.07
	January	0.52	Sky Diff	0.41
	August	0.4		0.31
EGYPT	January	0.7	Direct beam	0.212
	August	0.45		0.06
	January	0.52	Sky Diff	0.4
	August	0.46		0.33
ISRAEL	January	0.78	Direct beam	0.24
	August	0.64		0.08
	January	0.57	Sky Diff	0.45
	August	0.63		0.47
IRAN	January	0.7	Direct beam	0.22
	August	0.64		0.08
	January	0.49	Sky Diff	0.38
	August	0.6		0.47
JORDAN	January	0.7	Direct beam	0.22
	August	0.65		0.09
	January	0.5	Sky Diff	0.38
	August	0.6		0.47
SAUDI ARABIA	January	0.69	Direct beam	0.168
	August	0.63		0.077
	January	0.55	Sky Diff	0.43
	August	0.68		0.54

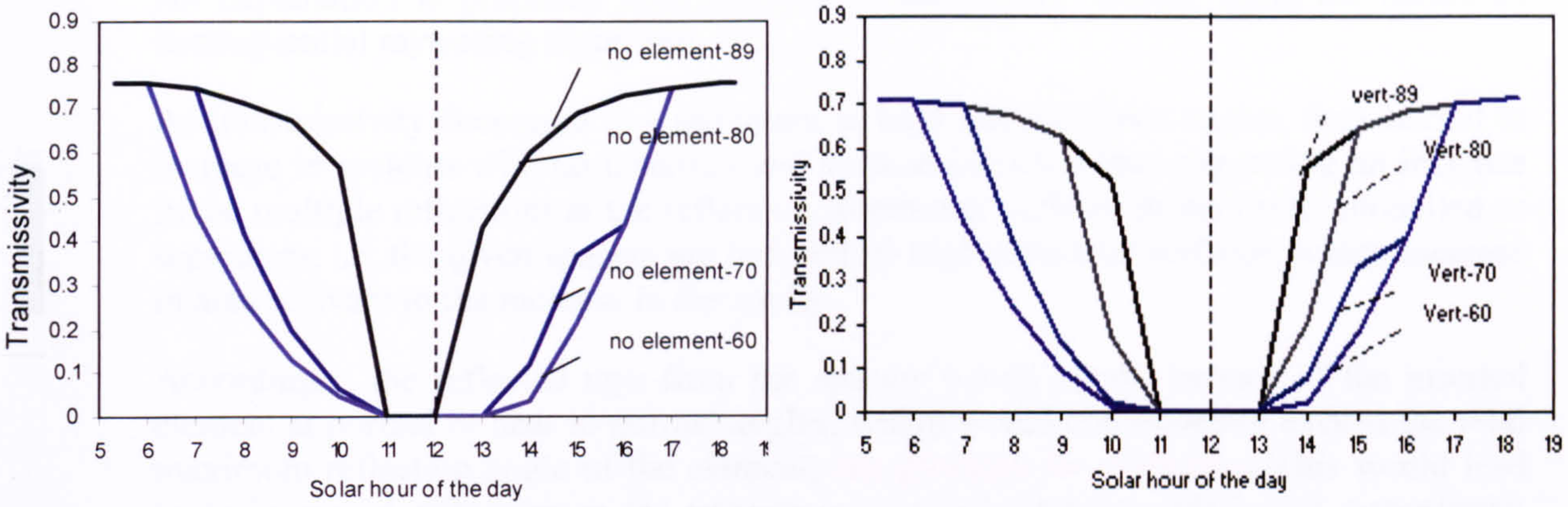

A) B)

Figure 6.10 Results for the diurnal direct beam transmissivity of the system for the 14th of August 1996/ Kuwait, for two scenarios' sets:
A- Case of a no insertion of the element in the cavity.
B- Case of a vertical element setting in the cavity.

NB; coloured graphs show the transmissivity, calculated by solar hour of the day for cavity widths corresponding to the element's insertion angles of 89° Black, 80° Grey, 70° Dark Blue, 60° Lighter Blue)

6.2.2 Comparison analysis

To fully assess the effect of the suggested inclined insertion on the (DB) transmissivity *see fig 6.09*; analysis was also needed to compare the system's behaviour with that of more conventional and commercial systems settings, e.g. those with either; (i) A normal angle insertion of the element. (ii) No insertion in the cavity.

Consequently, several scenarios were adopted, and were taken as similar in cavity widths to measurements projected from insertion angles of (89, 80, 70, 60°) respectively, for a modular system's cavity width of (~0.02, 0.18, 0.36 and 0.58 m) respectively.

Again the base for behaviour comparison sought for the glazing system, relates to the control of the rates of transmission of the incident direct component of the solar radiation during the periods of peak intensity.

Results obtained for transmissivities of various glazing system configurations showed again a fluctuating pattern of behaviour.

Figure 6.10 (A&B) shows unexpected behaviour of the (DB) transmissivity for some of those systems, once raytracing algorithm is applied as the base of analysis. In high solar angles scenarios, more blockage of the direct component was obtained by a normal angle element's insertion and a complete transmissivity blockage was obtained with a system with no element insertion.

The result is different from an expected behaviour; seen usually if the same simulations were to be run through other software e.g. that uses solid angle model or a centre of node algorithms for incident radiation calculation.

An explanation is proposed here, relevant to the pattern shown, using the nature of nonsequential raytracing algorithm.

As transmissivity decreased to a minimum at high sun incidence angles, then started to increase in systems with no insertion and vertical insertion thus suggesting an increase in the multiple reflections at the reflective aluminium surfaces in the cavity modelled as separators, i.e. the given spacers are induced by high reflective surfaces, which increase in area relevant to the increase in the cavity.

Accordingly, the reflected rays from the spacers would hit the surface of the inserted element at normal or near to normal angles, which would consequently exceed the total maximum reflection angle of the element; *see glossary for definition.* This would lead to an increased reflection on the transparent vertical element surface and a maximum decrease of overall transmissivity of the total system.

This would not be the case when relatively lower sun angles ensue, as the inclined element's insertion scenario would perform better in cutting down the (DB) transmissivity especially to that of a vertical setting.

This would also not be applicable with other incident components, i.e. those of the sky-diffuse and the albedo. They are more stable and would not change substantially with the change of cavity, which is understandable as they are assumed not to be angle dependant. However, such explanation would have to be backed by further work and investigation into the effect of spacers' materials and surfaces on the reflectivity, and the over all behaviour of the system.

Figure 6.11 shows results in percentage (%), of the (DB) transmissivity of the two other insertion scenarios compared to the suggested system's behaviour; i.e. comparing the (DB) transmissivity of a vertical element's insertion and that of a no insertion setting to the behaviour of an inclined element's insertion, taken for a band of cavity widths respectively.

Results show ascertained differences in transmissivity behaviour between the three systems, and that at low sun angles were minimal, e.g. 0.007% for relatively small cavity width band scenarios (0.0175-0.03m), while differences increased up to 3% for the vertical insertion and 9% for a no-element scenario, in favour of the suggested system using wider cavity modular widths.

For high sun angles, e.g. at noon, larger discrepancies in transmissivity results appeared between these two scenarios and the inclined insertion; it shows that the suggestion is a less performer than the other two scenarios especially using small cavity widths.

Those results indicates a stronger role for the inclined insertion setting in controlling the level of the transmitted direct incident component, compared to the behaviour of more conventional types of multiple glazing systems, especially at low sun angles and using relatively wider cavity widths. Results also show variable and fluctuating results for the "no insertion setting scenario" in controlling the (DB) transmissivity.

It should also be noted that such inhibiting effect might not be always favourable especially at lower sun angles and during the cold season where a steadier pattern of insolation transmissivity is needed to heat the inner spaces.

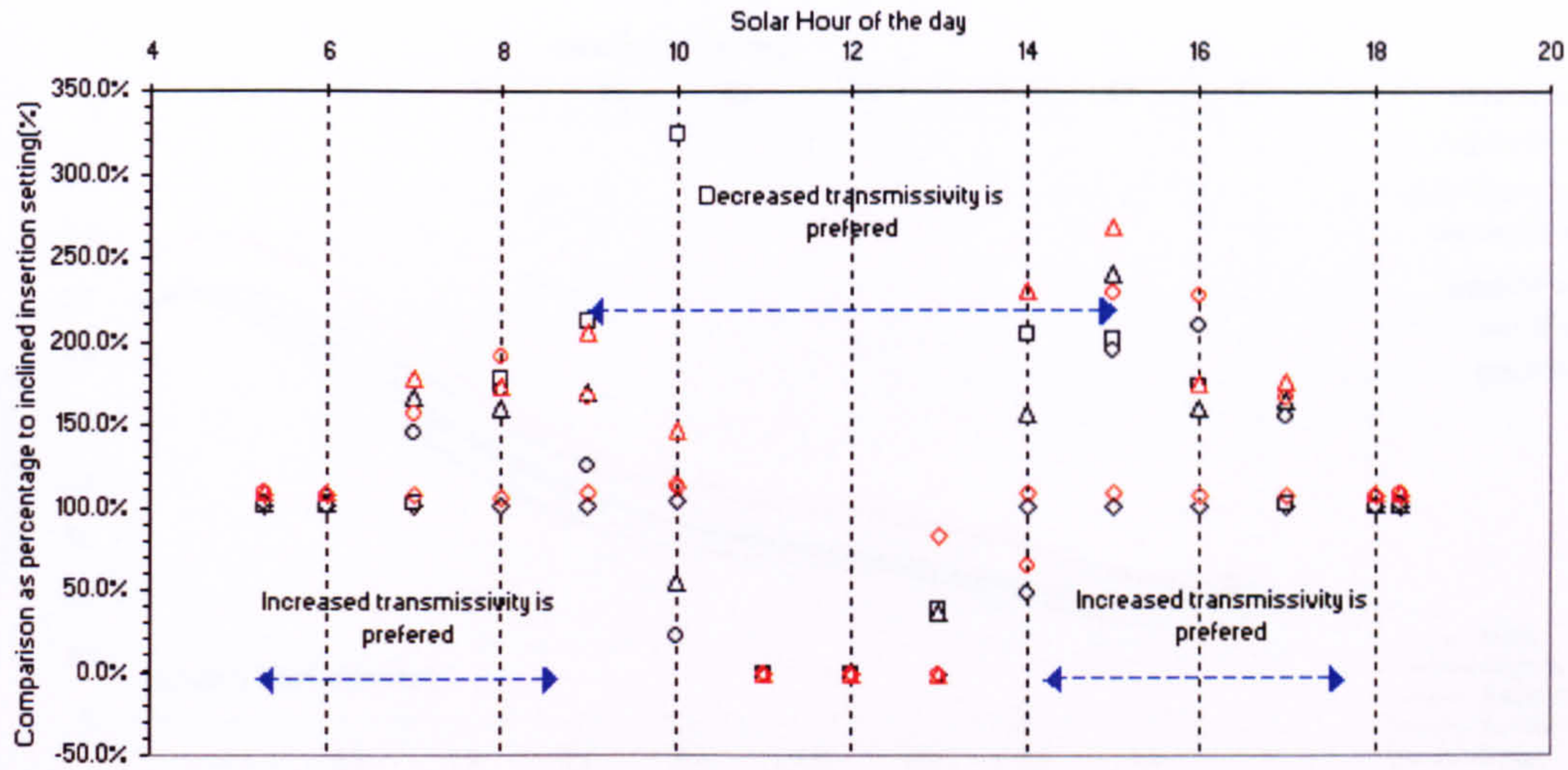

Scenario	Width bands			
Case of vertical to inclined insertion	◇ Angle 89-band	□ Angle 80-band	△ Angle 70-band	◇ Angle 60-band
Case of no element to inclined element	◇ Angle 89-band	□ Angle 80-band	△ Angle 70-band	◇ Angle 60-band

Figure 6.11 shows the variation of (DB) transmissivity comparisons (in %), using two scenarios (A, B)- for 14th August1996/Kuwait data. Comparisons are for:

A- A vertical-to-an inclined insertion setting.
B- No element-to-an inclined element setting.

6.2.3 Normalisation of transmissivity results

Consequently, a regression analysis was needed to show the relationship between the levels of insolation going through the proposed system and those of insertion angle of the element/ width of the cavity system, and with relevance to solar geometry.

A statistical approach was developed, which used the reported seasonal transmissivity data of the direct and diffused components of insolation for the participating countries. The process use was as follows:

i. Polynomial regressions were calculated for both of the direct and diffused components' transmissivity of the system, still accounting for seasonal changes for each of the enlisted countries and for a band of insertion angles (45-90°), i.e. relevant to a band of system's cavity widths (0.0175-1m); here still assuming a modular unit height for the system.

ii. Calculated regressions were then normalised by picking random data results from the graphs and adjusting the curves to the points, which would only return most accurate results, compared against the accumulated raytracing output data using the STDEV statistical method

Regressions of the fifth order were found to be the most representative of results; accordingly they were taken as base for the normalisation process.

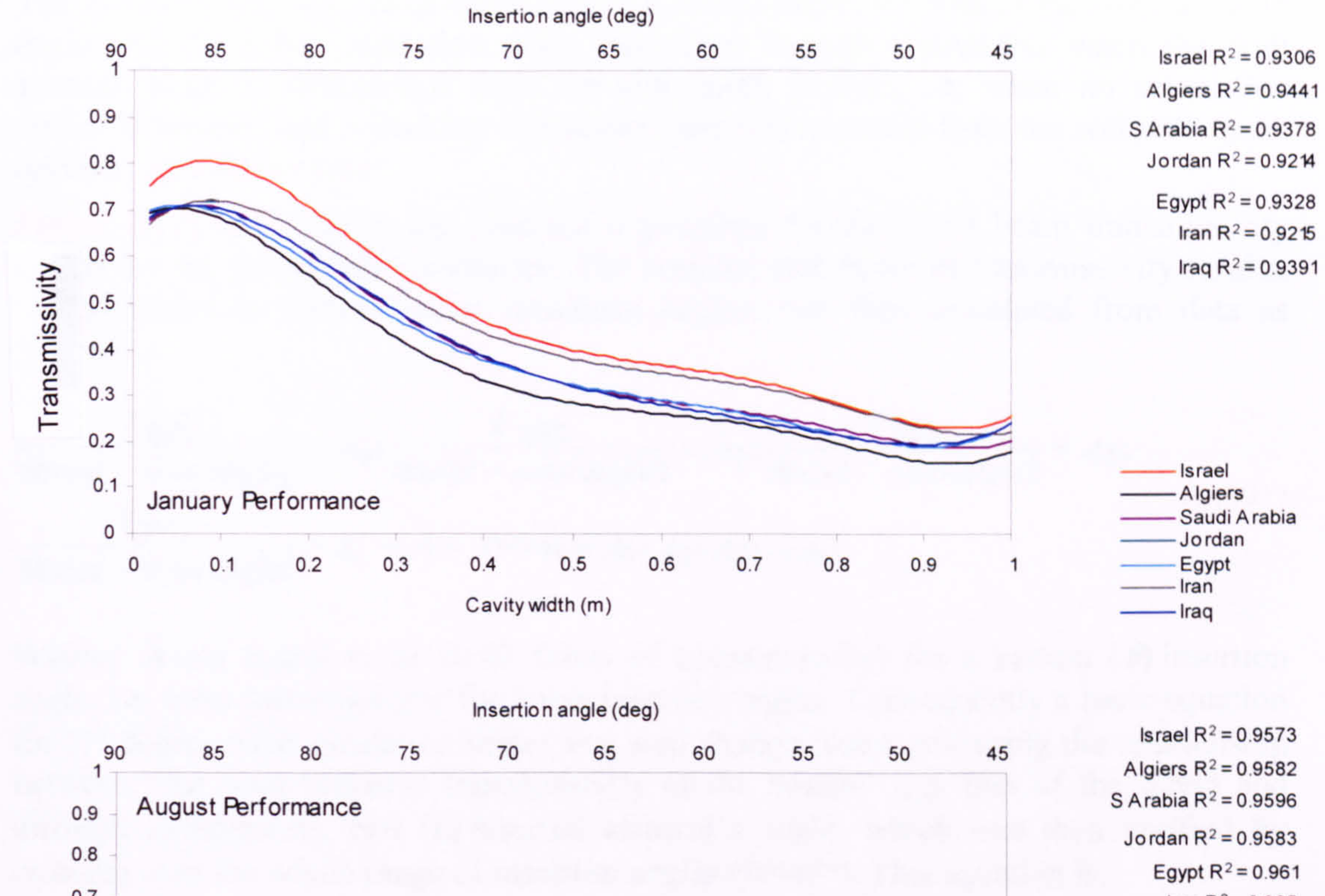

Figure 6.12 Seasonal (DB) transmissivity trend lines behaviour for the participating countries; Israel, Algiers, Saudi Arabia, Jordan, Egypt, Iran and Iraq:

A- During January (low sun angles).

B- During August (high sun angles).

iii. Normalised regressions were then compared to find the nominal step factor, i.e. weight factor, in transmissivity results associated with change in the solar incidence angles and the element's insertion angle, e.g. a regression where Y=change in transmissivity value corresponds to X=1° degree step change in the insertion element's angle.

iv. This process was repeated, for summer and winter data and, for both of the direct and diffused beam components, thus allowing the correlation to pick up any discrepancies in the frequency of the raytracing mapping, i.e. by comparing the normal trend of results using the direct beam and the diffused component scenarios data.

The assumed solar incidence angle here is a *profile angle*, for both of the solar azimuth angle and the solar inclination angle calculated through SMARTS2 when the wall azimuth angle is deactivated from the simulation process, i.e. when no orientation option is selected and a tracking sun device option is activated from the software menu options; *see chapter four*.

Figure 6.12(A&B) shows the finalised regressions for the direct beam transmissivity results for the participating countries. The nominal step factor of transmissivity results, i.e. compared to relevant solar incidence angles, was then calculated from data as follows:

$$\frac{T_{DB1}}{\theta incid-solarangle_1}=A_1;\frac{T_{DB2}}{\theta incid-solarangle2}=A_2;\frac{T_{DB3}}{\theta incid-solarangle3}=A_3;$$
$$\frac{T_{DBi}}{\theta incid-solarangle i}=A_i\rightarrow \bar{A}=Average(A_1;A_2;A_3;\dots A_i) \quad (6.001)$$

Where; $\bar{A}$ was found to be (0.03 times of transmissivity) for a certain (θ) insertion angle, i.e. more transmissivity for lower insertion angles. Consequently a basic equation for (1° degree solar incidence angle) as a step change factor governing the relationship between "the total radiative transmissivity of the system" e.g. that of the direct and diffused components, and (θ) inserted element's angle, which was then verified by crossing over the whole range of insertion angles (89-45°). This equation is:

$$\Delta\tau^{\theta incid-solarangle=1}=-1.6533(1/\tan\theta)^5+2.4667(1/\tan\theta)^4-0.474(1/\tan\theta)^3-$$
$$0.3378(1/\tan\theta)^2+0.0659(1/\tan\theta)+0.8234 \quad (6.002)$$

Where ($\Delta\tau$) is the step change in system's transmissivity and (θ) is the insertion element's angle for a ($\theta_{incid\text{-}solarangle}$)=1° deg solar incidence angle. Thus, the following equation were developed to present the correlation between the transmissivity and the system's inserted element's angle and relevant to the prevalent solar incidence angle, through splitting the annual solar geometry seasonal changes into summer and winter periods, i.e. similar to SMARTS2 weather files definition. For the summer and winter period respectively;

$$\bar{\tau}=\left|\begin{array}{l}[-1.6533(1/\tan\theta)^5+2.4667(1/\tan\theta)^4-0.474(1/\tan\theta)^3-\\ 0.3378(1/\tan\theta)^2+0.0659(1/\tan\theta)+0.8234\ ]/(0.03(\theta_{incid-solarangle}))\end{array}\right| \quad (6.003)$$

$$\bar{\tau}=\left|\begin{array}{l}(0.03(\theta_{incid-solarangle}))/[-1.6533(1/\tan\theta)^5+2.4667(1/\tan\theta)^4-0.474(1/\tan\theta)^3-\\ 0.3378(1/\tan\theta)^2+0.0659(1/\tan\theta)+0.8234\ ]\end{array}\right|$$

Where ($\bar{\tau}$) is the mean transmissivity value of the system, and (θ) is the inserted element angle, while ($\theta_{incid\text{-}solarangle}$) is the solar incidence angle relevant to the solar geometry of the specific site. The total insolation flux transferred across the system would be ($q_{in\text{-}solar}=q_{out\text{-}solar}\times\bar{\tau}$).

This value would be used later; *see 6.3.3*. (Obtained equations were then verified by using a random input of insertion angles to predict the (DB) transmissivity then to compare them with obtained data from the software results. Confidence coefficients; *see glossary for definition*, were shown to be between 91%-100%.

6.3 CFD RESULTS

Results of the rates of solar energy absorption obtained from the raytracing simulations of the Kuwait data were used as input to the CFD simulation platform, applying the imported 2D unstructured meshed models developed in GAMBIT. As previously indicated, the aims for the CFD simulations were to assess the effects of thermal convection and conduction modes arising from the cavities formed by the inserted element on the total rates of heat transfer across the glazing system. An additional objective was to find an overall U-value for the proposed glazing system from the collective heat transfer coefficients of the surface elements' of the module (i.e. spanning from the outer glazing surface of the system to the inner glazing surface respectively), and adding them to the heat transfer coefficient appertaining to the radiative heat transfer contribution.

As explained earlier, *see chapters four and five,* by using a 2D calculation environment with a linear heat transfer simulation, the surface areas of the model were not included in calculations.

Heat transfer effects in the frames of the glazing were also excluded, as these were assumed to be fixed parameters to simplify calculations. All tests were conducted for parameters of cavities widths between (0.02-0.12m), and accounting for summer/winter seasonal changes, using Kuwait weather files 1996;

Consequently, only heat transfer coefficients arising at the glazing areas, the insertion setting and the spacers were progressed to the final counter of collective heat transfer after adding the radiative mode, from the raytracing. The following derivation from (ISO/DIN 15099 2003) was adopted to account for the U-value of the system; *see also equations 4.002,3 and 4.004*.

$$U_{total} = \frac{1}{\frac{1}{h_t} + \frac{1}{h_{int}} + \frac{1}{h_{ext}}} \qquad (6.004)$$

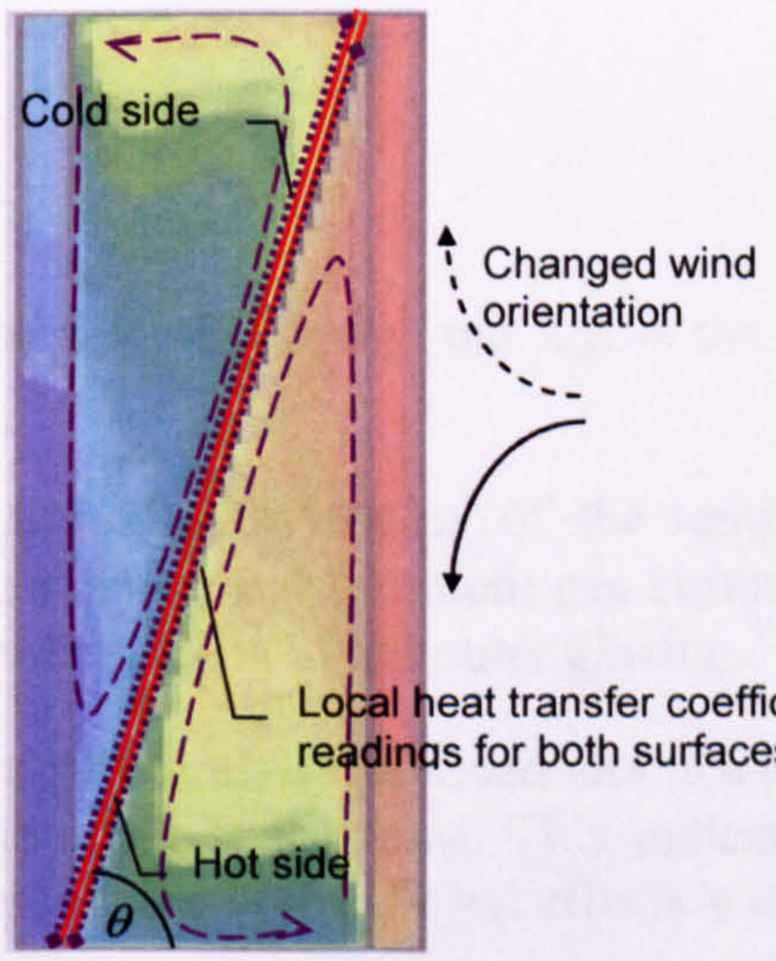

Figure 6.13 shows schematic zonal conditions assumed for the calculation.

Where U is the thermal transmittance (W/m^2K), h_{ext} and h_{int} are the external and internal transfer coefficients (W/m^2K) respectively; *see chapter four*; and h_t is the conductance of multiple glazing units (W/m^2K) and is taken from:

$$\frac{1}{h_t} = \sum_{i=1}^{n} \frac{1}{h_i} + \sum_{i=1}^{n} \frac{d}{k} \qquad (6.005)$$

Where h_i is the heat transfer coefficient for the i^{th} cavity space calculated from:

$$h_i = h_c + h_r \qquad (6.006)$$

Here (h_c) is the convectional heat transfer coefficient and (h_r) is the radiative heat transfer, which was calculated from the *longwave* radiative flux (q_i) on each element's surface (i) from the raytracing results *or*:

$$\varepsilon q_i = \varepsilon \sigma T_i^4 \qquad (6.007)$$

Where (ε) is the emissivity of the surface and (T_i) is surface temperature; for the first surface $T_i = T_{sky}$, which is the sky temperature in Kelvin and is equal to:

$$T_{sky} = T_{out} - 6 \qquad (6.008)$$

(T_{out}) is the outside temperature taken empirically or from available weather files. As a result (h_r) would be then determined from *equation 6.007* and using *equation 4.046*, *see chapter four*. Alternatively, convectional heat transfer coefficients (h_c) values for each cavity zone were calculated using the Nusselt number averaged from the CFD boundary layers results; *see 5.4.2, and fig. 6.13.*

Averaged (h_c) for the cavities were calculated using *equation 6009* (ISO/DIN 15099 2003): Averaged obtained (**Nu**) for vertical cavities were remodelled from:

$\mathbf{Nu=1+(Nu_{vertical}-1)\sin\theta}$ for inclined cavities from 90-180°; (θ) here, is the inclination angle of the setting (degrees),

$$h_c = \mathbf{Nu}\ \frac{\lambda_{air}}{d_{mean}} \qquad (6.009)$$

Where (d_{mean}) is the mean width of the cavity and λ_{air} is the air thermal conductivity (W/m.k).

Images of CFD results and the contour images of the temperature distribution and gaseous cavity velocity showed active and turbulent gas currents in the cavity, i.e. that of the Y velocity near to the inner surface of the outer glazing.

Such convectional forces were substantially subdued and disappeared near the inclined elements' surface and near the upper spacer area. This indicates an important role for the inserted element in suppressing the convectional effects within the cavity; *see figure 6.14(A&B)*.

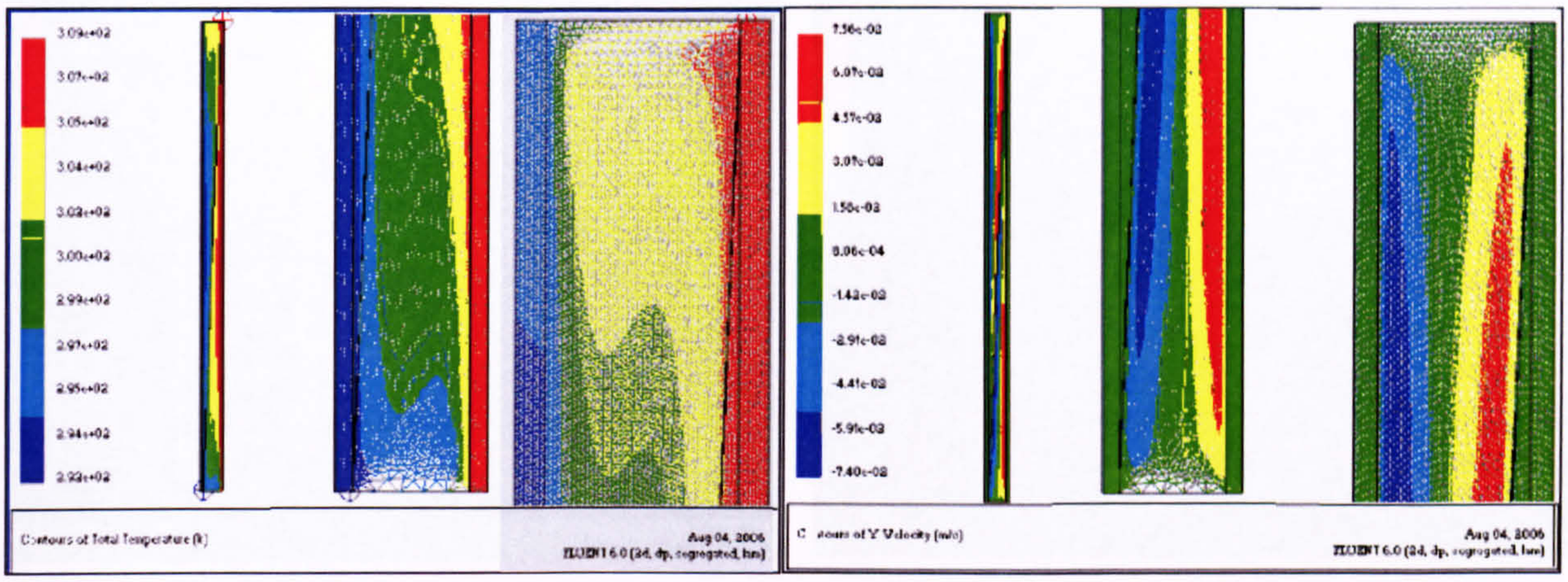

A 0.04m width-inclined insertionp; total temperature and Y velocity contours. (Summer)

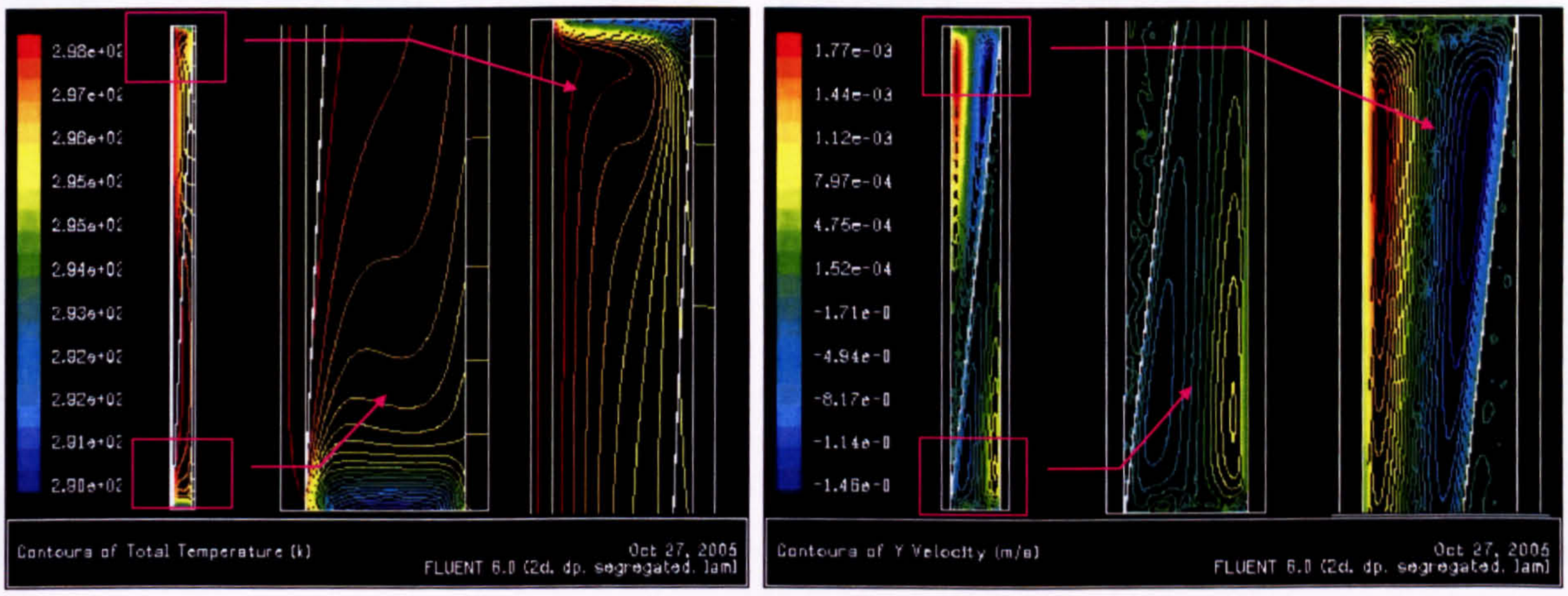

A- A 0.04, 0.1m width-inclined insertion; total temperature and Y velocity contours.(Winter).

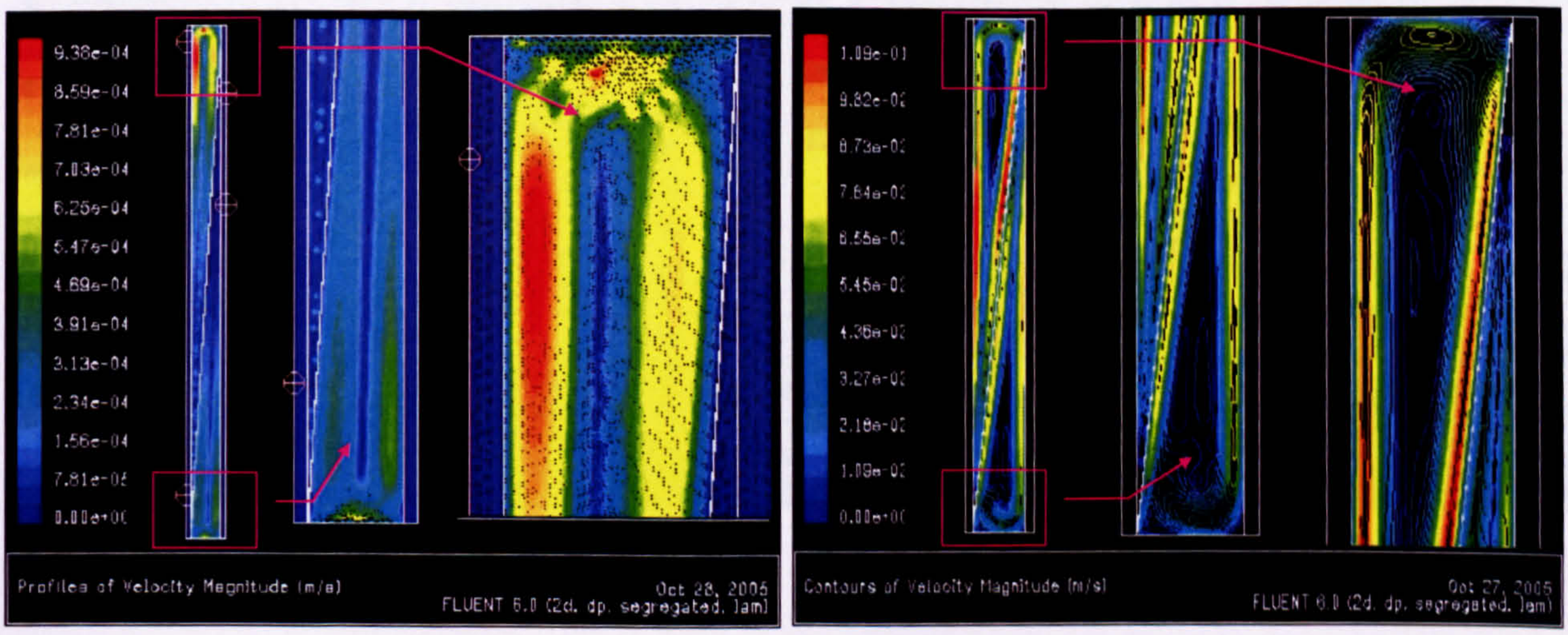

B- 0.06, 0.12m width-inclined insertion; total temperature and Y velocity contours.(Winter), NB: an increased level contours gradients were applied

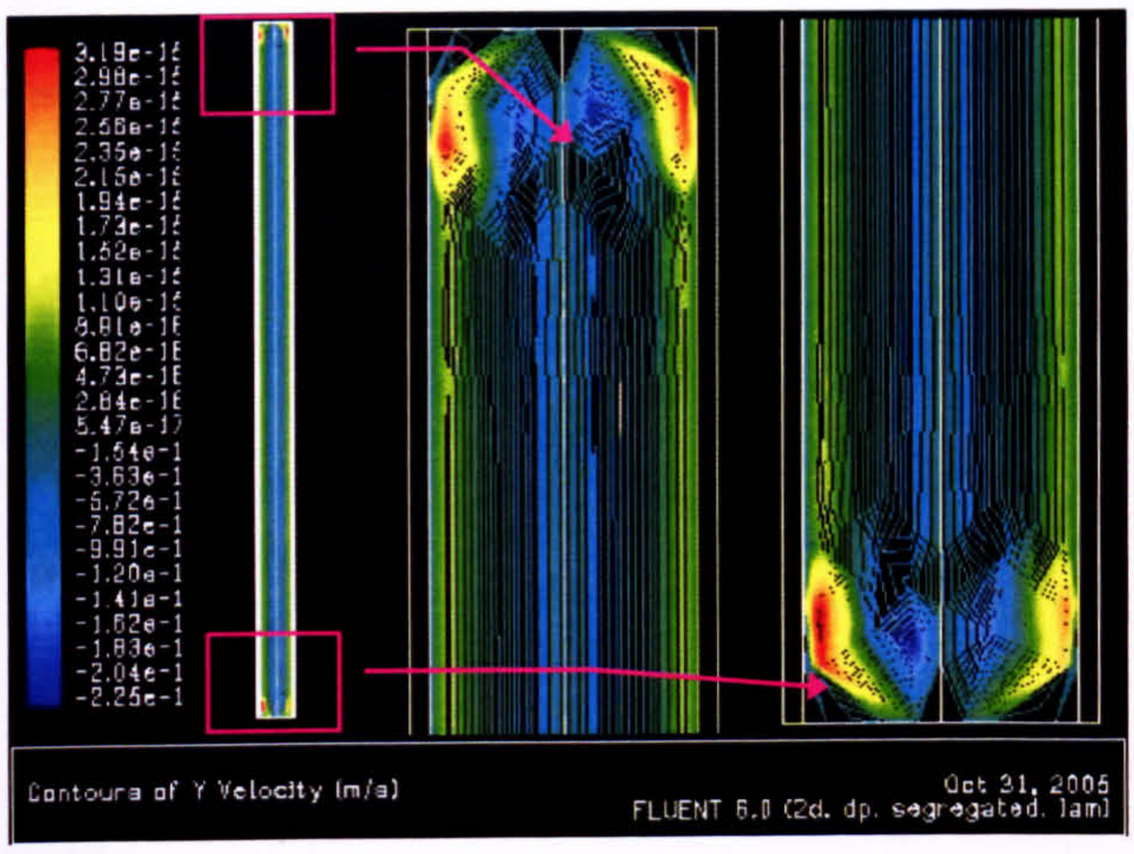

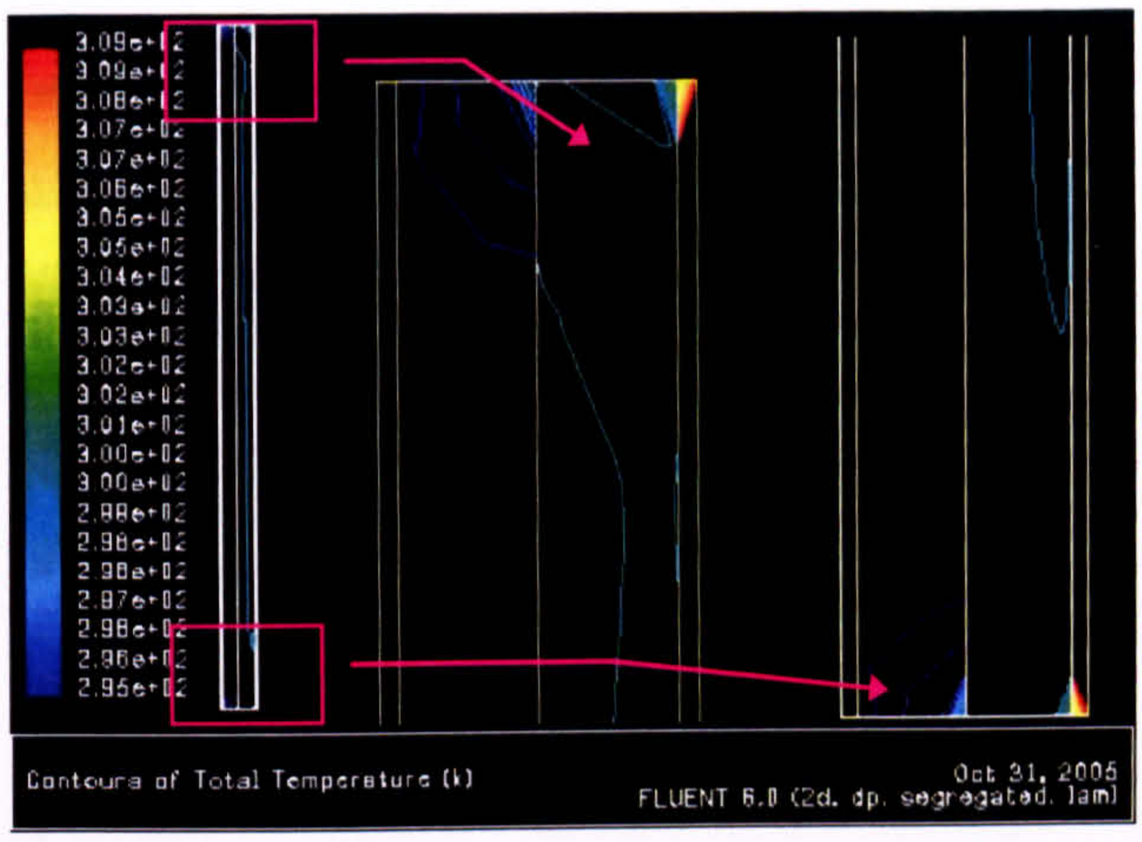

C- 0.05m width-vertical insertion for total temperature and Y velocity contours.(Winter).

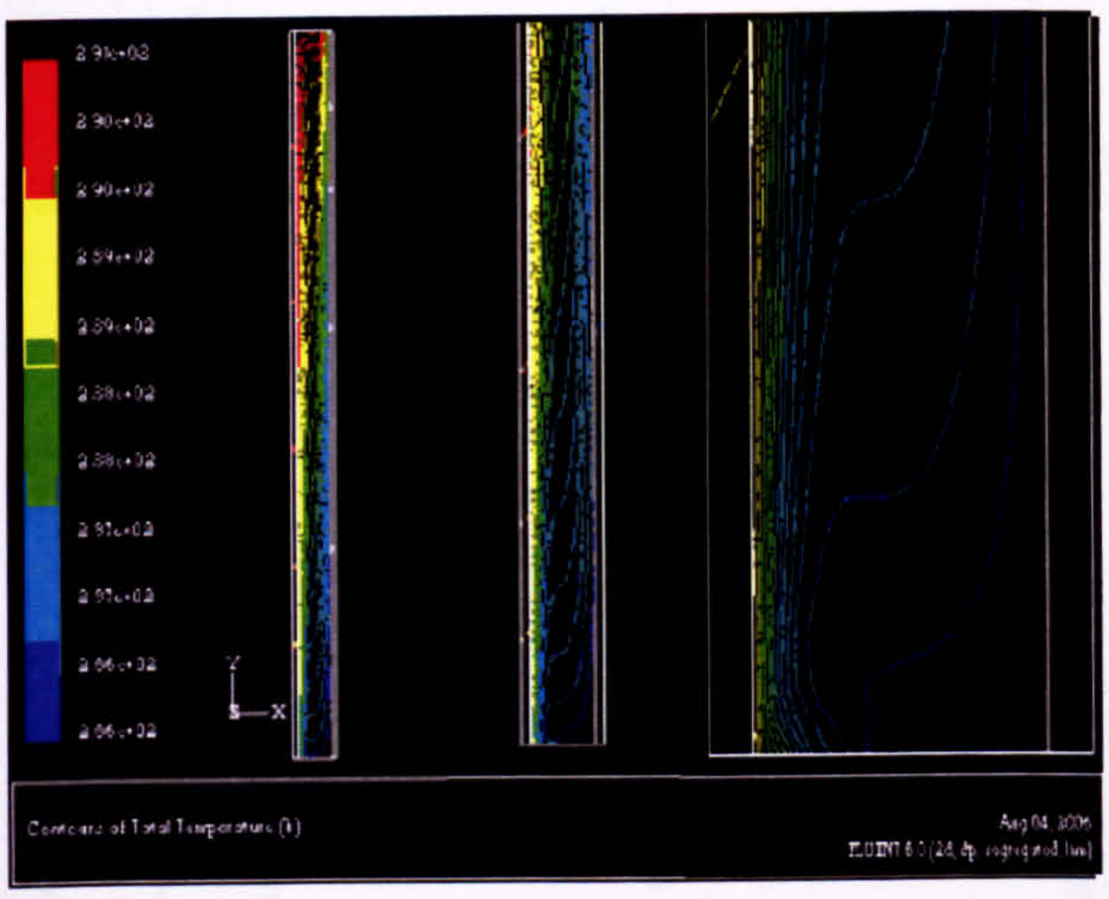

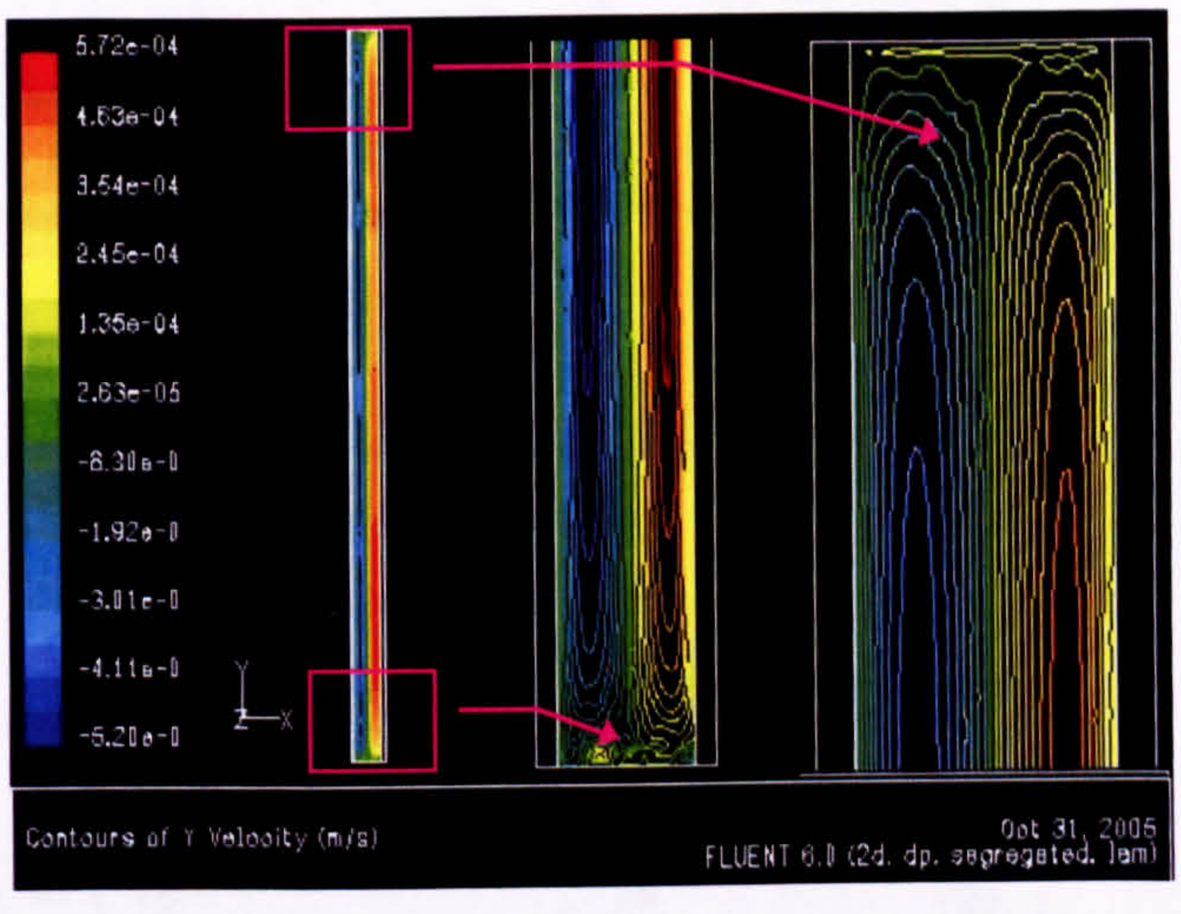

D- 0.05m width-no insertion; total wall temperature and Y velocity contours.(Winter).

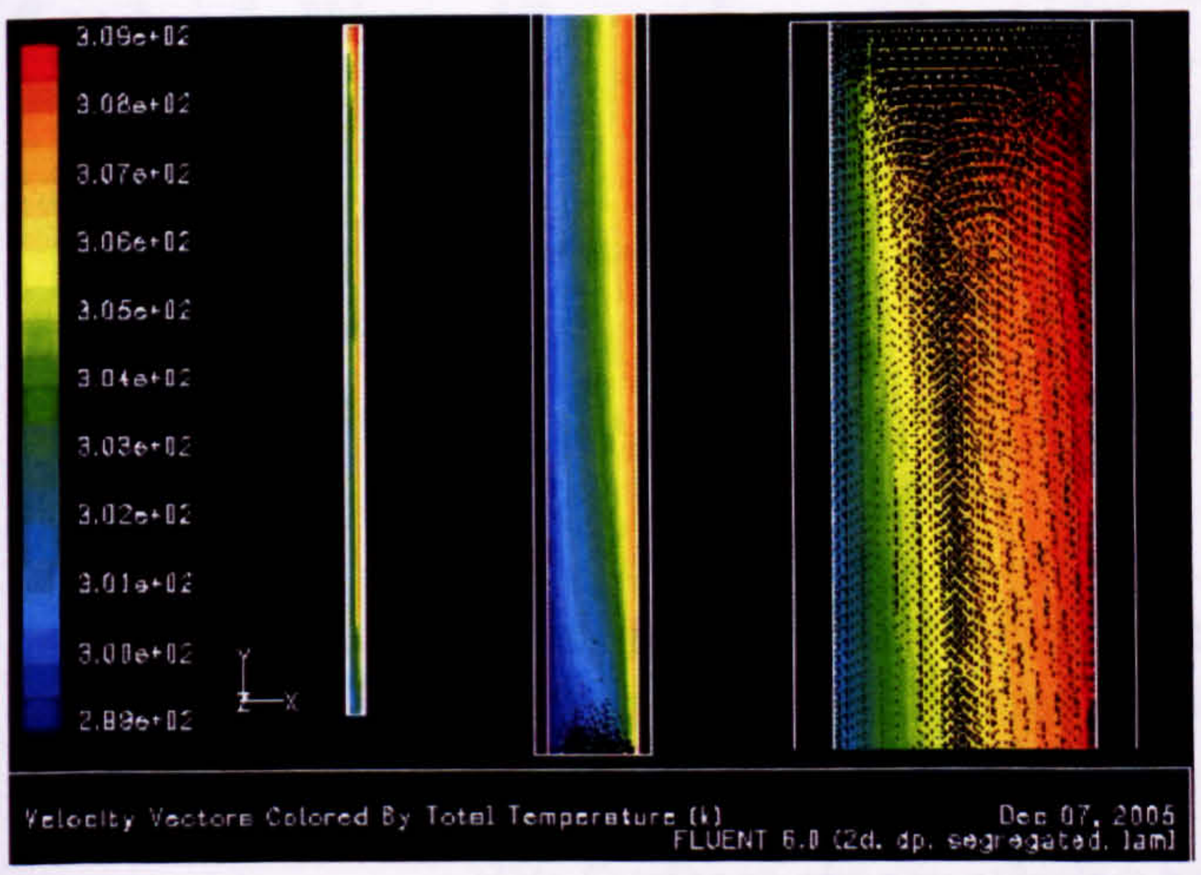

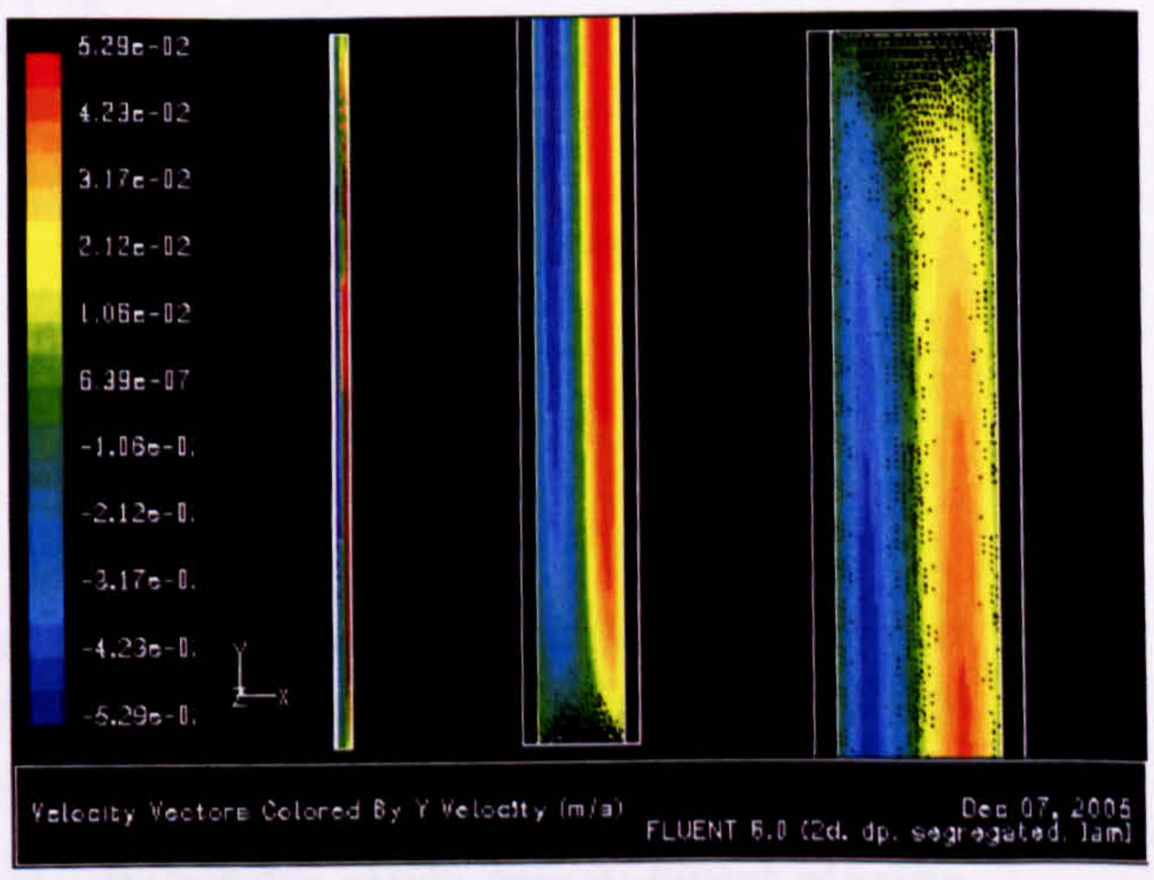

E- 0.02m width-no insertion; total temperature (contours) and Y velocity contours.(Summer).

Figure 6.14 shows several output results for different scenarios, with inclined insertion, vertical insertion and no inserted element.

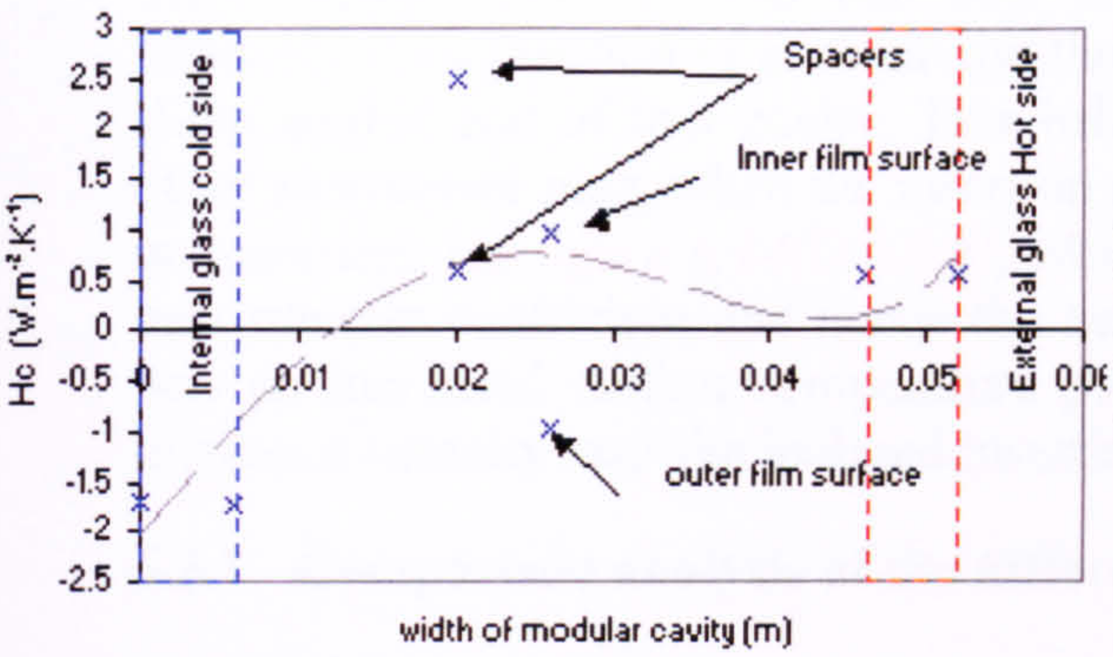

A- 0.04m

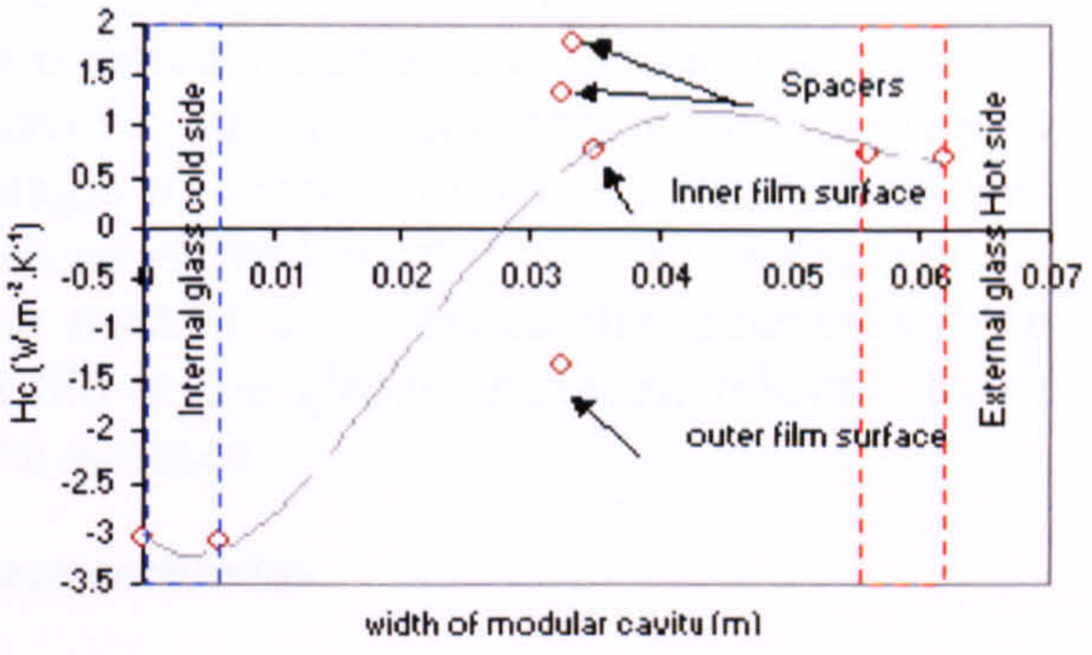

B-0.05m

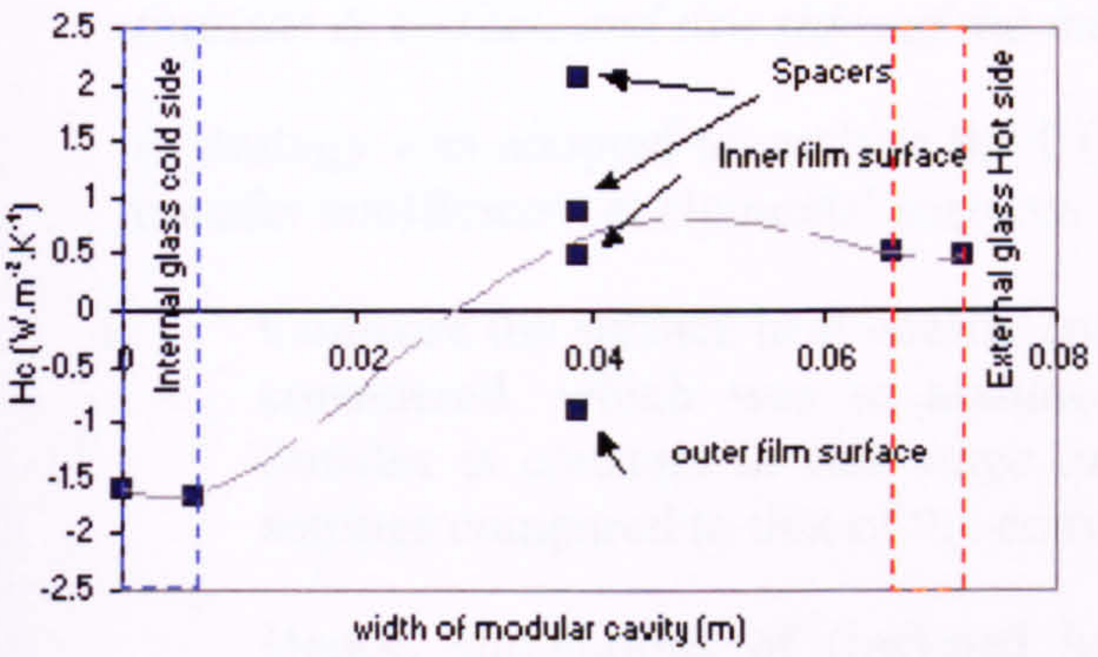

C-0.06m

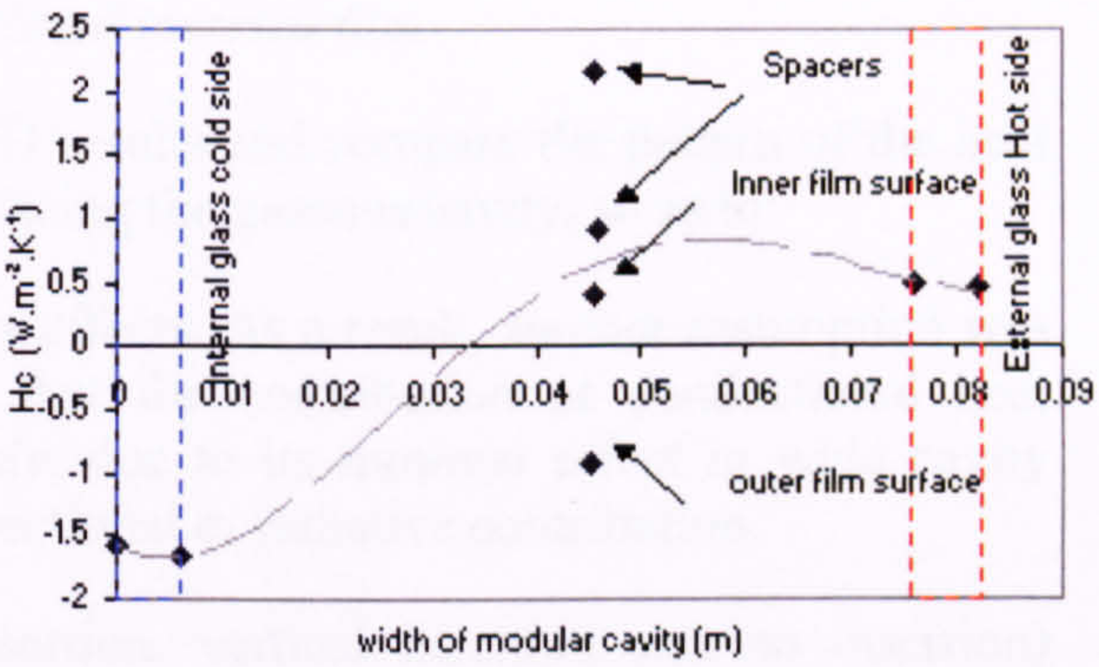

D-0.07m

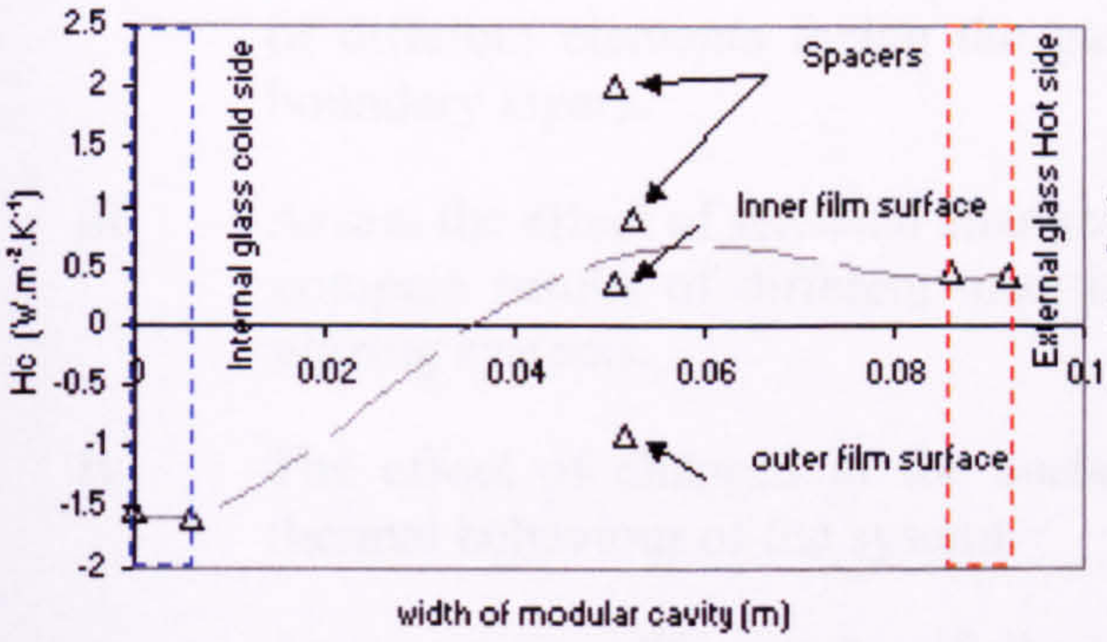

E-0.08m

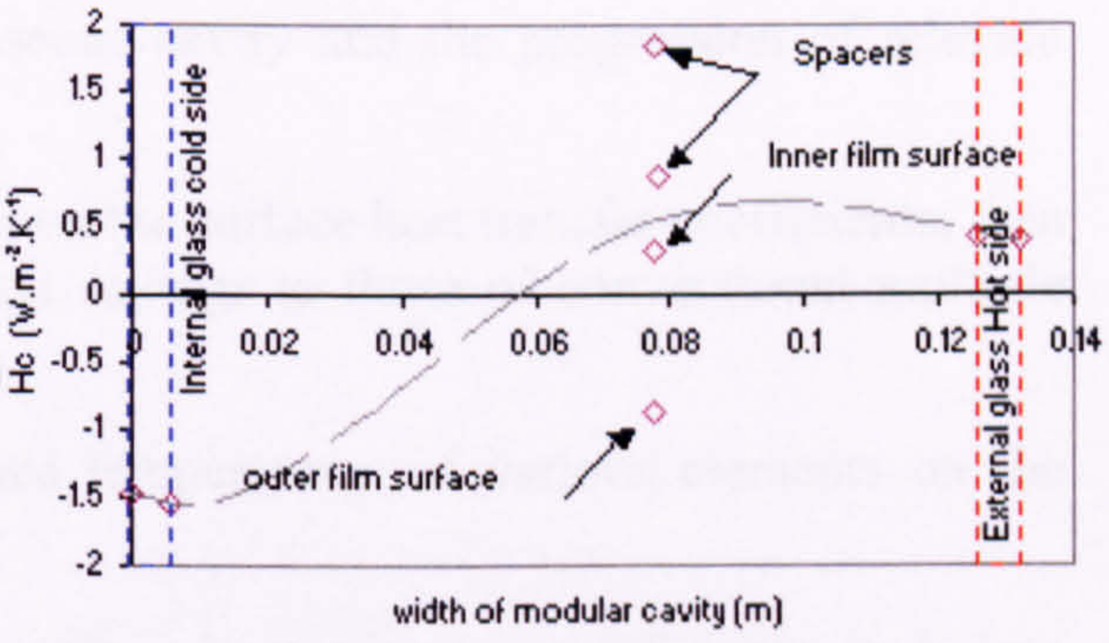

F-0.12m

Figure 6.15 shows mapping of the heat transfer coefficient of surfaces of an inclined element's insertion setting scenarios (A-F), between (0.04-0.12m) cavity widths scenarios, 3:00PM; 14th August, Kuwait,

NB: Surfaces shown relating to the "modular sets": are: external glazing (outside & inside), internal glazing (outside & inside), upper and lower separators, and the two sides of the inclined inserted film.

These images also showed that two parallel-coupled convectional currents in the relatively wider section of each cavity; those currents then tend to diminish towards the sharp angled end of that cavity. This behaviour was different from what is shown in other ascertained runs, when the insertion angle was normal or in cases where there was no insertion; *see figure 6.14(D,E&F)*, which could lead eventually to an increase in the heat transfer coefficient and hence the heat transfer. At wider cavities scenarios there was an increased surface temperature profile at the glazing surfaces, relevant to an increased velocity near the inclined insertion surfaces,

6.3.1 Comparison analysis of the different scenarios

Using CFD results, the convectional heat transfer coefficients were averaged for the surfaces of the following zones: *External glazing (outside & inside), internal glazing (outside & inside), and two sides of the inclined inserted film.*

A strategy was adopted to analyse the CFD results and compare the pattern of the heat transfer coefficients at elements' surfaces facing the gaseous cavity, so as to:

i. Compare the surface heat coefficients effects. As a result, another assumption was considered, which was to assume that the contribution of conductional heat transfer is constant *at this stage only*, due to its minimal effect in wide cavity settings compared to that of the convectional or radiative contribution.

   Hence, simulations of (inclined insertion, vertical insertion and no insertion) settings; were aimed at:

ii. Explore the transition and interaction of the convectional heat transfer coefficients of different elements facing the gaseous cavity and the progression of relevant boundary layers.

iii. Assess the effect of seasonal changes on the surface heat transfer coefficients; then compare results of different insertion settings to those of conventional multiple glazing systems.

iv. The effect of changes in the surface temperatures of various elements on the thermal behaviour of the system.

v. As presenting the results of the surface heat transfer coefficients took into consideration the direction of the convectional forces, i.e. an indicative +/- vector value was used in reference of the coefficient results and hot/cold surfaces; yet not assuming this presentation in consequent values calculation; *see Fluent 6 manual.*

Figure 6.15 shows heat transfer coefficients for the elements affecting the convective heat transfer in cavities with an inclined insertion system, of a 14th August/ Kuwait summer scenario.

Results show the behaviour of several scenarios of the suggestion cavities widths.

They showed that a considerable variation in heat transfer coefficients at relatively small cavities' widths would stabilise when those widths are increased, leading to relatively steady-value heat transfer coefficient.

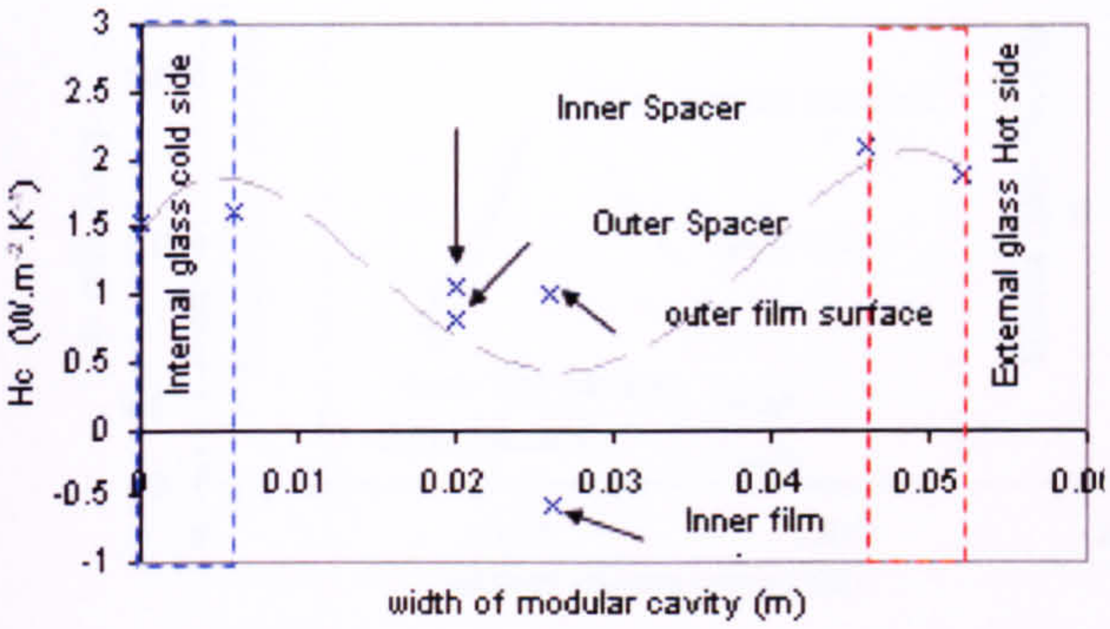

A- 0.04m

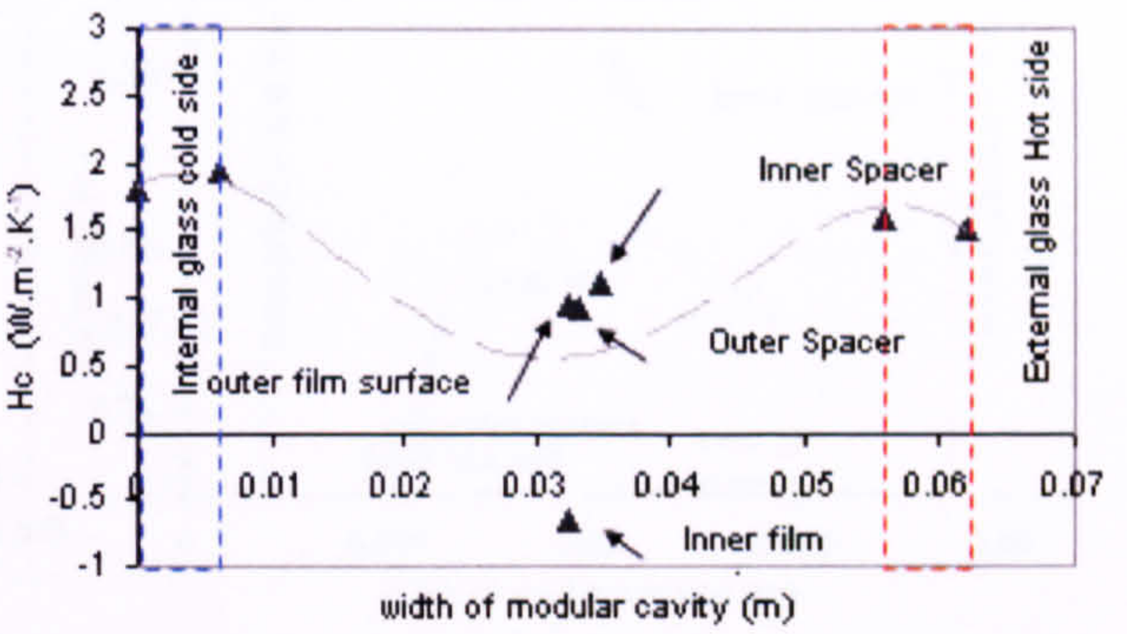

B-0.05m

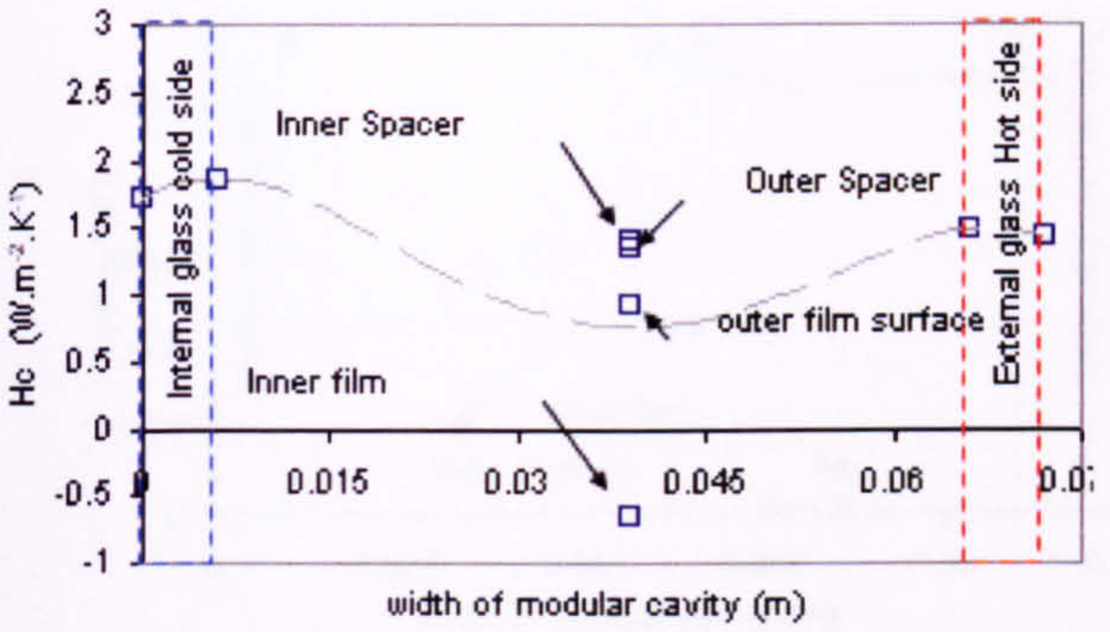

C-0.06m

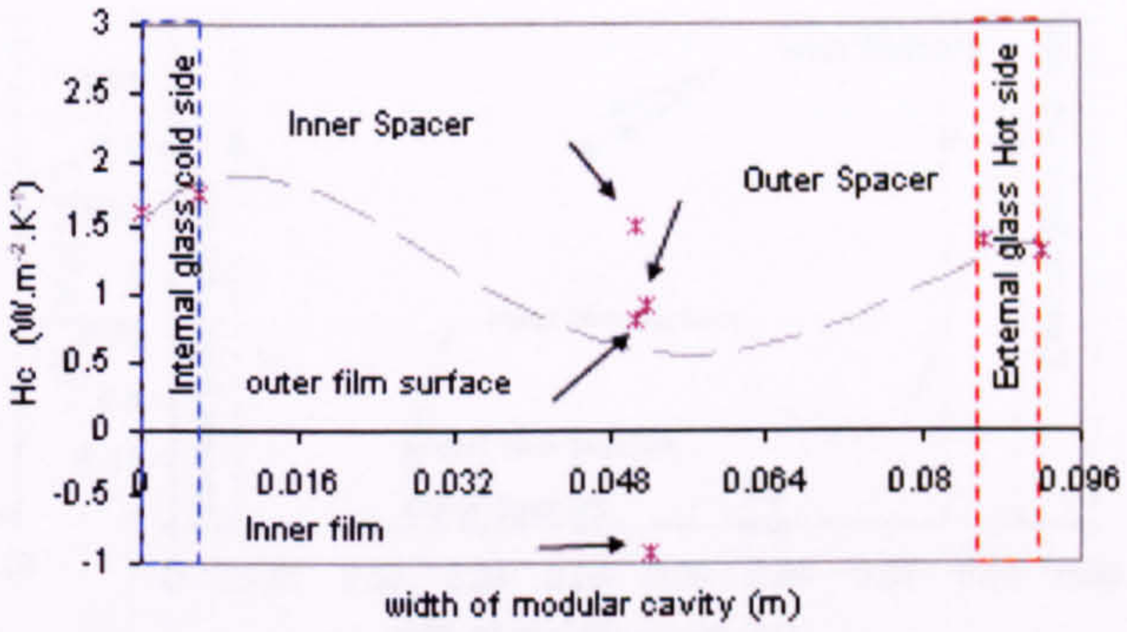

D-0.08m

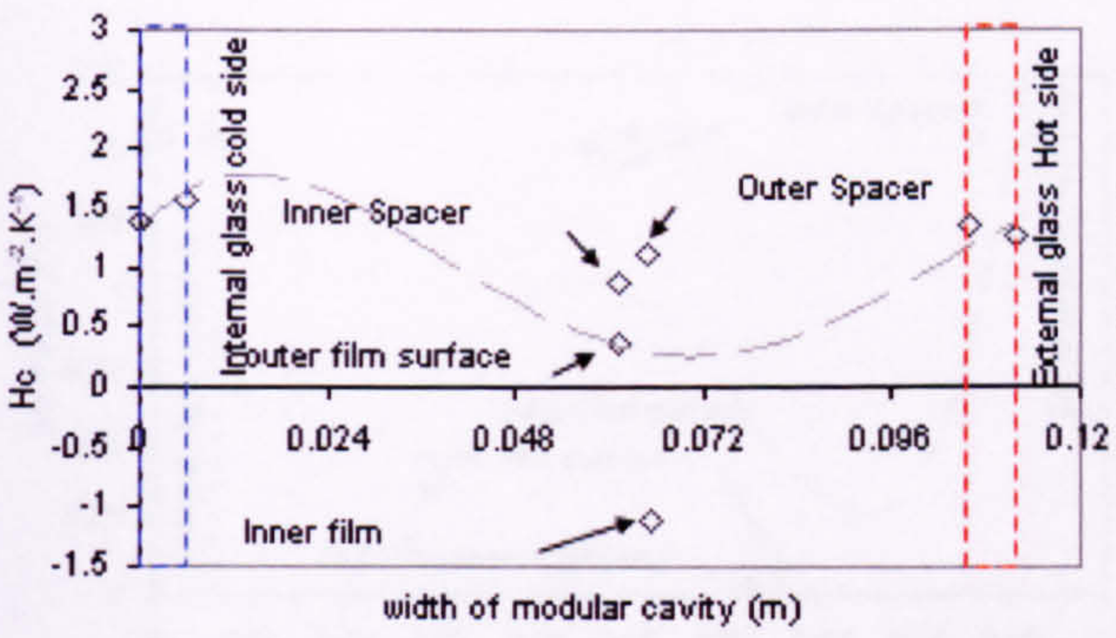

E-0.10m

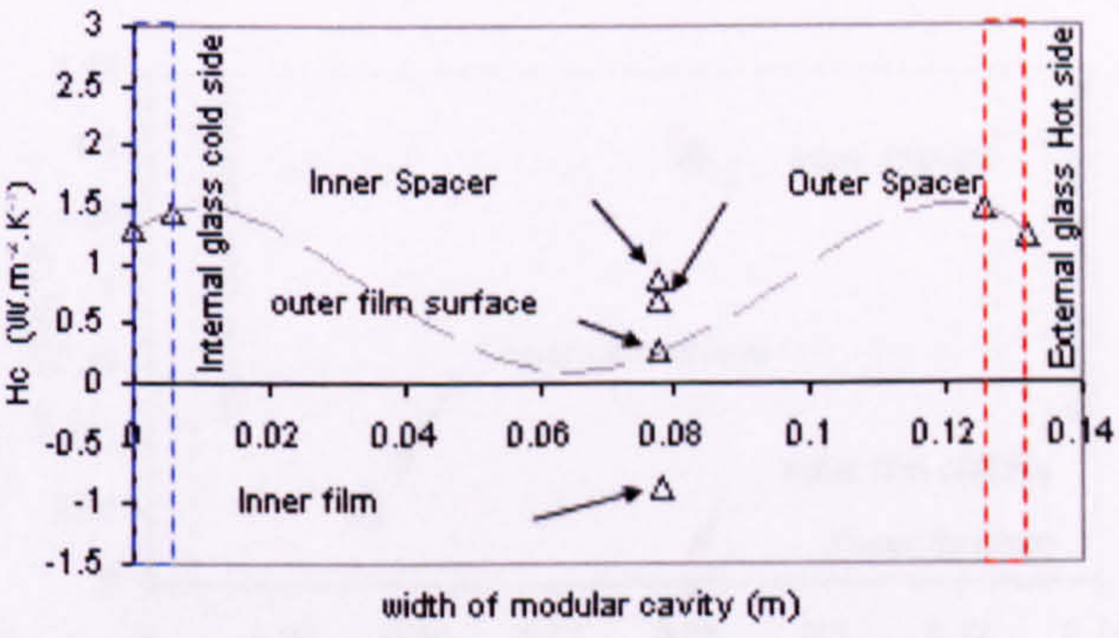

F-0.12

Figure 6.16 shows mapping of the heat transfer coefficient of surfaces of an inclined element's insertion setting scenarios (A-F) between (0.04-0.12m) cavity widths scenarios, 3:00PM; 14th January, Kuwait:

NB, red lines refer to the position of the external glazing h_c for each of the investigated cavity width of the modular sets.

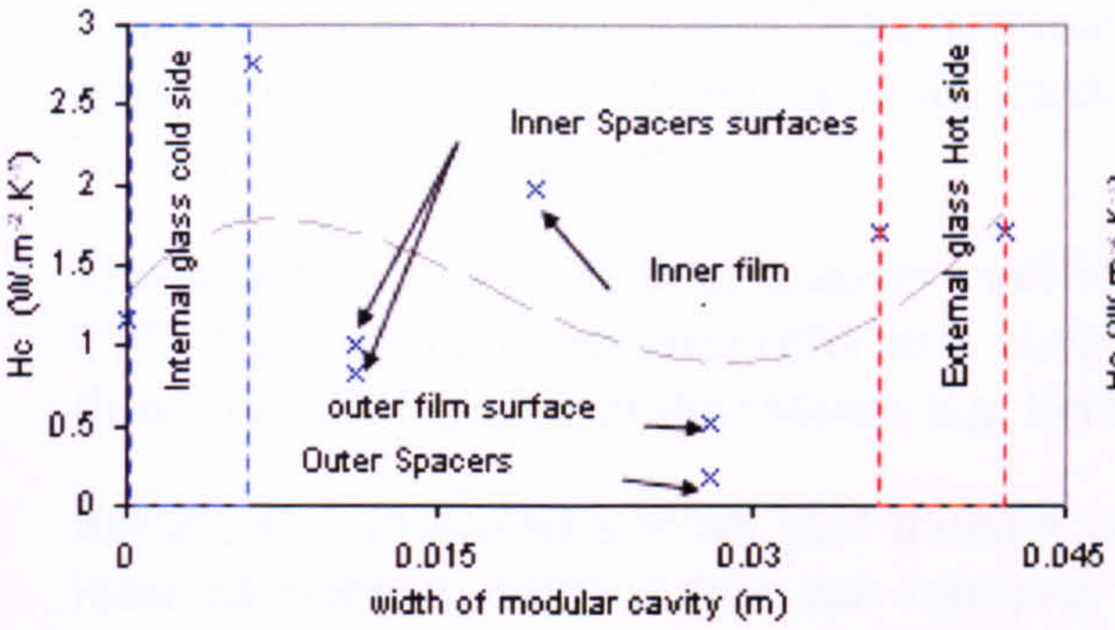

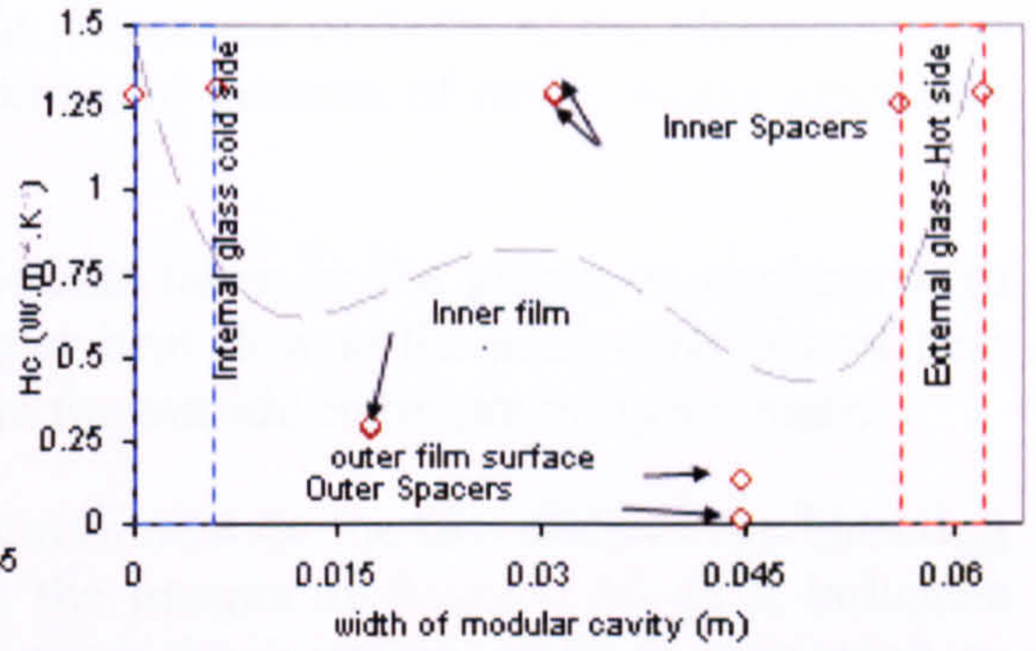

A- 0.03m

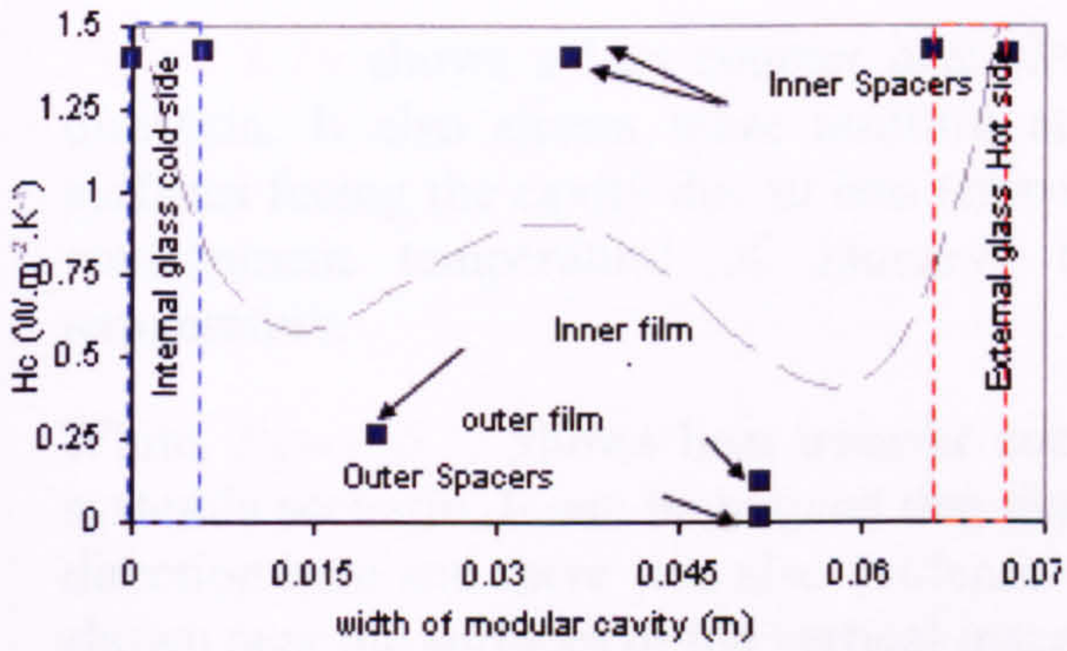

B- 0.05m

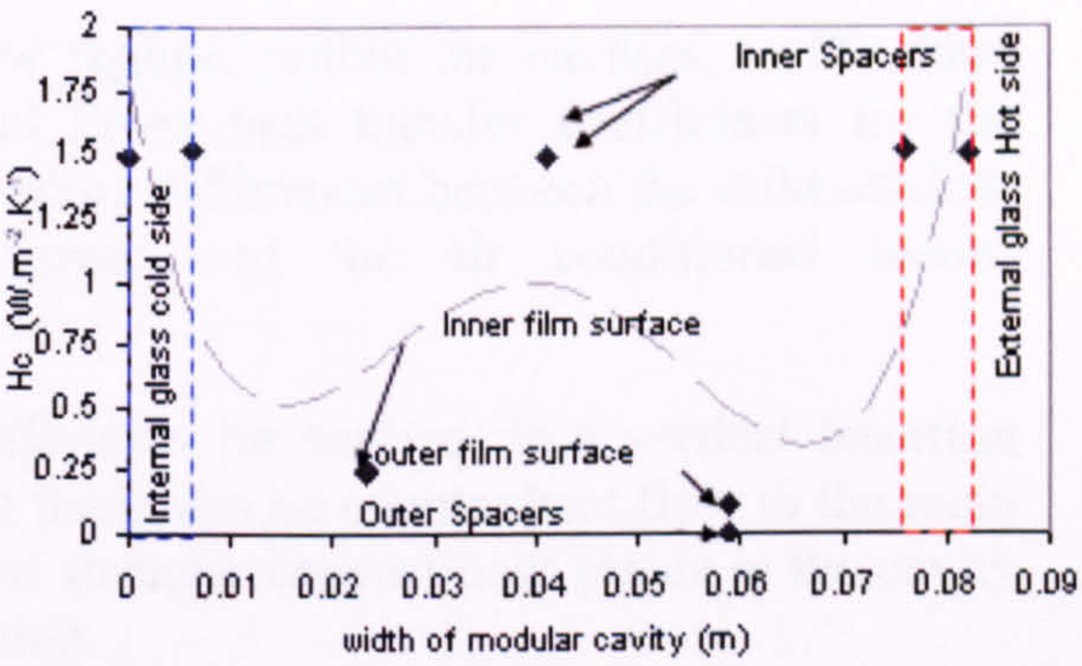

C-0.06m

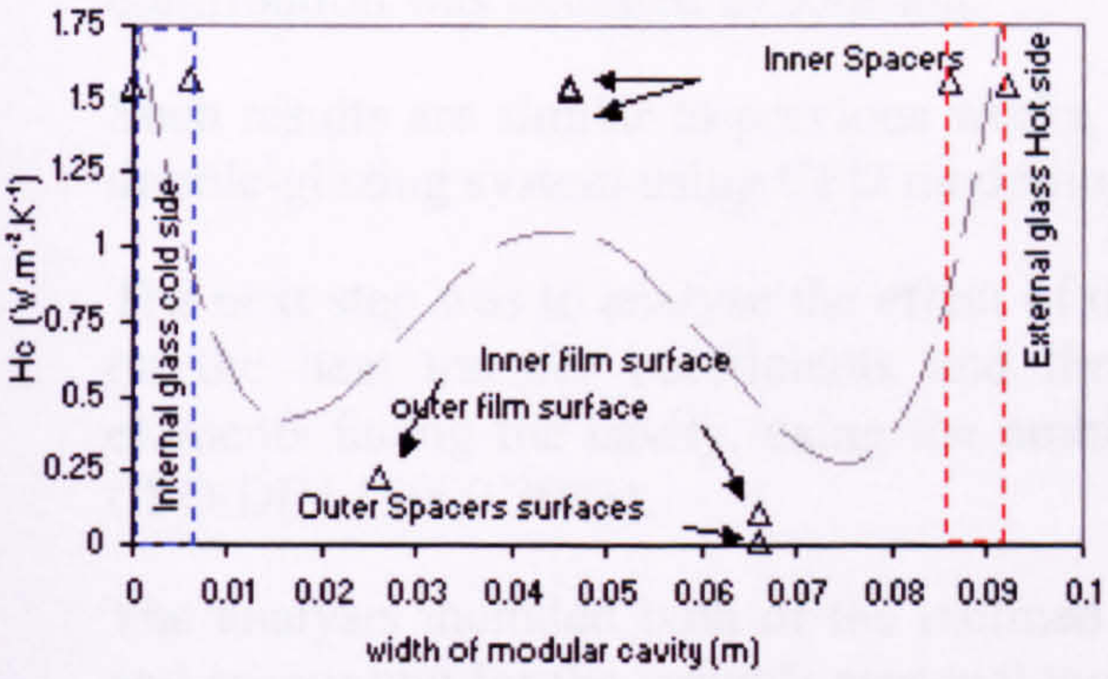

D-0.07m

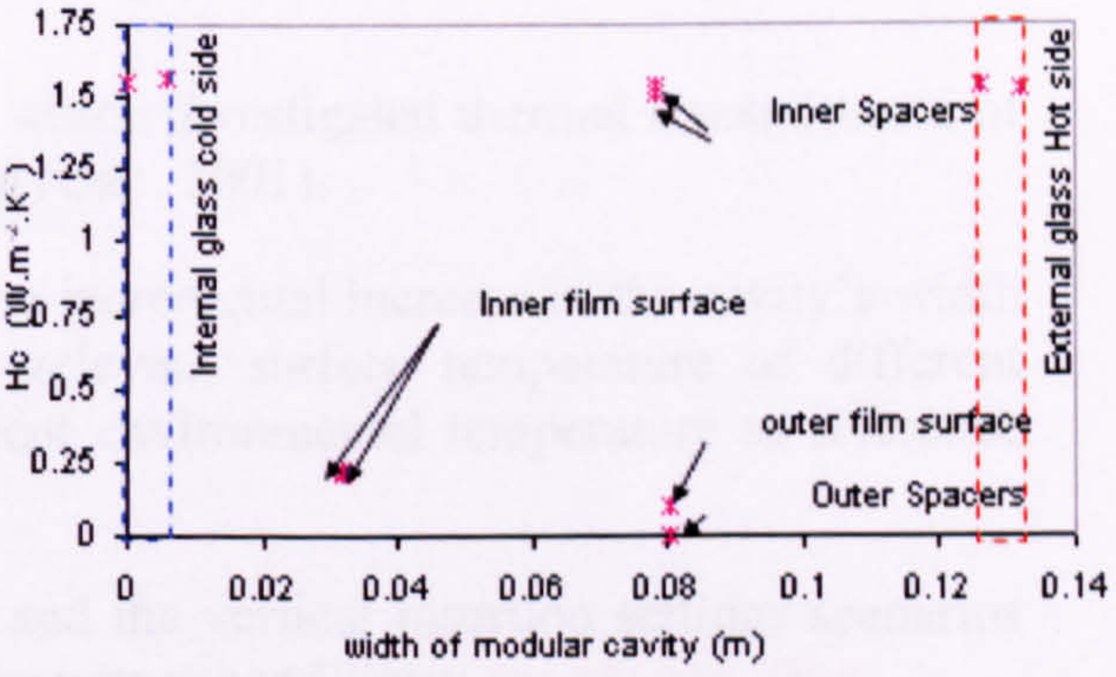

E- 0.08m

F- 0.12m

Figure 6.17 shows mapping of the heat transfer coefficient surfaces of a vertical element's insertion setting scenarios (A-F), between (0.03-0.12m) cavity widths scenarios, 3:00PM; 14th August, Kuwait.

Comparison of the output also indicated that a decrease of 3-7% of the elements' heat transfer coefficients is evident with the incremental increase of cavity width especially in wide cavity's widths scenarios.

The negative values of heat transfer coefficients taken in the graph, as explained, (a CFD presentation of results) refer to a counter heat flow to the main direction of heat flow from the hot side of the system, e.g. here the outside environment in summer.

Results also indicated a small heat transfer coefficient on the two sides of the bisecting inserted element. Such output can interpret the images of *figure 6.14*, as it indicates slower convectional heat transfer currents near the insertion surfaces compared to increasing convectional currents near the spacers with the increase of the cavity width.

Yet as the role of the conduction decreases respectively; the overall effect is semi stable.

Figure 6.16 shows a less counter heat flow regime, within the cavities, to the main direction. It also shows more uniform and lower heat transfer coefficients for the surfaces facing the cavity due to less temperature differences between the mild outdoor environment temperature of January/ Kuwait and the air conditioned indoor temperature.

While, *figure 6.17* shows heat transfer coefficients for surfaces in a vertical insertion system's scenario. It can be noticed that that there was no counter heat flow to the main direction here and there was also evidence of stronger convectional forces in the cavity shown near the surfaces of the vertical insertion.

Alternatively when simulating a system without an inserted element, it was found that the effect of increasing the cavity's width up to +0.05m, on the heat transfer coefficients would be minimal within temperature difference of (10-15K), if the conduction contribution was assumed as constant.

Such results are similar to previous works, which investigated thermal transmittance of double-glazing system using CFD modelling (Gan. 2001).

The next step was to analyse the effect of the incremental increase in the cavity's width on the heat transfer coefficients and the relevant surface temperature of different elements facing the cavity, using the ambient environmental temperature as reference (ISO/DIN 15099 2003).

The analysis included both of the inclined and the vertical insertion settings scenarios and accounting for the variable seasonal temperature conditions; *see chapter four*.

Figures 6.18(A&B) & 6.19 show that generally the heat transfer coefficients for all the surfaces investigated dropped to a steady and semi constant value after the width of the cavity increased beyond a certain point.

Results in *figure 6.19* also shows that ascertained heat transfer coefficient at the surface of a vertical element's insertion returned higher values than those at the surface of an inclined insertion for the same range of temperatures differences (~13K in Kuwait/ summer conditions).

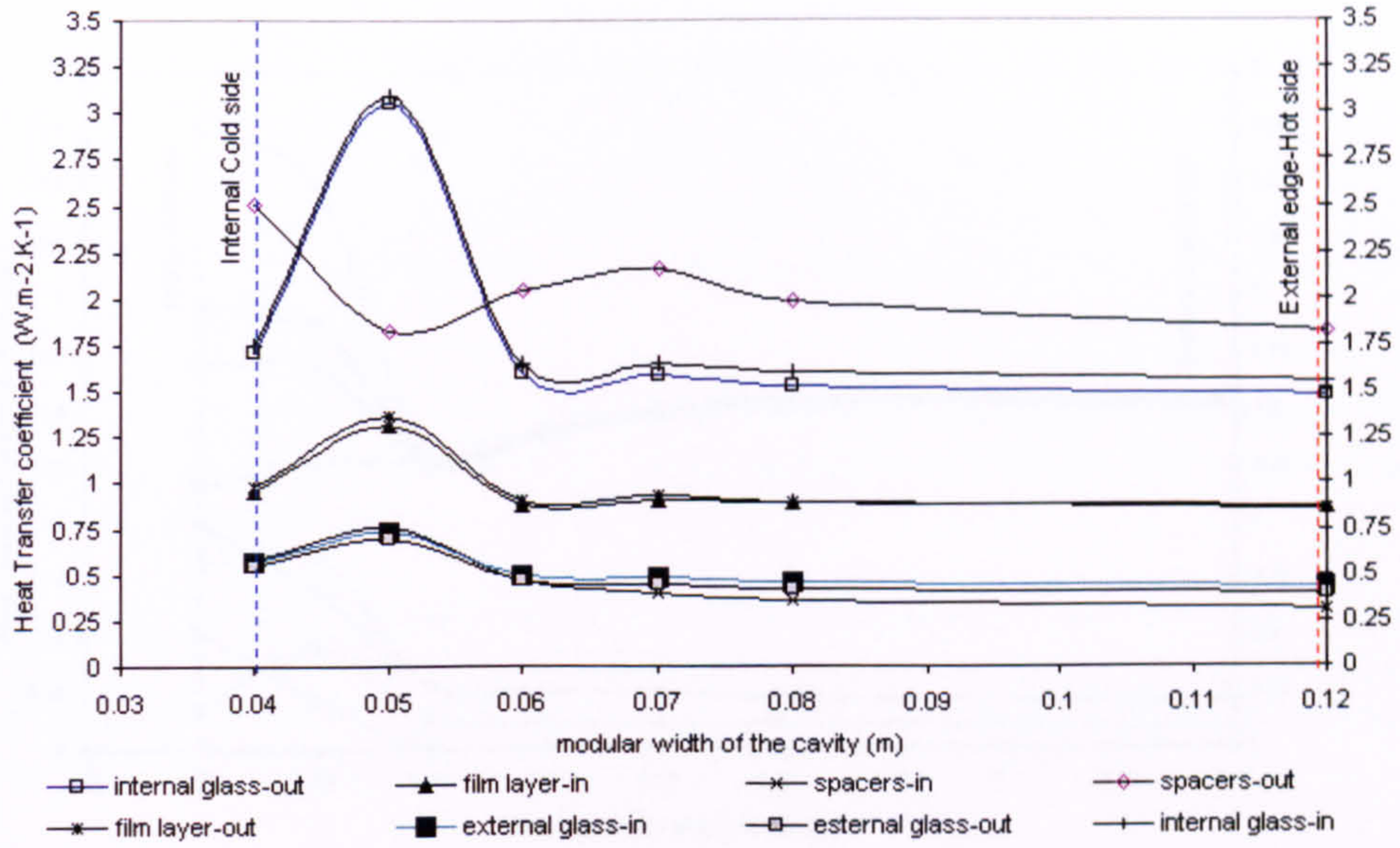

A- Summer conditions (temperature difference 13K).

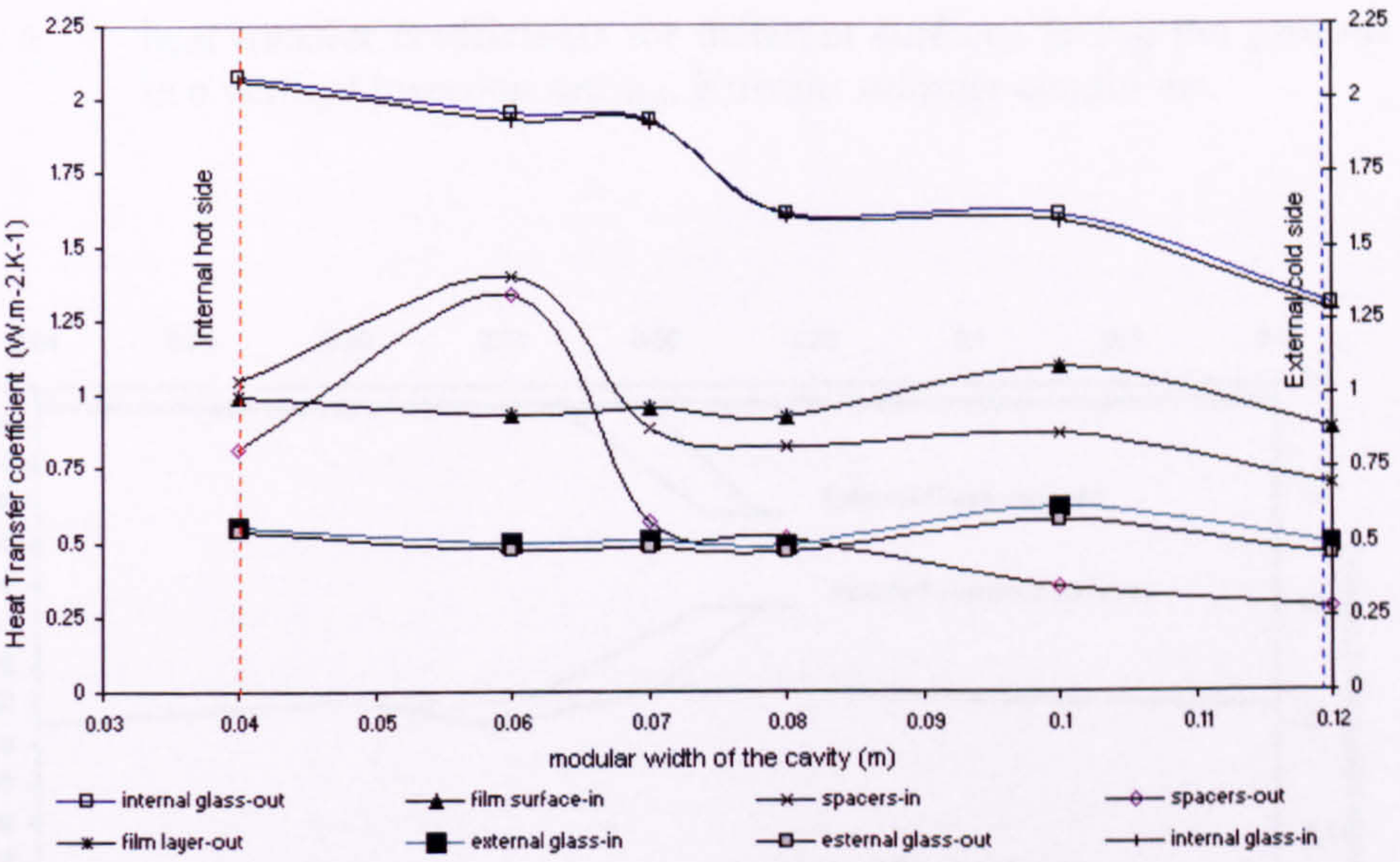

B- Winter conditions (temperature difference 5K)

Figure 6.18 heat transfer coefficients for different surfaces facing the gaseous cavity in an inclined insertion setting, Kuwait/ summer and winter conditions

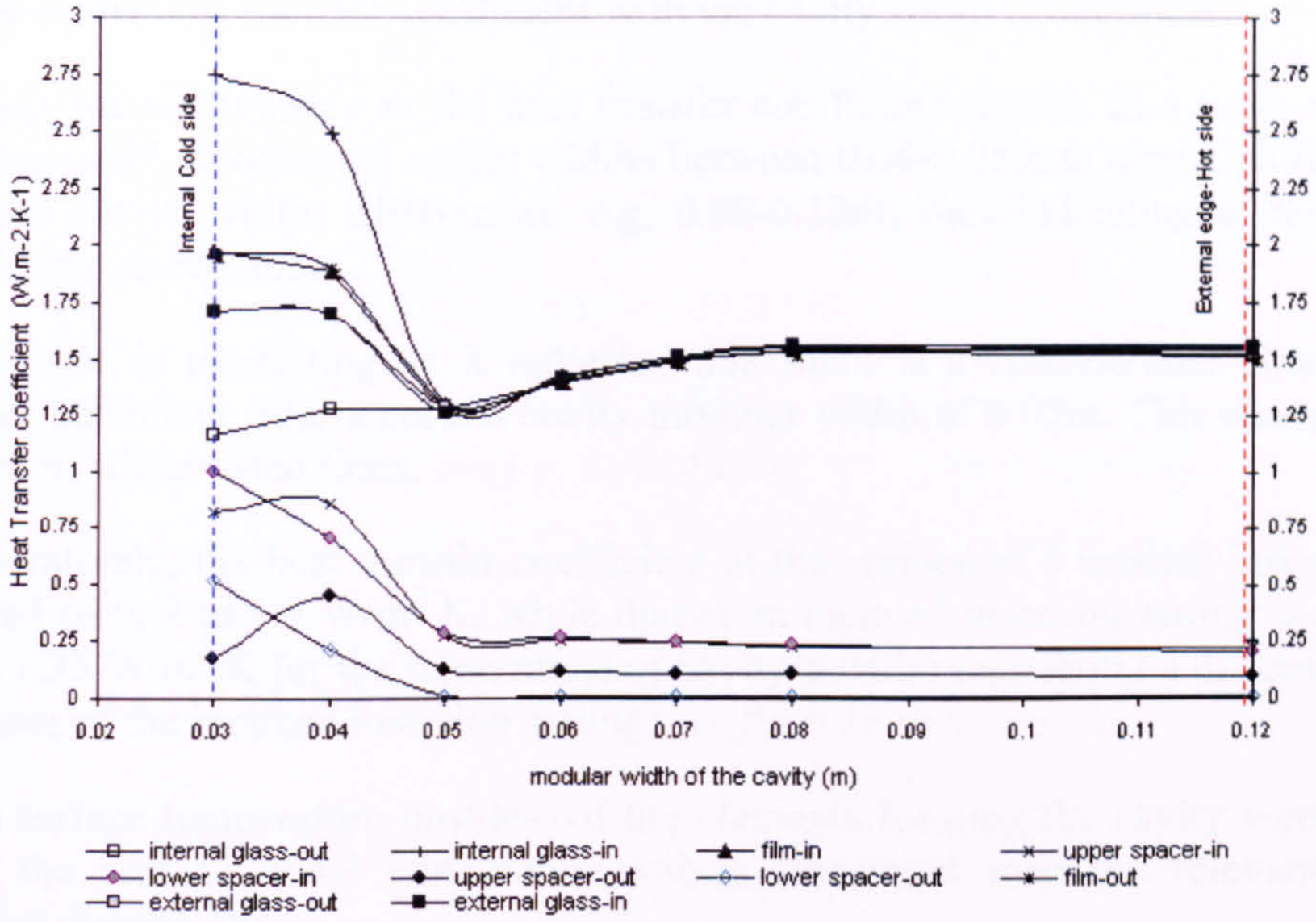

Figure 6.19 heat transfer coefficients for different surfaces facing the gaseous cavity in a vertical insertion setting, Kuwait/ summer conditions.

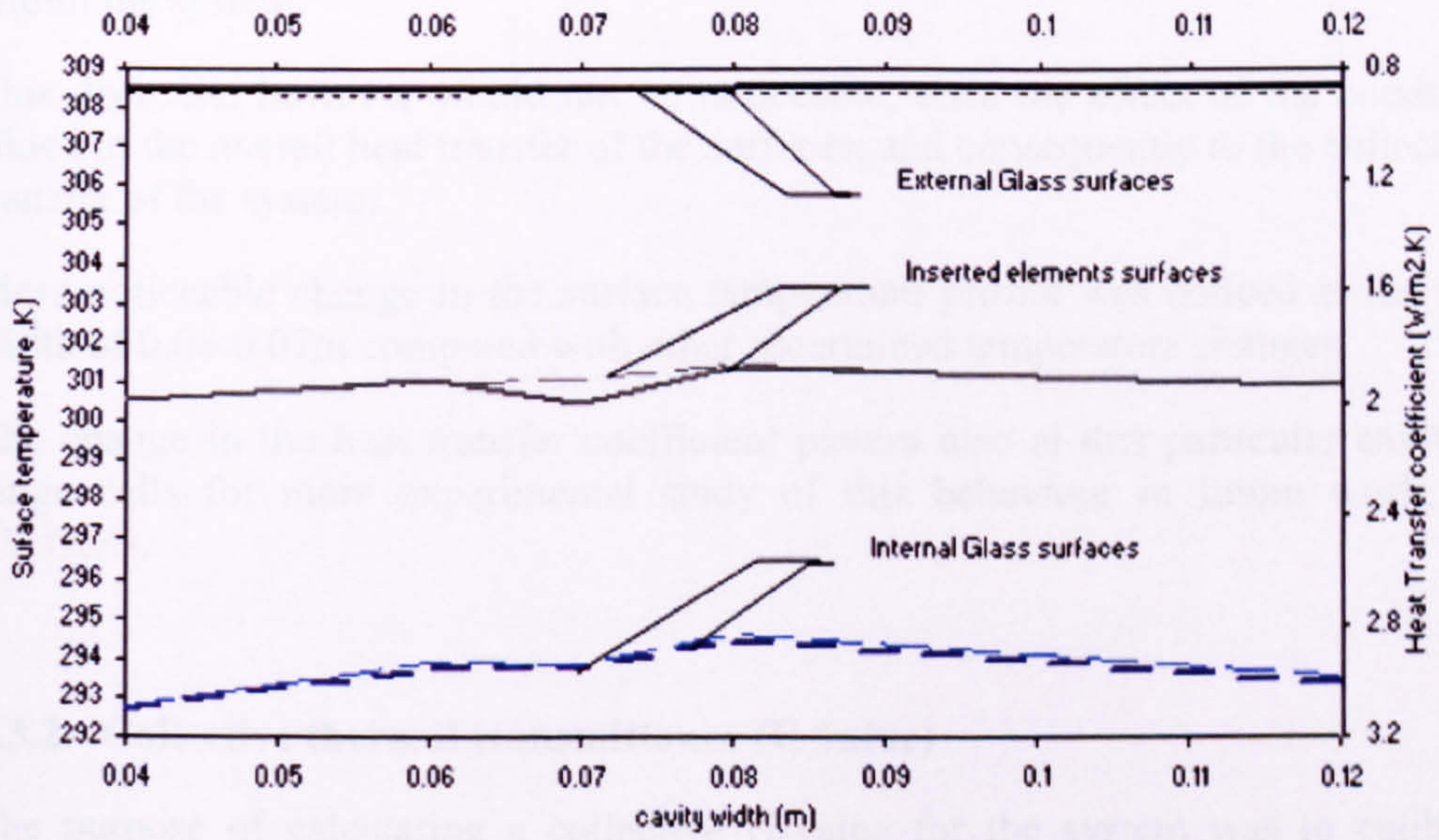

Figure 6.20 Relationship between heat transfer coefficient and the surface temperature for different elements facing the gaseous cavity; Kuwait/ summer; inclined insertion scenario.

Alternatively, *Figure 6.18(A&B)* also indicated that the relationship that governs the change in the heat transfer coefficient with the cavity width is not linear.

As such, the discrepancy in the heat transfer coefficient results, as a ratio, varied from 33% for small incremental cavity widths between 0.04-0.05m to a ratio as low as 2-4% at wider cavity widths differences, e.g. 0.08-0.12m; thus indicating a move towards semi linear correlation.

Such result is interesting as it indicates that there is a considerable change in heat transfer behaviour after a certain cavity modular width of 0.05m. This change was also evident in winter conditions; *see fig. 6.18(A&B)*.

Comparatively, the heat transfer coefficient at the surface of a vertical insertion setting dropped from 2 to 1.5 W/m^2 K, while that at an inclined insertion setting dropped from 1.5 to 1.25 W/m^2 K for the same range of cavity's width registering a difference of 20% in favour of the inclined insertion setting; *see fig 6.18 (A)& fig19*.

Mean surface temperature profiles, of the elements forming the cavity were generated using the surface nodal temperature values integrated over the relevant elements' modular dimensions.

Figure 6.20 shows that there was a noticeable drop in the temperature profile across the two cavities formed by the inserted element; surface temperature differences as small as 0.5C° were responsible for a noticeable change in the heat transfer coefficient at the outer and inner glazing surfaces.

The decrease in the heat transfer coefficient, e.g. as average ratio (%), with relevance to a specific temperature scenario, and with increasing the cavity width was between 3-4% within the system.

This decrease, however would not be noticeable, once the effect of the conduction is added to the overall heat transfer of the surfaces, and consequently to the collective heat transfer of the system.

More noticeable change in the surface temperature profile was noticed at the modular width of 0.06-0.07m compared with other ascertained temperature changes.

The change in the heat transfer coefficient pattern also at this particular cavity width range calls for more experimental study of this behaviour in future work; *see fig 21(A&B)*.

6.3.2 Collective thermal transmittance (U-value)

The purpose of calculating a collective U-value for the system was to calibrate the behaviour of the system through a recognised method as with thermal transmittance. Part of the evaluation process and optimising results was to compare the thermal behaviour, with regard to two main variables:

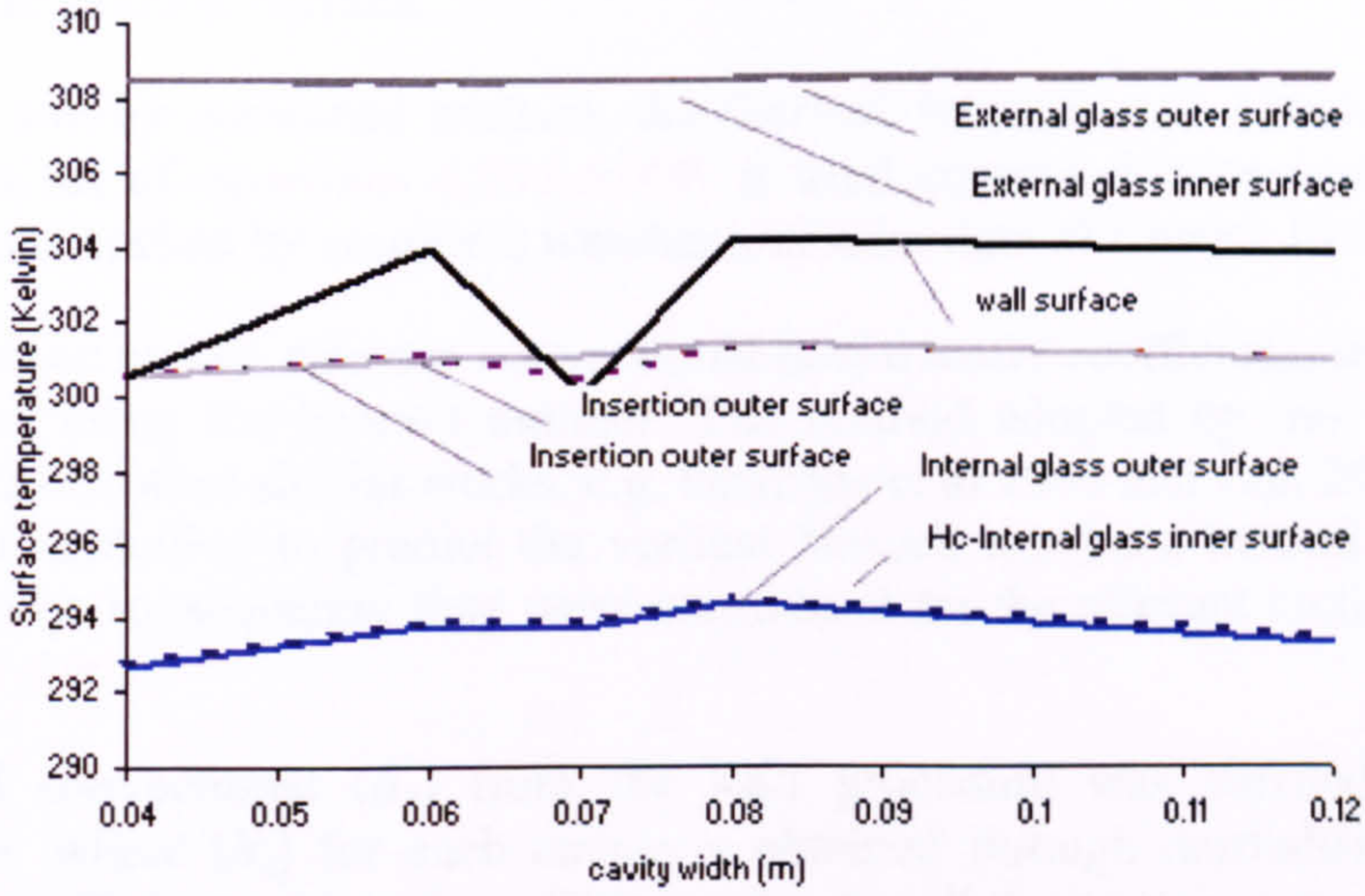

A. Inclined element's insertion

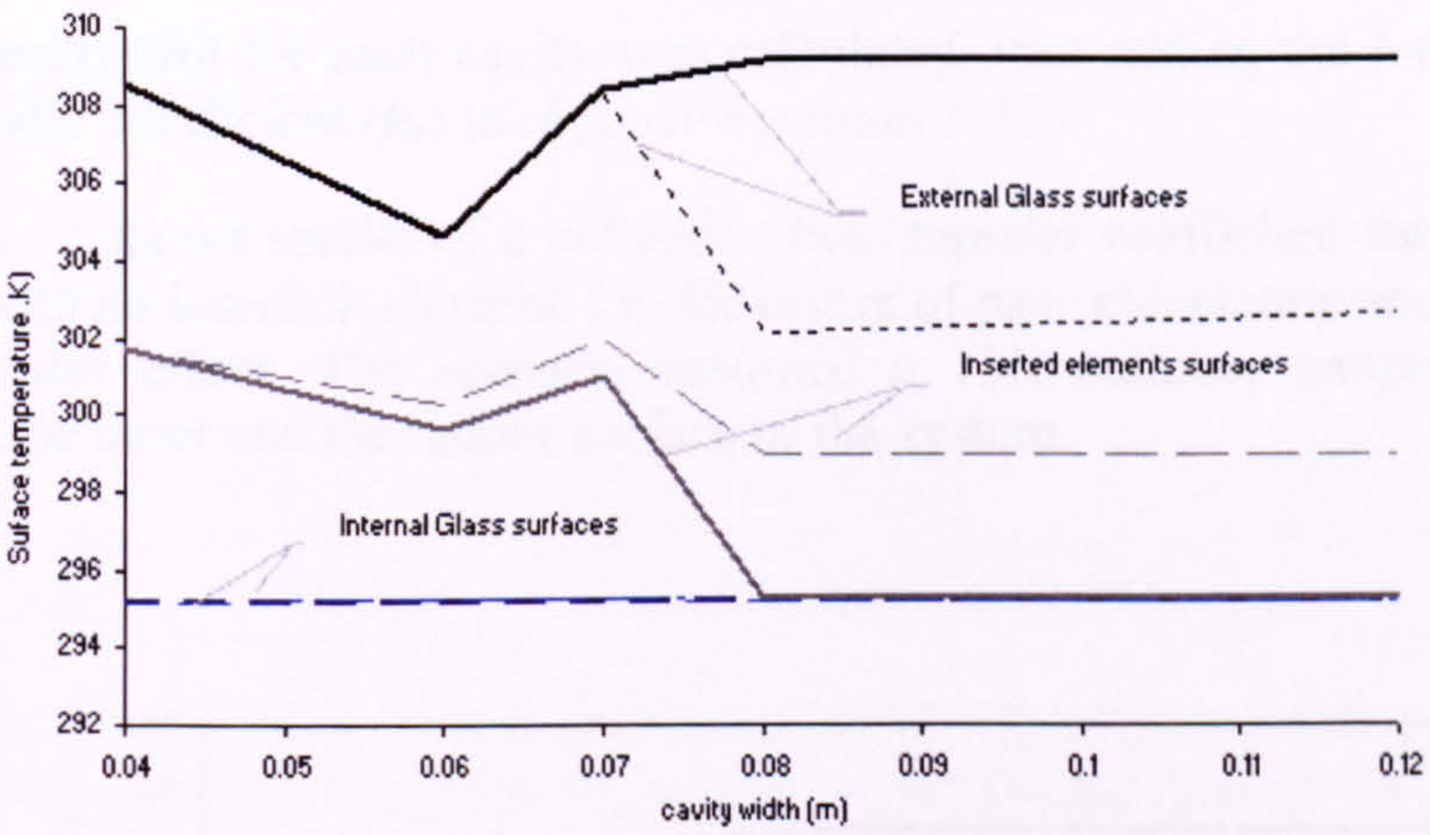

B. Vertical element's insertion

Figure 6.21 Variation of surface temperature at different elements' surfaces relevant to changing the insertion type and the cavity width, Kuwait/ summer.

- Changes in the overall U-value of the system with the change in the cavity width, i.e. the relevant insertion angle.
- Seasonal variation, i.e. temperature differences across the system

Then to compare the suggestion with other insertion scenarios, i.e. vertical insertion setting and no inserted element in the cavity.

In recent years, a method of CFD simulation combined with experimental work and empirical solar data was often used to calculate the thermal transmittance of multiple glazing systems. Most of the work concentrated on studying the heat flow regimes

across the centre of glazing systems, nature of heat transfer in the frames, and the aspect ratio of the glazing cavities.

Using a similar combined method, the thermal transmittance U-value was calculated using the set of *equations 6.004-6.009;* it used combined numerical and Fluent-CFD simulations backed by empirical weather and solar data of Kuwait 1996.

As explained earlier, relevant convectional heat transfer coefficients in each cavity were calculated using the Nusselt number. The method adopted by this research, slightly differed from other similar works, e.g. Griffiths et al 1997 and Gan 2001, in that it used the CFD modelling to predict the vertical Nusselt numbers, instead of being derived numerically; subsequently they were normalised for the relevant inclination angles, *see equation 6.009*.

Resulted convectional (h_c) from the said procedure was verified against another approach, where (h_c) for each cavity is obtained through normalising the local heat transfer coefficients, taken from CFD results, for all the participating surfaces along the path of the heat transfer. Differences in results between these two methods were marginal.

Consequently (h_i) for each cavity was calculated after adding the longwave (thermal) heat transfer coefficient (h_r) to (h_c), *see equation 6.006*.

Figure 6.22 shows results of a collective heat transfer coefficient for the cavities of a system with no insertion element, i.e. for centre of pane calculation and excluding frame heat transfer effect. The scenario assumed a 13K summer temperature difference between the outer and the indoor surface of the system.

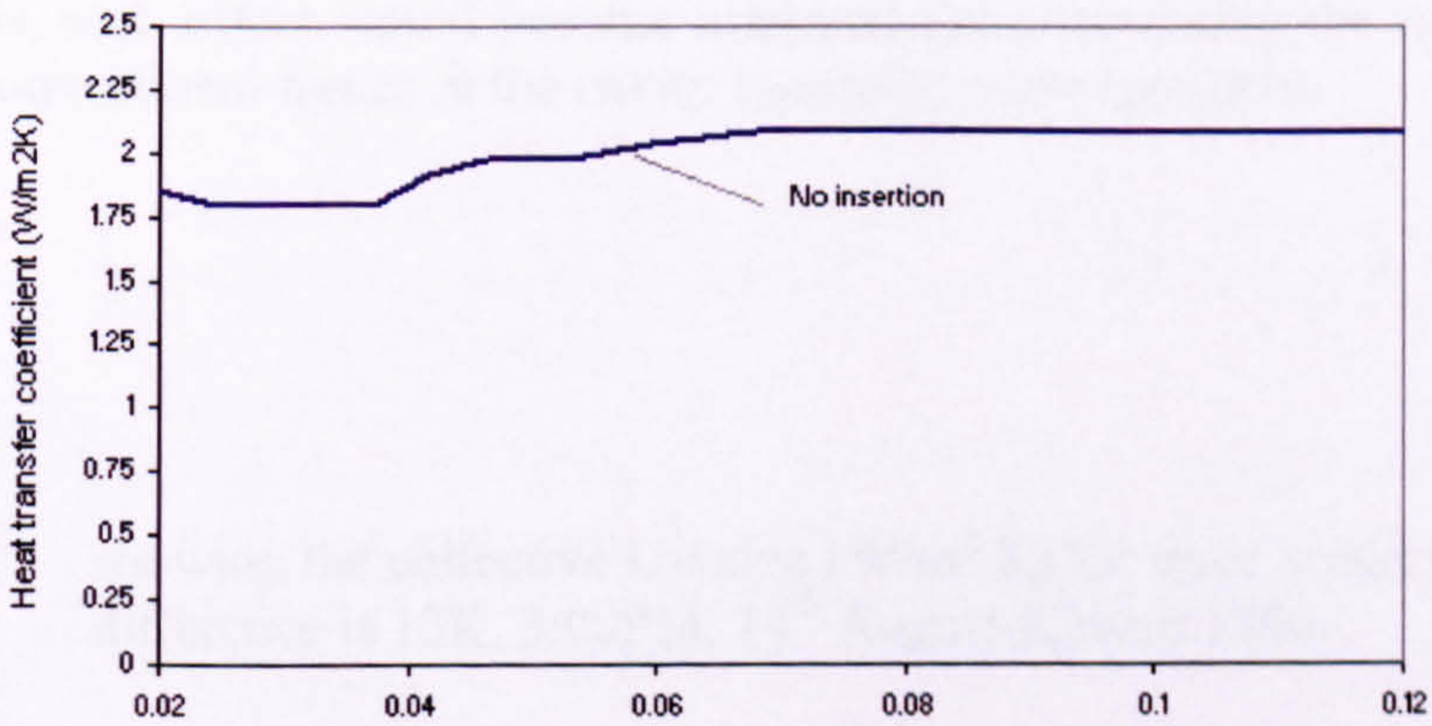

Figure 6.22 showing collective heat transfer coefficient (h) for a system with no insertion. Summer scenario, Kuwait 14th August 1996.Temperature difference across the system is 13K.

Results show that after an initial fluctuation at incremental modular cavity widths, the collective heat transfer coefficient stabilised with the increase of the cavity. Ascertained value was between 1.85-2.08 $W/m^2.K$ for cavity widths between 0.02-0.12m respectively.

Results of the U-value, as a guide for thermal transmittance, indicate that the inclined insertion proposed system performs better than the other settings, when the modular cavity width increase is incremental, e.g. between 0.02-0.04m.

Variance in U-values, between an inclined to vertical setting were 14% then decreased gradually with larger cavity widths to 0.004%, in favour of the inclined insertion; *see table 6.02, fig. 6.23 (A&B)* respectively.

As stated previously, these results only reflect U-values for centre of pane calculations and did not include the effect of the frames or the thermal transfer at the edges of the spacers

Alternatively, once compared to no insertion setting, differences were between 46% at small incremental widths then to 43% when cavity widths were 01.2m suggesting that the inclined system here also performs better at relatively small cavity widths range.

Figure 6.23(A) also suggests a semi fixed U-value for a system with no insertion with increasing the cavity width; this is compared to the inclined and/or vertical insertions settings which are more width sensitive.

Explanation is suggested; by using the inserted element settings i.e. an inclined or vertical option, would help in suppressing the convectional currents in small cavity widths range.

Afterwards, such effect would become marginal upon increasing the cavity width, and with the convectional forces in the cavity becoming more turbulent.

Table 6.02 showing the collective U-value ($W/m^2.K$) for three scenarios; temperature difference is 13K, 3:00PM, 14th August-Kuwait 1996.

Type of insertion	Width of the modular cavity (m)						
U- value (W/m^2K)	0.02	0.04	0.05	0.06	0.07	0.08	0.12
Inclined setting U-value	1.281	1.210	1.212	1.205	1.214	1.208	1.170
Vertical setting U value	1.593	1.437	1.178	1.177	1.176	1.175	1.175
No element U value	2.8	2.757	2.76	2.78	2.67	2.68	2.69

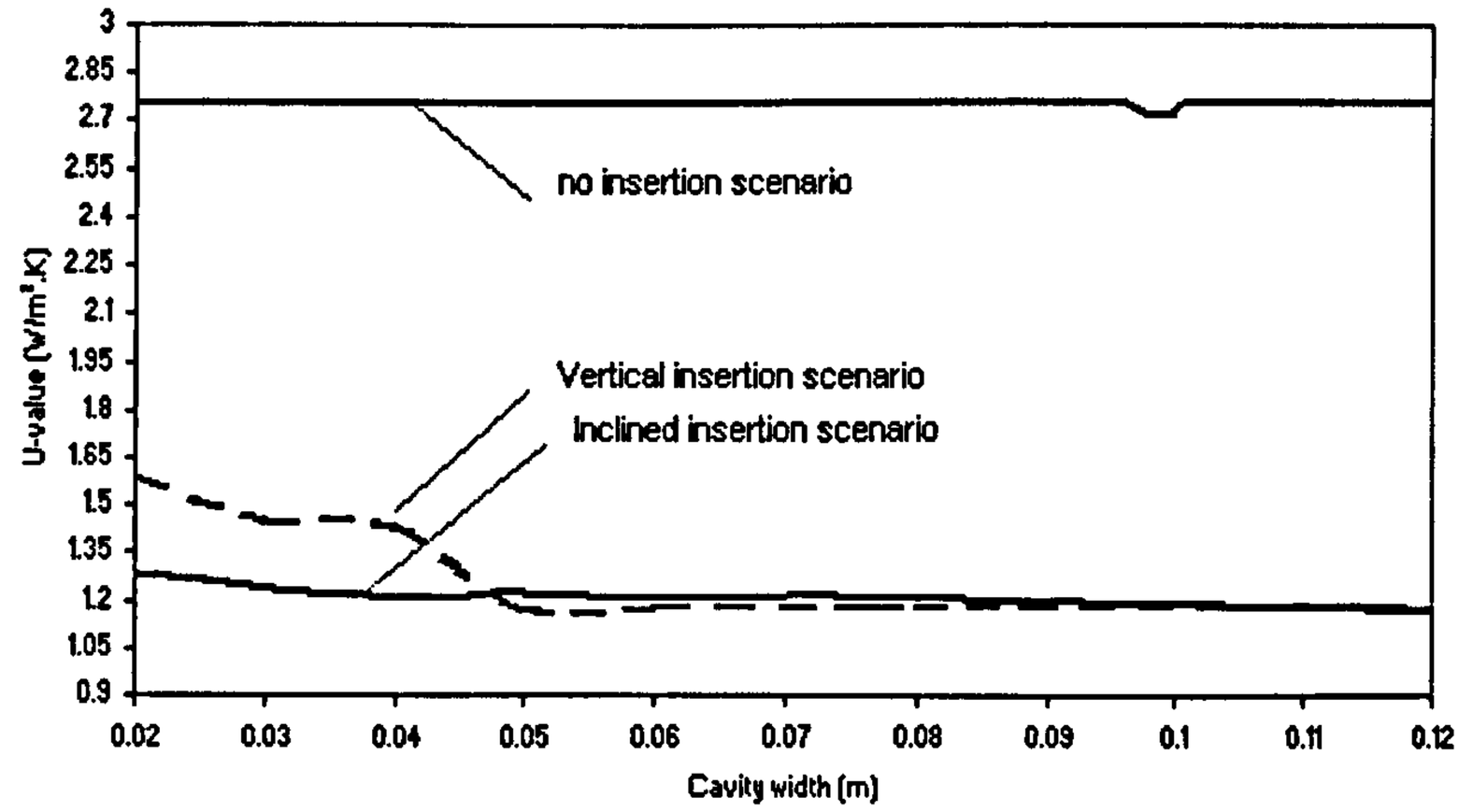

A. U value for three settings

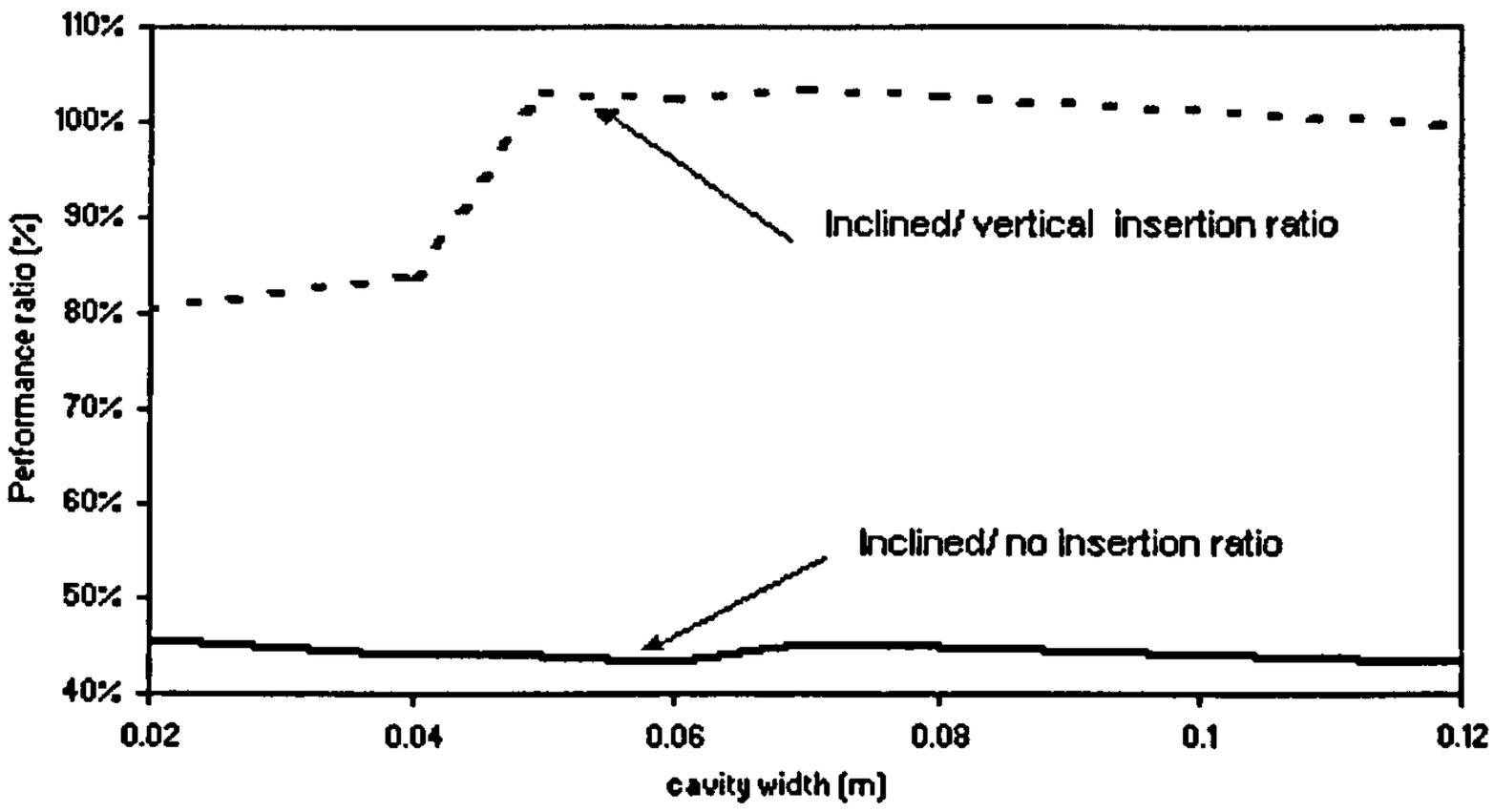

B. Comparison as behaviour ratio for the different settings

Figure 6.23 showing U-value for three scenarios; vertical, inclined and no insertion. Summer scenario, Kuwait 14th August 1996.Temperature difference across the system is 13K

Also, with the increased cavity width, the inserted element and spacers surfaces would even contribute to increase the local convectional currents in those cavities with their increased surface areas; they would also have a higher cavity aspect ratios that is normal to the direction of heat flow, i.e. that of width / Length of the cavity.

In such settings, the effect of the conductional forces would be limited, and then tend to be minimal with the increased cavity width.

The next step was to explore the possible correlation that governs the main thermal parameters of the settings: (i) The range of temperature difference across the system.

(ii) The insertion angle of the element/ the corresponding cavity width for a modular system. A method was adopted to optimise the U-value of an inclined insertion system as follows:

- Using a statistical method, the U-values were calculated for several temperature differences range across the system, e.g. 2, 3,5,10 and 13K respectively. The simulations accounted for any relevant changes in the outdoor or indoor conditions; *see fig 6.24.*

- The simulations were taken for a range of cavity widths (0.02-0.12m) to attune the U- value pattern upon changing the width of cavity or (**tan** θ^{1}) and the temperature difference (ΔT) across the system. Hence a correlation could be produced.

- A STDEV weight factor was identified=(0.01) that is correspondent to 1K temperature difference (between the outer environment conditions and the inner conditions); this was then substituted to normalise the basic step equation; *see equation 6.010* and *table 6.03*:

$$\underset{\Delta T=1K}{\Delta U} = [2076.6(\tan\theta^{-1})^4 - 1515.3(\tan\theta^{-1})^3 + 288.49(\tan\theta^{-1})^2 - 21.621(\tan\theta^{-1}) + 1.5837] \quad (6.010)$$

- The best fit for the equation was found to be in the fourth order. Multiplying the step factor (0.01) by (ΔT) and adding them as a variable to the basic equation, produced an equation that presents the relationship between the U_{total}-value of the system; the insertion angle (θ), temperature differences (ΔT) across the system.

$$U_{thermal} = [2076.6(\tan\theta^{-1})^4 - 1515.3(\tan\theta^{-1})^3 + 288.49(\tan\theta^{-1})^2 - 21.621(\tan\theta^{-1}) + 1.5837] + (0.01\Delta T) \quad (6.011)$$

Consequently, this equation can be used to calculate U-value of only the thermal heat transfer in the inclined and/or vertical insertion system, once the insertion angle and the temperature difference across the system are known; *see appendix -XII for results.* The next section deals with calculating the total transferred energy through the glazing system

Table 6.03 shows the development of the step weight factor used in the basic equation.

ΔT scenarios	Width of the cavity (m)							
	0.02	0.03	0.04	0.05	0.06	0.07	0.08	0.12
U- value 13k	1.281	1.256	1.210	1.292	1.205	1.214	1.208	1.170
U- value 5k	1.266	1.184	1.132	1.113	1.131	1.031	1.094	1.027
For 1k (Weight factor)	0.002	0.009	0.010	0.022	0.009	0.023	0.014	0.018
For 2k	0.004	0.018	0.019	0.045	0.018	0.046	0.028	0.036
Forf3k	0.006	0.027	0.029	0.067	0.028	0.069	0.043	0.054
U value-1K	1.258	1.148	1.094	1.024	1.095	0.939	1.037	0.955
U value-2K	1.260	1.157	1.104	1.046	1.104	0.962	1.052	0.973
U value-3K	1.262	1.166	1.113	1.069	1.113	0.985	1.066	0.991

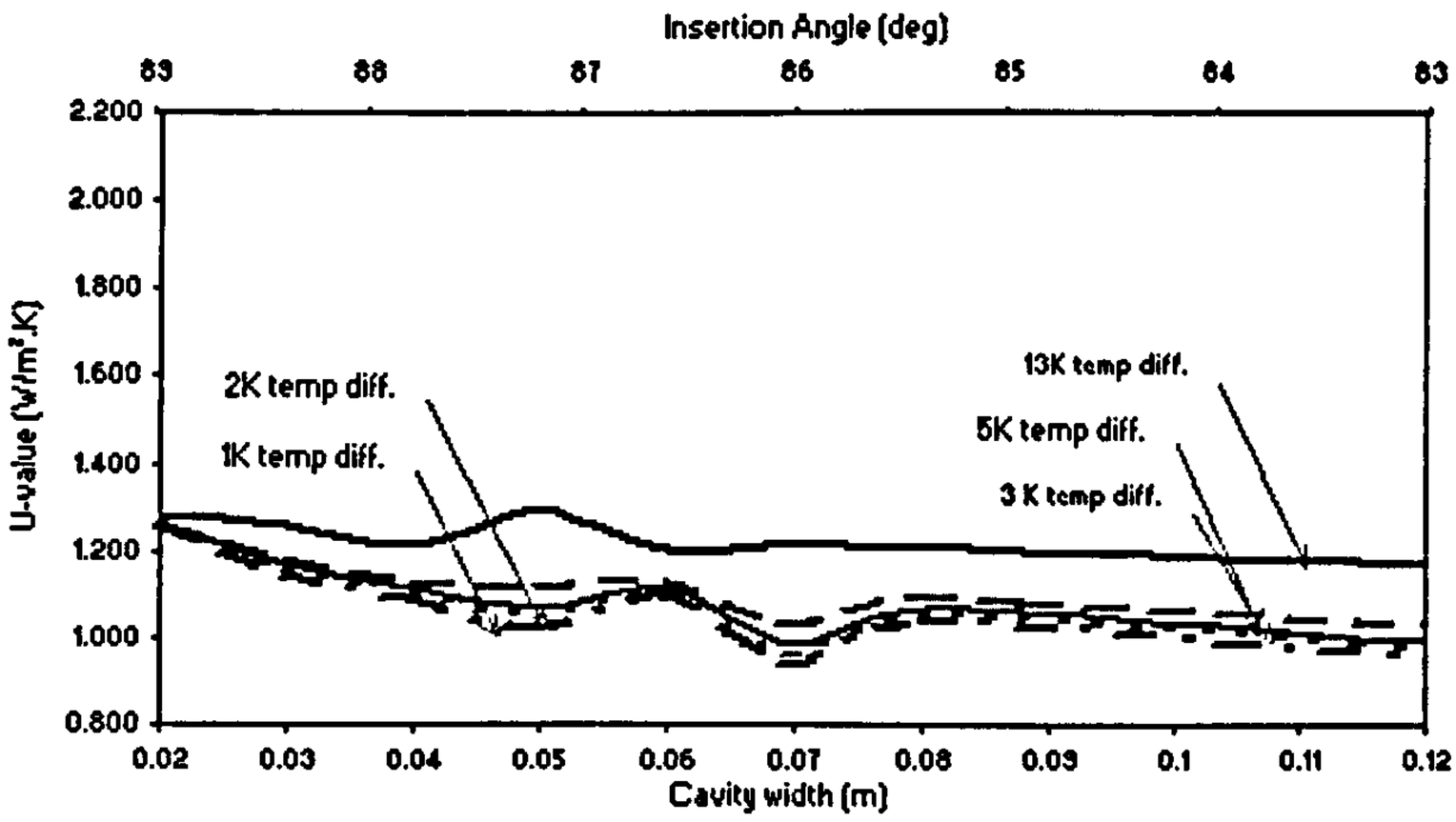

Figure 6.24 showing the method used to predict the U-value for an inclined insertion system, data used here is for Kuwait (August/summer and January/Winter) 1996.

6.3.3 Total transmitted energy

In such systems, the non-linearity and the thermally induced air circulation cause the total solar energy transmittance and the thermal transmittance to change with local temperatures. Temperatures change with incident solar radiation and absorption. Consequently, if incident solar radiation enters the equations, for whole calculation, it must be recognised that the thermal transmittance also changes simultaneously. Thus makes it virtually impossible to separate the two effects. By definition the thermal transmittance is assumed to be the transmittance without solar radiation (ISO/DIN 15099). As a consequence, when adding the incident solar heat flux with its components (the direct and diffused), the total energy transmittance is calculated as:

$$q_{in-nosolar} = U_{total}(T_{indoor} - T_{environment}) \tag{6.012}$$

Where ($q_{in\text{-}nosolar}$) is the heat gain received into the inner space as a thermal transmittance, when adding the effect of the insolation ($q_{in\text{-}solar}$), which is calculated from the collective *transmitted* solar insolation along with its visible wavelength contribution:

$$q_{in-total} = U_{total}(T_{indoor} - T_{environment}) + q_{in-solar} \tag{6.013}$$

This equation was used to calculate the total heat gain passing through the centre of glazing of the system, still excluding the effect at the heat transfer going through the frames.

In fig 6. 25 the shaded area refers to cavity widths between (0.03-0.04m) of the modular system where the transmitted energy drops substantially, it implies that those widths would be the best-fit width for (DB) transmissivity sought, so as to achieve good result with a practical cavity width.

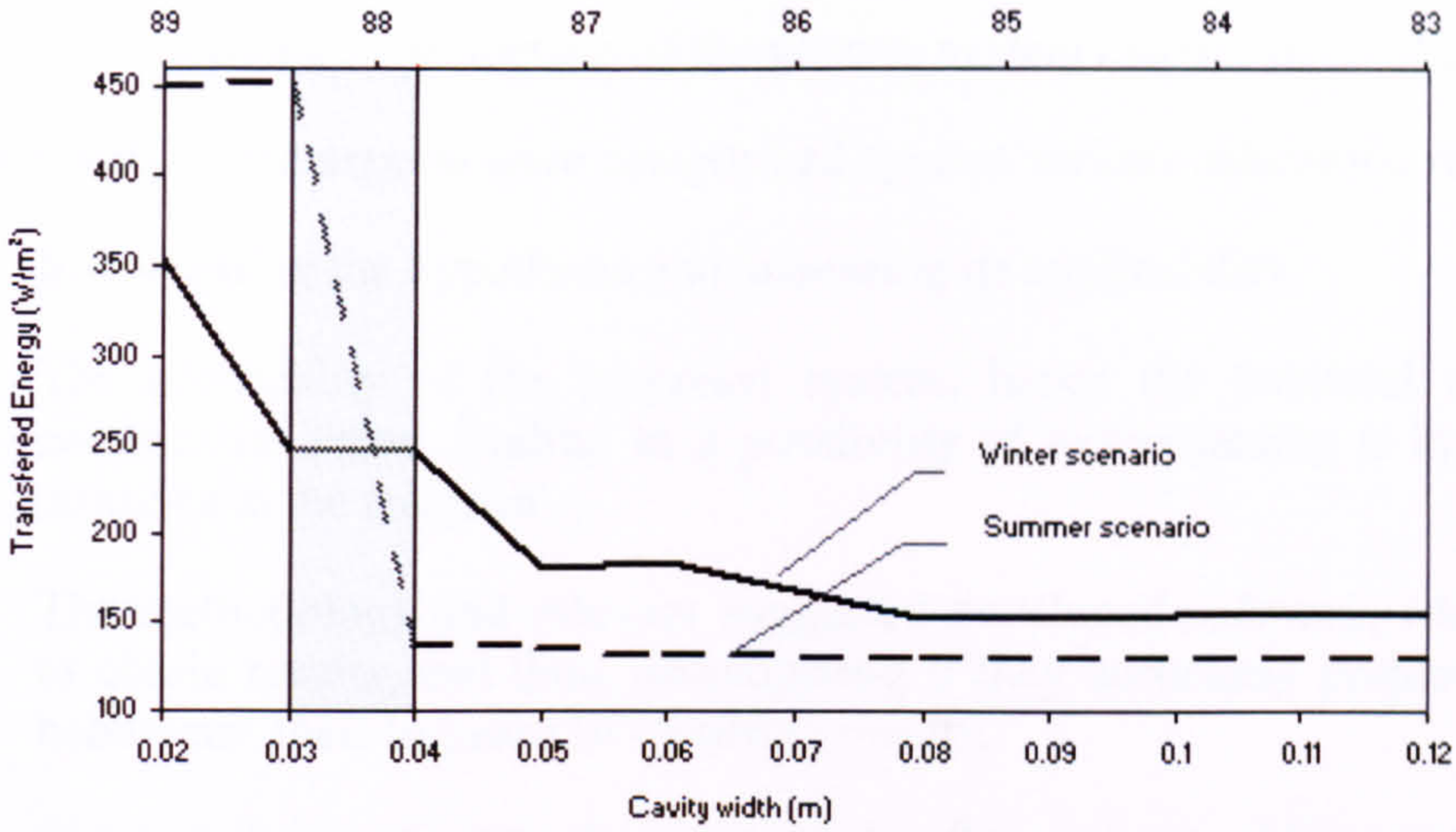

Figure 6.25 showing the total heat gain through the centre of glazing for the suggestion, summer and winter scenarios Kuwait 1996.

They correspond to a narrow range of insertion angles (88.28-87.7°), after which the transmitted energy dropped substantially with the increase in cavity width.

The graph also implies that the visible part contribution of the insolation is considerable in heating the inner space. The previous statement did not take account of other contributory factors in real life situations, e.g. frames, shading devices, which were excluded from calculation

The optimisation process to calculate the effectiveness of the whole system has to be weighed against the practicality of system dimensions that would be viable in real applications, relevant to the seasonal and diurnal needs and reflect the expected benefits.

For practicality reasons, wide cavity widths might not be advised to be used in windows openings due to various reasons, including aesthetical, structural and economical.

On the other hand, if a more acceptable module cavity width of (0.04m) was chosen, with an insertion element angle of 87.7°, it would lead to a varying effectiveness with regard to the reduction of direct solar gain. Still, this type of output behaviour might be preferable, as higher rates of solar energy intake are advantageous during the cold season. It also can be noted that the drop in Energy transmission in summer would be more significant. This would also reflect on the effectiveness of the system to reduce energy consumption rates across the different latitudes and with the different seasonal and diurnal changes.

Discussion

Several platforms and simulation settings were used to examine the behaviour of the proposed glazing system; two main aspects were considered as base for the analysis:

- Overall behaviour, with regard to a preferable reduction of the direct solar gain passing through the proposed system.

- Expected optical properties of the glazing system calculated as of a bulk sample.

Alternatively, these aspects were categorized against various indicators, relevant to:

(i) Investigating the hypothesis and, assessing its applicability.

(ii) The practicality of the proposed system, hence the potential of acquiring a commercial value, leading to a possibility of implementing it in the suggested latitudes in the research.

(iii) The methodology and relevant suggested developed software, which were used to obtain results; and thus, investigating if they accurately projected the system behaviour, their logistics in reporting results.

(iv) The possibility of using the developed software, in its different platforms, as a tool to assess other glazing systems.

As shown several equations were developed that could be taken further to a calculation block that could assess the overall behaviour of the system. The block could be relatively easy to use and does not require a considerable CPU time and could be included in any software that uses SMARTS2 in the background as solar model, and a simple finite element calculator platform, e.g. as in WINDOWS. The input could be scheduled as follows:

- OUTPUT from SMARTS2 for; the tilted direct beam, diffused and Albedo relevant to the solar geometry of the site, the solar incidence angle, i.e. as a profile angle, or an actual incidence angle if the wall azimuth angle, i.e. that defines the orientation is known.
- INPUT for; the insertion angle, optical and thermal properties of the materials used in the system. However, at this stage of development calculation of coatings on glazing panes are not included.
- Outdoor and indoor operating temperatures and prevailing wind profile.
- As shown, the block would calculate the total transmitted energy (solar and thermal) across the system; *see 6.3.1-6.3.3* respectively.
- Accuracy varied for the different components of the block; the insolation model accuracy was ±4 (91-100%), accuracy for the thermal model was 94-97%, *see figs 6.26& 6.27.*

(v) Possible future work, to further enhances the performance of the suggestion or to investigate the possibility of using it in other applications.

(vi) Investigating the added benefits from inserting a transparent element at a preferable set angle in a double-glazing cavity and the practicality of such regime; as the idea of suspending or inserting such an element.

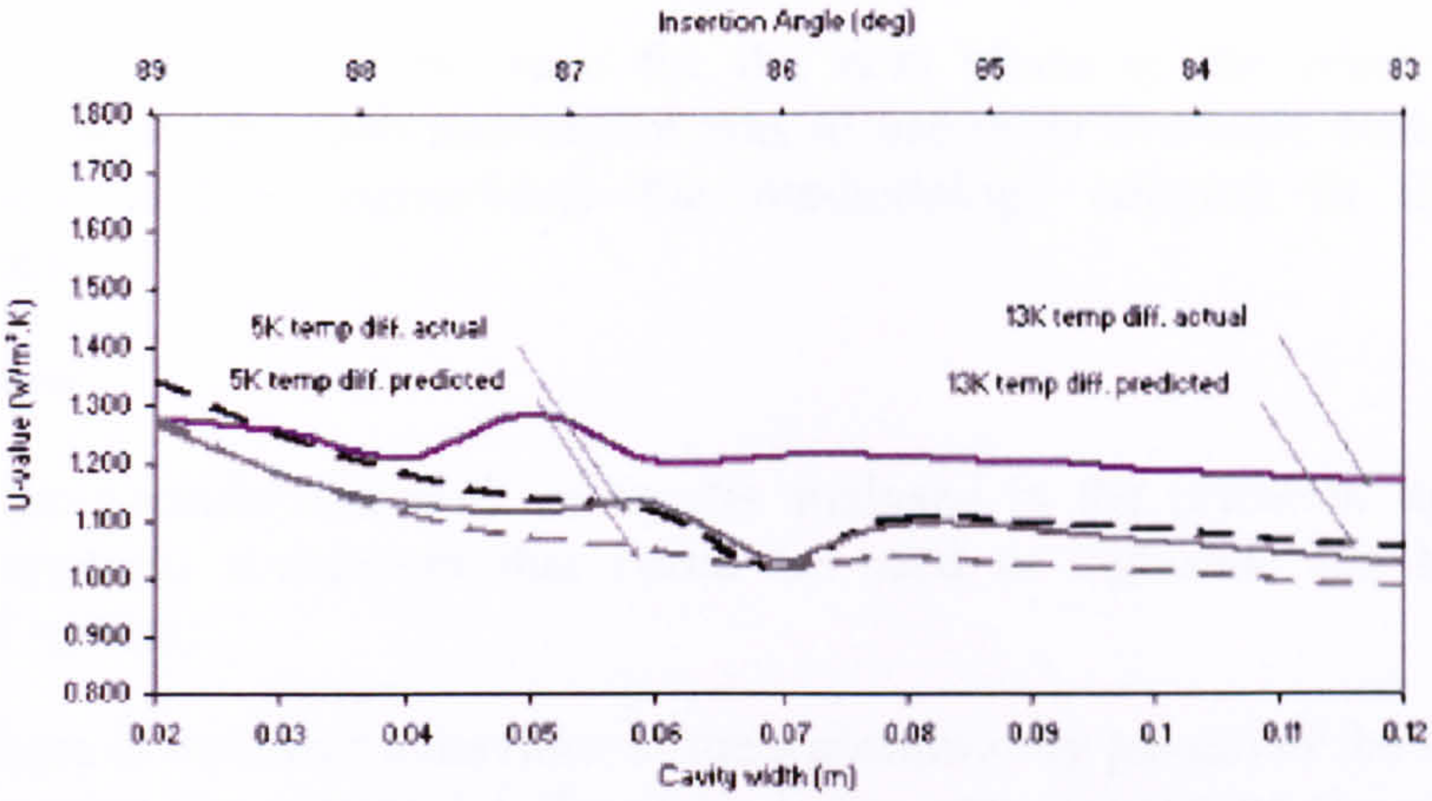

Figure 6.26 showing predicted U-value results for two scenarios, i.e. temperature differences across the system are 13K and 5K respectively, simulating summer and winter conditions in Kuwait August, January.

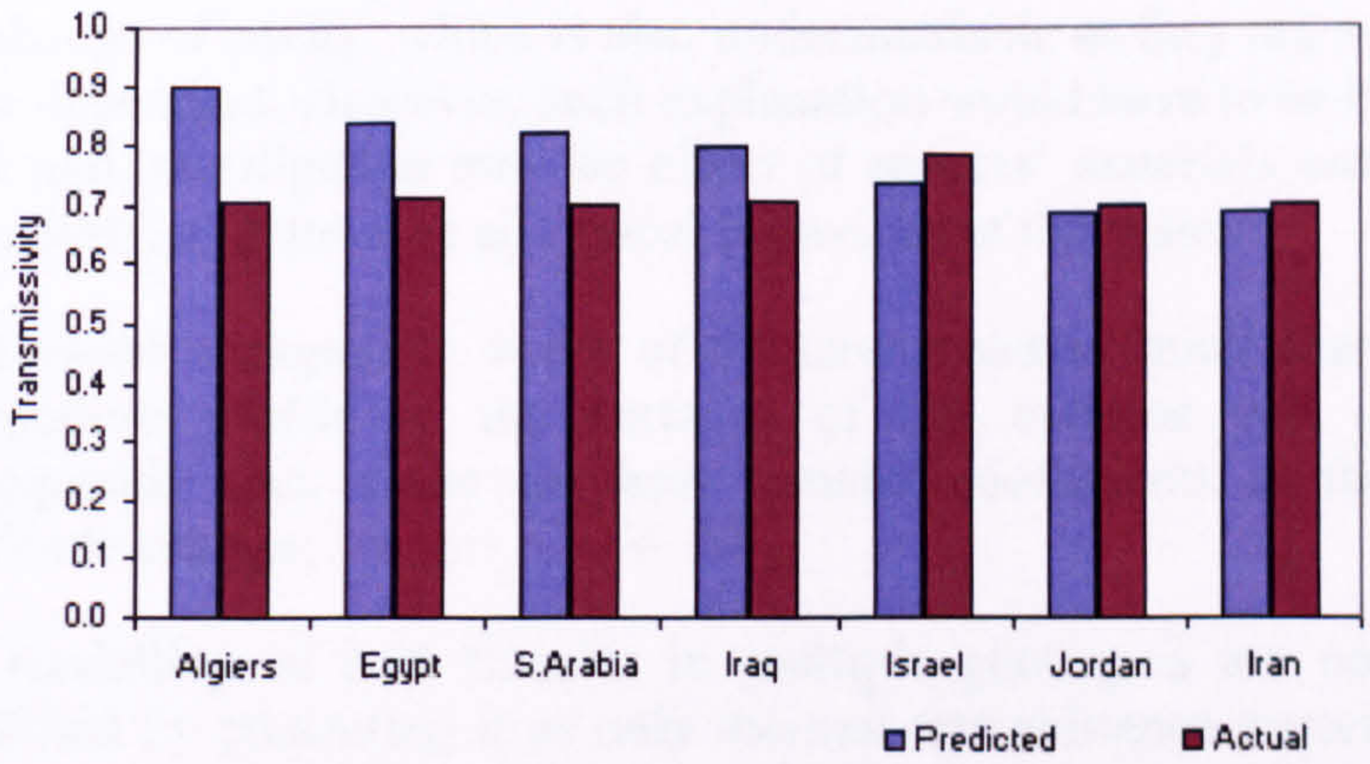

A- Winter

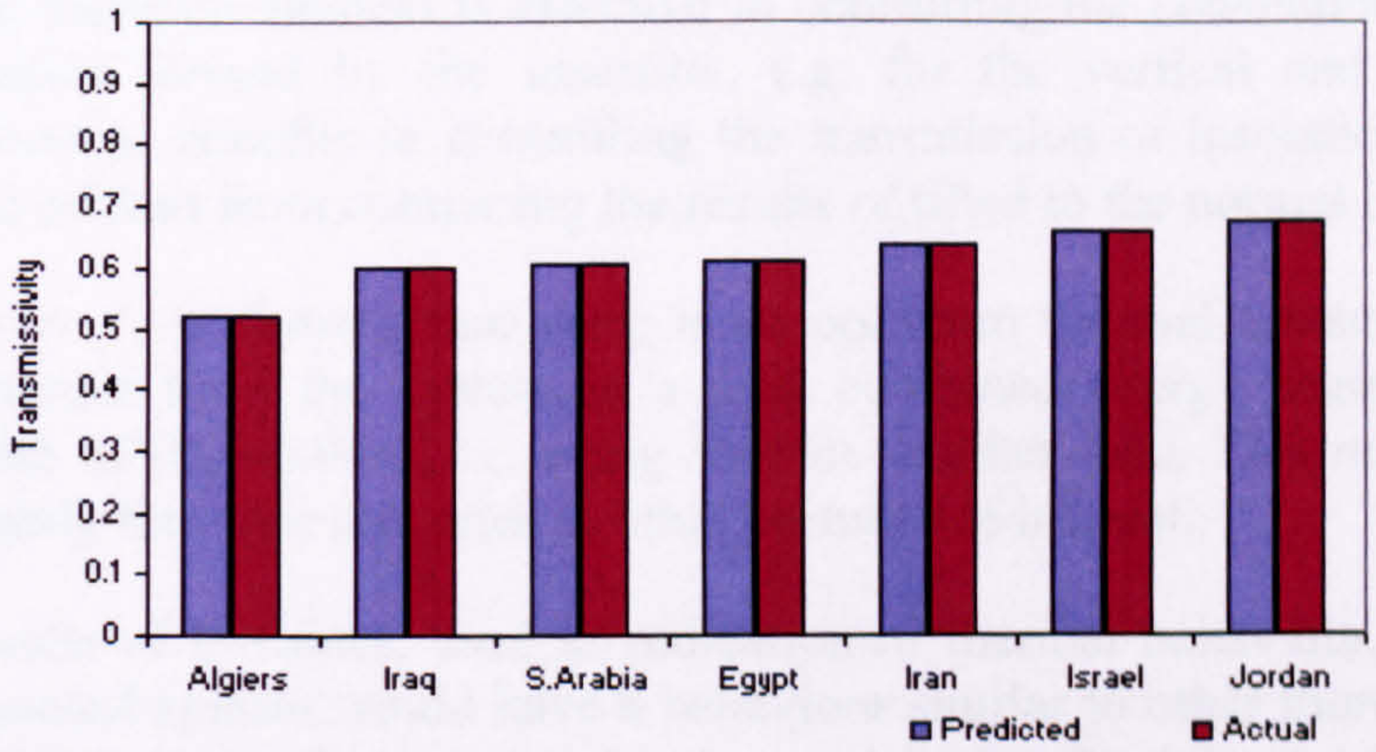

B- Summer

Figure 6.27 showing predicted Transmissivity results for two scenarios (i.e. winter and summer; e.g. assumed width of the cavity here is 0.04m
NB; Red columns=Actual data generated by the research method, Blue columns=predicted data accumulated from the developed equations.

The last statement was the base for the next phase of the research addressed in *chapter 7*. However, such assessment was to use other available commercial tools for comparison, and to consolidate the methodology adopted in this research for simulations.

Conclusion

Despite the considerable bulk of results analysed in the research, there seems to be several apparent statements that could be used to underline the behaviour of the proposed system:

(i) There is no linear behaviour in the transmissivity pattern of the solar components crossing the system, i.e. the direct beam, upon increasing the set insertion angle of the element. Such conclusion suggests more complex regime of reflection and absorption than usually assumed.

This would not the case with the other incident components, i.e. the sky-diffuse and the albedo. They are more stable and would not change substantially with the change of cavity, which is also understandable as they are assumed to be not angle dependant. However, such explanation would have to be backed by further work and investigation into the effect of spacers' materials and surfaces on the reflectivity, and the over all optical behaviour of the system.

(ii) Incremental changes the width of the cavity causes small changes in the local temperature profile at the surfaces of the external and internal glazing, consequently they cause the heat transfer coefficients at the corresponding cavities to change; *see figs 6.20 & 6.21*.

(iii) The modelling of heat transfer in multiple glazing is too complicated to be simplified by presenting it as only thermal transmittance process; more work is needed for better understanding and calibration of existing glazing system.

(iv) The insertion element is effective in controlling the convectional currents in the cavities formed by the insertion, e.g. for the vertical and inclined options. However, benefits in controlling the transmission of insolation were limited as was evident from comparing the results of tilted to the normal insertion.

(v) *Figure 6.25* showed that there is an optimum thermal transmittance behaviour expected from the system in a total combined energy transmission at cavity width of 0.03-0.04m, i.e. using Kuwait weather data. This result might change slightly for other scenarios at other latitudes of interest.

(vi) Results of U-values, used as indication of thermal behaviour, suggests that the proposed system would have a behaviour similar to other more complex glazing systems using advanced insulated materials, i.e. Dual Sealed Structural Silicone secondary sealed unit (The Glass Association of North America 2004:GANA, SIGMA and others).

(vii) Alternatively, the lengthy CPU time spent throughout the simulations, produced set of equations that could be developed and assimilated as a block in current commercial software, which could be used to assess such suggestion commercially.

References

1. Alamdari F, Hammond G.P, Improved data correlation for buoyancy-driven convection in rooms. Building services Engineering. Res. Technology 1983; 4(3): 106-112.

2. BS EN 573, Glass in building- determination of thermal resistance (U value)-calculation method, British Standards Institution, London 1998.

3. Energy Comfort 2000, Information Dossier, Windows –The Key to Low Energy Design; European Commission Thermie Project to reduce energy and improve comfort and environment; (5) March 1998.

4. Fang Y., Eames P., Trevor H., Norton B., Complex multimaterial insulating frames for windows with evacuated glazing. Solar Energy 2005; 79(3): 245-261.

5. Fluent 6 online index manual Apache Web server, Fluent incorporated 2003. See also: http://lis.dvo.ru/fluent/ug/node16.htm#4088

6. Hammond G.P, thermal performance of advanced glazing systems. Journal institute of Energy 2001; 74(March): 2-10.

7. GANA publications, sealed units. The glass association of North America; Topika, KS, USA 2004. See also: http://www.glasswebsite.com/

8. Gan G. Thermal transmittance of multiple glazing: computational fluid dynamics prediction. Applied Thermal Engineering Journal 2001; 21: 1583-1592.

9. Griffiths P, Norton B, Eames P.C, S. Lo, detailed simulation of heat transfer across evacuated glazing, Building Research and information. 1996; 24(3): 141-147.

10. ISO/DIN 15099, Thermal Performance of Windows, Doors and Shading Devices, Detailed Calculations, ISO Central Secretariat, Geneva, Switzerland 2003.

11. Nadia. Provider of Dust data. Kuwait: Institute for Scientific Research; 1996.

12. PRQC definitions, in performance, reliability, and quality of service committee, part of ATIS, USA, 2005. See also: http://www.atis.org/0010/index.asp.

13. Pfisterer R. *et al*, Modern ray-tracing software simplifies virtual prototyping. Laser Focus World Journal, 2003; December.

14. Rayica software manual from Mathematica©5.2, Wolfram Research Inc. See also: http://www.opticasoftware.com/documentation/Rayica/RayicaGuide/#.

`CHAPTER SEVEN

COMPARSION AND ASSESSMENT

Introduction

Lack of experimental backup data can be a main disadvantage in the process of testing new glazing applications, as it would limit the ability to validate any associated developed codes or models, especially if one of the research objectives is to include developed algorithms and codes as new blocks in current dynamic simulation packages. Hence, the need to compare new applications with those of well-established commercial tools, and try if possible, to operate within the same inputs and environments used for developed models.

Most of the commercial packages share the same theoretical background (i.e. as a foundation for calculations); yet they differ in the degree of freedom given for the user in aspects of inputs of geometry, calculation environment, range and specification of materials in their compiled libraries.

Thus, part of the objectives sought for using those tools, were to check if results, in general would be relevant to those obtained from the method of calculation used in this research.

The method of comparison used here, followed the same steps of the research's own approach to evaluate performance of the inclined inserted element in relation to that of vertical setting, then to draw a pattern of relation between transmissivity and the change of the cavity width.

For the purpose of comparison several known commercial tools were used; software and a mathematical code (*see chapter three*), to compare the output of the new proposed glazing system and the associated newly developed codes and software.

7.1 WINDOWS PACKAGE

General overview:

WINDOWS (and its related editions) is a Microsoft Windows™ based computer program, developed by *Lawrence Berkeley National Laboratory* (LBNL) for use by manufacturers, engineers etc, to determine the thermal and solar optical properties of the glazing and frame of window systems (Mitchell R. *et* a*l*, 2003). It consists of three software tiers with the following interfaced libraries:

- Continuously updated algorithms library consistent with ASHRAE SPC142 and ISO15099, (Mitchell *et* al 2002).
- A Condensation Resistance Index library in accordance with a draft version of NFRC 500 (i.e. National Fenestration Registration Council).

- A surface temperature mapping code.
- An integrated database of related material properties.
- Links to other LBNL window analysis software:
- *THERM*, for calculating 2-D frame and edge effects (i.e. using a quad mesh generating method)
- *RESFEN*, for calculating the energy effects of windows in typical houses throughout the United States.
- *Optics* for the optical properties of all coated and uncoated glazings, laminates, and applied films.

The program uses centre of nodes calculation for meshed geometries (i.e. finite elements method) to calculate the heat transfer modes across a 2D environment. It has also the capacity to switch between different methods of convection or radiation (i.e. ASHRAE/NFRC, Fixed Convection Coefficient method, Yazdanian-Klems and Kimura, etc.), depending on the type of inputs available.

Limitation of the calculation environments

The latest editions of *THERM5.1*, *WINDOW5.2a* and *Optics5.2* were used to check the new glazing behaviour. However, there are certain limitations to the amount of inputs that could be used to emulate the suggested written codes. Those could be summarised as:

(i) **Set insertion angle of each element**: the first part of the program (i.e. *THERM5*) gives the user the ability to change separately the set angle of each component of any glazing system. It has a graphical/mesh interface and allows scaling and changing in local coordinates whilst maintaining global coordinates.

Alternatively, other tiers; *WINDOW5* and *Optics* can only rotate the set angles of glazing geometries within a context of a whole inseparable entity.

(ii) **Calculation Method**: *THERM5* uses only a quad mesh generator; this would reduce the accuracy of calculation in any geometry with angled set elements, due to skewness, non alignment and overlapped meshed cells, especially around sharp edges of geometries causing problems between set boundary layers and error in generated results.

Other mitigating factors include; the number of allowable quad mesh tree ranges, i.e. between 6~9, which is relatively low compared to other comprehensive CFD tools, and the maximum allowed number of iterations per simulation, which again would affect the accuracy of results. On the other hand, *WINDOW5* uses built-in centre of nodes equations, *see fig 7.01*.

In general, the three parts of the software work only in a 2D environment, though *Optics* has the ability to show results as a graphical interface of 3D environment.

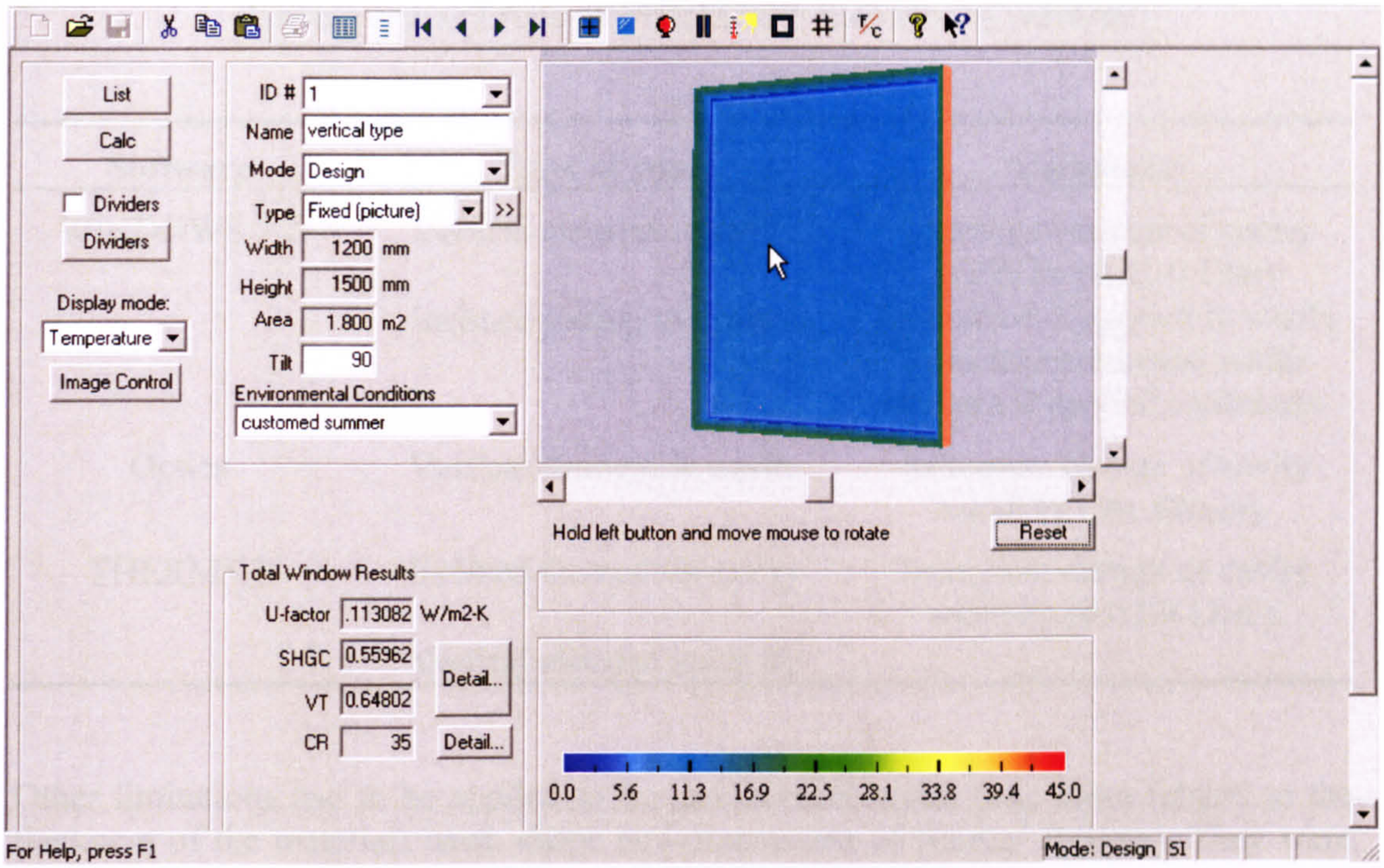

Figure 7.01 Showing the type of display of *WINDOWS5* program results of a run with vertical element and 0.08m cavity width.

(iii) Output options: the three legs of the software were developed primarily to jointly evaluate the behaviour of a whole final glazing product (i.e. a window with its frame, panes, spacers, etc.). This is reflected in the type of available output data from the different parts of the software. Hence, *WINDOW5* and *THERM5* can only generate outputs of U-values, as a collective output of intersecting isotherm surfaces of the whole window unit including the surrounding frame and normal to the global coordinates), thus limiting the ability to analyse the individual optical behaviour of the components (i.e. glazing panes, spacers, etc.).

For other types of outputs; *THERM5* can only generate graphical mapping for the distribution of (temperature, Isotherms, heat and velocity fluxes), while *WINDOW5* and *Optics* can generate output for the optical behaviour of the glazing/unit involved ($\boldsymbol{T_{vis}}$, $\boldsymbol{R_f}$, $\boldsymbol{R_b}$, etc).

Setting the general parameters:

The research used two types of generic runs, relevant to the specific limitations, discussed earlier, for each part of the software. *Table 7.01* shows the types of those runs relevant to each part of the software.

Parameters of one type of environment (i.e. summertime) were used as inputs in all the different parts of the software to minimise overlapping of runs.

Table 7.01 showing types of runs associated with each type of software.

Software	Type of runs	Comments
WINDOWS 5.2	Vertical element in cavity	Increment change of cavity width by (0.02-0.12m)
	Inclined setting of system	Inclination is applied to whole system; incremental width increase is applied separately.
Optics	Vertical element in cavity	Increment change of cavity width by (40, 80mm).
THERM5.2	Inclined element in cavity	Increment change of cavity width by (0.02-0.12m).
	Vertical element in cavity	

Other limitations had to be applied to the geometrical inputs (e.g. those related to the thickness of the materials used, shape and dimensions of frames/ spacers). They were considered as constants for the purpose of simplifying the simulation:

7.1.1 WINDOWS 5

Assumptions used for this program were as follows:

- Types of glass used; are 6mm generic white float glass; optical properties used: $\mathbf{T}_{sol}$ is 0.78, outer emissivity is 0.840.
- Gas used for the cavity; is pure air with a conductivity of 0.024069 W/m^{-K}, *Cp* is 1006.103271 J/kg^{-K}, density is 1.292171 kg/m^3, Prandtl number of 0.7197.
- A customised new material file was added to the library for a polystyrene sheet with the following standard optical data: ($\boldsymbol{T}_{sol}$: 0.834, $\boldsymbol{T}_{vis}$: 0.899, $\boldsymbol{R}_{soll,2}$: 0.075); $\boldsymbol{R}_{soll,2}$ here refers to the front and the back reflectivity respectively.
- A customised weather file was created; simulations were taken for summer season with an outside temperature of 309.95K and an inside temperature of 295.15K, using the built-in U-factor method of calculation.
- Spacers used; were of aluminium ordinary type with a U value of $10.790 W/m^2.K$.
- Area of selected window was taken from the software library as a "fixed (picture)/NFRC" with a width of 1200×1500mm, specific area of the glazing is $1.207m^2$. Due to the limitation of applying an inclined element setting, the research had to assume that the whole window setting, including the frame, is inclined.

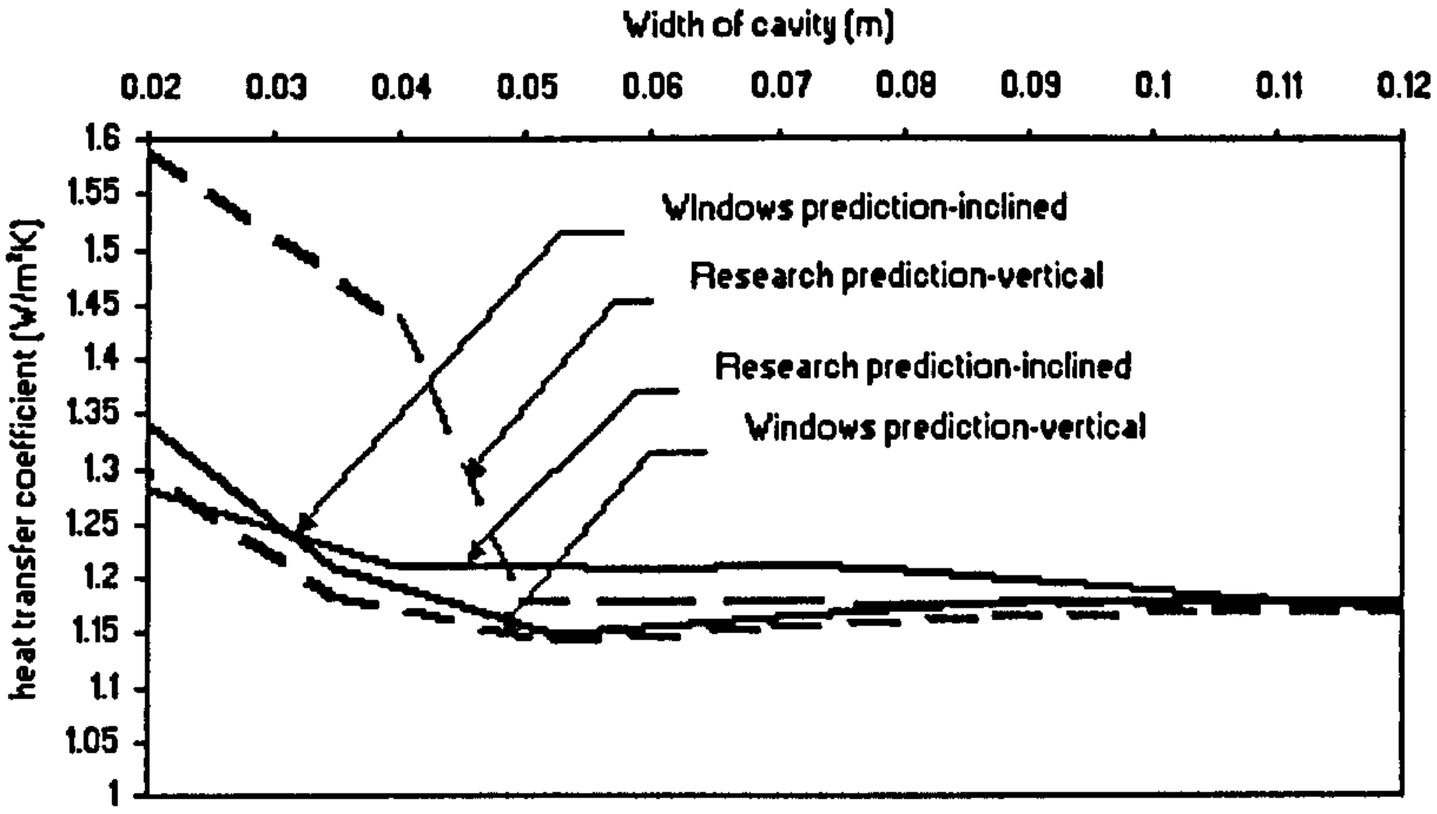

Figure 7.02 Showing comparison of centre of glazing U-value calculated through WINDOWS5 and that of the research method. Scenarios are for inclined and vertical insertion.

- To simulate the inclined insertion, the whole system was tilted corresponding to the inserted element's angles of the suggestion method while the cavity widths were increased manually in WINDOWS5 to emulate an increased cavity area along with the inclination increase.

Fig 7.02 shows output results for the centre of glazing U value for two scenarios, e.g. the inclined and vertical settings, simulated through WINDOWS and compared to results obtained through the research method.

As expected, results show that there is no significant difference between a vertical and an inclined setting; if simulated through WINDOWS.

Differences in results for the inclined insertion between the two methods are 93-99% in small range cavity widths to those of the research method. However, the figure also shows that there are considerable differences in results between the two methods, when comparing results for the vertical insertion. This could be due to the followings:

(i) As the software deals with the centre of glazing calculation method and has limitation in its tilting options, it presumes a fixed value for the transmitted irradiative heat flux with the increased tilt angle, thus minimising accuracy.

(ii) WINDOWS 5.2 uses modified Nusselt number for tilted cavities (ISO/DIN 15099, 2003) as base for calculation, however it is less accurate in results (Yang and Curcija 2003) with small range tilting angles that near to the normal setting, e.g. angles 89-86° deg. This would justify the discrepancies shown in results of the two methods, especially at this range.

(iii) The software uses a numerical regression to model radiation, hence using diffuse radiation method to calculate the transmissivity.

Still, WINDOWS 5.02 output indicate that the proposed system performs well in controlling the heat gain. Results showed that an optimum U factor was achieved of 1.15 ($W/m^2.K$), with an optimum angle, for this setting, of $\approx 87.0^{\circ}$.

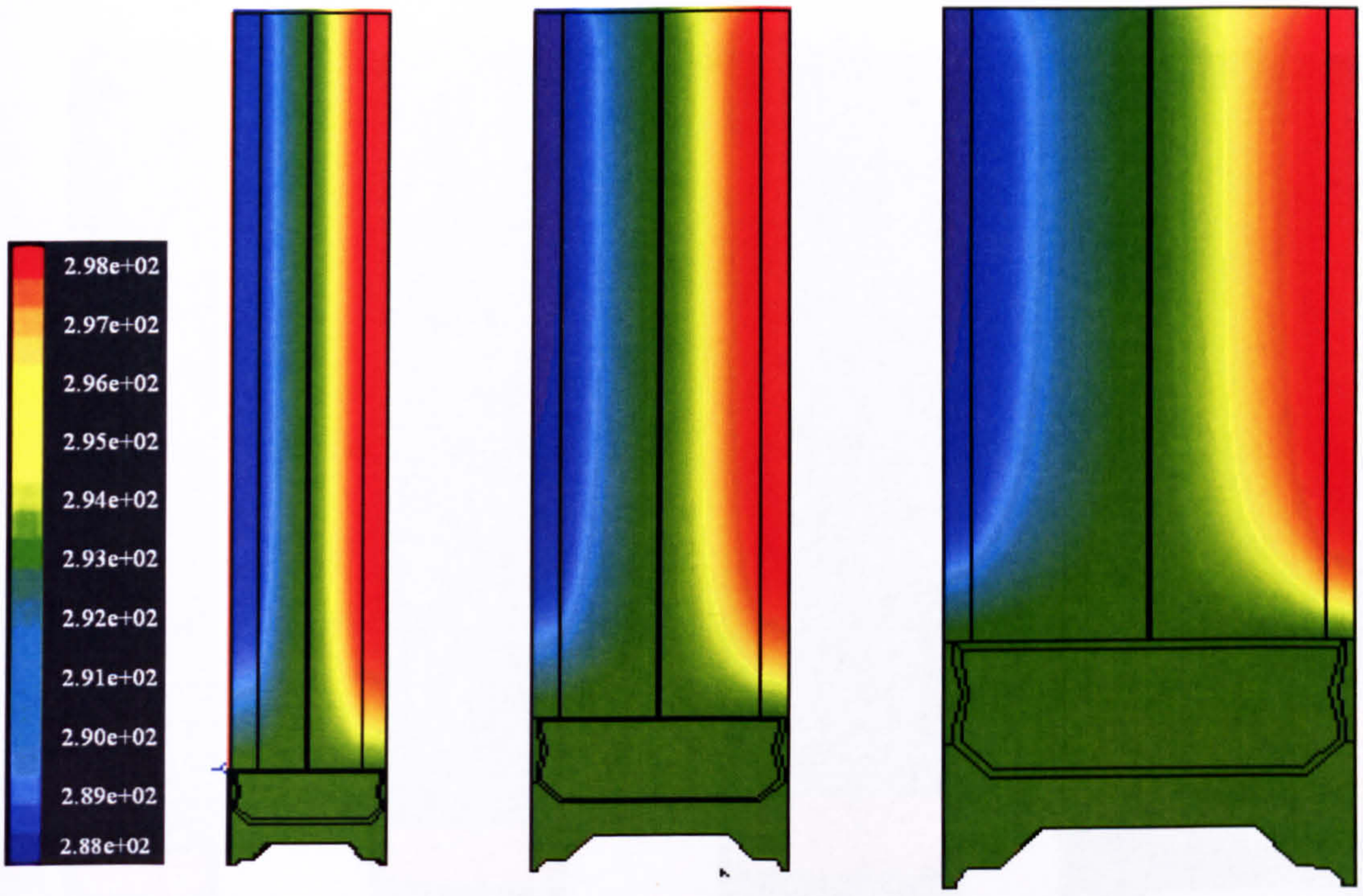

a) Vertical element; Planar temperature range in cavity: 15.00~25.00C◦

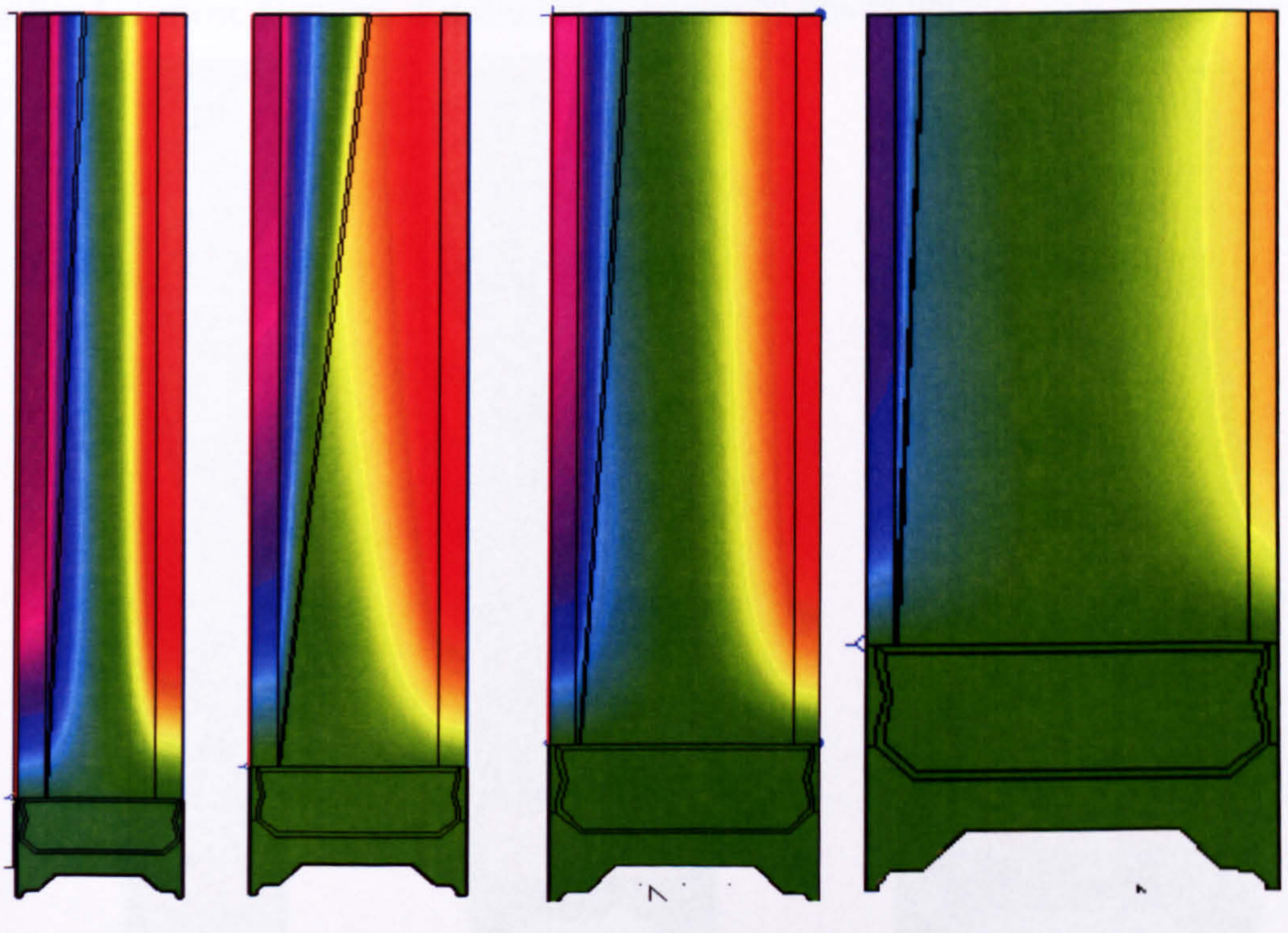

b) Inclined element; Planar temperature range in cavity: 15~25.00C◦

Figure 7.03 showing temperature distributions for two scenarios of insertion
a) Vertical cavity widths: 0.02, 0.04, 0.08m
b) Inclined cavity widths: 0.02, 0.03, 0.06 , 0.08m

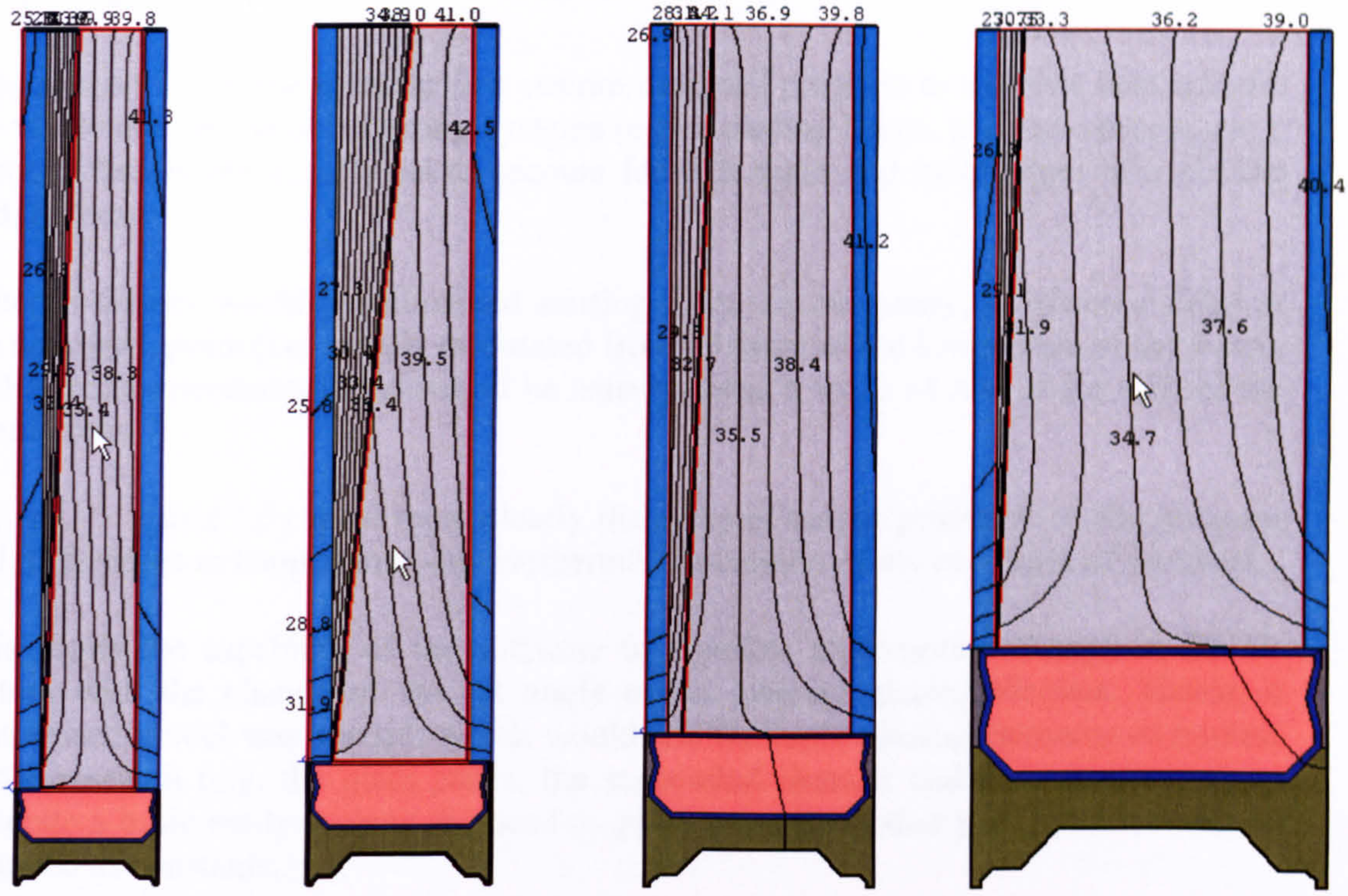

a) Inclined element; Isotherm distribution in cavity: 22.00~45.00C◦

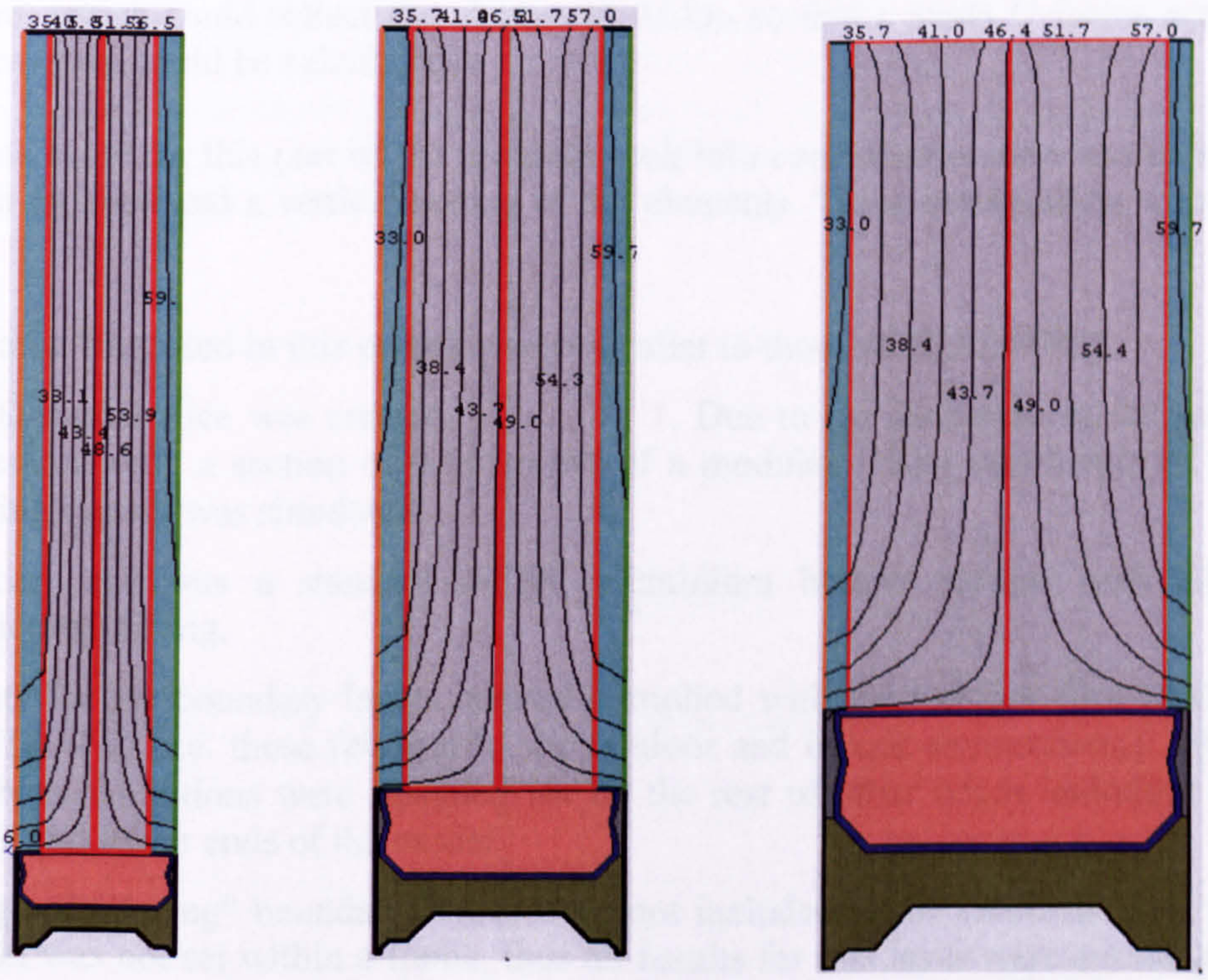

b) Vertical element; Planar Isotherm distribution in cavity: 32.00~65.00C◦

Figure 7.04 showing Isotherm distribution for two possibilities of insertion

a) Inclined; cavity widths:0.02, 0.03, 0.055 , 0.08m

b) Vertical; cavity widths: 0.02, 0.04, 0.08m

7.1.2 THERM5

This second tier of the software is a custom-designed program to simulate heat transfer for whole and inseparable glazing systems (e.g. including frame, glazing, spacers, etc.). Input U-factors are initially set to account for only outer and inner edges of a glazing and its frame.

Other U-factors would be calculated starting from, an imaginary, "*Estimated Edge of the Glazing*", point (i.e. usually calculated from 63.5mm of the lower edge of the frame, NFRC recommendation), and would be usually given a value of zero at the start of the simulations.

Figures 7.03 and 7.04 show more clearly the types of output generated by the program and differences in tempertature and isothermal distrubtion of the two types of insertion.

This limits the capability of the software to simulate an expected change in the U-factors with the change of the set angle of an inserted glazing element. Hence, a customised model was needed, which would use the basic glazing elements of interest to the research (e.g. the glass panes, the suspended element and separators) so as to generate a basic entity without the need to go into detail of other parts, which could be assumed as constants.

Consequently, customised boundary layers were created for the simulation's environment, which could reflect the change in width, so that a mean U-factor across the glazing system could be calculated.

Assumptions made for this part of the program took into consideration two sets of runs (i.e. with an inclined and a vertical setting of the element). Those assumptions were as follows:

- Material files used in this program were similar to those of *WINDOWS5*.
- A 2D model slice was created, *see fig 7.03*. Due to the limitation of the mesh generator, only a section of 0.016m out of a modular 1.00m unit-height of the glazing system was simulated.
- Spacer used was a standard NFRC aluminium hollow section with silica (desiccant) filling.
- Inputs for the boundary layers created complied with the weather files used in *WINDOWS5* (i.e. those relevant to the outdoor and indoor environment); while adiabatic conditions were assigned for all the rest of other edges including the upper and lower ends of the model.
- "Edge of Glazing" boundary layers were not included in the calculation, as the model was not set within a frame, thus all results for this layer were assumed as 0.00.
- Quad tree mesh parameters were taken as 9 per grid size of 5×5mm; maximum iterations taken were 25 per cell (those settings are the maximum allowable parameters within the program).
- Convergence tolerance: 1e-006, relaxation parameter: 1, adjustment step:-0.01.

Fig 7.05 shows output results, (i.e. centre of nodes calculation method), for two types of inserted element runs (i.e. vertical and inclined).

As the program gives the user the option to calculate the U-value of isothermal lines across a bulk sample from inside out and vice-versa, results could also show that the overall behaviour of the U-values for the two ways are similar to those of WINDOWS.

Results also show that an inclined element setting is more efficient than a similar system with a vertical setting. It can also be noted that the behaviour curve of an inclined-element setting tends to have a trend similar to that obtained from Fluent; *see chapter 6.*

The graph shows that the U-value starts to deccrease for both of the vertical and the inclined glazing systems after it has attained a 1.36 and 1.32 W/m2.K U-values for the vertical and inclined insertion respectively and as the cavity width increases.

Another interesting outcome shown in the figure, is that best expected optical behaviour for the inclined setting, i.e. assuming a modular height of 1.00m, is for a cavity width between (0.03~0.05m), giving an average U-value of 1.188 W/m^2.K for the vertical insertion; while the optium expected behaviour for the inclined insertion occurs with a U-value of 1.147 W/m^2.K. After this band width the U-value curves increased slightly before dropping again slightly to a steady trend.

Again these results are explained by the method in which Therm5 performs its calculation, as it assumes a minimised contribution to the thermal transmittance by conduction. Results have also to be kept in the context of the limitations of the software itself, as shown in *fig 7.06*, where the irregularities in the meshing of an inclined element setting could affect results*; see appendix xi for results and calculation.*

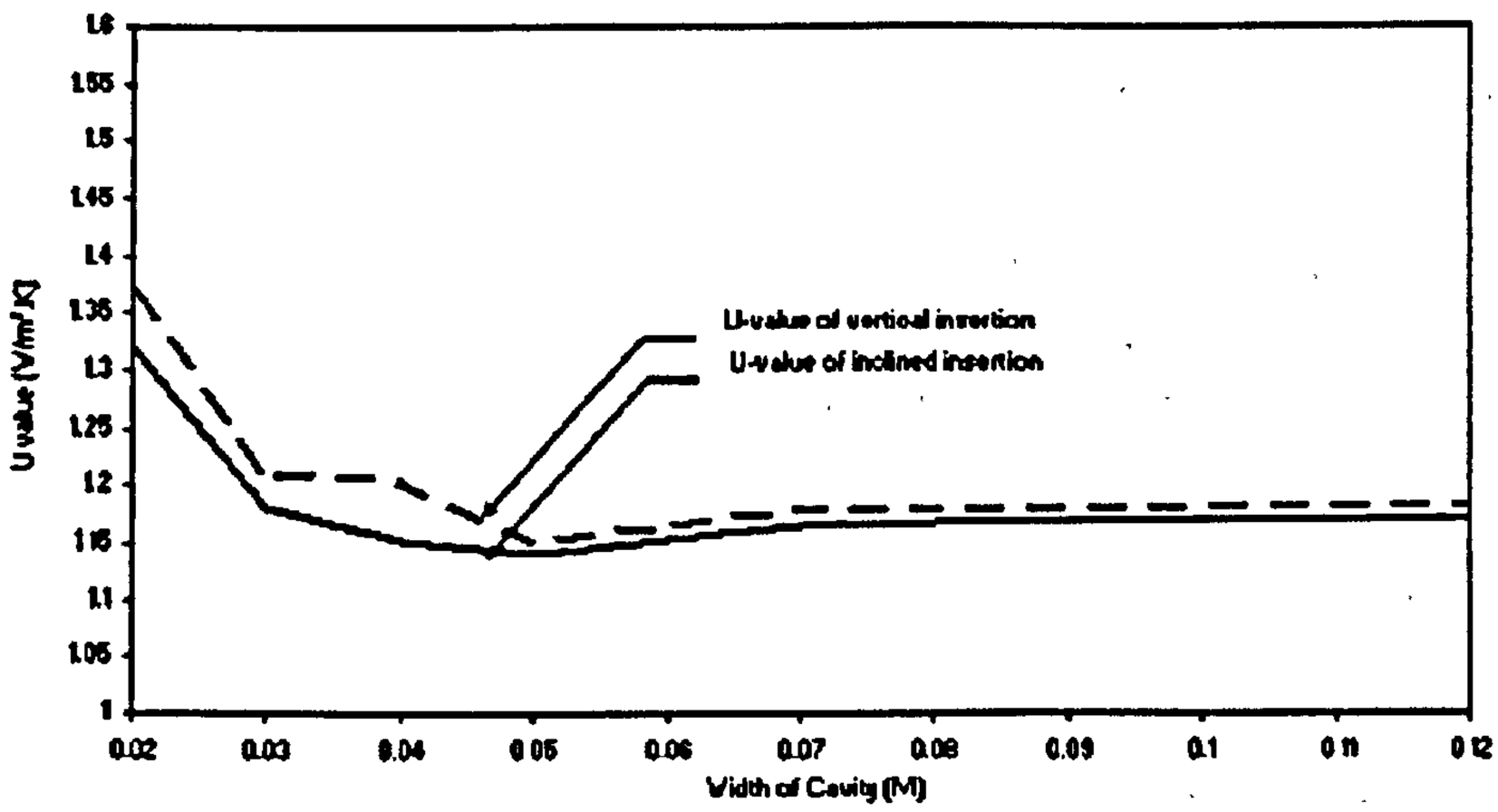

Figure 7.05 showing the mean U-value of the Glazing system in THERM5 with:

- Vertical element setting
- Inclined element setting.

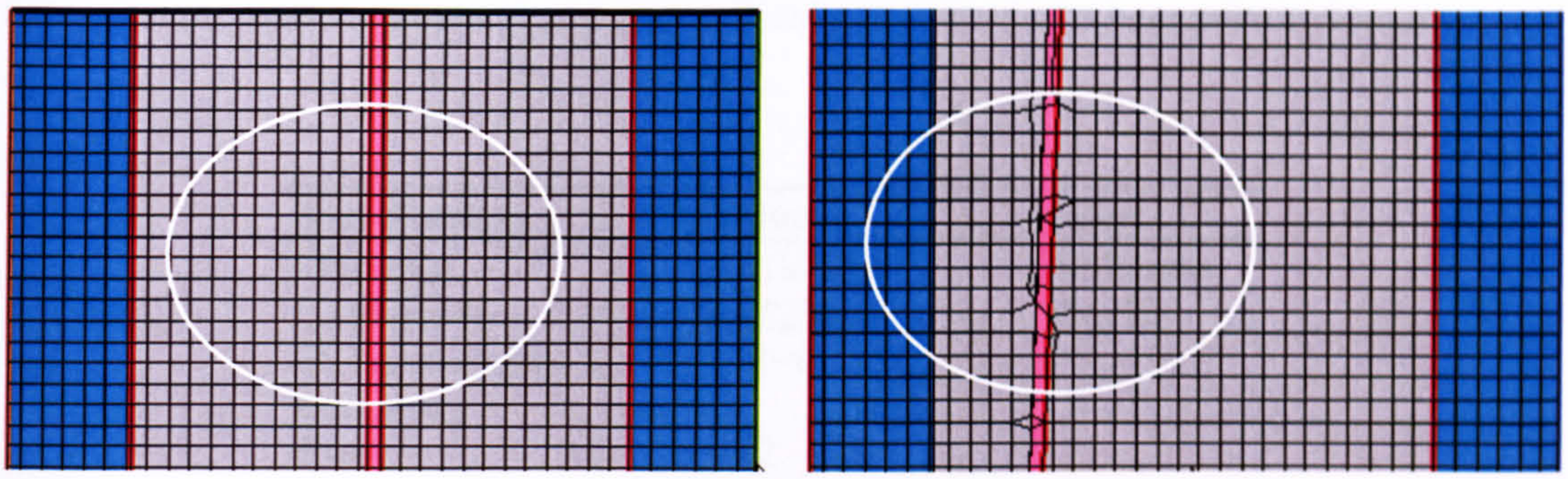

Figure 7.06 showing two sets of meshing options by *THERM5*, the mesh of the inclined option shows irregularities in meshing due to the limitation of the program to quad-meshes generation only

7.1.3 OPTICS 5

This program is used to generate a profile of optical properties of an examined sample. It relies on backup data of a large number of commercial glazings. Data is contained in a single Microsoft Access database file (*Glazing.mdb*) and can be imported or exported by Optics5 in the form of spectral data text files, which are backward compatible with WINDOW 5. It is also possible to read in newly measured data.

Due to limitation of this tier, there is no method to simulate an inclined element insertion while maintaining a vertical setting for other attached elements of the glazing system.

The program could only simulate a change of the incident angle of insolation or a change of tilt angle of a whole inseparable system from the cardinal coordinates. Thus, a customised model was built only to check the optical properties an inserted stand-alone thin element only.

Table 7.02 shows the type of profile, generated by the software, of the optical and geometrical parameters of an imported film (from the program library) that was customised to simulate an inserted element at 75° degrees from the horizon.

Figure 7.07 shows the optical behaviour of such setting; indicating a constant transmissivity across the two sides of the elements while different reflectivity ensues for each of the faces of the inserted element, i.e. still assuming a specific setting of a 75 °tilt angle of the element.

By displaying a fixed transmissivity for the two faces of the element, the result would consequently, suggest a varied absorptivity for each face of the element. Still, this result would only represent the optical characteristics of the element only not those of the whole suggested glazing system; thus concluding that this software can not fully assess the behaviour of a whole system.

Table 7.02 Showing optical and geometrical parameters of a heat mirror element.

Specifications	**Value**	**Units**
Thickness	3.81E-02	SI/Microns
Conductivity	0.1523	W/m.K
IR Transmittance	TIR=0	
Emissivity		
Front	0.82	
Back	0.85	
Product Name:		
Manufacturer:	CPFilms	Inc.
NFRC ID:	2504	
Type:	Film	
Material:	N/A	
Coating Name:	N-1035 (Neutral)	SR CDF
Coated Side:	Back	
Substrate Filename:	N/A	
Film Filename:	N/A	
Appearance:	Neutral	
Acceptance:		
Uses:		
Availability:		
Structure:		

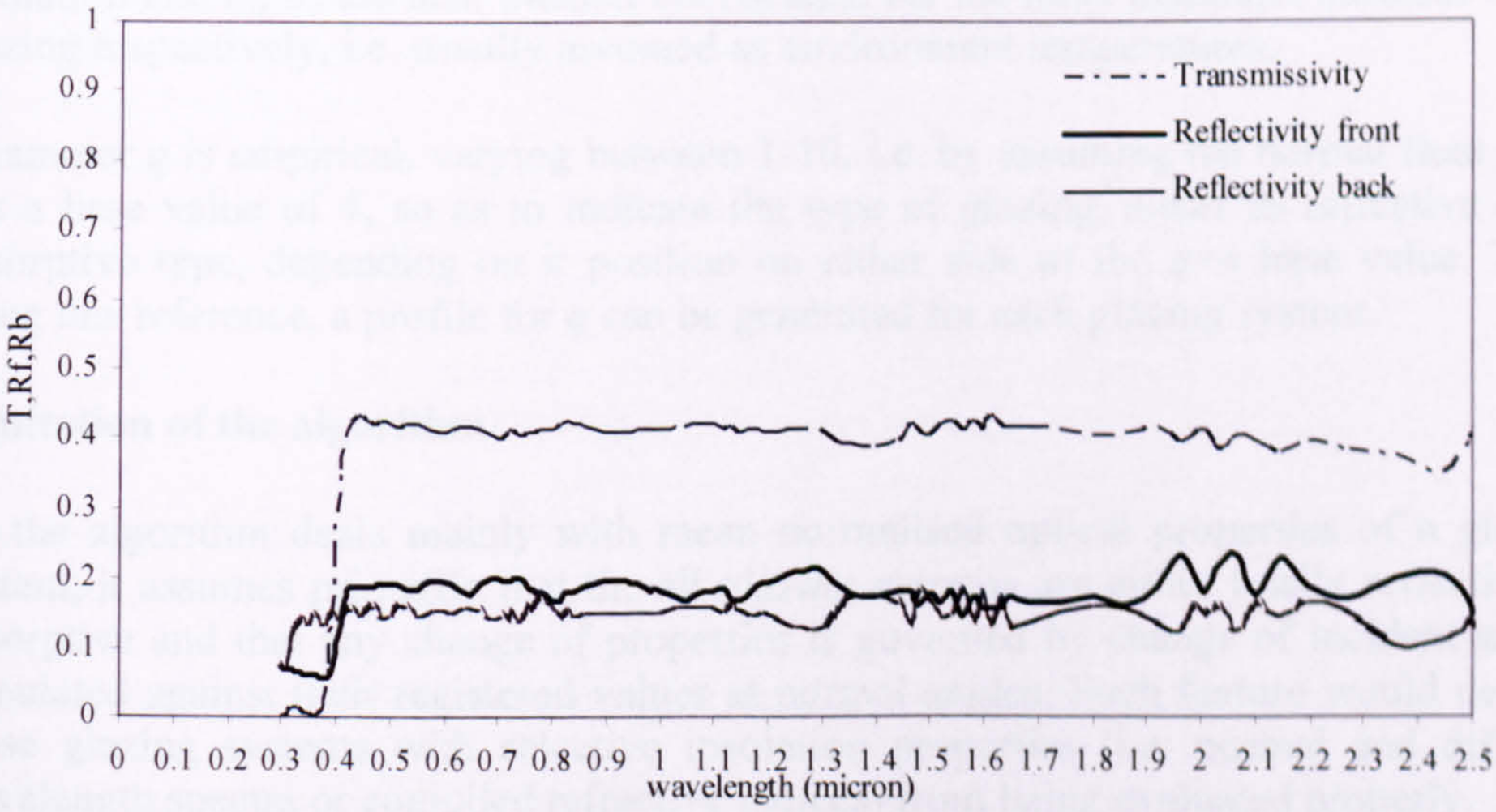

Figure 7.07 Results of Optical properties of a customised inclined glazing element (i.e. a 0.0003m PVC sheet) set at an angle of 75 degrees, using *OPTICS 5*.

7.2 CUSTOMISED ALGORITHM; THE (q) METHOD.

This algorithm was developed primarily to compare manufactured glazing systems behaviours across a widely existing variety giving an overall estimate of a system behaviour relative to its optical properties.

The method uses a customised algorithm to define an annual mean energy transmittance for glazing systems (i.e. a parameter q) at any incidence angle in the cardinal direction, relevant to the prediction of a "g-value", defined as the solar transmittance plus the absorbed part of the radiation, which is re-emitted inside the building.

(q-value) is sometimes referred to as relevant to TSET- *Total Solar Energy* Transmittance or SHGC-*solar Heat Gain Coefficient*. It is also dependent on the number of panes used in the system. The correlations between those parameters are:

$$f(p,q)_{\theta=0\text{-}90} = q(i)^{*}p(i)^{*}g_{(\theta=90)} \tag{7.001}$$

Where:

$$g_t = T_{sol} + q_i \tag{7.002}$$

And

$$q_i = A_{sol}\frac{h_i}{h_e + h_i} \tag{7.003}$$

p here is the number of panes of a glazing system, T_{sol} is the mean solar transmittance at normal incidence, i.e. this parameter is usually obtained from the glazing manufacturers. q_i here is for a single pane, A_{sol} is the visible area of the glazing subjected to the insolation and h_i, h_e are heat transfer coefficients for the inner and outer surfaces of the glazing respectively, i.e. usually assumed as environment temperatures.

Parameter q is empirical, varying between 1-10, i.e. by assuming the normal float glass has a base value of 4, so as to indicate the type of glazing, either as reflective or as absorptive type, depending on it position on either side of the q=4 base value. Thus, using this reference, a profile for q can be generated for each glazing system.

Limitation of the algorithm

As the algorithm deals mainly with mean normalised optical properties of a glazing system, it assumes primarily that the all glazing systems are either totally reflective or absorptive and that any change of properties is governed by change of incident angles calculated against their registered values at normal angles. Such feature would deprive those glazing systems with selective insolation properties (i.e. normal and diffused wavelength spectra or compiled refractive indices) from being evaluated properly.

Setting the test parameters:

Assumptions were made for a 3-layered, i.e. p=3, modular glazing of 1.00m height with a cavity width of 0.04m with an inclined element setting.

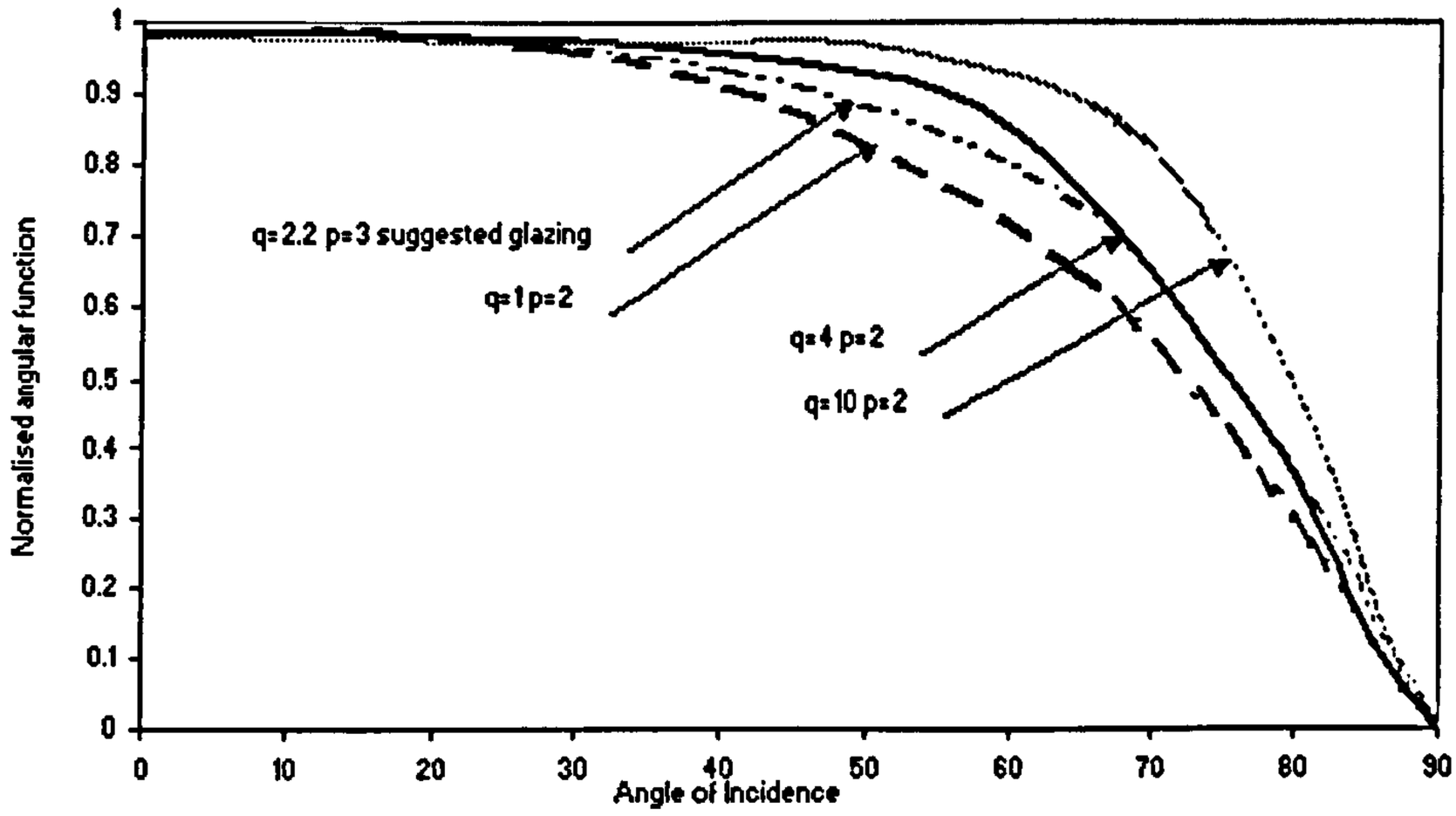

Figure 7.08 Behaviour of 0.04m width inclined element setting, using (*q*-value) polynomial curve formula.

T_{sol} was taken here as 0.6 relevant to the mean transmittance behaviour of 0.04m setting using the weather file of Kuwait/May 1996.

On applying the same methodology to predict other relevant values; it was found that q_3=2.2 and g_t=2.8, for a p=3 *See appendix xi.*

*Figure 7.08*shows the behaviour of this specific setting of the glazing calibrated by the polynomial curve and compared to other assumed types of glazing. Using the assumed base value curve where q=4 and p=2, as indicative of normal float glass double glazing. All curves results obtained to the right of this base curve would represent reflective glazing types, while those to the left of the base curve are indicative of an absorptive type. Consequently, the glazing is shown here to perform as an absorbing type (with a high extinction coefficient, K).

The result is somehow different from what is expected of such system to be a "*reflecting type*" according to results of the raytracing model.

Alternatively, changing the values for (q, g) could even generate different results, depending on changing the setting and the width of the cavity.

7.3 CUSTOMISED ALGORITHM; THE (T_{SOL}) METHOD

Another comparison was conducted using the T_{sol}, i.e. mean solar transmittance, as a base for behaviour against other relevant commercial types of coated glazing.

In this example, and still using the same input parameters of previous tests to obtain a similar value for q, the new proposal was compared with two widely used reflecting types of glazing and two other imaginary types with q=*1* and q=*2* respectively.

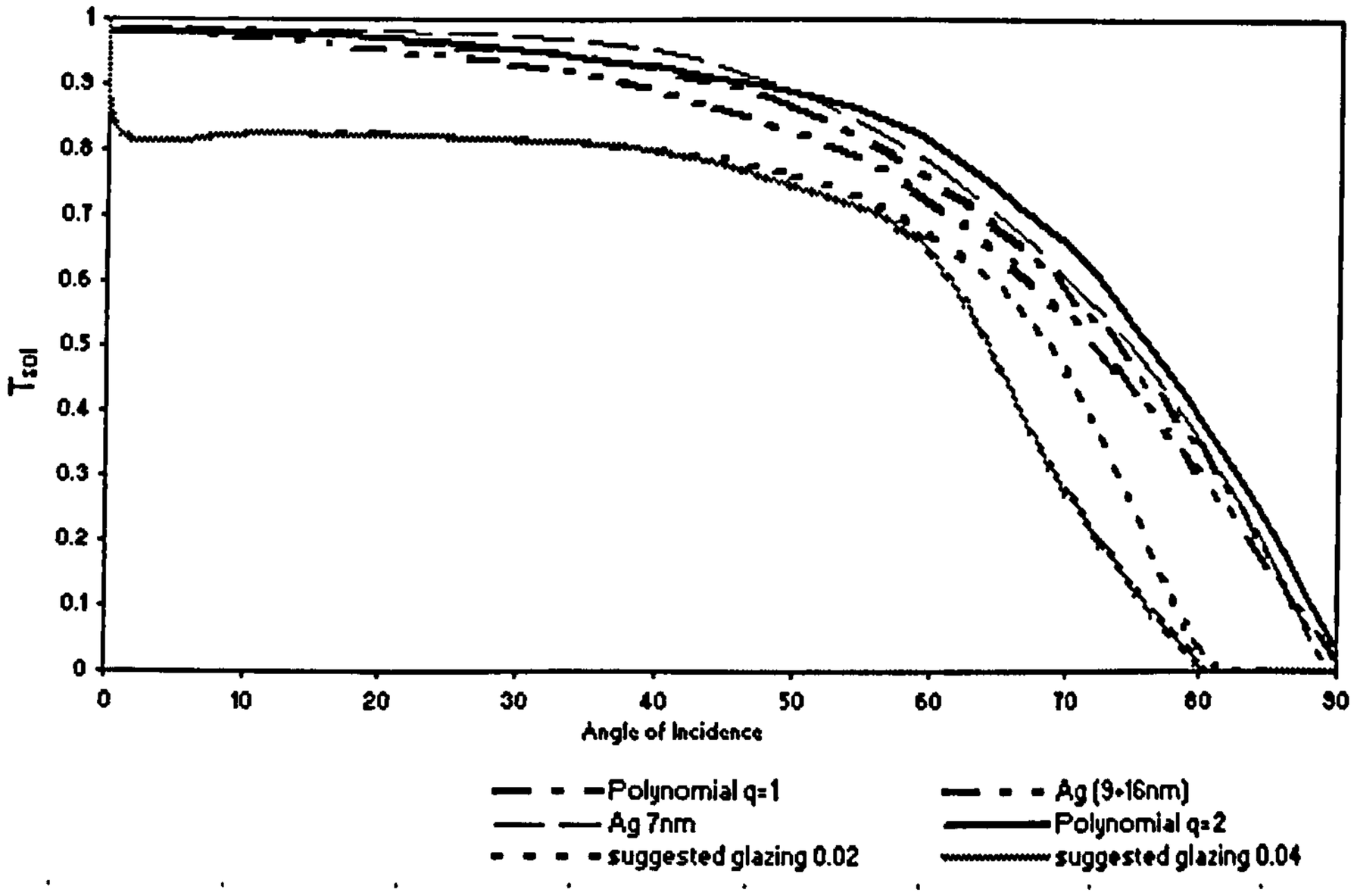

Figure 7.09 Behaviour of 0.02m, 0.04m widths inclined element setting, using (T_{sol}) polynomial curve formula compared to other known types.

A different result can be noticed here, *see fig 7.9*, when modelling two cavity widths of 0.02, 0.04m. It shows an interesting behaviour of T_{sol} when compared to the other types, i.e. due to the varying reflective ability of the inserted element with the change in the solar incidence angle.

Still, results show a substantial difference in mean solar transmissivity, compared with the other *q=1* and *q=2*, which in turn are supposed to be better reflectors, *see fig. 7.09.*

These results lead to the conclusion that this method is limited and would not be adequate to calibrate systems with selective glazing properties.

7.4 THE PROPOSED SYSTEM AS A COMMERCIAL PRODUCT

It would be impossible to make an assessment of the commercial viability of the proposed system as a product without experimental work to assess its behaviour in real life conditions and address the practical issues that would not be noticeable in a simulation environment.

However if the proposed system is to be compared to a list of similar products (Energy comfort 2000), e.g. double and triple glazing systems, with or without high performance coating or inert gases, it can be noticed that the system can be classified as a reflective type product with a relatively low U-value and reasonable $T_{visible}$ and T_{sol} values; *see table 7.03.*

The values quoted in the table are for centre of glazing U-values, they are also normalised over the range of solar incidence angles between 0-90° and for the range of latitudes considered; the behaviour of the suggestion would vary with the change in those angle.

Table 7.03 shows the suggestion compared against other known commercial systems.

type of pane	U-value W/m^2K	$T_{visible}$ %	T_{solar} %
clear glass			
single glass 0.004m	6	88	83
Double glass with air (4-12-4)	3	80	76
Double glass, low-E coating, with Argon (4-12-4)	1.5	77	65
Triple glass, with air (4-12-4-12-4)	2	72	67
Triple glass, with Low E coating & Argon	1.2	70	60
Vacuum pane with Low-E coating (4-12-4)	0.5	77	65
Reflective glass			
Double medium reflective glass with Low-E coating (6-12-6)	1.6	29	39
Double glass, Bronze+ Low-E coating with Argon (6-12-6)	1.6	9	13
Proposed system, floating glass+ Polystyrene with Air (6-10-0.0001-10-6)	1.28	52	69

Finally, the proposed system is relatively similar in behaviour to glazing systems with vertical insertion, e.g. heat mirror types, which are patented by Westside Technologies™.

Conclusion

Behaviour of the proposed glazing system was verified using various commercial tools. Two main aspects of its behaviour were analysed through the calibration process:

- U-values for the centre of glazing across the simulated environments.
- Expected optical properties of the system calculated as a performance of a bulk sample.

Despite geometric and meshing limitations in the modelling techniques of those tools; the research worked on matching, whenever possible, the calculation environment, type of materials used and physical dimensions of the 2D models involved.

Several points could be highlighted from this comparison:

(i) Though, those tools currently do not have the ability to calibrate angle-selective types of glazing; the type of results obtained suggests a similar behaviour in inhibiting direct solar radiation as expected of the proposed glazing system.

(ii) The behaviour of the suggested glazing as a separate bulk sample could not be calibrated efficiently by any of those tools, thus suggesting a lesser possibility to

include the new suggestion model as a new block within the existing commercial tools, without adding the calculation block suggested; *see chapter 6 discussion.*

(iii) Results from THERM and WINDOWS are similar in nature but they are different to those obtained through FLUENT for the same parameters.

(iv) Having an inclined angle with the inserted element yields different results to those obtained from a vertical setting.

(v) Results obtained show a similarity, to FLUENT results, of the optimal suggested width for best behaviour. Thus again calling for experimental work to validate the simulated results.

(vi) Discrepancies in results can be explained by the different theoretical background of the software used and the degree of accuracy sought in them.

(vii) Initially, the suggestion has a commercial potential, when compared to other conventional systems.

References

1. Mitchell R. et al, Therm 5 / WINDOW5, NFRC. Simulation manual. California USA, Lawrence Berkeley National Laboratory 2002.
2. Energy Comfort 2000, Information Dossier, Windows –The Key to Low Energy Design; European Commission Thermie Project to reduce energy and improve comfort and environment; (5) March 1998.
3. ISO/DIN 15099, Thermal Performance of Windows, Doors and Shading Devices, Detailed Calculations, ISO Central Secretariat, Geneva, Switzerland 2003.
4. Yang Y, Supervisor: Curcjia D.C, Natural convective flow and heat transfer in vertical and inclined glazing cavities. Master thesis; Graduate School of the University of Massachusetts Amherst. USA, September 2003

CHAPTER EIGHT

CONCLUSIONS AND EXPECTED FUTURE WORK

Introduction

Several developments are introduced daily to the market of commercial glazing systems. Most of these developments are mainly to deal with enhancing the performance of glazing systems by introducing either:

(i) New glazing materials, i.e. coatings, films and or other enhanced types of glazing and glass.

(ii) New gases, i.e. filling the gaseous cavities in multiple systems.

(iii) New insulation materials and methodology to minimise heat losses and thermal bridging across the glazing system and its components.

(iv) New geometries for the systems; either by introducing multiple glazing panes or new methods for insertion of elements that would either inhibit or enhance transfer of energy across the glazing system, relevant to the functions sought.

(v) Smart windows.

(vi) A combination of some or all of the above.

The proposed glazing system discussed in this research would fall into the new geometry category (iv). However, the type of results obtained from the simulation suggests that there is still a considerable amount of future work needed to prove the hypothesis and back up the system performance results by experimental and analytical data.

Several points could be specifically highlighted from reading into the separate conclusions at the end of each chapter. Those points would establish the frame to consider the whole exercise and assess its performance and practicality as an application. The research tried to summarise the main points highlighted throughout the research:

8.1 HIGHLIGHTS OF THE CONCLUSIONS

(i) A novel type of multiple glazing system was *proposed* for latitudes of high rates of insolation, which can inhibit the direct component of insolation while allowing acceptable amounts of the diffused component (day light) to enter the buildings.

(ii) Selective glazing technology has advanced significantly in the last three decades, with two main trends of solar selective glazing that could be roughly redefined as; glazing with wavelength selectivity and glazing with incorporated angular selectivity.

It was shown that for best performance of the angular selective types, i.e. similar to the proposed system, they should be used in multi-layers to enhance their solar control performance, which will weaken respectively their visible transmittance and view maintenance, hence the need for a new and more simplified approach to selective incorporated angular selectivity glazing.

(iii) Different methods exist to calibrate the performance and rating of current glazing systems, relevant to countries, manufacturers and the purpose of the glazing. There is ongoing research to have a unified base upon which most systems could be calibrated.

(iv) Several current commercial glazing models, i.e., WINDOWS5.2, *THERM5*.2 of NBL, etc. were investigated, also customised algorithms, i.e., g-value of (karlsson & Ross 1999), or following models of (*p and q*) (karlsson 2000). All of these models and algorithms, apart from the *Equivalent Models*"(EM), (Montechi *et al.* 1999), shared one apparent disadvantage; the software can simulate a glazing system if the whole system is tilted on its global axis, as there is no built-in capacity to simulate heat transfer in a vertical system with components tilted individually. Such statement could be explained by looking into the inherited theoretical background for all of these systems, i.e., using centre of nodes approach in their finite element methodology. Recent release of WINDOWS6 has included new blocks within the software to simulate integrated shading devices within the cavity; the blocks solve mainly the fixed angles integrated slats using numerical regressions.

On the other hand, more complex tools, e.g. CFD software might not be able to simulate the optical properties or assess properly the performance of the semi transparent materials of glazing systems, as they are considered as grey objects in calculation. Hence, the need for an angle dependant simulation package i.e., raytracing technique, combined with a CFD modelling for convection and conduction, (Ćurčija C 2002). to cater for losses in energy transfer, through reflection and not just in absorption.

(v) The research *developed* customised raytracing software that uses the non-sequential algorithm of raytracing to assess the optical behaviour of the proposed system, as part of the comprehensive assessment process. Using the customised algorithm has helped in better understanding of the radiative heat transfer process, still there were issues regarding the level of accuracy of results needed and lack of experimental work to verify obtained data.

(vi) SMARTS2 was chosen as a base for the first tier of the assessment tool, i.e. as an insolation model, despite several reservations on the software and the algorithm it uses, which are registered and reported; *see chapter two*. It was felt that the type of input needed for the software are more relevant to the available empirical data, hence the decision.

(vii) Studying the input parameters at the different tiers of SMARTS2 software, especially turbidity factors have indicated that there is a stronger relation, than that was previously anticipated, between turbidity factors, humidity and the diffuse component of insolation.

(viii) Consequently, the research also *developed* a turbidity local code for Kuwait weather using the local meteorological and dust concentration data of 1996. Results were more in agreement with available empirical irradiation data than those obtained through built in data in SMARTS2 software. However, further investigation is recommended which would be beyond the boundary of the current work, *see chapter five.*

(ix) Numerous geometrical settings for the suggestion were investigated, e.g. angle dependent, type of insertion, and different simulation scenarios were assessed e.g. time and latitude related, to ascertain the hypothesis, *see chapter six.*

Results showed that there is a more positive and stable contribution by the proposed system towards inhibiting the convection regimes, i.e. in heat transfer, rather than that to the radiation regime, i.e. relevant to the direct component of insolation.

This could also means that the suggestion could be used commercially and with practical width of cavity measurement setting.

There would be a incremental difference in systems' transmissivity behaviour, about 4% between an inclined inserted element, at a set angle e.g. 89-87° with a practical cavity width of 0.02-0.04m from that of a normal angle insertion setting, i.e. with regard to inhibiting the radiative effect of the direct component; *see chapter six, figs. 6.09&6.10* respectively. This would apply especially in high incidence angles.

However the latter statement would change inversely in favour of the proposed system by increasing the cavity width or when the incidence angles are low. Difference in transmissivity could be up to 30%. The proposed system would also perform better than other commercial systems if comparison were based on the level of control on the transmission of the diffused component of insolation.

(x) The lengthy CPU time spent, throughout the simulations, suggests that the adopted methodology of calculation, e.g. SMARTS2+the new raytracing software+Fluent would be difficult to assimilate, as a simulation block, in the current commercial software. Still new research is increasingly suggesting that raytracing techniques are becoming more reliable to simulate radiative heat transfer in glazing systems, (Anderson M. 2003).

(xi) The research has also *developed* a new set of correlation-based equations that might be further developed to a simulation block that could be plugged into current commercial software, e.g. WINDOWS, if those software use SMARTS2 and finite element blocks as platforms for their simulations; *see chapter six discussions.*

(xii) Regarding cost effectiveness, only basic glazing materials for modelling the new proposed system were used, leading to competent results compared to the performance of current commercial systems that use enhanced and more expensive optical materials. This suggests that the system has the potential to have a commercial viability and competence with regard to relevant types of multiple glazing systems.

(xiii) Another task of any next phase of the research would be to look into applying the methodology of suspension into systems with more enhanced optical materials to evaluate any added benefit, oversee the logistic problems of suspension in the cavity and the operational and/or optimum insertion angles.

It is also worth mentioning that the patent method of suspended semi transparent thin elements in glazing systems is currently managed by only one American group (*i.e. Westside technologies*).

(xiv) Additionally, more suggested work is still to be done to explore and resolve other aspects of the proposal, i.e. materials used, method of inserting and sustaining the transparent element in the system's cavity, or changing the number and types of the insertion. Such stipulated work should look at:

8.2 EXPERIMENTAL WORK

Experimental work is needed to support the findings of the current research. Such future work would concentrate on assessing the visual, optical and thermal aspects of the proposed system. It would also be able to address other operational factors that relate to:

- The method of keeping the inserted element accurately suspended at an optimal angle without distorting, due to the effect of gravity or the effect of the gaseous cavity convectional forces.

- The Practicality and aesthetics, of the proposal by investigating an acceptable width to height proportion in the system's geometry and, thus, the method of integrating the system within the current structural fabric of buildings.

- The possibility of using the same hypothesis for glazing systems used in cold countries, i.e. latitudes 54-69°North. A suggestion could be introduced where the system is rotated on its Y-global axis, so the angle of insertion would face the inner side of i.e. a room space. Such modification would allow the system theoretically to reduce the effect of heat losses by thermal radiation and still minimise the convectional forces in the gaseous cavity.

8.3 MATERIALS:

As shown, basic properties were assumed for the materials, used in the simulations, so as to be considered as constants in calculations:

- 6.00mm Float glass was assumed for the glass panes.

- Normal optical and transparent polystyrene was assumed for the inserted element.

- Dry air was assumed to replace the inert gases, commonly used in the gaseous cavity.

- Standard aluminium with a grated or un-polished surface was used as a material for the spacers in the gaseous cavity.

Such decision was taken, as previously indicated, to minimise the CPU time needed for the simulations.

Alternatively, more work could be directed to investigate the performance of the system, if such basic materials are to be replaced with others of enhanced optical and thermal properties.

Part of the recommended research would be, then, directed to investigate the feasibility of using such enhancements and stipulate the level of system's efficiency and performance both thermally and optically.

8.4 GEOMETRY OF THE SUGGESTION

A modification to the proposed system geometry could be considered for enhancing the performance. It tries to address the issue of increased convectivity with the increase of the width of the cavity, so to achieve an optimal insertion angle.

Maintaining one inserted element in the cavity could be seen as a limitation to the hypothesis, as achieving an optimal insertion angle would be affected by aesthetical and structural constraints governed by a practical height to a width ratio for the glazing system geometry.

A modification to the current geometry is to be introduced where more set angled elements are set into the cavity (i.e. still maintaining an optimal set angle of insertion, which has to be calculated), *see figure 8.01*; thus forming a set of transparent "*louvers*" within the gaseous cavity and eventually, maintaining a practical width for the cavity without forsaking performance.

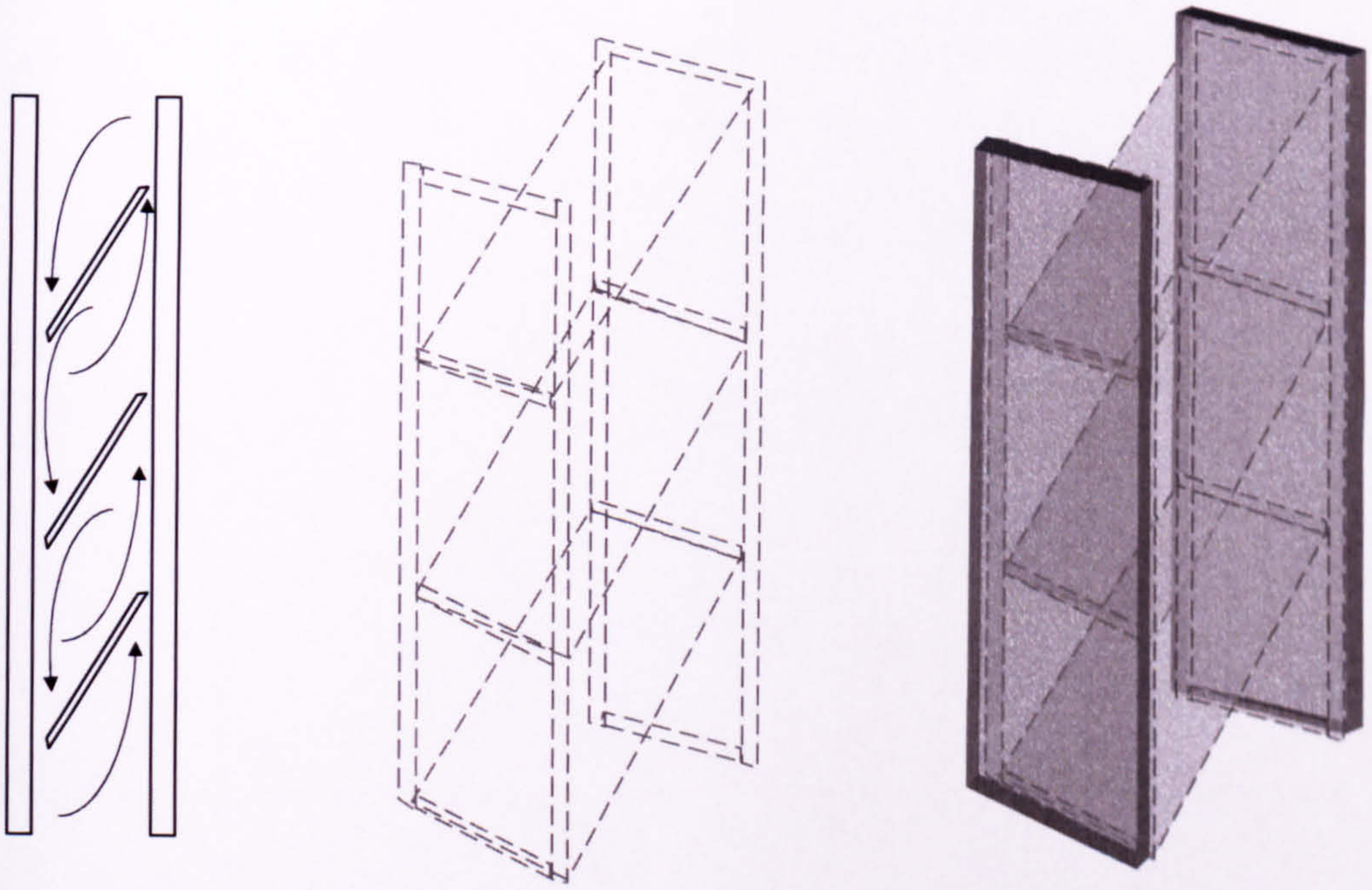

a. *b.* *c.*

Figure 8. 01 shows a sketch of the suggested system.

a. Cross-section of the system. b. Axonometric of the louvers. c. Overall layout of the system

Such modification seeks to further inhibit the effect of convection forces in the cavity. As the angled *louvers* would be set to not to touch the surface of the outer or the inner glazing and as with minimal cross-area, there will be minimal effect of an increased conduction. Such statement could be further explained by the set up of the transparent "*louvers*", *see fig. 8. 01, b*; it shows that they would be joined by a skeletal frame of the same transparent material running along the side spacers of the glazing system, thus causing the *louvers* to be freely suspended in the gaseous cavity.

Also, such enhanced system would cause minimal obstruction to visibility, as it would have the same refraction index of the adjacent glass panes, hence not causing *optical edges.* The future work will set to investigate how such proposal would be able to perform.

On the other hand, having the ability to bend the system's geometry, due to the small spans of the insertion, without affecting the performance would increase the possibility of its applications (i.e. could be used in vaulted or arched openings or in automobile windshields).

LIST OF PUBLICATIONS

1. Askar H., Probert S.D., Batty W.J. Windows for buildings in hot arid countries In: Applied Energy, Elsevier Science Ltd, 2001,70: 77–101.

2. Askar H., Batty W.J. Suggestion for a new multiple glazing system for hot arid countries. Editor: CISBAT 2001, Solar Energy in Buildings-International conference, Ecole polytechnique fédérale de Lausanne. Lausanne, Switzerland, 3-4 October 2001.

3. Askar H., Batty W.J. Assessing the performance of SMARTS2 in a first tier of software using empirical weather data. Conference paper in: Measurement and modeling of solar radiation & daylight- Challenges for the 21st Century, Napier University, Edinburgh, Scotland 2003.

4. *Askar H., Batty W.J. Assessing the performance of the "Simple Model of the Atmospheric Radiative Transfer of Sunshine" (SMARTS2) in a first tier of software using empirical weather data. In: Energy, Elsevier Science Ltd, 2005, 30(9): 1577-1588.*

LIST OF APPENDICES

Please refer to the attached CD for details of appendices.

(i) Appendix i: SMARTS2 Software:
i.1: appendices\appendix i\appendix i dry_sand.dat
i.2: appendices\appendix i\Appendix i smarts2.FOR.txt
i.3: appendices\appendix i\appendix i SMARTS2 read me file.doc

(ii) Appendix ii: Raytracing Software:
ii.1: appendices\appendix ii\appendix ii-1 SOFTWARE RAYTRACIN1.doc
ii.2: appendices\appendix ii\appendix ii-2 RAYTRACING README.doc

(iii) Appendix iii: Empirical data
iii.1:appendices\appendix iii\appendix iii-1 kw monthly rad.xls
iii.2:appendices\appendix iii\appendix iii-2 dust21 kuwait.xls
iii.3: appendices\appendix iii\appendix iii-3 kw quarterly dust.xls

(iv) Appendix iv: Astronom Software Results:
iv.1: appendices\appendix iv\appendix iv-1 Algers file.txt
iv.2:appendices\appendix iv\appendix iv-2 Egypt file.txt
iv.3:appendices\appendix iv\appendix iv-3 Iran file.txt
iv.4:appendices\appendix iv\appendix iv-4 iraq file.txt
iv.5:appendices\appendix iv\appendix iv-5 Israel file.txt
iv.6: appendices\appendix iv\appendix iv-6 Jordan file.txt
iv.7: appendices\appendix iv\appendix iv-7 kuwait file.txt
iv.8:appendices\appendix iv\appendix iv-8 Saudi Arabia file.txt

(v) Appendix v CFD Raw Data:
v.1:appendices\appendix v\appendix 10-materials properties.doc
v.2: appendices\appendix v\appendix Hc Values Summer
v.3: appendices\appendix v\appendix Hc Values Winter
v.4: appendices\appendix v\appendix Hc-Vertical-Summer
v.5: appendices\appendix v\appendix Results Study
v.6: appendices\appendix v\appendix CFD Contours Results
v.7: appendices\appendix v\appendix Refractive Index

(vi) Appendix vi: countries- SMARTS2
Algers:
vi.1.a: appendices\appendix vi\vi-1 Algers\August\vi-1.a Algers_inp.htm
vi.1.b: appendices\appendix vi\vi-1 Algers\August\vi-1.b Algers_OUT.htm
vi1.c:appendices\appendix vi\vi-1 Algers\January\vi.1.c Algers _OUT.htm
vi.1.d:appendices\appendix vi\vi-1 Algers\January\vi-1.d Alger_inp.htm
Egypt:
vi.2.a:appendices\appendix vi\vi-2 Egypt\August\vi-2.a Egypt_inp.htm
vi.2.b:appendices\appendix vi\vi-2 Egypt\August\vi-2.b egypt_OUT.htm
vi.2.c:appendices\appendix vi\vi-2 Egypt\January\vi-2.c Egypt_inp.htm
vi.2.d:appendices\appendix vi\vi-2 Egypt\January\vi-2.d egypt_OUT.htm
Iran:
vi.3.a: appendices\appendix vi\vi-3 Iran\August\vi-3.a Iran_inp.htm

vi.3.b:appendices\appendix vi\vi-3 Iran\August\vi-3.b iran_OUT.htm
vi3.c: appendices\appendix vi\vi-3 Iran\January\vi-3.c Iran_inp.htm
vi.4.d:appendices\appendix vi\vi-3 Iran\January\vi-3.d iran_OUT.htm
Iraq:
vi.4.a:appendices\appendix vi\vi-4 Iraq\August\vi-4.a Iraq_inp.htm
vi.4.bappendices\appendix vi\vi-4 Iraq\August\vi-4.b iraq_OUT.htm
vi.4.cappendices\appendix vi\vi-4 Iraq\January\vi-4.c Iraq_inp.htm
vi.4.dappendices\appendix vi\vi-4 Iraq\January\vi-4.d iraq_OUT.htm
Israel:
vi.5.a.:appendices\appendix vi\vi-5 Israel\August\vi-5.a Israel_inp.htm
vi.5.b:appendices\appendix vi\vi-5 Israel\August\vi-5.b israel_OUT.htm
vi.5.c:appendices\appendix vi\vi-5 Israel\January\vi-5.c Israel_inp.htm
vi.5.d:appendices\appendix vi\vi-5 Israel\January\vi-5.d israel_OUT.htm
Jordan:
vi.6.a:appendices\appendix vi\vi-6 Jordan\August\vi-6.a Jordan_inp.htm
vi.6.b:appendices\appendix vi\vi-6 Jordan\August\vi-6.b jordan_OUT.htm
vi.6.c:appendices\appendix vi\vi-6 Jordan\January\vi-6.c Jordan_inp.htm
vi.6.d:appendices\appendix vi\vi-6 Jordan\January\vi-6.d jordan_OUT.htm
Saudi Arabia:
vi.7.a:appendices\appendix vi\vi-7 Saudi Arabia\August\vi-7.a Saud_inp.htm
vi.7.b:appendices\appendix vi\vi-7 Saudi Arabia\August\vi-7.b Saud_OUT.htm
vi.7.c:appendices\appendix vi\vi-7 Saudi Arabia\January\vi-7.c Saud_inp.htm
vi.7.d:appendices\appendix vi\vi-7 Saudi Arabia\January\vi-7.d saud_OUT.htm

(vii) Appendix vii: SMARTS2-Kuwait
vii.1.a: appendices\appendix vii\Kuwait vii.1\vii.1.a kuwait_inp.htm
vii.1.b: appendices\appendix vii\Kuwait vii.1\vii.1.b kuwait_OUT.htm
February:
Vii2.a:appendices\appendix vii\Kuwait vii.2\vii.2.a kuwait_inp.htm
vii.2.b:appendices\appendix vii\Kuwait vii.2\vii.2.b kuwait1_OUT.htm
March
vii.3.a:appendices\appendix vii\Kuwait vii.3\vii.3.a kuwait_inp.htm
vii.3.b:appendices\appendix vii\Kuwait vii.3\vii.3.b kuwait_OUT.htm
April:
vii.4.a:appendices\appendix vii\Kuwait vii.4\vii.4.a kuwait_inp.htm
vii.4.b:appendices\appendix vii\Kuwait vii.4\vii.4.b kuwait_OUT.htm
May:
vii.5.a:appendices\appendix vii\Kuwait vii.5\vii.5.a kuwait_inp.htm
vii.5.b:appendices\appendix vii\Kuwait vii.5\vii.5.b kuwait1_OUT.htm
June:
vii.6.a:appendices\appendix vii\Kuwait vii.6\vii.6.a kuwait1_inp.htm
vii.6.b:appendices\appendix vii\Kuwait vii.6\vii.6.b kuwait1_OUT.htm
July:
vii.7.a:appendices\appendix vii\Kuwait vii.7\vii.7.a kuwait1_inp.htm
vii.7.b:appendices\appendix vii\Kuwait vii.7\vii.7.b kuwait1_OUT.htm
August:
vii.8.a:appendices\appendix vii\Kuwait vii.8\vii.8.a kuwait1_inp.htm
vii.8.b:appendices\appendix vii\Kuwait vii.8\vii.8.b kuwait1_OUT.htm
September:
vii.9.a:appendices\appendix vii\Kuwait vii.9\vii.9.a kuwait1_inp.htm
vii.9.b:appendices\appendix vii\Kuwait vii.9\vii.9.b kuwait1_OUT.htm
October:
vii.10.a:appendices\appendix vii\Kuwait vii.10\vii.10.a kuwait1_inp.htm
vii.10.b:appendices\appendix vii\Kuwait vii.10\vii.10.b kuwait1_OUT.htm
November:

vii.11.a:appendices\appendix vii\Kuwait vii.11\vii.11.a kuwait1_inp.htm
vii.11.b:appendices\appendix vii\Kuwait vii.11\vii.11.b kuwait1_OUT.htm
December:
vii.12.a:appendices\appendix vii\Kuwait vii.12\vii.12.a kuwait1_inp.htm
vii.12.b:appendices\appendix vii\Kuwait vii.12\vii.12.b kuwait1_OUT.htm

(viii) Appendix viii: Kuwait-SMARTS2 (2)
viii.1: appendices\appendix viii\kuwait6_OUT.txt
viii.2: appendices\appendix viii\kuwait7_OUT.txt
viii.3:appendices\appendix viii\kuwait8_OUT.txt
viii.4:appendices\appendix viii\kuwait9_OUT.txt
viii.5:appendices\appendix viii\kuwait10_OUT.txt
viii.6:appendices\appendix viii\kuwait11_OUT.txt
viii.7:appendices\appendix viii\kuwait12_OUT.txt
viii.8:appendices\appendix viii\kuwait13_OUT.txt
viii.9:appendices\appendix viii\kuwait14_OUT.txt
viii.10:appendices\appendix viii\kuwait15_OUT.txt
viii.11:appendices\appendix viii\kuwait16_OUT.txt
viii.13:appendices\appendix viii\kuwait17_OUT.txt
viii.14:appendices\appendix viii\kuwait18_OUT.txt

(ix) Appendix ix: Countries Rayrtracing
Algers:
ix.1.a: appendices\appendix ix\Algers\ix.1.a algers-nb-Jan input.txt
ix.1.b: appendices\appendix ix\Algers\ix.1.b algers-nb-Jan output.txt
ix1.c: appendices\appendix ix\Algers\ix.1.c algers-db-Jan input.txt
ix.1.d: appendices\appendix ix\Algers\ix.1.d algers-db-Jan output.txt
ix.1.e:appendices\appendix ix\Algers\ix.1.e algers-nb-Aug input.txt
ix.1.f:appendices\appendix ix\Algers\ix.1.f algers-nb-Aug output.txt
ix.1.g:appendices\appendix ix\Algers\ix.1.g algers-db-Aug input.txt
ix.1.h:appendices\appendix ix\Algers\ix.1.h algers-db-Aug output.txt
Egypt:
ix.2.a: appendices\appendix ix\Egypt\ix.2.a Egypt-nb-Jan input.txt
ix.2.b: appendices\appendix ix\Egypt\ix.2.b Egypt-nb-Jan output.txt
ix.2.c: appendices\appendix ix\Egypt\ix.2.c Egypt-db-Jan input.txt
ix.2.d: appendices\appendix ix\Egypt\ix.2.d Egypt-db-Jan output.txt
ix.2.d:appendices\appendix ix\Egypt\ix.2.e Egypt-nb-Aug input.txt
ix.2.e:appendices\appendix ix\Egypt\ix.2.f Egypt-nb-Aug output.txt
ix.2.f:appendices\appendix ix\Egypt\ix.2.f Egypt-nb-Aug output.txt
ix.2.g:appendices\appendix ix\Egypt\ix.2.g Egypt-db-Aug input.txt
ix.2.h:appendices\appendix ix\Egypt\ix.2.h Egypt-db-Aug output.txt
Iran
ix.3.a: appendices\appendix ix\Iran\ix.3.a Iran-nb-Jan input.txt
ix.3.b: appendices\appendix ix\Iran\ix.3.b Iran-nb-Jan output.txt
ix3.c: appendices\appendix ix\Iran\ix.3.c Iran-db-Jan input.txt
ix.3.d:appendices\appendix ix\Iran\ix.3.d Iran-db-Jan output.txt
ix.3.e:appendices\appendix ix\Iran\ix.3.e Iran-nb-Aug input.txt
ix.3.f:appendices\appendix ix\Iran\ix.3.f Iran-nb-Aug output.txt
ix.3.g:appendices\appendix ix\Iran\ix.3.g Iran-db-Aug input.txt
ix.3.h:appendices\appendix ix\Iran\ix.3.h Iran-db-Aug output.txt
Iraq:
ix.4.a:appendices\appendix ix\Iraq\ix.4.a Iraq-nb-Jan input.txt
ix.4.b:appendices\appendix ix\Iraq\ix.4.b Iraq-nb-Jan output.txt
ix.4.c: appendices\appendix ix\Iraq\ix.4.c Iraq-db-Jan input.txt
ix.4.d:appendices\appendix ix\Iraq\ix.4.d Iraq-db-Jan output.txt

ix.4.e:appendices\appendix ix\Iraq\ix.4.e Iraq-nb-Aug input.txt
ix.4.f:appendices\appendix ix\Iraq\ix.4.f Iraq-nb-Aug output.txt
ix.4.g:appendices\appendix ix\Iraq\ix.4.g Iraq-db-Aug input.txt
ix.4.h:appendices\appendix ix\Iraq\ix.4.h Iraq-db-Aug output.txt
Israel:
ix.5.a.: appendices\appendix ix\Israel\ix.5.a Israel-nb-Jan input.txt
ix.5.b: appendices\appendix ix\Israel\ix.5.b Israel-nb-Jan output.txt
ix.5.c: appendices\appendix ix\Israel\ix.5.c Israel-db-Jan input.txt
ix.5.d:appendices\appendix ix\Israel\ix.5.d Israel-db-Jan output.txt
ix.5.e: appendices\appendix ix\Israel\ix.5.e Israel-nb-Aug input.txt
ix.5.f: appendices\appendix ix\Israel\ix.5.f Israel-nb-Aug output.txt
ix.5.g: appendices\appendix ix\Israel\ix.5.g Israel-db-Aug input.txt
ix.5.h : appendices\appendix ix\Israel\ix.5.h Israel-db-Aug output.txt
Jordan:
ix.6.a: appendices\appendix ix\Jordan\ix.6.a jordan-nb-Jan input.txt
ix.6.b: appendices\appendix ix\Jordan\ix.6.b jordan-nb-Jan output.txt
ix.6.c: appendices\appendix ix\Jordan\ix.6.c jordan-db-Jan input.txt
ix.6.d:appendices\appendix ix\Jordan\ix.6.d jordan-db-Jan output.txt
ix.6.e:appendices\appendix ix\Jordan\ix.6.e Jordan-nb-Aug input.txt
ix.6.f:appendices\appendix ix\Jordan\ix.6.f Jordan-nb-Aug output.txt
ix.6.g: appendices\appendix ix\Jordan\ix.6.g jordan-db-Aug input.txt
ix.6.h: appendices\appendix ix\Jordan\ix.6.h jordan-db-Aug output.txt
Saudi Arabia:
ix.7.a: appendices\appendix ix\Saudi Arabia\ix.7.a Saudi-nb-Jan input.txt
ix.7.b:appendices\appendix ix\Saudi Arabia\ix.7.b Saudi-nb-Jan output.txt
ix.7.c: appendices\appendix ix\Saudi Arabia\ix.7.c Saudi-db-Jan input.txt
ix.7.d: appendices\appendix ix\Saudi Arabia\ix.7.d Saudi-db-Jan output.txt
ix.7.e: appendices\appendix ix\Saudi Arabia\ix.7.e Saudi-nb-Aug input.txt
ix.7.f:appendices\appendix ix\Saudi Arabia\ix.7.f Saudi-nb-Aug output.txt
ix.7.g: appendices\appendix ix\Saudi Arabia\ix.7.g Saudi-db-Aug input.txt
ix.7.h: appendices\appendix ix\Saudi Arabia\ix.7.h Saudi-db-Aug output.txt
ix8 :Performance Of Countries

(x) Appendix x: Raytracing Kuwait
x.1: appendices\appendix x\Kuwait (Jan)/
0.02m, 0.04m, 0.06m,….0.36m/Diffused Beam/ Test
/Test.Out
/Normal Beam/ Test
/Test.Out
x.2: appendices\appendix x\Kuwait (Feb)/
0.02m, 0.04m, 0.06m,….0.36m/Diffused Beam/ Test
/Test.Out
/Normal Beam/ Test
/Test.Out
x.3: appendices\appendix x\Kuwait (Mar)/
0.02m, 0.04m, 0.06m,….0.36m/Diffused Beam/ Test
/Test.Out
/Normal Beam/ Test
/Test.Out
x.4: appendices\appendix x\Kuwait (April)/
0.02m, 0.04m, 0.06m,….0.36m/Diffused Beam/ Test
/Test.Out
/Normal Beam/ Test
/Test.Out
x.5: appendices\appendix x\Kuwait (May)/

0.02m, 0.04m, 0.06m,….0.36m/Diffused Beam/ Test
/Test.Out
/Normal Beam/ Test
/Test.Out
x.6: appendices\appendix x\Kuwait (Jun)/
0.02m, 0.04m, 0.06m,….0.36m/Diffused Beam/ Test
/Test.Out
/Normal Beam/ Test
/Test.Out
x.7: appendices\appendix x\Kuwait (Jul)/
0.02m, 0.04m, 0.06m,….0.36m/Diffused Beam/ Test
/Test.Out
/Normal Beam/ Test
/Test.Out
x.8: appendices\appendix x\Kuwait (Aug)/
0.02m, 0.04m, 0.06m,….0.36m/Diffused Beam/ Test
/Test.Out
/Normal Beam/ Test
/Test.Out
x.9: appendices\appendix x\Kuwait (Sept)/
0.02m, 0.04m, 0.06m,….0.36m/Diffused Beam/ Test
/Test.Out
/Normal Beam/ Test
/Test.Out
x.10: appendices\appendix x\Kuwait (Oct)/
0.02m, 0.04m, 0.06m,….0.36m/Diffused Beam/ Test
/Test.Out
/Normal Beam/ Test
/Test.Out
x.11: appendices\appendix x\Kuwait (Nov)/
0.02m, 0.04m, 0.06m,….0.36m/Diffused Beam/ Test
/Test.Out
/Normal Beam/ Test
/Test.Out
x.12: appendices\appendix x\Kuwait (Dec)/
0.02m, 0.04m, 0.06m,….0.36m/Diffused Beam/ Test
/Test.Out
/Normal Beam/ Test
/Test.Out
x.13: appendices\appendix x\Kuwait-insertion angles/
/July-47,…../July-89
/August-86, …../August-89
x.14: appendices\appendix x\Kuwait-diurnal
x.15: appendices\appendix x\sensitivity performance (Kuwait)1

(xi) Appendix xi: Comparative tools
xi.1:appendices\appendix xi\appendix xi./ Assessment-Windows-Tv-q.xls

(xii) Appendix xii: Results and analysis
xii.1:appendices\appendix xii\ insertion surface temp
/0.04mouter surface temp,.....0.12m outer surface temp
xii.2:appendices\appendix xii\ vert insert surface temp
/0.02mouter surface temp,.....0.12m outer surface temp
xii.3:appendices\appendix xii\ Assessment summer
xii.4:appendices\appendix xii\ Assessment-no insertion

xii.5:appendices\appendix xii\ Assessment-vertical
xii.6:appendices\appendix xii\ Assessment-wintercheck

(xiii) Appendix xii: Published papers

xiii.1: Windows for buildings in hot arid countries.
xiii.2: Suggestion for a new multiple glazing system for hot arid countries
xiii.3: Assessing the performance of smarts2 in a first tier of software using empirical weather data (conference paper)
xiii.4: Assessing the performance of smarts2 in a first tier of software using empirical weather data (journal paper)